JSCSEN 75(11)1463–1616(2010)

Journal of the Serbian Chemical Society

Electronic Version

VOLUME 75

No 11

BELGRADE 2010

Available on line at

www.shd.org.rs/JSCS/

The full search of JSCS is available through

DOAJ DIRECTORY OF OPEN ACCESS JOURNALS

www.doaj.org

Journal of the Serbian Chemical Society
JSCS-info@shd.org.rs • www.shd.org.rs/JSCS

J. Serb. Chem. Soc. Vol. 75, No. 11 (2010)

CONTENTS

Published by the Serbian Chemical Society
Karnegijeva 4/III, 11000 Belgrade, Serbia
Printed by the Faculty of Technology and Metallurgy
Karnegijeva 4, P.O. Box 35-03, 11120 Belgrade, Serbia

Journal of the Serbian Chemical Society
JSCS-info@shd.org.rs • www.shd.org.rs/JSCS
J. Serb. Chem. Soc. 75 (11) 1463–1471 (2010)
JSCS–4068
UDC 547.79+547.286.2:547.496.3–304.2:542.913
Original scientific paper

Synthesis and characterization of some 1,2,4-triazole-3-thiones obtained from intramolecular cyclization of new 1-(4-(4-X-phenylsulfonyl)benzoyl)-4-(4-iodophenyl)-3-thiosemicarbazides

OLGA D. CRETU[1], STEFANIA F. BARBUCEANU[2]*, GABRIEL SARAMET[3] and CONSTANTIN DRAGHICI[4]

[1]*University of Medicine and Pharmacy "Carol Davila", Faculty of Pharmacy, Pharmaceutical Botany Department, Traian Vuia Street 6, 020956, Bucharest,* [2]*University of Medicine and Pharmacy "Carol Davila", Faculty of Pharmacy, Organic Chemistry Department, Traian Vuia Street 6, 020956, Bucharest,* [3]*Pharmaceutical Techniques and Drug Industry Department, Faculty of Pharmacy, Traian Vuia Street 6, 020956 Bucharest and* [4]*The Organic Chemistry Centre "Costin. D. Neniţescu", Romanian Academy, Splaiul Independenţei 202B, 060023, Bucharest, Romania*

(Received 21 December 2009, revised 12 July 2010)

Abstract: This paper presents new heterocyclic compounds from the class of 1,2,4-triazole-3-thione which were obtained by intramolecular cyclization, in basic media of some acylthiosemicarbazides containing diphenyl sulfone moieties. The new 1-(4-(4-X-phenylsulfonyl)benzoyl)-4-(4-iodophenyl)-3-thiosemicarbazides (**7a**–**c**) were obtained by the reaction of 4-(4-X-phenylsulfonyl)-benzoic acid hydrazides (**6a**–**c**) (X = H, Cl or Br) with 4-iodophenylisothiocyanate. The cyclization of the acylthiosemicarbazides **7a**–**c** in the presence of an 8 % NaOH solution resulted in the formation of the new 5-(4-(4-X-phenylsulfonyl)phenyl)-4-(4-iodophenyl)-2,4-dihydro-3*H*-1,2,4-triazole-3-thiones (**8a**––**c)**. The structures of the newly synthesized compounds were elucidated by spectral methods (IR, UV–Vis, ^{1}H-NMR, ^{13}C-NMR and MS spectroscopy) and elemental analysis.

Keywords: 1-acylthiosemicarbazide; intramolecular cyclization; 1,2,4-triazole--3-thione.

INTRODUCTION

The synthesis of compounds containing 1,2,4-triazole rings in their structure has attracted widespread attention, mainly in connection with their wide range of pharmacological properties. A variety of biological activities, such as anti-inflammatory,[1] analgesic,[1,2] antibacterial,[3,4] antifungal,[3] antitubercular,[5] antiviral,[5]

* Corresponding author. E-mail: stefaniafelicia_barbuceanu@yahoo.com
doi: 10.2298/JSC091221122C

antitumoral,[6] anticonvulsant[7] and antidepressant,[8] have been reported for mercapto- and thione-substituted 1,2,4-triazole systems.

1,2,4-Triazole-3-thiones have been prepared by different methods. One of the most common routes to these compounds involves cyclodehydration of acylthiosemicarbazides with a variety of basic reagents, such as sodium hydroxide,[9–11] potassium hydroxide,[12] sodium carbonate,[13] triethylamine,[14] *etc*.

In addition, it is known that acylthiosemicarbazides, the key intermediates used in the synthesis of 1,2,4-triazoles, are compounds with various pharmacological activities: analgesic,[15] antibacterial,[16] antifungal,[17,18] antitubercular[19] and antitumoral.[17] Moreover, a literature survey revealed that diphenyl sulfone derivatives possess antibacterial activities.[20,21]

In view of the above-mentioned findings and in continuation of our research in the domain of heterocyclic compounds of the 1,2,4-triazole class with expected biological activity,[22–25] herein, the syntheses of some new acylthiosemicarbazides and their cyclization compounds from the 1,2,4-triazole class containing the diphenylsulfone moiety with potential biological activity are described. The new synthesized compounds were characterized by IR, UV-Vis, ^{1}H--NMR, ^{13}C-NMR and mass spectrometry and elemental analysis.

EXPERIMENTAL

Materials, methods and instruments

All chemicals used in this study were supplied by Sigma-Aldrich and Merck. Melting points were determined using a Böetius apparatus and are uncorrected. The infrared spectra were registered with a Vertex 70 Bruker spectrometer using potassium bromide disc technique and the results are expressed in wave number (cm^{-1}). The nuclear magnetic resonance (^{1}H-NMR and ^{13}C-NMR) spectra were registered on a Varian Gemini 300 BB spectrometer working at 300 MHz for ^{1}H- and 75 MHz for ^{13}C-NMR, using DMSO-d_6 as the solvent. Chemical shifts are expressed in δ (ppm) using TMS as the internal standard. The mass spectra were obtained with a triple quadrupole mass spectrometer Varian 1200 L/MS/MS, with an electrospray interface (ESI), coupled with a high performance liquid chromatograph with a Varian ProStar 240 SDM ternar pump. The sample solution (2 μg ml^{-1} in chloroform/methanol 1/1, v/v) was introduced into the ESI interface by direct infusion, after a hundred-fold dilution with methanol, at a flow rate of 20 μl min^{-1}. The instrument was operated in the negative ion mode. For negative ionization, a 10 % ammonia solution was added. The ESI needle was subjected to a DC voltage of ±5 kV, and for dispersion, nitrogen at a pressure of 42 psi (14 psi ≈ 1 atm) was used. The drying gas was air at 200 °C and 19 psi and the collision gas was argon (Linde, 99.9999 %) at a pressure of about 1 mTorr. The UV–Vis spectra were recorded on a Specord 40 Analytik Jena spectrometer, in methanol (2.5×10^{-5} M) in the wavelength range 200–600 nm. The elemental analyses were realized with a Perkin-Elmer 2400 instrument.

*General procedure for the preparation of 1-(4-(4-X-phenylsulfonyl)benzoyl)-4-(4-iodophenyl)-3-thiosemicarbazides (**7a**–**c**)*

Equimolar quantities of hydrazide **6** (1.0 mmol) and 4-iodophenyl isothiocyanate (1.0 mmol) in absolute ethanol (3.0 mL) were refluxed for 10 h. The formed precipitate was filtered off and washed with a few mL of cold ethanol. The resulting solid was dried in air and recrystallized from ethanol.

*General procedure for the preparation of the 5-(4-(4-X-phenylsulfonyl)phenyl)-4-(4-iodophenyl)-2,4-dihydro-3*H*-1,2,4-triazole-3-thiones (**8a–c**)*

A mixture of acylthiosemicarbazide **7** (1.0 mmol) and sodium hydroxide solution (8 %, 8.0 mL) was heated under reflux for 4 h. The obtained solution was filtered, allowed to cool and then adjusted to pH 5.5–6.0 with a dilute solution of HCl. The crude product was filtered off, washed with water and recrystallized from $CHCl_3$/petroleum ether (1:1, v/v).

RESULTS AND DISCUSSION

The synthetic pathway followed for the preparation of the title compounds was accomplished as shown in Scheme 1. 4-(4-X-Phenylsulfonyl)benzoic acid hydrazides **6a**–**c** (X = H, Cl or Br), the key intermediates used in the synthesis of the 1-acylthiosemicarbazides **7a**–**c**, were synthesized according to a literature method.[26] Thus, the diaryl sulfones **3a**–**c** were obtained by a Friedel–Crafts reaction between benzene or halobenzene **1a**–**c** (X = Cl or Br) and *p*-toluenesulfonyl chloride **2**. The diaryl sulfones **3a**–**c** were converted into the 4-(4-X-phenylsulfonyl)benzoic acids **4a**–**c** by oxidation in presence of chromic acid and acetic acid. The acids **4a**–**c** were reacted with ethanol in sulfuric acid media to yield the corresponding esters **5a**–**c**. The latter were converted to the desired 4-(4-X-phenylsulfonyl)benzoic acid hydrazides **6a**–**c** upon treatment with hydrazine hydrate in ethanol.[26] The new 1-(4-(4-X-phenylsulfonyl)benzoyl)-4-(4-iodophenyl)-3--thiosemicarbazides **7a**–**c** were obtained by nucleophilic addition of 4-(4-X-phenylsulfonyl)benzoic acid hydrazides **6a**–**c** to 4-iodophenyl isothiocyanate. For the

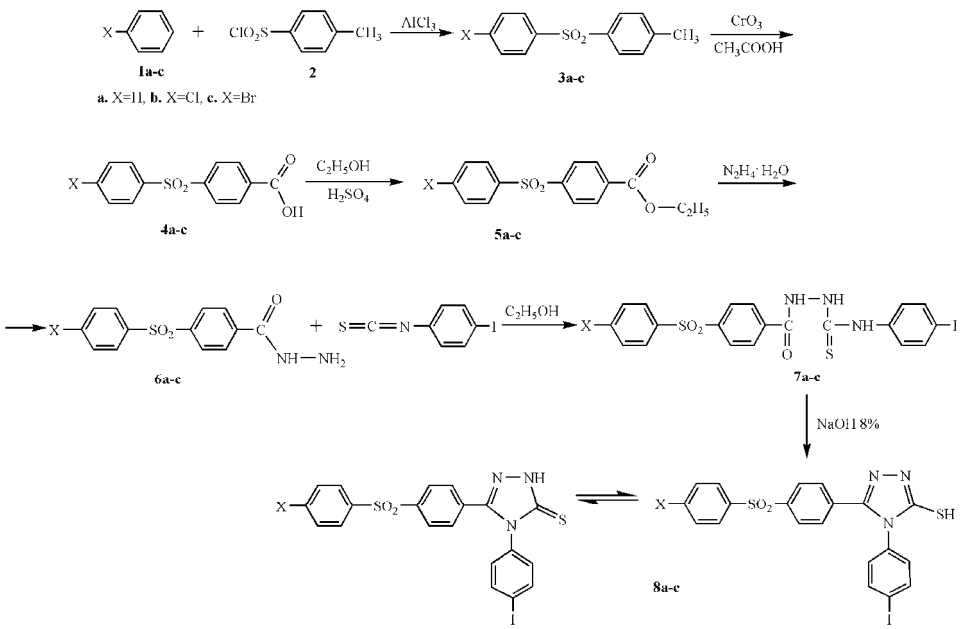

Scheme 1. The synthetic route of the title compounds.

synthesis of the new 5-(4-(4-X-phenylsulfonyl)phenyl)-4-(4-iodophenyl)-2,4-dihydro-3*H*-1,2,4-triazole-3-thiones **8a**–**c**, the acylthiosemicarbazides **7a**–**c** were subjected to intramolecular cyclization in 8 % sodium hydroxide solution under reflux.

The cyclization of the acylthiosemicarbazides **7a**–**c** to the 1,2,4-triazoles **8a**–**c** could be explained by the following mechanism (Scheme 2).[27]

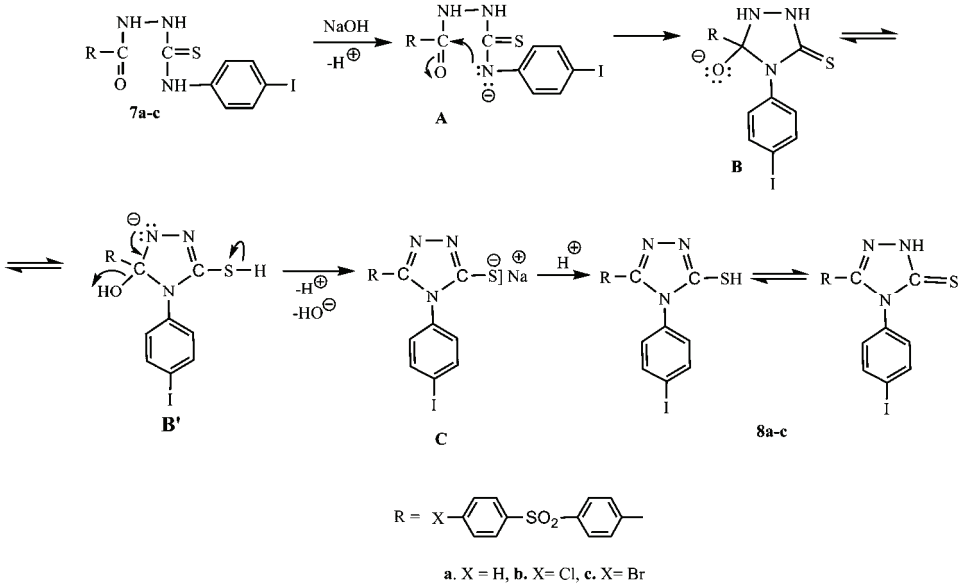

Scheme 2. Proposed mechanism for the formation of the 1,2,4-triazoles **8a**–**c**.

The intermediate tautomer anion **B** was formed by cyclization of the initially obtained anion **A** in basic media from the acylthiosemicarbazides **7a**–**c**. The tautomer anion **B'** was converted into the sodium salt **C** of 1,2,4-triazole **8a**–**c** by elimination of water.

The analytical and spectral data for the newly prepared acylthiosemicarbazides **7a**–**c** are given below.

*4-(4-Iodophenyl)-1-(4-(phenylsulfonyl)benzoyl)-3-thiosemicarbazide (**7a**)*. Yield: 90 %; m.p. 228–230 °C. Anal. Calcd. for $C_{20}H_{16}IN_3O_3S_2$ (FW 537.39): C, 44.70; H, 3.00; S, 11.93; N, 7.82 %. Found: C, 44.77; H, 2.92; S, 11.89; N, 7.76 %. IR (KBr, cm^{-1}): 3365, 3291 (N–H stretching), 3085, 3064, 3038 (C–H stretching of aromatic ring), 1667 (C=O stretching), 1572, 1545, 1523, 1486 (C=C stretching of aromatic ring), 1326, 1295, 1156 (SO_2 stretching), 1226 (C=S stretching), 502 (C–I stretching). ^{1}H-NMR (300 MHz, DMSO-d_6, δ / ppm): 10.80 (1H, *s*, NH), 9.90 (1H, *br s*, NH), 9.80 (1H, *br s*, NH), 8.11 (4H, *s*, aromatic), 7.99 (2H, *dd*, aromatic, J = 7.9 and 1.2 Hz), 7.65 (5H, *m*, aromatic), 7.26 (2H, *br*

s, aromatic). ^{13}C-NMR (75 MHz, DMSO-d_6, δ / ppm): 181.32 (C=S), 164.90 (C=O), 143.93, 140.69, 139.17, 137.18, 136.95, 134.21, 130.04, 129.38, 128.33, 127.64, 127.59, 89.84 (aromatic ring). MS (APCI, *m*/*z*): 536 [M–H]$^-$, 1073 [2M––H]$^-$. UV–Vis (CH_3OH) (λ_{max} / nm (log ε)): 204 (4.55), 246 (4.47).

1-(4-(4-Chlorophenylsulfonyl)benzoyl)-4-(4-iodophenyl)thiosemicarbazide (***7b***). Yield: 83 %; m.p. 213–215 °C. Anal. Calcd. for $C_{20}H_{15}ClIN_3O_3S_2$ (FW 571.84): C, 42.01; H, 2.64; S, 11.21; N, 7.35 %. Found: C, 42.10; H, 2.59; S, 11.15; N, 7.43 %. IR (KBr, cm^{-1}): 3325, 3166 (N–H stretching), 3091, 3070, 3050 (C–H stretching of aromatic ring), 1687 (C=O stretching), 1578, 1541, 1525, 1484 (C=C stretching of aromatic ring), 1321, 1260, 1159 (SO_2 stretching), 1224 (C=S stretching), 761 (C–Cl stretching), 509 (C–I). ^{1}H-NMR (300 MHz, DMSO-d_6, δ / ppm): 10.81 (1H, *br s*, NH), 9.90 (1H, *br s*, NH), 9.80 (1H, *br s*, NH), 8.12 (4H, *s*, aromatic), 8.01 (2H, *d*, aromatic, *J* = 8.8 Hz), 7.66 (2H, *d*, aromatic, *J* = 8.8 Hz), 7.65 (2H, *d*, aromatic, *J* = 8.8 Hz), 7.28 (2H, *br s*, aromatic). ^{13}C-NMR (75 MHz, DMSO-d_6, δ / ppm): 181.53 (C=S), 164.60 (C=O), 143.26, 139.84, 139.08, 139.25, 137.26, 136.78, 130.03, 129.51, 129.29, 127.97, 127.53, 89.92 (aromatic ring). MS (APCI, *m*/*z*): 570 [M–H]$^-$, 572 [M–H]$^-$. UV––Vis (CH_3OH) (λ_{max} / nm (log ε)): 203 (4.69), 249 (4.55).

1-(4-(4-Bromophenylsulfonyl)benzoyl)-4-(4-iodophenyl)thiosemicarbazide (***7c***). Yield: 89 %; m.p. 228–230 °C. Anal. Calcd. for $C_{20}H_{15}BrIN_3O_3S_2$ (FW 616.29): C, 38.98; H, 2.45; S, 10.41; N, 6.82 %. Found: C, 39.06; H, 2.50; S, 10.49; N, 6.75 %. IR (KBr, cm^{-1}): 3329, 3309, 3163 (N–H stretching), 3090, 3046, 3013 (C–H stretching of aromatic ring), 1689 (C=O stretching), 1576, 1542, 1522, 1484 (C=C stretching of aromatic ring), 1320, 1261, 1160 (SO_2 stretching), 1225 (C=S stretching), 573 (C–Br stretching), 505 (C–I stretching). ^{1}H-NMR (300 MHz, DMSO-d_6, δ / ppm): 10.81 (1H, *br s*, NH), 9.90 (1H, *br s*, NH), 9.87 (1H, *br s*, NH), 8.12 (4H, *s*, aromatic), 7.92 (2H, *d*, aromatic, *J* = 8.8 Hz), 7.84 (2H, *d*, aromatic, *J* = 8.8 Hz), 7.66 (2H, *d*, aromatic, *J* = 8.8 Hz), 7.28 (2H, *br s*, aromatic). ^{13}C-NMR (75 MHz, DMSO-d_6, δ / ppm): 180.03 (C=S), 164.88 (C=O), 143.26, 139.44, 139.05, 137.23, 136.76, 132.96, 129.50, 129.28, 128.48, 128.28, 127.51, 89.76 (aromatic ring). MS (APCI, *m*/*z*): 614 [M–H]$^-$, 616 [M–H]$^-$. UV–Vis (CH_3OH) (λ_{max} / nm (log ε)): 203 (4.59), 252 (4.43).

The analytical spectral data for the newly prepared 1,2,4-triazole-3-thiones **8a**–**c** are given below.

*4-(4-Iodophenyl)-5-(4-(phenylsulfonyl)phenyl)-2,4-dihydro-3*H*-1,2,4-triazole-3-thione* (***8a***). Yield: 75 %; m.p. 300 °C. Anal. Calcd. for $C_{20}H_{14}IN_3O_2S_2$ (FW 519.38): C, 46.25; H, 2.72; S, 12.35; N, 8.09 %. Found: C, 46.36; H, 2.64; S, 12.30; N, 8.15 %. IR (KBr, cm^{-1}): 3411 (N–H stretching), 3091, 3059 (C–H stretching of aromatic ring), 1616 (C=N stretching of triazole ring), 1579, 1536, 1490 (C=C stretching of aromatic ring); 1323, 1290, 1159 (SO_2 stretching), 1239 (C=S stretching), 531 (C–I). ^{1}H-NMR (300 MHz, DMSO-d_6, δ / ppm): 7.96 (2H,

d, aromatic, *J* = 8.8 Hz), 7.94 (2H, *dd*, aromatic, *J* = 7.7; 1.7 Hz), 7.85 (2H, *d*, aromatic, *J* = 8.8 Hz), 7.68 (1H, *tt*, aromatic, *J* = 7.7; 1.7 Hz), 7.60 (2H, *t*, aromatic, *J* = 7.7 Hz), 7.54 (2H, *d*, aromatic, *J* = 8.8 Hz), 7.17 (2H, *d*, aromatic, *J* = = 8.8 Hz). ^{13}C-NMR (75 MHz, DMSO-d_6, δ / ppm): 169.04 (C3), 149.00 (C5), 142.61, 140.39, 138.51, 134.05, 130.91, 130.51, 130.44, 130.02, 129.58, 127.81, 127.68, 96.53. MS (APCI, *m*/*z*): 518 $[M–H]^-$. UV–Vis (CH_3OH) (λ_{max} / nm (log ε)): 204 (4.69), 240 (4.51), 249 (4.48), 323 (3.91).

*5-(4-(4-Chlorophenylsulfonyl)phenyl)-4-(4-iodophenyl)-2,4-dihydro-3*H-*-1,2,4-triazole-3-thione (**8b**)*. Yield: 94 %; m.p. 293–295 °C. Anal. Calcd. for $C_{20}H_{13}ClIN_3O_2S_2$ (FW 553.82): C, 43.37; H, 2.37; S, 11.58; N, 7.59 %. Found: C, 43.29; H, 2.29; S, 11.51; N, 7.70 %. IR (KBr, cm^{-1}): 3409 (N–H stretching), 3088, 3061, 3027 (C–H stretching of aromatic ring), 1617 (C=N stretching of triazole ring), 1579, 1539, 1490 (C=C stretching of aromatic ring); 1322, 1284, 1158 (SO_2 stretching), 1237 (C=S stretching), 768 (C–Cl stretching); 534 (C–I). ^{1}H-NMR (300 MHz, DMSO-d_6, δ / ppm): 7.96 (2H, *d*, aromatic, *J* = 8.8 Hz), 7.95 (2H, *d*, aromatic, *J* = 8.5 Hz), 7.85 (2H, *d*, aromatic, *J* = 8.8 Hz), 7.67 (2H, *d*, aromatic, *J* = 8.5 Hz), 7.54 (2H, *t*, aromatic, *J* = 8.8 Hz), 7.17 (2H, *d*, aromatic, *J* = 8.5 Hz). ^{13}C-NMR (75 MHz, DMSO-d_6, δ / ppm): 169.06 (C3), 148.96 (C5), 142.14, 139.42, 139.19, 138.52, 134.05, 130.91, 130.69, 130.17, 129.69, 129.64, 127.88, 96.54; MS (APCI, *m*/*z*): 552 $[M–H]^-$, 554 $[M–H]^-$. UV–Vis (CH_3OH) (λ_{max} / nm (log ε)): 204 (4.62), 241 (4.47), 251 (4.30), 322 (3.84).

*5-(4-(4-Bromophenylsulfonyl)phenyl)-4-(4-iodophenyl)-2,4-dihydro-3*H-*-1,2,4-triazole-3-thione (**8c**)*. Yield: 70 %; m.p. 285–286 °C. Anal. Calcd. for $C_{20}H_{13}BrIN_3O_2S_2$ (FW 598.27): C, 40.15; H, 2.19; S, 10.72; N, 7.02 %. Found: C, 40.25; H, 2.31; S, 10.65; N, 6.97 %. IR (KBr, cm^{-1}): 3410 (N–H stretching), 3086, 3061, 3028 (C–H stretching of aromatic ring), 1617 (C=N stretching of triazole ring), 1572, 1540, 1490 (C=C stretching of aromatic ring), 1323, 1280, 1158 (SO_2 stretching), 1238 (C=S stretching), 574 (C–Br); 534 (C–I). ^{1}H-NMR (300 MHz, DMSO-d_6, δ / ppm): 7.95 (2H, *d*, aromatic, *J* = 8.8 Hz), 7.90 (2H, *d*, aromatic, *J* = 8.8 Hz), 7.84 (2H, *d*, aromatic, *J* = 8.5 Hz), 7.84 (2H, *d*, aromatic, *J* = 8.5 Hz), 7.54 (2H, *d*, aromatic, *J* = 8.5 Hz), 7.17 (2H, *d*, aromatic, *J* = 8.5 Hz). ^{13}C-NMR (75 MHz, DMSO-d_6, δ / ppm): 169.08 (C3), 149.00 (C5), 142.11, 139.64, 138.54, 134.08, 133.14, 130.92, 130.69, 129.73, 129.65, 128.56, 127.90, 96.56. UV–Vis (CH_3OH) (λ_{max} / nm (log ε)): 204 (4.67), 239 (4.42), 255 (4.40), 324 (3.83).

The spectral data of all the newly synthesized compounds from the 1,2,4-triazoles and thiosemicarbazides were in accordance with the proposed structures.

The infrared spectra of the new acylthiosemicarbazides **7a**–**b** confirmed that the nucleophilic addition of hydrazides **6a**–**c** to 4-iodophenyl isothiocyanate occurred by the appearance of a new absorption band due to stretching vibration of C=S group at 1224–1226 cm^{-1}. In addition, the C=O and N–H stretching bands

were present at 1667–1689 and 3365–3163 cm^{-1}, respectively. In the 1,2,4-triazoles **8a**–**c**, the disappearance of the C=O stretching band from the acylthiosemicarbazides and the detection of the C=N stretching band at ≈1617 cm^{-1} is evidence for ring closure. 1,2,4-Triazoles **8a**–**c** may exist in the thiol and thione forms. According to the IR spectral data of compounds **8a**–**c** which have the triazole-3-thione structure, the observation of C=S stretching bands at 1237–1239 cm^{-1} and the absence of an absorption band in the 2300–2600 cm^{-1} region cited for the SH group [11,28] proved that, in the solid state, these new derivatives exist predominantly in the thionic form. The N–H stretching bands of 1,2,4-triazoles **8a**–**c** were observed at 3409–3411 cm^{-1}.

All protons were seen in the ^{1}H-NMR spectra with the expected chemical shifts and integral values. The NH protons of the acylthiosemicarbazides were observed as singlets at 9.80–10.81 ppm. The ^{13}C-NMR spectra of the newly synthesized compounds (**7a**–**c** and **8a**–**c**) showed the number of signals which were consistent with the number of carbon atoms in the molecule. The C=O carbon signal in the ^{13}C-NMR spectra of the acylthiosemicarbazides **7a**–**c** was observed at 164.60–164.90 ppm, whereas the C=S carbon signal appeared in the range 180.03–181.53 ppm. The ^{13}C-NMR spectra of compounds **8a**–**c** contained the resonance signals C3 and C5 of the triazole ring at ≈ 169 and ≈ 149 ppm, respectively. The presence of the signal at ≈ 169.00 ppm, characteristic for the carbon of a C=S group, indicated that these compounds from the 1,2,4-triazoles class existed in solution predominantly in the thione form.[29,30]

The mass spectra of compounds **7a**–**c** and **8a,b** showed an $(M–H)^-$ peak in agreement with their molecular formula. In the case of compounds which contain halogen, two molecular ion peaks were observed as expected, due to the isotopic chlorine or bromine atom in the molecule.

CONCLUSIONS

A series of novel heterocyclic compounds from the 1,2,4-triazole-3-thione class **8a**–**c** were synthesized by treatment of the corresponding acylthiosemicarbazides **7a**–**c** with a sodium hydroxide solution, at reflux. The new acylthiosemicarbazides were synthesized by nucleophilic addition of 4-(4-X-phenylsulfonyl)benzoic acid hydrazides **6a**–**c** to 4-iodophenyl isothiocyanate. The structures of these new compounds were determined by spectral data and elemental analyses. These new compounds will be tested for their biological activity.

ИЗВОД

СИНТЕЗА И КАРАКТЕРИСАЊЕ НЕКИХ 1,2,4-ТРИАЗОЛ-3-ТИОНА ДОБИЈЕНИХ ИНТРАМОЛЕКУЛСКОМ ЦИКЛИЗАЦИЈОМ НОВИХ 1-(4-(4-X-ФЕНИЛСУЛФОНИЛ)БЕНЗОИЛ)-4-(4-ЈОДФЕНИЛ)-3-ТИОСЕМИКАРБАЗИДА

OLGA D. CRETU[1], STEFANIA F. BARBUCEANU[2], GABRIEL SARAMET[3] и CONSTANTIN DRAGHICI[4]

[1]University of Medicine and Pharmacy "Carol Davila", Faculty of Pharmacy, Pharmaceutical Botany Department, Traian Vuia Street 6, 020956, Bucharest, [2]University of Medicine and Pharmacy "Carol Davila", Faculty of Pharmacy, Organic Chemistry Department, Traian Vuia Street 6, 020956, Bucharest, [3]Pharmaceutical Techniques and Drug Industry Department, Faculty of Pharmacy, Traian Vuia Street 6, 020956 Bucharest u [4]The Organic Chemistry Centre "Costin. D. Neniţescu", Romanian Academy, Splaiul Independenţei 202B, 060023, Bucharest, Romania

У раду су приказани нови деривати 1,2,4-триазол-3-тиона, добијени интрамолекулском циклизацијом, у базним условима, из неких ацилтиосемикарбазида који садрже дифенил-сулфонску структуру. Нови 1-(4-(4-X-фенилсулфонил)бензоил)-4-(4-јодфенил)-3-тиосемикарбазиди **7a**–**c** добијени су реакцијом хидразида 4-(4-X-фенилсулфонил)-бензоеве киселине **6a**–**c** (X = H, Cl, Br) са 4-јодфенил-изотиоцијанатом. Циклизацијом ацилтиосемикарбазида **7a**–**c** у присуству 8 % раствора NaOH добијени су 5-(4-(4-X-фенилсулфонил)фенил)-4-(4-јодфенил)-2,4-дихидро-3*H*-1,2,4-триазол-3-тиони **8a**–**c**. Структуре нових једињења утврђене су спектралним методама (IR, UV–Vis, ^{1}H-NMR, ^{13}C-NMR и MS спектри) и елементалном анализом.

(Примљено 21. децембра 2009, ревидирано 12. јула 2010)

REFERENCES

1. M. Amir, S. Kumar, *Acta Pharm*. **57** (2007) 31
2. M. Gokce, B. Cakir, K. Erol, M. F. Sahin, *Arch. Pharm*. **334** (2001) 279
3. I. R. Ezabadi, C. Camoutsis, P. Zoumpoulakis, A. Geronikaki, M. Soković, J. Glamočlija, A. Ćirić, *Bioorg. Med. Chem.* **16** (2008) 355
4. G. Mazzone, F. Bonina, R. Arrigo Reina, G. Blandino, *Farmaco* **36** (1981) 181
5. I. Küçükgüzel, E. Tatar, Ş. G. Küçükgüzel, S. Rollas, E. De Clercq, *Eur. J. Med. Chem*. **43** (2008) 381
6. H. N. Dogan, A. Duran, S. Rollas, *Indian J. Chem. Sect. B.* **44** (2005) 2301
7. J. M. Kane, M. A. Staeger, C. R. Dalton, F. P. Miller, M. W. Dudley, A. M. L. Ogden, J. H. Kehne, H. J. Ketteler, T. C. McCloskey, Y. Senyah, P. A. Chmieleweski, J. A. Miller, *J. Med. Chem.* **37** (1994) 125
8. J. M. Kane, M. K. Dudley, S. M. Sorensen, F. P. Miller, *J. Med. Chem*. **31** (1988) 1253
9. M. Wujec, M. Pitucha, M. Dobosz, U. Kosikowska, A. Malm, *Acta Pharm*. **54** (2004) 251
10. M. Pitucha, M. Wujec, M. Dobosz, *J. Chin. Chem. Soc*. **54** (2007) 69
11. K. Zamani, K. Faghihi, T. Tofighi, M. R. Shariatzadeh, *Turk. J. Chem*. **28** (2004) 95
12. A.-R. Farghaly, H. El-Kashef, *Arkivoc* **XI** (2006) 79
13. N. Guelerman, S. Rollas, M. Uelgen, *Boll. Chim. Farm*. **137** (1998) 140
14. U. Salgin-Gökşen, N. Gökhan-Kelekçi, Ö. Göktaş, Y. Köysal, E. Kiliç, Ş. Işik, G. Aktay, M. Özalp, *Bioorg. Med. Chem*. **15** (2007) 5738
15. M. A. Bhat, N. Siddiqui, S. A. Khan, *Indian J. Pharm. Sci.* **68** (2006) 120
16. A. M. Qandil, H. N. Tumah, M. A. Hassan, *Acta Pharm. Sci.* **48** (2006) 95
17. N. K. Singh, S. B. Singh, A. Shrivastav, S. M. Singh, *Proc. Indian Acad. Sci. (Chem. Sci.)* **113** (2001) 257

18. N. Kalyoncuoğlu, S. Rollas, D. Sür-Altiner, Y. Yeğenoğlu, Ö. Anğ, *Pharmazie* **47** (1992) 796
19. S. Bahadur, A. K. Goel, *Indian J. Pharm*. **38** (1976) 71
20. E. F. Elslager, Z. B. Gavrilis, A. A. Phillips, D. F. Worth, *J. Med. Chem.* **12** (1969) 357
21. R. Wolf, H. Matz, E. Orion, B. Tuzun, Y. Tuzun, *Dermatol. Online J*. **8** (2002) 2
22. S.-F. Barbuceanu, G. L. Almajan, I. Saramet, C. Draghici, R. Socoteanu, F. Barbuceanu, *J. Serb. Chem. Soc.* **74** (2009) 1041
23. G. L. Almajan, S.-F. Barbuceanu, E.-R. Almajan, C. Draghici, G. Saramet, *Eur. J. Med. Chem.* **44** (2009) 3083
24. O. D. Cretu, S.-F. Barbuceanu, I. Saramet, C. Draghici, C. Enache, *Rev. Chim. (Bucharest)* **60** (2009) 816
25. I. Şaramet, C. Drăghici, C. Bărcuţean, V. Rădulescu, T. Loloiu, M. D. Banciu, *Heterocycl. Commun.* **7** (2001) 369
26. A. Mavrodin, V. Zotta, M. Stoenescu, D. Oţeleanu, *Pharm. Zentralhalle Dtschl*. **95** (1956) 353
27. I. Şaramet, C. Drăghici, C. Bărcuţean, V. Rădulescu, T. Loloiu, M. D. Banciu, *Rev Roum. Chim.* **47** (2002) 139
28. S. Baluja, S. Chanda, R. Chabhadiya, N. Kachhadia, R. Nair, A. Solanki, *J. Serb. Chem. Soc.* **72** (2007) 539
29. C. Kuş, G. Ayhan-Kilcigil, B. C. Eke, M. Işcan, *Arch. Pharm Res.* **27** (2004) 156
30. M. Wujec, U. Kosikowska, P. Paneth, A. Malm, *Heterocycles* **71** (2007) 2617.

Journal of the Serbian Chemical Society
JSCS-info@shd.org.rs • www.shd.org.rs/JSCS
J. Serb. Chem. Soc. 75 (11) 1473–1479 (2010)
JSCS–4069
UDC 547.239–304.2+66.095.252.091.7:547.594.3
Original scientific paper

Synthesis of nitrogen-containing dispiroheterocycles using nitrilimines (II)

HANY M. DALLOUL[1]* and AHMED S. ABU SAMAHA[2]

[1]*Chemistry Department, Faculty of Science, Al-Aqsa University of Gaza, P.O. Box 4051, 76888 Gaza and* [2]*Biology Department, Faculty of Science, Al-Aqsa University of Gaza, P.O. Box 4051, 76888 Gaza, Palestine*

(Received 24 August 2009, revised 12 July 2010)

Abstract: A series of 1,2,4,9,10,12-hexaazadispiro[4.2.4.2]tetradeca-2,10-dienes **5a**–**j** was synthesized by the reaction of 1,4-cyclohexanedione dioxime (**3**) with appropriate nitrilimines (**2**). The microanalysis and spectral data of the synthesized compounds are in full agreement with their molecular structure. The microbial features of some of the synthesized compounds were studied by a known method.

Keywords: Dispiroheterocycles; 1,4-cyclohexanedione oxime; nitrilimines; cycloaddition.

INTRODUCTION

Recently, a versatile and efficient one-pot synthesis of octaazadispiroheterocyclic compounds was described in which 1,4-cyclohexanedione methyl hydrazone and nitrilimines, generated *in situ* from the corresponding hydrazonoyl halides by the action of a suitable base, were utilized.[1] As part of our continuing interest in the construction of spiroheterocyclic systems by means of the nitrilimine 1,3-dipolar cycloaddition methodology,[2–5] the reaction of *C*-substituted-*N*--arylnitrilimines (**2**) with 1,4-cyclohexanedione dioxime (**3**) in an attempt to synthesize the hitherto unknown hexaazadispiroheterocyclic compounds **5a**–**j** is reported herein, with the aim of investigating their biological activities.

RESULTS AND DISCUSSION

The hydrazonoyl halides **1a**–**j** were prepared by a modified literature procedure[6–14] and the nitrilimines **2** were generated *in situ* from **1** by reaction with triethylamine (Et_3N). The non-isolatable nitrilimines **2** reacted readily with 1,4--cyclohexanedione dioxime **3** affording the corresponding 1,2,4,9,10,12-hexaaza-

* Corresponding author. E-mail: hmdalloul60@yahoo.com
doi: 10.2298/JSC090824119D

dispiro[4.2.4.2]tetradeca-2,10-dienes **5a**–**j** (Scheme 1). The formation of compounds **5a**–**j** is assumed to involve the primary cycloadducts **4**, which tautomerize to amine oxide-type intermediates that are deoxygenated by triethylamine to NH triazoles **5a**–**j**. It is worth mentioning that the nitrile oxides generated *in situ* from the respective hydroxamoyl chlorides with triethylamine as the base react with oximes to give 4-hydroxy-4,5-dihydro-1,2,4-oxadiazoles.[15]

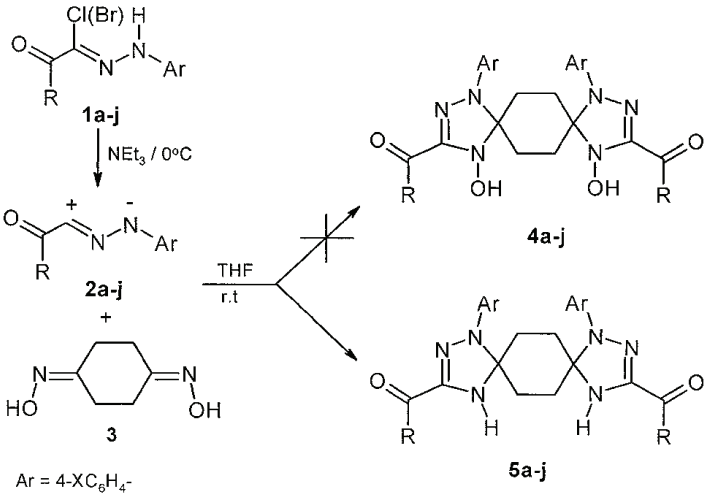

Entry	a	b	c	d	e	f	g	h	i	j
R	Me	Me	MeO	Ph	PhNH	PhNH	PhNH	2-$C_{10}H_7$	2-C_4H_3O	2-C_4H_3S
X	H	Cl	Cl	Cl	Cl	Br	Me	Cl	Cl	Cl

Scheme 1. Synthetic pathway for the preparation of compounds **5a–j.**

Characterization data for the synthesized compounds

*3,11-Diacetyl-1,9-diphenyl-1,2,4,9,10,12-hexaazadispiro[4.2.4.2]tetradeca--2,10-diene (**5a**)*. Yield: 47 %; m.p. 180–182 °C. Anal. Calcd. for $C_{24}H_{26}N_6O_2$ (FW 430.51): C, 66.96; H, 6.09; N, 19.52 %. Found: C, 67.18; H, 5.90; N, 19.40 %. IR (KBr, cm^{-1}): 3385 (NH), 1678 (C=O), 1622 (C=N), 630 (C–Cl). ^{1}H-NMR (DMSO-d_6, δ / ppm): 7.42–7.12 (10H, *m*, aromatic), 5.74 (2H, *s*, 2 NH, D_2O exchangeable), 2.48 (6H, *s*, 2 CH_3), 2.17–2.03 (8H, *m*, 4 CH_2). ^{13}C-NMR (DMSO--d_6, δ / ppm): 189.65 (C=O), 147.95 (C=N), 141.46–120.18 (C=C Ar), 87.45 (spiro carbons), 35.07, 34.83 (2 CH_2), 26.45 (CH_3); MS (*m/z*): 430 ($M^{+\bullet}$).

*3,11-Diacetyl-1,9-bis(4-chlorophenyl)-1,2,4,9,10,12-hexaazadispiro[4.2.4.2]-tetradeca-2,10-diene (**5b**)*. Yield: 45 %; m.p. 186–188 °C. Anal. Calcd. for $C_{24}H_{24}Cl_2N_6O_2$ (FW 499.40): C, 57.72; H, 4.84; N, 16.83 %. Found: C, 57.88; H, 4.74; N, 16.71 %. IR (KBr, cm^{-1}): 3385 (NH), 1676 (C=O), 1620 (C=N), 631

(C–Cl). ^{1}H-NMR (DMSO-d_6, δ / ppm): 7.48–7.14 (8H, *m*, aromatic), 5.74 (2H, *s*, 2 NH, D_2O exchangeable), 2.47 (6H, *s*, 2 CH_3), 2.16–2.01 (8H, *m*, 4 CH_2). ^{13}C-NMR (DMSO-d_6, δ / ppm): 189.71 (C=O), 147.96 (C=N), 141.94–121.10 (C=C Ar), 87.22 (spiro carbons), 35.10, 34.86 (2 CH_2), 26.48 (CH_3). MS (*m/z*): 498/500 (M^+, chlorine isotopes).

*1,9-Bis(4-chlorophenyl)-3,11-bis(methoxycarbonyl)-1,2,4,9,10,12-hexaaza-dispiro[4.2.4.2]tetradeca-2,10-diene (**5c**)*. Yield: 50 %; m.p. 173–175 °C. Anal. Calcd. for $C_{24}H_{24}Cl_2N_6O_4$ (FW 531.40): C, 54.25; H, 4.55; N, 15.81 %. Found: C, 54.46; H, 4.41; N, 15.95 %. IR (KBr, cm^{-1}): 3380 (NH), 1720 (C=O), 1625 (C=N), 628 (C–Cl). ^{1}H-NMR (DMSO-d_6, δ / ppm): 7.57–7.20 (8H, *m*, aromatic), 5.74 (2H, *s*, 2 NH, D_2O exchangeable), 3.74 (6H, *s*, 2 OCH_3), 2.18-2.04 (8H, *m*, 4 CH_2). ^{13}C-NMR (DMSO-d_6, δ / ppm): 156.69 (O–C=O), 147.90 (C=N), 141.90–121.16 (C=C Ar), 88.95 (spiro carbons), 54.22 (OCH_3), 35.56, 34.72 (2 CH_2). MS (*m/z*): 530/532 (M^+, chlorine isotopes).

*3,11-Dibenzoyl-1,9-bis(4-chlorophenyl)-1,2,4,9,10,12-hexaazadispiro[4.2.4.2]-tetradeca-2,10-diene (**5d**)*. Yield: 52 %; m.p. 179–181 °C. Anal. Calcd. for $C_{34}H_{28}Cl_2N_6O_2$ (FW 623.55): C, 65.49; H, 4.53; N, 13.48 %. Found: C, 65.30; H, 4.70; N, 13.65 %. IR (KBr, cm^{-1}): 3365 (NH), 1665 (C=O), 1618 (C=N), 620 (C–Cl). ^{1}H-NMR (DMSO-d_6, δ / ppm): 8.46–7.26 (18H, *m*, aromatic), 5.74 (2H, *s*, 2 NH, D_2O exchangeable), 2.00–1.95 (8H, *m*, 4 CH_2). ^{13}C-NMR (DMSO-d_6, δ / ppm): 184.86 (C=O), 148.10 (C=N), 142.15–121.19 (C=C Ar), 91.50 (spiro carbons), 35.54, 34.76 (2 CH_2). MS (*m/z*): 622/624 (M^+, chlorine isotopes).

*1,9-Bis(4-chlorophenyl)-3,11-bis(phenylaminocarbonyl)-1,2,4,9,10,12-hexa-azadispiro[4.2.4.2]-tetradeca-2,10-diene (**5e**)*. Yield: 47 %; m.p. 196–198 °C. Anal. Calcd. for $C_{34}H_{30}Cl_2N_8O_2$ (FW 653.58): C, 62.48; H, 4.63; N, 17.14 %. Found: C, 62.30; H, 4.72; N, 17.02 %. IR (KBr, cm^{-1}): 3375, 3248 (NH), 1655 (C=O), 1615 (C=N), 622 (C–Cl). ^{1}H-NMR (DMSO-d_6, δ / ppm): 8.90 (2H, *s*, 2 PhNH), 7.76–7.03 (18H, *m*, aromatic), 5.68 (2H, *s*, 2 NH, D_2O exchangeable), 2.13–2.06 (8H, *m*, 4 CH_2). ^{13}C-NMR (DMSO-d_6, δ / ppm): 159.36 (C=O), 147.86 (C=N), 141.43–121.10 (C=C Ar), 89.52 (spiro carbons), 35.50, 34.90 (2 CH_2); MS (*m/z*): 652/654 (M^+, chlorine isotopes).

*1,9-Bis(4-bromophenyl)-3,11-bis(phenylaminocarbonyl)-1,2,4,9,10,12-hexa-azadispiro[4.2.4.2]-tetradeca-2,12-diene (**5f**)*. Yield: 45 %; m.p. 201–203 °C. Anal. Calcd. for $C_{34}H_{30}Br_2N_8O_2$ (FW 742.48): C, 55.00; H, 4.07; N, 15.09 %. Found: C, 55.22; H, 3.95; N, 14.90 %. IR (KBr, cm^{-1}): 3380, 3257 (NH), 1654 (C=O), 1612 (C=N), 631 (C–Br). ^{1}H-NMR (DMSO-d_6, δ / ppm): 8.87 (2H, *s*, 2 PhNH), 7.78–7.15 (18H, *m*, aromatic), 5.67 (2H, *s*, 2 NH, D_2O exchangeable), 2.11–2.05 (8H, *m*, 4 CH_2). ^{13}C-NMR (DMSO-d_6, δ / ppm): 159.40 (C=O), 147.84 (C=N), 141.62–116.50 (C=C Ar), 89.60 (spiro carbons), 35.26, 34.90 (2 CH_2). MS (*m/z*): 742/744 (M^+, bromine isotopes).

*1,9-Bis(4-methylphenyl)-3,11-bis(phenylaminocarbonyl)-1,2,4,9,10,12-hexaazadispiro[4.2.4.2]-tetradeca-2,12-diene (**5g**)*. Yield: 48 %; m.p. 191–193 °C. Anal. Calcd. for $C_{36}H_{36}N_8O_2$ (FW 612.74): C, 70.57; H, 5.92; N, 18.29 %. Found: C, 70.45; H, 4.79; N, 18.42 %. IR (KBr, cm^{-1}): 3380, 3260 (NH), 1655 (C=O), 1612 (C=N). ^{1}H-NMR (DMSO-d_6, δ / ppm): 8.89 (2H, *s*, 2 PhNH), 7.80––7.13 (18H, *m*, aromatic), 5.67 (2H, *s*, 2 NH, D_2O exchangeable), 2.26 (6H, *s*, $2CH_3$), 2.10–2.04 (8H, *m*, 4 CH_2). ^{13}C-NMR (DMSO-d_6, δ / ppm): 159.24 (C=O), 147.90 (C=N), 141.55–119.94 (C=C Ar), 89.65 (spiro carbons), 35.50, 34.96 (2 CH_2), 23.40 (CH_3); MS (*m/z*): 612 (M^+).

*1,9-Bis(4-chlorophenyl)-3,11-di-2-naphthoyl-1,2,4,9,10,12-hexaazadispiro-[4.2.4.2]tetradeca-2,10-diene (**5h**)*. Yield: 54 %; m.p. 216–218 °C. Anal. Calcd. for $C_{42}H_{32}Cl_2N_6O_2$ (FW 723.67): C, 69.71; H, 4.46; N, 11.61 %. Found: C, 69.50; H, 4.35; N, 11.70 %. IR (KBr, cm^{-1}): 3365 (NH), 1650 (C=O), 1605 (C=N), 630 (C–Cl). ^{1}H-NMR (DMSO-d_6, δ / ppm): 8.45–7.22 (22H, *m*, aromatic), 5.74 (2H, *s*, 2 NH, D_2O exchangeable), 2.10–2.03 (8H, *m*, 4 CH_2). ^{13}C--NMR (DMSO-d_6, δ / ppm): 184.56 (C=O), 148.32 (C=N), 142.12–120.86 (C=C Ar), 91.63 (spiro carbons), 35.30, 34.75 (2 CH_2); MS (*m/z*): 722/724 (M^+, chlorine isotopes).

*1,9-Bis(4-chlorophenyl)-3,11-di-2-furoyl-1,2,4,9,10,12-hexaazadispiro-[4.2.4.2]tetradeca-2,10-diene (**5i**)*. Yield: 48 %; m.p. 194–196 °C. Anal. Calcd. for $C_{30}H_{24}Cl_2N_6O_4$ (FW 603.47): C, 59.71; H, 4.01; N, 13.93 %. Found: C, 59.85; H, 3.90; N, 13.85 %. IR (KBr, cm^{-1}) 3370 (NH), 1665 (C=O), 1615 (C=N), 627 (C–Cl). ^{1}H-NMR (DMSO-d_6, δ / ppm): 7.80–7.16 (14H, *m*, aromatic), 5.64 (2H, *s*, 2 NH, D_2O exchangeable), 2.16–2.10 (8H, *m*, 4 CH_2). ^{13}C--NMR (DMSO-d_6, δ / ppm): 174.56 (C=O), 148.25 (C=N), 143.20–121.58 (C=C Ar), 94.85 (spiro carbons), 35.41, 34.83 (2 CH_2). MS (*m/z*): 602/604 (M^+, chlorine isotopes).

*1,9-Bis(4-chlorophenyl)-3,11-di-2-thenoyl-1,2,4,9,10,12-hexaazadispiro-[4.2.4.2]tetradeca-2,10-diene (**5j**)*. Yield: 50 %; m.p. 180–182 °C. Anal. Calcd. for $C_{30}H_{24}Cl_2N_6O_2S_2$ (FW 635.60): C, 56.69; H, 3.81; N, 13.22 %. Found: C, 56.80; H, 3.65; N, 13.06 %. IR (KBr, cm^{-1}): 3375 (NH), 1660 (C=O), 1610 (C=N), 628 (C–Cl). ^{1}H-NMR (DMSO-d_6, δ / ppm): 7.84–7.12 (14H, *m*, aromatic), 5.65 (2H, *s*, 2 NH, D_2O exchangeable), 2.15–2.06 (8H, *m*, 4 CH_2). ^{13}C--NMR (DMSO-d_6, δ / ppm): 175.82 (C=O), 148.30 (C=N), 143.73–121.68 (C=C Ar), 94.64 (spiro carbons), 35.35, 34.66 (2 CH_2); MS (*m/z*): 634/636 (M^+, chlorine isotopes).

Spectral data analysis

Compounds **5a**–**j** gave satisfactory analyses for the proposed structures which are confirmed on the bases of their spectroscopic data. The electron impact (EI) mass spectra displayed the correct molecular ions (M^+) in accordance with the suggested structures. The base peak in all these compounds was that of the con-

jugated vinyl triazole cation (Scheme 2). This fragmentation pattern is well known for cycloalkanones.[16]

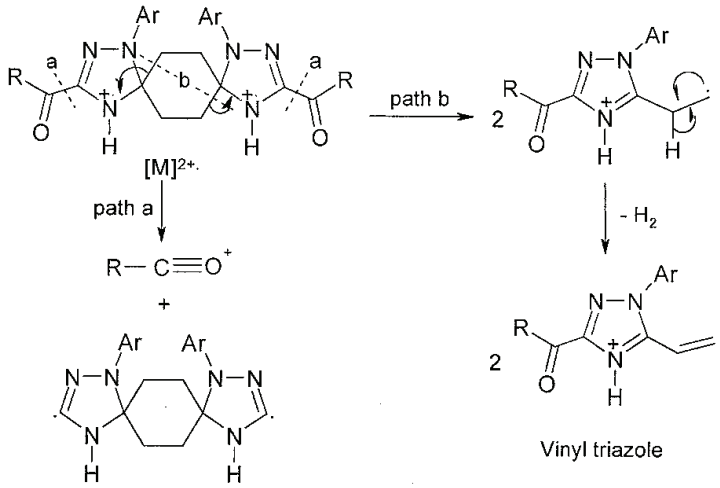

Scheme 2. The main fragmentation of compounds **5a**–**j**.

The IR spectra for **5a**–**j** showed absorption bands in the region 3380–3360 cm^{-1} and 1680–1650 cm^{-1}, assignable to NH and carbonyl group signals, respectively. Their ^{1}H-NMR spectra revealed, besides aromatic protons at 8.5–7.1 ppm, a D_2O exchangeable singlet signal in the region 5.7–5.6 ppm, assignable to the triazole ring NH proton. The ^{13}C-NMR spectra showed all the signals expected for the proposed structures and, in particular, the C5 and C8 signals (spiro carbons) were found at about 95–85 ppm. This is similar to reported values for spiro carbons flanked by two nitrogen atoms in five-membered heterocycles,[3–5] which provides strong evidence in support of the structures **5a**–**j**. The signal at about 148 ppm was attributed to the C=N of the triazole ring. The ^{15}N-NMR spectra of similar triazoles, such as 3-acetyl-5,5-dimethyl-1-phenyl-4,5-dihydro-1,2,4-triazole, which displayed a doublet for NH at 284.26 ppm relative to nitromethane ($^1J_{N–H}$ = 85 Hz, $^3J_{N–CH_3}$ = 2.5 Hz) were reported to support the suggested structure of the reaction products.[17] Further work on the structures of the synthesized compounds is ongoing.

Antimicrobial activity

The obtained antimicrobial activity data is reported in Table I as the average of three experiments. The results showed that all the tested compounds exhibited a marked degree of activity against bacteria and fungi compared with well-known antibacterial and antifungal substances, such as tetracycline and fluconazole. According to NCCLS (2004), zones of inhibition for tetracycline and fluconazole < 14 mm were considered resistant, between 15 and 18 mm as weakly

sensitive and > 19 mm sensitive. In addition, the results showed the degree of inhibition varied between the tested compounds.

TABLE I. Antimicrobial screening results of the tested compounds (zone of inhibition in mm)

Compound	Bacteria					Fungi	
	Enterococcus sp.	*E. coli*	*S. aureus*	*Klebsiella.* sp.	*Proteus* sp.	*C. albicans*	*A. niger*
5a	14	19	11	10	0	11	10
5c	14	18	12	0	0	13	8
5d	17	13	12	17	14	15	14
5f	12	15	10	8	0	12	12
5h	9	9	14	19	0	13	0
5j	15	12	10	15	11	14	10
DMF	–	–	–	–	–	–	–

EXPERIMENTAL

All melting points were determined on an A. Krüss Melting Point Meter equipped with a thermometer and are uncorrected. The IR spectra were measured as potassium bromide pellets using a Satellite 3000 Mid infrared spectrophotometer. The ^{1}H-NMR and ^{13}C-NMR spectra were recorded on a Bruker AM 300 MHz spectrometer at room temperature in DMSO-d_6 solution using tetramethylsilane (TMS) as the internal reference. Chemical shifts were recorded as δ values in ppm downfield from the internal TMS. Electron impact (EI) mass spectra were run on a Shimadzu GCMS-QP1000 EX spectrometer at 70 eV. Elemental analyses were performed at Cairo University, Egypt. The hydrazonoyl halides **1a**–**j**[6-14] and 1,4-cyclohexanedione dioxime **3**[18] were prepared according to literature procedures. Tetrahydrofuran (THF) and triethylamine were purchased from Avocado Research Chemicals, England, and used without further purification.

*General procedure for the reaction of nitrilimines **2** with 1,4-cyclohexanedione dioxime (**3**)*

Triethylamine (0.05 mol, 7 mL) in tetrahydrofuran (10 mL) was added dropwise to stirred mixture of oxime **3** (0.025 mol) and the appropriate hydrazonoyl halides **1a**–**j** (0.05 mol) in tetrahydrofuran (70 mL) at –5–0 °C. The reaction temperature was allowed to rise slowly to room temperature and stirring was continued over night. The precipitated salts were filtered off and the solvent was then evaporated. The residue was washed with water (100 mL) and in few cases the gummy products were triturated with ethanol (10 mL). The crude solid product was collected and recrystallized from ethanol to give the desired compounds.

Antimicrobial activity testing

Six of the newly synthesized compounds were screened *in vitro* for their antimicrobial activity against a variety of bacterial strains, such as *Enterococcus* sp., *Escherichia coli*, *Staphylococcus aureus*, *Klebsiella* sp. and *Proteus* sp., and fungi, such as *Aspergillus niger*, *Candida albicans*, employing the nutrient agar disc diffusion method[29-21] at a concentration of 10 mg mL^{-1} in dimethylformamide (DMF) and disc diameter of 6.5 mm by measuring the average diameter of the inhibition zone in mm.

CONCLUSIONS

Several new 1,2,4,9,10,12-hexaazadispiro[4.2.4.2]tetradeca-2,10-dienes were synthesized and characterized, and some of them proved to have potent antibac-

terial and antifungal activity. The results confirm that the antimicrobial activity is strongly dependent on the nature of the substituents at C3 and C11 of the triazole rings.

Acknowledgements. The authors are thankful to the Union of Arab Universities (UAU), Supporting Box of Palestinian Universities, Amman, Jordan, for financial support.

ИЗВОД

СИНТЕЗА АЗОТОВИХ ДИСПИРОХЕТЕРОЦИКЛА УПОТРЕБОМ НИТРИЛИМИНА (II)

HANY M. DALLOUL[1] и AHMED S. ABU SAMAHA[2]

[1]*Chemistry Department, Faculty of Science, Al-Aqsa University of Gaza, P.O. Box 4051, 76888 Gaza и*
[2]*Biology Department, Faculty of Science, Al-Aqsa University of Gaza, P.O. Box 4051, 76888 Gaza, Palestine*

Синтетисана је серија 1,2,4,9,10,12-хексаазадиспиро[4.2.4.2]тетрадека-2,10-диена **5a–j** реакцијом 1,4-циклохексадион-диоксима (**3**) и одговарајућих нитрилимина (**2**). Резултати микроанализе и спектрални подаци у складу су са претпостављеном структуром једињења. Испитане су микробиолошке активности једињења.

(Примљено 24. августа 2009, ревидирано 12. јула 2010)

REFERENCES

1. H. M. Dalloul, *Arkivoc* **XIV** (2008) 234
2. H. M. Dalloul, P. H. Boyle, *Heterocycl. Commun.* **9** (2003) 507
3. H. M. Dalloul, *Chem. Heterocycl. Compd.* **40** (2004) 1402
4. H. M. Dalloul, P. H. Boyle, *Turk. J. Chem.* **30** (2006) 119
5. H. M. Dalloul, P. H. Boyle, *Heterocycl. Commun.* **13** (2007) 155
6. M. M. El-Abadelah, A. Q. Hussein, B. A. Thaher, *Heterocycles* **32** (1991) 1879
7. A. S. Shawali, A. O. Abdelhamid, *Bull. Chem. Soc. Jpn.* **49** (1976) 321
8. H. M. Hassaneen, A. S. Shawali, N. M. Elwan, N. M Abounada, *Sulfur Lett.* **13** (1992) 273
9. H. M. Hassaneen, A. S. Shawali, N. M. Elwan, N. M. Abounada, *Org. Prep. Proced. Int.* **24** (1992) 171
10. P. Frohberg, G. Drutkowski, C. Wagner, *Eur. J. Org. Chem.* (2002) 1654
11. M. M. El-Abadelah, A. Q. Hussein, M. R. Kamal, K. H. Al-Adhami, *Heterocycles* **27** (1988) 917
12. A. S. Shawali, H. M. Hassaneen, A. Shetta, A. Osman, F. Abdel-Galil, *Heterocycles* **19** (1982) 57
13. A. M. Farag, M. S. Algharib, *Org. Prep. Proced. Int.* **20** (1988) 521
14. A. O. Abdelhamid, F. H. El-Shiaty, *Phosphorus Sulfur Relat. Elem.* **39** (1988) 45
15. S. Morrocchi, A. Ricca, *Chim. Ind. (Milan)* **49** (1967) 629
16. M. Hesse, H. Meier, B. Zeeh, *Spectroscopic Methods in Organic Chemistry*, Thieme, Stuttgart, 1997, p. 229
17. A. R. S. Ferwanah, *Asian J. Chem.* **11** (1999) 480
18. B. Furniss, A. Hannford, V. Rogers, P. Smith, A. Tachell, *Vogel's Text Book of Practical Organic Chemistry, Including Qualitative Organic Analysis*, 4th ed., Longman, London, 1978, pp. 1113–1196
19. C. H. Collins, P. M. Lyne, J. M. Granga, *Microbiological Methods*, 6th ed., Butterworths, London, 1989, p. 410
20. O. N. Irob, M. Moo-Yung, W. A. Anderson, *Int. J. Pharm.* **34** (1996) 87
21. R. J. Grayer, J. B. A. Harborne, *Phytochemistry* **37** (1994) 19.

Journal of the Serbian Chemical Society
JSCS-info@shd.org.rs • www.shd.org.rs/JSCS
J. Serb. Chem. Soc. *75* (11) 1481–1489 (2010)
JSCS–4070
UDC 577.112+577.175.72:539.2:543.544
Original scientific paper

An investigation of the different molecular forms of IGFBP-1 using immobilised metal-, immuno- and lectin-affinity chromatography

DRAGANA LAGUNDŽIN*#, ROMANA MASNIKOSA#, GORAN MILJUŠ#, DRAGANA ROBAJAC# and OLGICA NEDIĆ#

Institute for the Application of Nuclear Energy – INEP, University of Belgrade, Banatska 31b, 11080 Belgrade, Serbia

(Received 30 March, revised 2 July 2010)

Abstract: The insulin-like growth factor-binding protein 1 (IGFBP-1) is a member of a family of six homologous proteins that regulate the action of the insulin-like growth factors. IGFBP-1 is a 25 kDa protein that, in addition to its native form, may exist in several phosphoforms (30 kDa), which are predominant in the circulation of humans. Phosphorylation of IGFBP-1 is a post-translational modification that has a great influence on the action of IGF-I. IGFBP-1 forms multimers and complexes with α2-macroglobulin (α2M). Polymerisation of IGFBP-1 was also reported. In order to analyse and separate these IGFBP-1 molecular species, affinity chromatography methods were used in this study. The results demonstrated that most of the IGFBP-1 circulates in complexes with α2M, which can be isolated by affinity chromatography using immobilised anti-α2M antibodies. IGFBP-1/α2M complexes may be differentiated from IGFBP-1 dimer and multimers using lectin-affinity chromatography, since the latter do not interact with lectins. It seems that the complexes contain not only monomeric IGFBP-1, but also its multimers. The dimer and multimers are stable under reducing conditions, suggesting a covalent linkage between the units. Free IGFBP-1 monomer can be separated from multimers using Con A-affinity chromatography. The concentration of free IGFBP-1 is relatively low in the circulation.

Keywords: IGFBP-1; isoforms; complexes; affinity chromatography.

INTRODUCTION

Insulin-like growth factors (IGF-I and IGF-II) are polypeptides, which regulate cell growth, differentiation and metabolism.[1] In the circulation they are associated with IGF binding proteins (IGFBPs), a family that consists of six homo-

* Corresponding author. E-mail: draganal@inep.co.rs
# Serbian Chemical Society member.
doi: 10.2298/JSC100330090L

logous proteins that modulate the bioactivity of IGFs. IGFBPs can either inhibit or enhance the activity of IGFs or have IGF independent effects.[2] Only the free (unbound) form of IGF is considered to be biologically active.[3]

IGFBP-1 is synthesised in many cell types, including hepatocytes, ovarian granulose cells, decidualised endometrium[2] and cells of connective tissue.[4] It is the predominant binding protein in amniotic fluid. In healthy individuals, the concentration of circulating IGFBP-1 fluctuates tenfold or more within a few hours as a response to changes in insulin concentration.[3] The concentrations of insulin and IGFBP-1 alter in opposite directions.

IGFBP-1 is a 25 kDa protein that may exist in several phosphoforms of approximately 30 kDa.[5] Up to five IGFBP-1 forms, varying in the degree of phosphorylation, have been identified.[6,7] Numerous studies have indicated that human IGFBP-1 may both potentiate or inhibit IGF-I stimulated biological activity.[8,9] The differences in IGFBP-1 actions are due to differential phosphorylation of IGFBP-1 that alters its affinity for IGF-I.[10] Potential phosphorylation sites of human IGFBP-1 are Ser101, Ser119 and Ser169.[9] Highly phosphorylated IGFBP-1 is the predominant isoform of IGFBP-1 in the circulation of a healthy adult, having affinity for IGF-I that is six- to eightfold higher than that of non-phosphorylated IGFBP-1.[11] Since the non-phosphorylated form binds IGF-I less tightly, enhancing its actions,[9,11] a delicate equilibrium between phosphorylated and non-phosphorylated isoforms is responsible for the regulation of IGF-I activity.

In the circulation, IGFBP-1 associates with the glycoprotein α_2-macroglobulin (α_2M, ≈700 kDa), which protects IGFBP-1 from proteolysis.[6] Thus, the IGFBP-1/α_2M complex may have an important role in controlling IGF-I action by regulating the amount of free IGFBP-1. In tissues, IGFBP-1 was found to form multimers, the role of which in the action of IGF remains to be determined.[12]

The aim of this study was to investigate IGFBP-1 isoforms, multimers and complexes in the circulation of healthy persons, using different affinity chromatography matrices. The affinity chromatography methods were based on the following interactions: metal ion–phosphoprotein, antigen–antibody and lectin–glycoprotein.

EXPERIMENTAL

Samples

Blood samples were obtained from healthy adult volunteers (n = 10). Venous blood was collected after 12 h fasting. The serum was separated by centrifugation within 45 min and kept frozen at –20 °C until used. The study was approved by the local ethics committee of the Institute for the Application of Nuclear Energy.

Immobilised metal-affinity chromatography (IMAC)

Iminodiacetic acid-agarose (IDA) was purchased from Sigma-Aldrich (Steinheim, Germany) and 1 mL of gel was packed into a column. After the column had been washed with distilled water, 1.0 mL of 0.10 mol L^{-1} ferric chloride solution was applied in order to saturate

the column with ferric ions. Unbound metal ions were washed out with 5 ml of distilled water and 5 ml of 0.1 % acetic acid. The column was equilibrated with dilution buffer: 0.05 mol L^{-1} MES (2-(*N*-morpholino)ethanesulphonic acid)/0.5 mol L^{-1} NaCl buffer pH 5.5.[13] Serum samples (100 μL diluted in 900 μL of dilution buffer) were circulated through the column for 1 h to ensure maximal binding. The unbound material was washed out with 5 mL of MES buffer. Elution of the bound molecules was performed using 8 mL of 0.2 mol L^{-1} Na-phosphate buffer pH 8.0. The column was regenerated using 10 mL of 0.1 mol L^{-1} Na-borate/1.0 mol L^{-1} NaCl buffer pH 10.0 and 10 mL of distilled water, followed by saturation with ferric chloride. The collected fractions (1.0 mL each) were kept at –20 °C until electrophoresis and immunoblotting were performed.

Immunoaffinity chromatography (IgY-C)

An IgY-12 column (1.2 mL of microbeads) was purchased from Beckman Coulter (Fullerton, USA, Proteomelab IgY-12 High Capacity Proteome Partitioning kit). The matrix with immobilised antibodies enables the binding and removal of albumin, IgG, IgA, IgM, α1-antitrypsin, haptoglobin, transferrin, orosomucoid, α_2M, HDL (apo A-I and apo A-II) and fibrinogen. The IgY column was loaded with 20 μL of serum diluted with 480 μL of dilution buffer: 10 mmol L^{-1} Tris (tris(hydroxymethyl)aminomethane)–HCl/1 mol L^{-1} NaCl buffer pH 7.4, and incubated for 15 min at room temperature using a rotator.[14] Unbound proteins were separated by centrifugation for 30 s at 2000 × g and the column was washed three times with dilution buffer. Bound proteins were eluted with 500 μL of elution buffer: 0.1 mol L^{-1} glycine–HCl buffer pH 2.5, for 3 min at room temperature using a rotator. They were separated from the gel by centrifugation and immediately neutralised with 50 μL of 1 mol L^{-1} Tris–HCl buffer pH 8.0. The column was washed three times with the elution buffer, neutralised with 600 μL of 2 mol L^{-1} Tris–HCl buffer pH 8.0 and washed with a dilution buffer prior to the next chromatographic cycle. The collected fractions (1 mL each) were kept at –20 °C until electrophoresis and immunoblotting were performed.

Lectin-affinity chromatography (LAC)

Eleven agarose-immobilised lectins purchased from Vector Laboratories (Burlingame, CA, USA) were packed into columns: Con A (lectin from *Canavalia ensiformis*), SNA (*Sambucus nigra* agglutinin), RCA-I (*Ricinus communis* agglutinin I), PHA-E (*Phaseolus vulgaris* erythroagglutinin), PHA-L (*Phaseolus vulgaris* leukoagglutinin), WGA (wheat germ agglutinin), succinylated WGA, ECL (*Erythrina cristagalli* lectin), UEA (*Ulex europaeus* agglutinin), LCA (*Lens culinaris* agglutinin) and MAL (lectin from *Maackia amurensis*). All columns except Con A- and LCA-agarose were equilibrated in 0.01 mol L^{-1} HEPES buffer, containing 0.15 mol L^{-1} NaCl, 0.8 g L^{-1} NaN_3, pH 7.5 (HBS). The Con A-agarose was equilibrated in 0.02 mol L^{-1} HEPES buffer containing 0.5 mol L^{-1} NaCl, 0.8 g L^{-1} NaN_3, 1.0 mmol L^{-1} $CaCl_2$, $MgCl_2$ and $MnCl_2$, pH 7.5, whereas the LCA-agarose was equilibrated in 0.01 mol L^{-1} HBS containing 0.8 g L^{-1} NaN_3, 0.1 mmol L^{-1} $CaCl_2$ and 0.01 mmol L^{-1} $MnCl_2$, pH 7.5. The HBS used for ECL-, SNA-, UEA- and MAL-agarose equilibration contained 0.1 mmol L^{-1} $CaCl_2$, whereas the HBS used for the equilibration of PHA-E and PHA-L-agarose contained 0.1 mmol L^{-1} $CaCl_2$ and 0.01 mmol L^{-1} $MnCl_2$. The pH of the HBS for the PHA-E-agarose equilibration was 8.0. Serum samples (100 μL diluted with 900 μL of the corresponding HBS) were circulated through the columns for 1 h. The unbound material was washed out with 20 mL of the appropriate HBS. The elution of the bound glycoproteins was generally performed in two consecutive steps: 1) neutral elution using hapten sugar dissolved in 15 mL of the appropriate HBS, pH 7.5 and 2) acidic elution with 7 mL of hapten sugar solution in 0.1 M

acetic acid, pH 3.0. The PHA-E and PHA-L-agarose columns were eluted in one-step only, using 10 mL of a 0.1 mol L^{-1} acetic acid solution. The hapten sugars used for specific elutions were: 0.5 mol L^{-1} lactose for MAL- and SNA-agarose, a mixture of 0.2 mol L^{-1} methyl-α-glucopyranoside and 0.2 mol L^{-1} methyl-α-mannopyranoside for Con A- and LCA-agarose, 0.2 mol L^{-1} lactose for the RCA I- and ECL-agarose, 0.5 mol L^{-1} *N*-acetyl-glucosamine for the WGA- and succinylated WGA-agarose and 0.1 mol L^{-1} fructose for the UEA-agarose.[15] The most concentrated protein fractions (1 ml each) were collected and the acidic fractions were immediately neutralised using 150 μL of 2 mol L^{-1} Tris–HCl buffer pH 8.9. The fractions were dialysed first against distilled water for 3 h at room temperature and then against 0.15 mol L^{-1} NaCl overnight at 4 °C. After being concentrated to approximately 1.0 ml on Microcon centrifugal filter device (Millipore, Billerica, MA, USA) with a 10 kDa cut-off membrane, the samples were kept frozen at –20 °C until electrophoresis and immunoblotting.

Electrophoresis and Western immunoblotting (WIB)

The most concentrated protein fractions obtained after affinity chromatography were subjected to: native polyacrylamide gel electrophoresis (nPAGE), denaturing non-reducing sodium dodecyl sulphate–polyacrylamide gel electrophoresis (SDS-PAGE) and denaturing reducing SDS-PAGE with 10 % 2-mercaptoethanol (v/v) in the sample buffer (rSDS-PAGE) using 12 % gels.[16]

Immunoblotting was performed using goat polyclonal anti-IGFBP-1 antiserum (DSL, Webster, USA), followed by an anti-goat IgG antibody coupled to horseradish peroxidase (Biosource, Camarillo, CA, USA) and a rabbit polyclonal anti-α2M antibody (IgG fraction, AbD Serotec, Oxford, UK), followed by an anti-rabbit IgG antibody coupled to horseradish peroxidase (Pierce Biotechnology, Rockford, IL, USA). The immunoreactive proteins were visualised using an enhanced chemiluminescence (ECL) reagent kit (Pierce, Minneapolis, MN, USA).[16] Molecular mass markers were from BioRad Laboratories (Hertfordshire, UK) and the cytosol from human placental cells was used as a source of a physiological marker of IGFBP-1.[17]

RESULTS AND DISCUSSION

Several post-translational modifications are known to modify the affinity of IGFBPs for IGFs, including phosphorylation,[7,18] proteolysis[19] and polymerisation.[20] The mechanisms accounting for these changes remain to be elucidated.[12] Phosphorylation of human IGFBP-1 leads to inhibition of IGF-I action.[9,11] The non-phosphorylated isoform forms multimers more rapidly and to a greater extent compared to the phosphorylated isoform.[12] When complexed to α_2M, IGFBP-1 is protected from proteolysis, but still able to bind IGFs and, thus may be expected to influence the IGF action as well.[6]

In order to assess the importance of various molecular forms of IGFBP-1, it is crucial to develop analytical tools for their investigation. To fulfil this goal, affinity chromatography methods based on three types of molecular recognition, *i.e.*, IMAC, immunoaffinity chromatography and LAC, were employed. Electrophoretic separation followed by immunoblotting of the fractionated proteins was used to identify the different molecular forms of IGFBP-1. Fractions of all serum samples were subjected to SDS-PAGE, rSDS-PAGE and nPAGE. Since all

samples showed the same pattern of IGFBP-1 distribution upon immunoblotting, only the representative results are shown in the figures.

SDS-PAGE revealed that almost all immunoreactive IGFBP-1 forms bound to the IDA column (Fig. 1a). Anti-IGFBP-1 antibodies recognised high molecular mass species as a very wide protein band (or several bands that could not be clearly distinguished) at ≈100 kDa, a protein at ≈60 kDa together with proteins at the start. IGFBP-1 monomer (≈30 kDa) was hardly visible. Matrices with immobilised IDA and chelated ions are widely used for the isolation of phosphoproteins.[13] Phosphate groups are electron-donors and, hence, can serve as ligands for coordination of metal ions. Ions that have the greatest affinity for binding to phosphoproteins are Fe^{3+}, Ga^{3+} and Ni^{2+}, Fe^{3+} being the most widely used metal ion in IMAC.[13,21,22] According to the presented results, different molecular species of IGFBP-1 could not be separated using IMAC, since all of them bound to the matrix. rSDS-PAGE was performed in order to investigate the stability of IGFBP-1 complexes in the presence of 2-mercaptoethanol. Almost all high molecular mass complexes, both in the bound and unbound fractions, dissociated, which resulted in the appearance of proteins of predominantly ≈60 and ≈30 kDa (Fig. 1b). This result implicates the existence of disulphide bonds that maintain molecules within the complex. It also suggests that the ≈ 60 kDa form is stable and resists dissociation into IGFBP-1 monomers. nPAGE was performed aiming to differentiate between the phosphoforms of IGFBP-1 monomer. Unfortunately, all isoforms appeared clustered in the middle of the gel and they could not be clearly separated from one another (Fig. 1c). Only proteins at the start were identified by immunoblotting with anti-α_2M antibodies (Fig. 1d), suggesting that these species of very high molecular mass were IGFBP-1/α_2M complexes. Cytosol

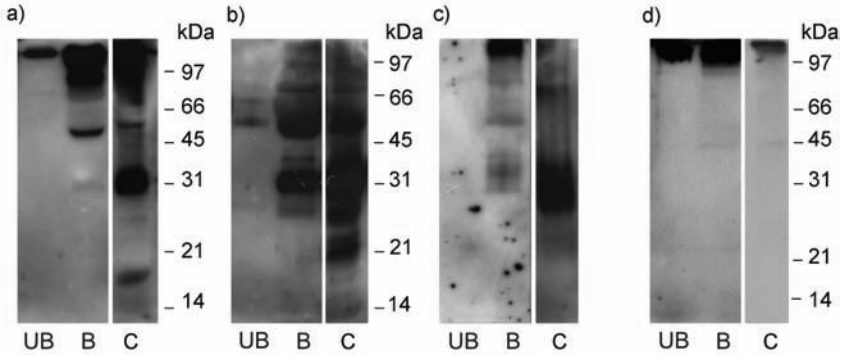

Fig. 1. Immunoblotting of the unbound (UB) and bound (B) fractions obtained after IMAC with anti-IGFBP-1 antibodies after a) SDS-PAGE, b) rSDS-PAGE c) nPAGE, as well as with anti-α_2M antibodies after d) SDS-PAGE. IGFBP-1 from placental cytosol (C) was used as a physiological marker. The positions of the molecular mass markers are indicated on the right side.

gave a different protein profile than that of serum, mostly in terms of the intensity of the bands, as it contains a different proportion of IGFBP-1 molecular forms than serum. The positions of some protein bands in the two types of samples varied slightly due to a difference in sample milieu (the number and abundance of other proteins).

After IgY-C, proteins in the bound fraction were identified as at least three bands of high molecular mass (Fig. 2a), one band at ≈60 kDa and a weak band at ≈30 kDa. In the unbound fraction, high molecular mass bands appeared together with monomer IGFBP-1. In rSDS-PAGE (Fig. 2b) high molecular mass species dissociated giving predominantly a ≈60 kDa protein band in the bound fraction and a ≈30 kDa protein band in the unbound fraction. nPAGE (Fig. 2c), again, proved itself not to be useful for the study of the isoform pattern of IGFBP-1. Immunoblotting with anti-α_2M antibodies (Fig. 2d) confirmed that only proteins at the start of the gel were IGFBP-1/α_2M complexes.

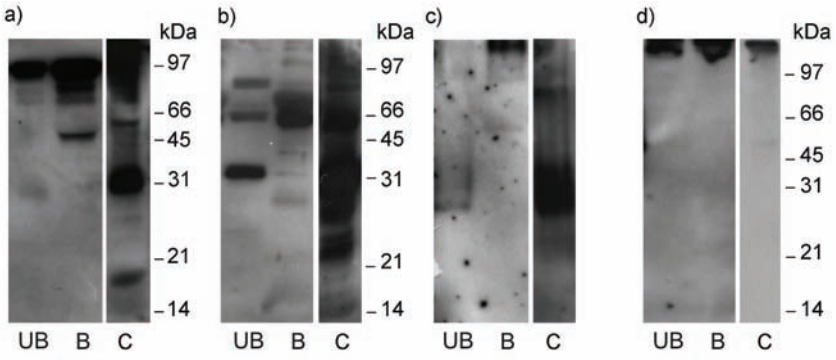

Fig. 2. Immunoblotting of unbound (UB) and bound (B) fractions obtained after IgY-C with anti-IGFBP-1 antibodies after a) SDS-PAGE, b) rSDS-PAGE c) nPAGE, as well as with anti-α_2M antibodies after d) SDS-PAGE. IGFBP-1 from placental cytosol (C) was used as a physiological marker. The positions of the molecular mass markers are indicated on the right side.

The IgY matrix contains immobilised antibodies against α_2M and, according to the intensity of the stained protein band, the majority of IGFBP-1 in circulation is engaged in complex formation with α_2M. The presence of other protein bands in the bound fraction after SDS-PAGE was most likely due to the dissociation of complexes either during the elution of the sample (acidic buffer) and/or during sample preparation for electrophoresis. Since anti-α_2M antibodies recognised only proteins positioned at the start, the immunoreactive bands of ≈100 and ≈60 kDa do not contain fragments of α_2M. These proteins are likely to be multimers of IGFBP-1. The immunoreactive band of ≈60 kDa most likely represents dimeric IGFBP-1, the formation of which may be catalysed by a transglutaminase.[12] To date, dimers were identified only in tissues consisting predominantly

of the non-phosphorylated IGFBP-1 form. IGFBP-1 forms having a mass greater than 60 kDa are most likely higher multimers, resisting the reduction by 2-mercaptoethanol. Multimers of ≈100 kDa were also found in tissues.[12]

Another way to differentiate IGFBP-1 complexes with α_2M from IGFBP-1 multimers is to employ lectins. Lectins have become very important analytical tool in glycoproteomics.[23] In the present study, complexes of IGFBP-1 with glycoprotein α_2M were expected to interact with certain lectins, whereas IGFBP-1 multimers were not, since IGFBP-1 is not glycosylated. The reactivity was tested with eleven immobilised lectins covering a wide range of saccharide specificity. IGFBP-1 immunoreactive forms were detected in pH 7.5 eluates from: Con A-, SNA-, RCA-I- and WGA-agarose as well as in pH 3.0 eluates from Con A- and PHA-E-agarose (Fig. 3a). As expected, anti-IGFBP-1 antibodies recognised only the high molecular mass species (complexes with α_2M).

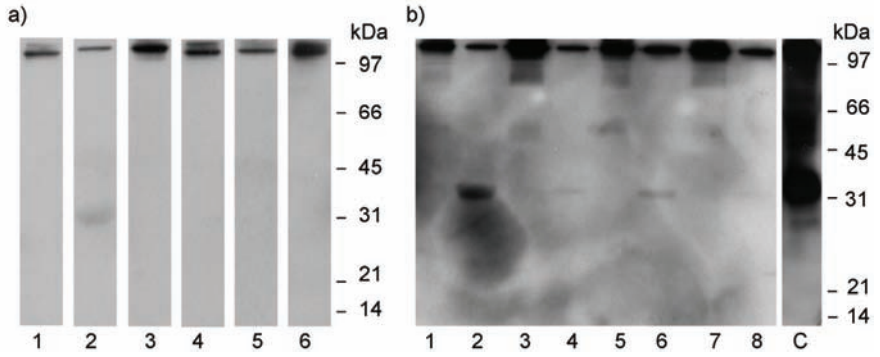

Fig. 3. Immunoblotting with anti-IGFBP-1 antibodies of the bound fractions obtained after LAC and SDS-PAGE. a) The presented samples were eluted from: Con A-agarose (pH 7.5 and 3.0; lanes 1 and 2), SNA-agarose (pH 7.5; lane 3), RCA-I-agarose (pH 7.5; lane 4), PHA-E-agarose (pH 3.0; lane 5) and WGA-agarose (pH 7.5; lane 6); b) The presented samples were eluted from Con A-agarose: in the presence of Ca^{2+}, Mn^{2+} and Mg^{2+} (pH 7.5 and 3.0; lanes 1 and 2), in the presence of Ca^{2+} and Mg^{2+} (pH 7.5 and 3.0; lanes 3 and 4), in the presence of Ca^{2+} and Mn^{2+} (pH 7.5 and 3.0; lanes 5 and 6) and in the presence of Mn^{2+} and Mg^{2+} (pH 7.5 and 3.0; lanes 7 and 8). IGFBP-1 from placental cytosol (C) was used as a physiological marker. The positions of the molecular mass markers are indicated on the right side.

Despite the fact that IGFBP-1 is not glycosylated at all, it bound to Con A and was eluted with the pH 3.0 buffer (Fig. 3a, lane 2). In order to investigate further the nature of this interaction, a series of experiments were performed by varying the presence of ions required for Con A activation (Ca^{2+}, Mn^{2+} and Mg^{2+}). It was demonstrated that all three ions are necessary for the interaction between IGFBP-1 and Con A (Fig. 3b). The absence of Mg^{2+} and Mn^{2+} reduced the binding of IGFBP-1 to some extent, while the absence of Ca^{2+} inhibited the interact-

tion completely. Lectin Con A is a metalloprotein, the 3D structure of which can adopt two conformational states, a “locked” form and an “unlocked” form.[24] The unlocked form of Con A weakly binds metal ions and a saccharide ligand, while the locked form binds two metal ions per monomer, enabling its full binding capacity for the saccharide. Many metastable complexes can be formed as well. Binary, ternary and quaternary complexes having both Con A conformers were identified.[25] Although Con A preferably binds methyl α-D-mannopyranoside and α-D-mannosyl groups, the synthesised ligand peptides, which structurally imitate these saccharides, can also bind to this lectin.[26] The specificity of Con A is not limited to saccharide units, but sugar-mimics may be identified by Con A binding sites as well. Therefore, the binding of IGFBP-1 monomer to Con A-agarose could be explained in the light of the appropriate conformational recognition. Metal ions, especially Ca^{2+}, are crucial for the interaction to occur.

CONCLUSIONS

The results obtained in this study demonstrated that most of the IGFBP-1 circulates associated with α_2M. These complexes can be isolated by affinity chromatography with immobilised anti-α_2M antibodies. IGFBP-1/α_2M complexes may be differentiated from IGFBP-1 dimer and multimers using lectin-affinity chromatography, since the latter do not interact with lectins. It seems that the complexes contain not only monomeric IGFBP-1, but also its multimers. Dimer and multimers are stable under reducing conditions, suggesting covalent linkage between the units. Free IGFBP-1 monomer can be separated from the multimers using Con A-affinity chromatography. The concentration of free IGFBP-1 in circulation is relatively low.

Acknowledgement. This work was supported by the Ministry of Sciences and Technological Development of Serbia, Grant No. 143019.

ИЗВОД

ИСПИТИВАЊЕ РАЗЛИЧИТИХ IGFBP-1 МОЛЕКУЛСКИХ ФОРМИ ПРИМЕНОМ АФИНИТЕТНЕ ХРОМАТОГРАФИЈЕ СА ИМОБИЛИЗОВАНИМ МЕТАЛНИМ ЈОНОМ, АНТИТЕЛИМА И ЛЕКТИНИМА

ДРАГАНА ЛАГУНЏИН, РОМАНА МАСНИКОСА, ГОРАН МИЉУШ, ДРАГАНА РОБАЈАЦ и ОЛГИЦА НЕДИЋ

Институт за примену нуклеарне енергије – ИНЕП, Универзитет у Београду, Банатска 31б, 11080 Београд

Везујући протеин тип 1 за инсулину сличне факторе раста (IGFBP-1) је члан фамилије која садржи шест хомологих везујућих протеина, чија је улога у регулацији активности инсулину сличних фактора раста. IGFBP-1 је протеин од 25 kDa, који осим нативне, може постојати и у облику неколико фосфоформи (30 kDa), које доминирају у циркулацији људи. Фосфориловање IGFBP -1 је пост-транслациона модификација која има велики утицај на активност IGF-I. IGFBP-1 формира мултимере и комплексе са α_2-макроглобулином (α_2M). У циљу анализе и раздвајања IGFBP-1 молекулских врста, у овом раду су примењене методе афинитетне хроматографије. Резултати су показали да се већина IGFBP-1 у циркулацији на-

лази у комплексима са α_2M, који се могу изоловати применом афинитетне хроматографије са имобилизованим анти-α_2M антителима. IGFBP-1/α_2M комплекси се могу раздвојити од IGFBP-1 димера и мултимера применом афинитетне хроматографије са имобилизованим лектинима, пошто се олигомери не везују за лектине. Димерна форма и мултимери су стабилни при редукционим условима, што указује на ковалентну везу између јединица. Слободни IGFBP-1 мономер је присутан у релативно малој концентрацији у циркулацији и може се раздвојити од мултимера применом афинитетне хроматографије са имобилизованим лектином Con A.

(Примљено 30. марта, ревидирано 2. јула 2010)

REFERENCES

1. V. R. Sara, K. Hall, *Physiol. Rev.* **70** (1990) 591
2. S. M. Firth, R. C. Baxter, *Endocr. Rev.* **23** (2002) 824
3. P. D. K. Lee, C. A. Conover, D. R. Powell, *Proc. Soc. Exp. Biol. Med.* **204** (1993) 4
4. J. L. Olesen, K .M. Heinemeier, C. Gemmer, M. Kjær, A. Flyvbjerg, H. Langberg, *J. Appl. Physiol.* **102** (2007) 214
5. M. Westwood, J. M. Gibson, A. J. Davies, R. J. Young, A. White, *J. Clin. Endocrinol. Metab.* **79** (1994) 1735
6. M. Westwood, J. D. Aplin, I. A. Collinge, A. Gill, A. White, J. M. Gibson, *J. Biol. Chem.* **276** (2001) 41668
7. J. I. Jones, A. J. D'Ercole, C. Camacho-Hubner, D. R. Clemmenson, *Proc. Natl. Acad. Sci. U.S.A.* **88** (1991) 7481
8. R. D. Elgin, W. H. Busby, D. R. Clemmons, *Proc. Natl. Acad. Sci. U.S.A.* **84** (1987) 3254
9. J. I. Jones, W. H. Busby, G. Wright, C. E. Smith, N. M. Kimack, D. R. Clemmons, *J. Biol. Chem.* **268** (1993) 1125
10. M. Iwashita, K. Sakai, Y. Kudo, Y. Takeda, *Growth Horm. IGF Res.* **8** (1998) 487
11. M. Westwood, J. M. Gibson, A. White, *Endocrinology* **138** (1997) 1130
12. K. Sakai, W. H. Busby, J. B. Clarke, D. R. Clemmons, *J. Biol. Chem.* **276** (2001) 8740
13. M. Machida, H. Kosako, K. Shirakabe, M. Kobayashi, M. Ushiyama, J. Inagawa, J. Hirano, T. Nakano, Y. Bando, E. Nishida, S. Hattori, *FEBS J.* **274** (2007) 1576
14. O. Nedić, R. Masnikosa, *J. Chromatogr. B* **877** (2009) 743
15. R. Masnikosa, I. Baričević, D. Lagundžin, O. Nedić, *Biochimie* **92** (2010) 97
16. O. Nedić, R. Masnikosa, *Metabolism* **57** (2008) 658
17. R. Masnikosa, B. Živković, O. Nedić, *J. Serb. Chem. Soc.* **74** (2009) 707
18. W. G. Hoeck, V. R. Mukku, *J. Cell. Biochem.* **56** (1994) 262
19. K. Sakai, M. Iwashita, Y. Takeda, *Endocr. J.* **44** (1997) 409
20. W. H. Busby, P. Hossenlopp, D. R. Clemmenson, *Endocrinology* **125** (1989) 773
21. L. Andersson, J. Porath, *Anal. Biochem.* **154** (1986) 250
22. M. G. Gravett, M. J. Novy, R. G. Rosenfeld, A. P. Reddy, T. Jacob, M. Turner, A. McCormack, J. A. Lapidus, J. Hitti, D. A. Eschenbach, C. T. Roberts Jr., S. R. Nagalla, *J. Am. Med. Assoc.* **292** (2004) 462
23. R. Qiu, F. E. Regnier, *Anal. Chem.* **77** (2005) 72
24. R. D. Brown, C. F. Brewer, S. H. Koenig, *Biochemistry-US*, **16** (1997) 3883
25. C. F. Brewer, R. D. Brown, S. H. Koenig, *J. Biomol. Struct. Dyn.* **1** (1983) 961
26. J. K. Scott, D. Loganathan, R. B. Easley, X. Gong, I. J. Goldstein, *Proc. Natl. Acad. Sci. U.S.A.* **89** (1992) 5398.

Journal of the Serbian Chemical Society
JSCS-info@shd.org.rs • www.shd.org.rs/JSCS
J. Serb. Chem. Soc. 75 (11) 1491–1501 (2010)
JSCS–4071
UDC 635.74+549.742.114:
615.322–188(560.4)
Original scientific paper

Sage-called plant species sold in Turkey and their antioxidant activities

ILKAY ERDOGAN-ORHAN[1]*, ELIF BAKI[1,2], SEZER ŞENOL[1] and GÜLDEREN YILMAZ[3]

[1]*Department of Pharmacognosy, Faculty of Pharmacy, Gazi University, 06330 Ankara,* [2]*Social Security Institution, Ministry of Labor and Social Security, Ankara and* [3]*Department of Pharmaceutical Botany, Faculty of Pharmacy, Ankara University, 06100 Ankara, Turkey*

(Received 22 March, revised 30 April 2010)

Abstract: Sage is commonly consumed as a herbal tea in Anatolia, where not only *Salvia* species, but also *Sideritis* species are called "sage" by the local people. Therefore, it was decided to investigate the most common species of sage-called plants sold in aktars (traditional herb-selling stores). Eighty-seven samples randomly purchased from 21 provinces throughout Turkey were identified, which finally led to the identification of 7 species; *Salvia tomentosa*, *Salvia fruticosa*, *Sideritis congesta*, *Sideritis pisidica* var. *termessi*, *Sideritis arguta*, *Sideritis perfoliata* and *Sideritis libanotica* subsp. *linearis*. Infusions prepared from all samples were preliminarily tested for their antioxidant activity and 7 representative species were further evaluated by the 2,2-diphenyl-1--picrylhydrazyl (DPPH) free radical scavenging, ferrous ion-chelating and ferric-reducing antioxidant power (FRAP) tests at 0.25, 0.50, and 1.0 mg ml^{-1} and for their anti-acetylcholinesterase activity. The infusions were subjected to the DPPH bioautographic revelatory test, which led to the conclusion that a flavonoid derivative seemed to be responsible for the antioxidant activity in *S. congesta* and *S. pisidica* var. *termessi*.

Keywords: sage; *Salvia*; *Sideritis*; infusion; antioxidant; acetylcholinesterase.

INTRODUCTION

In Turkey, sage is known as "adaçayı" and is commonly consumed as teas, which are also used in Anatolian folk medicine.[1] *Salvia* species (*Lamiaceae*) are known as "sage" in English, usually referring to *S. officinalis*, whereas throughout Turkey, species of several plant genera, *Salvia*, *Sideritis* and very rarely *Stachys*, are usually known as sage and sold in aktars (traditional herb-selling stores).[2,3] As these three genera belonging to *Lamiaceae* are similar to each other

* Corresponding author. E-mail: iorhan@gazi.edu.tr
doi: 10.2298/JSC100322115E

in terms of their morphology, they are easily confused by local people. In addition, as *Salvia* and *Sideritis* species are represented by approximately 90 and 40 species, respectively, in Turkey,[4–6] the aim of the current study was to survey which species (taxa) are sold as sage (adaçayı) in aktars and local bazaars. It was also decided to determine their antioxidant activity by three different *in vitro* methods, *i.e.*, by the 2,2-diphenyl-1-picrylhydrazyl (DPPH) free radical scavenging, ferrous ion-chelating, and ferric-reducing antioxidant power (FRAP) tests. Moreover, some *Salvia* species have also been reported for memory enhancement in European folk medicine.[7] Thus the inhibitory activity of the infusions towards acetylcholinesterase (AChE), the key enzyme in the pathogenesis of Alzheimer's disease (AD),[8] was also investigated using the spectrophotometric Ellman method.

EXPERIMENTAL

Plant materials

The name of the aktars and provinces, purchase date and identification of 87 sage-called plant materials which were sold as sage (adaçayı in Turkish) and used in this study are listed in Table I. The obtained materials (already in dried form) were identified by three taxonomists; namely Prof. Dr. Hayri Duman (Department of Biology, Faculty of Art and Science, Gazi University, Ankara), Dr. Gülderen Yilmaz (Department of Pharmaceutical Botany, Faculty of Pharmacy, Ankara University, Ankara, Turkey), and Dr. Ferhat Celep (Department of Biology, Middle East Technical University, Ankara, Turkey). The samples are kept at the Pharmacognosy Research Laboratory of the Faculty of Pharmacy, Gazi University, Ankara, Turkey.

TABLE I. Name of the aktars and provinces, purchase dates, and identification as well as the yields of the aqueous extract of the sage-called plant materials used in this study

Sample No.	Name of the aktars and province	Purchase date	Identification of the plant materials	Aqueous extract yields, % (w/w)
1	Yenigül Vip Kuruyemiş, Ankara	2007	*Salvia tomentosa*	3.98
2	Tuzabat Köyü, Mugla	2007	*Salvia fruticosa*	3.93
3	Şekeroğlu Baharat, Kilis	2007	*Sideritis congesta*	9.76
4	Ulucami Baharatçısı, Bursa	2007	*Salvia fruticosa*	4.66
5	Etem Baharatları, Trabzon	2007	*Sideritis pisidica* var. *termessi*	15.0
6	Etem Baharatları, Trabzon	2007	*Salvia fruticosa*	11.4
7	Bağdat Ticaret Gıda Limited Şti., Ankara	2007	*Sideritis congesta*	8.26
8	Emre Baharat, Kastamonu	2007	*Sideritis congesta*	10.58
9	Gıda Pazarı, Ankara	2008	*Salvia fruticosa*	4.74
10	Yeni Belediye İş Merkezi, Çankiri	2007	*Salvia fruticosa*	6.03
11	Lokman Baharat, Karabük	2007	*Salvia fruticosa*	8.68
12	Ulukuş Alternatif Tıbbın Doğal Çaylar ve Şifalı Nebatat Bitkileri, Gaziantep	2007	*Sideritis congesta*	8.68
13	Yaşam Eren Baharat, Edirne	2007	*Salvia fruticosa*	4.14
14	Yayla Baharat, Istanbul	2008	*Salvia fruticosa*	6.51

TABLE I. Continued

Sample No.	Name of the aktars and province	Purchase date	Identification of the plant materials	Aqueous extract yields, % (w/w)
15	Özşen Lokman Hekim Baharat, Ankara	2008	*Sideritis congesta*	9.0
16	Arifoğlu Baharat, Çanakkale	2007	*Salvia fruticosa*	6.25
17	Sümbül Efendi Baharatçısı, Istanbul	2008	*Salvia fruticosa*	4.46
18	Aksel Baharat, Istanbul	2008	*Salvia fruticosa*	7.12
19	Özçiçek Kuruyemiş, Istanbul	2008	*Salvia fruticosa*	4.32
20	Şifa Sultan Bitkisel Ürünler, Istanbul	2008	*Salvia fruticosa*	7.54
21	İnan baharatları ve Aktar, Istanbul	2008	*Salvia fruticosa*	7.69
22	Mesut Güneş Aktar ve Baharat, Istanbul	2008	*Salvia fruticosa*	7.16
23	Muhittin Lokman Hekim, Ankara	2008	*Salvia fruticosa*	5.02
24	Muhittin Lokman Hekim, Ankara	2008	*Sideritis congesta*	12.02
25	Doğa Baharat Dünyası, Istanbul	2008	*Salvia fruticosa*	7.21
26	Nur Baharat, Istanbul	2008	*Salvia fruticosa*	4.89
27	Kırk Ambar, Istanbul	2008	*Salvia fruticosa*	8.57
28	Yeni Çavuşoğlu Baharatları, Istanbul	2008	*Salvia fruticosa*	2.04
29	Karabulut Şifa Baharatçısı, Istanbul	2008	*Salvia fruticosa*	5.09
30	Paşam Baharat (Mısır Çarşısı), Istanbul	2008	*Salvia fruticosa*	7.71
31	Gözde Baharat ve Kuruyemiş, Istanbul	2008	*Salvia fruticosa*	9.01
32	Lokman Baharat, Istanbul	2008	*Salvia fruticosa*	5.88
33	Atlar Baharat, Istanbul	2008	*Salvia fruticosa*	4.08
34	Hazerbaba, Istanbul	2008	*Sideritis congesta*	12.64
35	Antep Pazarı, Istanbul	2008	*Salvia fruticosa*	5.59
36	Uğur Kuruyemiş, Istanbul	2008	*Salvia fruticosa*	3.81
37	Sena Baharat, Istanbul	2008	*Salvia fruticosa*	5.10
38	Kardeşler Baharat, Kirikkale	2008	*Salvia fruticosa*	7.72
39	Ünlü Lokman Hekim, Kirikkale	2008	*Salvia fruticosa*	7.28
40	Coşkun Kuruyemiş, Ankara	2008	*Salvia fruticosa*	3.97
41	Hünkar Tohumculuk, Ankara	2008	*Salvia fruticosa*	6.58
42	Lokman Hekim, Ankara	2008	*Salvia fruticosa*	2.50
43	Avan Kuruyemiş ve Baharat, Ankara	2008	*Salvia fruticosa*	4.71
44	Paşa Süpermarket ve Mandıra, Ankara	2008	*Salvia fruticosa*	5.84
45	Safari Kuruyemiş, Ankara	2008	*Salvia fruticosa*	3.98
46	Akkaynak Süper Market, Ankara	2008	*Salvia fruticosa*	1.58
47	Coşkunlar Gıda, Ankara	2008	*Salvia fruticosa*	5.41
48	Zeyveli Gıda Pazarı, Ankara	2008	*Sideritis congesta*	6.49
49	Mert Gıda, Ankara	2008	*Sideritis congesta*	7.67

TABLE I. Continued

Sample No.	Name of the aktars and province	Purchase date	Identification of the plant materials	Aqueous extract yields, % (w/w)
50	Berat Baharatları, Ankara	2008	*Sideritis congesta*	9.90
51	Kuruyemiş Dünyası, Ankara	2008	*Sideritis congesta*	15.0
52	İmalatçı Erhan Zeytincilik, Ankara	2008	*Salvia fruticosa*	5.01
53	Erpaş Gıda, Ankara	2008	*Salvia fruticosa*	6.57
54	Şifa Baharatları, Elazig	2008	*Salvia fruticosa*	4.65
55	Özgıda, Elazig	2008	*Sideritis congesta*	12.60
56	Efka Baharat, Mugla	2008	*Salvia fruticosa*	6.19
57	Seçkin Manav, Mugla	2008	*Salvia fruticosa*	5.36
58	Balcı Gökmen, Mugla	2008	*Salvia fruticosa*	4.30
59	Merve Gıda, Çorum	2008	*Salvia fruticosa*	5.53
60	Ebru Kuruyemiş, Bingöl	2008	*Salvia fruticosa*	7.13
61	Nur Gıda Pazarı, Bingöl	2008	*Salvia fruticosa*	3.30
62	Hatemoğlu Kuruyemiş, Ankara	2008	*Sideritis congesta*	12.50
63	Arıvital, Ankara	2008	*Salvia fruticosa*	4.53
64	Gizem Lokman Hekim, Ankara	2008	*Salvia fruticosa*	3.06
65	Can Baharat, Ankara	2008	*Salvia fruticosa*	5.83
66	Çağrı Baharat, Ankara	2008	*Sideritis congesta*	12.41
67	Ünlü Lokman, Ankara	2008	*Sideritis congesta*	10.0
68	Ünlü Lokman, Ankara	2008	*Salvia fruticosa*	9.36
69	Sabuncu Kemal Hoca, Ankara	2008	Could not be identified	9.97
70	Dr. Ali Nazmi Lokman Hekim, Ankara	2008	*Sideritis congesta*	8.65
71	Candan Lokman, Agri	2008	*Salvia fruticosa*	8.72
72	Esen Lokman Baharat, Agri	2008	*Salvia fruticosa*	3.05
73	Çerçi Hüsnü Yusuf, Adana	2008	*Salvia fruticosa*	8.84
74	Ağar Bakkaliyesi, Adana	2008	*Salvia fruticosa*	5.76
75	Kantarmacılar Çerçi Mehmet, Adana	2008	*Salvia fruticosa*	7.71
76	Kantarmacılar Çerçi Mehmet, Adana	2008	*Sideritis congesta*	9.93
77	Has Çerçi Yusuf, Adana	2008	*Salvia fruticosa*	8.52
78	Çerçi Uğur Yusuf Ticaret, Adana	2008	*Salvia fruticosa*	2.42
79	Metin Baharat, Sivas	2008	*Sideritis congesta*	8.58
80	Özfidan Baharat, Sivas	2008	*Sideritis congesta*	8.42
81	Mevsim Ticaret, Sivas	2008	*Sideritis congesta*	12.26
82	Köylüoğlu Baharat, Afyon	2008	*Salvia fruticosa*	3.58
83	Karaca Baharat, Afyon	2008	*Salvia fruticosa*	6.86
84	Kamburoğlu Baharat, Afyon	2008	*Salvia fruticosa*	2.33
85	Oktaş Baharat, Antalya	2008	*Sideritis perfoliata*	18.50
86	Halk Pazarı, Antalya	2008	*Sideritis arguta*	5.53
87	Mustafa Şimşek Baharatçı,Antalya	2008	*Sideritis libanotica* subsp. *linearis*	2.62

Preparation of the infusions

Approximately 10 g from each of the 87 samples sold as "sage" was weighed accurately on a digital balance and 150 ml of boiling distilled water was poured onto each sample and left for 10 min at room temperature in order to prepare the infusions, which is in accordance with the traditional method for sage tea preparation in Anatolia. The aqueous parts of each infusion was filtrated and lyophilized. The lyophilized extracts, the yields (w/w) of which are given in Table I, were employed in the AChE inhibitory and antioxidant activity tests.

Antioxidant activity tests

DPPH radical scavenging activity. The stable DPPH radical scavenging activity was determined by the Blois method.[9] Gallic acid and butylated hydroxyanisol (BHA) were employed as the references. Inhibition of DPPH (*I*) in percent was calculated as:

$$I\,(\%) = 100((A_{\text{blank}}–A_{\text{sample}}) / A_{\text{blank}}) \quad (1)$$

where A_{blank} is the absorbance of the control reaction (containing all reagents except the test sample) and A_{sample} is the absorbance in the presence of the extracts/reference. The analyses were run in triplicate and the results are expressed as average values with the standard error mean (SEM).

Ferrous ion-chelating effect. The ferrous ion-chelating effect of all the infusions was estimated by the method of Chua.[10] The ratio of inhibition of the formation of the ferrozine–Fe^{2+} complex was calculated by Eq. (1), where A_{blank} is the absorbance of the control reaction (containing only $FeCl_2$ and ferrozine), and A_{sample} is the absorbance in the presence of the extracts/reference. The analyses were run in triplicate and the results are expressed as average values with the standard error mean (*SEM*).

Ferric-reducing antioxidant power assay (FRAP). The ferric-reducing power (FRAP) of the infusions was tested using the assay of Oyaizu.[11] The analyses were performed in triplicate. Increased absorbance of the reaction mixture indicated increased reducing power.

Bioautographic DPPH revelatory test

The infusions belonging to *Salvia tomentosa*, *Salvia fruticosa*, *Sideritis congesta*, *Sideritis pisidica* var. *termessi*, *Sideritis arguta*, *Sideritis perfoliata* and *Sideritis libanotica* subsp. *linearis* were subjected to thin layer chromatography (TLC) using a solvent system consisting of ethyl acetate:methanol:water (60:20:5). The plate after drying at room temperature was examined under UV 254 and 366 nm light and sprayed with 4 % DPPH solution. The radical scavenging spots turned to a yellow color on a purple background.

Analysis of the active spots in the bioautographic DPPH revelatory test

The spots which were found to be active in the DPPH revelatory test were subjected to TLC again using the same solvent system and treated with three different spraying agents: namely 5 % sulfuric acid, 1 % vanillin and naturstoff reagent in order to obtain preliminary information about phytochemical nature of the compounds.

Anti-AChE activity

Anti-AChE activity was assayed by the spectrophotometric method of Ellman.[12] Electric eel AChE (Type-VI-S, EC 3.1.1.7, Sigma) was used as the enzyme source, while acetylthiocholine iodide (Sigma, St. Louis, MO, USA) was employed as the substrate of the reaction. 5,5'-Dithio-bis(2-nitrobenzoic)acid (DTNB, Sigma, St. Louis, MO, USA) was used for the measurement of the cholinesterase activity. All the other reagents and conditions were same as

described in a previous publication.[13] The experiments were performed in triplicate. Galanthamine (Sigma, St. Louis, MO, USA) was the reference.

Total phenol and total flavonoid contents

Phenolic contents of the extracts were assayed according to the Folin-Ciocalteu method.[14] The samples were mixed with Folin-Ciocalteu reagent (Sigma) and sodium carbonate (7.5 %). After incubation at 40 °C for 30 min, the absorption was measured at 760 nm. The total phenolic contents are expressed as gallic acid equivalents (GAE, mg g^{-1} extract). The total flavonoid contents were calculated by the aluminum chloride colorimetric method.[15] The absorbance of the reaction mixture was measured at 415 nm.

RESULTS AND DISCUSSION

In this study, the species of 87 plant samples, which were sold as "sage", were identified as *Salvia fruticosa* (61 samples), *Sideritis congesta* (20 species), *Salvia tomentosa* (1 species), *Sideritis pisidica* var. *termessi* (1 species), *Sideritis arguta* (1 species), *Sideritis perfoliata* (1 species), *Sideritis libanotica* subsp. *linearis* (1 species) and one unidentified species. In accordance with the traditional method of preparing sage tea in Anatolia, infusions from the 87 samples were prepared and the preliminary antioxidant activity of all infusions was determined using the DPPH radical scavenging test at a concentration of 1.0 mg ml^{-1}. Their radical scavenging activity against DPPH was found to change between 12.69 and 71.39 % (Table II). Further antioxidant activity tests were only performed on the infusions of the 7 identified species given above using DPPH radical scavenging, ferrous ion-chelating and ferric-reducing antioxidant power (FRAP) tests at concentrations of 0.25, 0.50, and 1.0 mg ml^{-1}. Among them, the *S. fruticosa* (65.04 %), *S. arguta* (60.70 %), and *S. congesta* (59.90 %) infusions had the highest scavenging effect towards DPPH (Table III), while *S. fruticosa* (2.303) and *S. arguta* (1.190) gave the best FRAP results (Table IV). All infusions displayed an insignificant effect in the ferrous ion-chelating tests (Table IV). These 7 infusions were tested for their *in vitro* acetylcholinesterase inhibition at concentrations of 0.25, 0.50, and 1.0 mg ml^{-1} using an ELISA microplate reader and were found to exert no activity in this assay.

The calibration equations for the total phenol and flavonoid contents of the infusions were found to be $y = 0.0009x + 0.0018$ ($r^2 = 0.87$) and $y = 2.0447x$ – – 0.0302 ($r^2 = 0.99$), respectively. Accordingly, the richest infusion in terms of both total phenol and total flavonoid contents belonged to *S. congesta* (Table III). Subsequently, the 7 infusions were monitored by TLC and post spraying with a 4 % DPPH solution. Only two spots having DPPH radical scavenger activity, evidenced by a yellow color on a purple background, were found, belonging to the infusions of *S. congesta* and *S. pisidica* var. *termessi*. Those spots possessed the same R_f value, which seemed to be the same compound, and were sprayed with 5 % sulfuric acid, 1 % vanillin and naturstoff reagents. The spots became bright yellow with 1 % sulfuric acid and the naturstoff reagent, which led to the con-

clusion that a flavonoid derivative was responsible for the antioxidant activity of the infusions of *S. congesta* and *S. pisidica* var. *termessi*.

TABLE II. DPPH free radical scavenging activity as percentage of inhibition±*SEM* (standard error mean), %, of the aqueous extracts of the sage-called species at 1.0 mg/ml

Sample No.	Value	Sample No.	Value	Sample No.	Value
1	34.01±1.01	32	71.12±0.18	63	37.11±0.85
2	48.51±1.79	33	32.49±1.17	64	55.07±0.32
3	47.23±0.44	34	46.80±0.21	65	50.45±0.52
4	52.31±1.47	35	41.73±0.10	66	48.74±1.69
5	36.76±1.84	36	21.12±1.00	67	35.81±0.11
6	63.14±1.72	37	46.46±0.64	68	45.31±1.05
7	39.35±1.72	38	53.59±1.08	69	88.23±1.30
8	56.86±0.32	39	27.84±0.49	70	61.33±1.16
9	43.00±0.57	40	39.59±1.39	71	45.16±1.05
10	32.69±1.07	41	28.69±0.11	72	65.04±0.65
11	33.46±0.74	42	58.02±0.43	73	50.75±0.74
12	66.40±0.32	43	45.01±0.42	74	51.12±1.05
13	57.83±0.63	44	47.40±0.63	75	51.42±0.21
14	40.41±1.06	45	42.03±0.21	76	41.14±1.27
15	56.57±0.32	46	42.40±0.52	77	46.28±1.15
16	63.71±0.74	47	46.95±0.84	78	12.69±0.32
17	17.04±1.02	48	50.84±1.07	79	34.88±0.63
18	34.48±0.63	49	59.90±1.67	80	36.04±0.11
19	22.14±1.55	50	64.16±1.37	81	32.49±0.21
20	52.71±0.90	51	55.44±0.21	82	34.43±0.15
21	70.12±1.12	52	53.72±0.73	83	59.66±1.37
22	64.78±1.49	53	29.36±0.70	84	23.25±1.47
23	38.54±0.62	54	23.60±1.28	85	43.39±1.68
24	61.67±1.89	55	55.89±1.05	86	60.70±0.11
25	71.39±0.10	56	29.05±0.31	87	16.27±0.10
26	42.62±0.93	57	62.67±0.54		
27	47.79±1.94	58	40.76±0.95		
28	16.19±1.04	59	48.36±0.31		
29	42.70±0.32	60	31.15±1.64		
30	47.77±0.53	61	38.75±0.63		
31	28.22±0.99	62	50.45±0.53		
References					
Gallic acid			92.57±0.10		
Butylated hydroxyanisol (BHA)			81.60±1.67		

The antioxidant and anti-AChE activities of the infusions obtained from the 7 representative plant species were also determined in order to find out if there were any differences between them. The infusions of the seven taxa identified as *S. fruticosa*, *S. congesta*, *S. tomentosa*, *S. pisidica* var. *termessi*, *S. arguta*, *S. perfoliata*, and *S. libanotica* subsp. *linearis* showed no inhibitory effect against

AChE. Previous research revealed that the components of sage which are active against AChE were the monoterpenes 1,8-cineole and α-pinene found in major amounts in the essential oils.[16] The ineffectiveness of the infusions towards AChE could be that the essential oil and its components are not soluble in water.

TABLE III. Total phenol and total flavonoid contents, and DPPH free radical scavenging activity (inhibition percentage±*SEM* (standard error mean)) of the aqueous extracts of 7 identified taxa out of 87 samples of sage-called species

Specimen	Total phenol content[a]±*SEM*[b], %	Total flavonoid content[c]±*SEM*, %	Percentage of inhibition±*SEM* against DPPH radical, %		
			DPPH concentration, mg ml^{-1}		
			0.25	0.50	1.0
Salvia tomentosa	87.87±0.32	46.31±2.35	9.53±0.11	33.28±1.20	34.01±1.01
Salvia fruticosa	129.94±0.62	71.66±3.14	22.27±0.74	47.23±1.33	65.04±0.65
Sideritis arguta	88.09±2.52	63.23±1.11	14.09±0.10	25.72±1.38	60.70±0.11
Sideritis congesta	154.10±2.60	138.75±2.94	17.54±0.10	35.16±0.11	59.90±1.67
Sideritis libanotica subsp. *linearis*	55.64±1.26	35.94±1.25	8.33±0.11	10.27±0.31	16.27±0.10
Sideritis perfoliata	88.74±2.44	42.49±0.52	16.19±0.85	33.28±1.20	43.39±1.68
Sideritis pisidica var. *termessi*	119.72±1.34	96.56±2.24	9.75±0.21	21.52±0.96	36.76±1.84
References					
Gallic acid			ND[d]	91.61±0.06	92.57±0.10
BHA			ND	77.99±0.48	81.60±1.67

[a]Data expressed in mg equivalent of gallic acid (GAE) to 1 g of extract; [b]standard error mean; [c]data expressed in mg equivalent of quercetin to 1 g of extract; [d]not determined

On the other hand, the preliminary antioxidant activity screening of the infusions at a concentration of 1.0 mg ml^{-1} by the DPPH radical scavenging test displayed a great variance with percentage if inhibition values from 12.69 to 71.39 %. These results clearly indicate that the sage-called plant samples had different phytochemical contents. Since the plant samples were sold in aktars under no serious official authority inspection, the collection time, date and name of the identifier are not clear. In addition, the preserving and storage conditions were not good, hence, some plant samples may have been exposed to direct sunlight or kept in open sacks. Thus, all these factors could affect the phytochemical content of the plants. Consistently, the analysis of the total phenol and flavonoid contents of the sage-called samples also showed remarkable variations (Table III).

In the further antioxidant assays for the 7 representative plant species, the *S. fruticosa* infusion exerted the best activity in the DPPH radical scavenging and FRAP assays (Tables III and IV). Several studies also showed significant antioxidant activity of the polar (water, ethanol, methanol, *etc*.) extracts of *S. fruticosa*, which was attributed to the existence of phenolic compounds, including rosmarinic acid, caffeic acid, carnosol, apigenin, and luteolin.[17–20] Accordingly, it could be speculated that the high antioxidant activity of this species could result from the presence of similar phenolic compounds in the infusion. However, not all the *S. fruticosa* samples purchased for this study displayed high radical scavenging activity (Table I). This variation could again depend on when and where the samples were obtained by the aktars as well as the duration of the storage time. Interestingly, in the DPPH bioautographic test, 7 infusions were subjected to TLC under the same conditions but only two infusions (*S. congesta* and *S. pisidica* var. *termessi*) were found to contain two active components, the colors of which turned into yellow on a purple background. In the TLC assay, chlorogenic acid, caffeic acid, gallic acid, rutin, quercetin, and kaempferol were used as references. However the two spots had different R_f value to those of the references. Therefore, the spots were sprayed separately with 5 % sulfuric acid, 1% vanillin, and naturstoff reagents. The color of flavonoid derivatives is known to become bright yellow with sulfuric acid and naturstoff reagents, which were in accordance with the present results. The vanillin reagent is more specific in revealing terpenic substances. Consequently, this led to the consideration that the active component of the above-mentioned *Sideritis* infusions could be a flavonoid derivative.

TABLE IV. Ferric ion-chelating effect and ferric-reducing antioxidant power (FRAP, absorbance at 700 nm±*SEM*) of the aqueous extracts of 7 identified taxa out of 87 samples of sage-called species

Aqueous extracts	Ferric ion-chelating capacity (inhibition±*SEM*[a], %)			Ferric-reducing antioxidant power (absorbance at 700 nm±*SEM*)		
	Ferric ion concentration, mg ml^{-1}					
	0.25	0.50	1.0	0.25	0.50	1.0
Salvia tomentosa	–[b]	2.59±0.45	19.35±0.40	0.38±0.01	0.68±0.08	1.12±0.01
Salvia fruticosa	–	3.70±0.97	6.95±1.70	0.96±0.02	1.64±0.05	2.30±0.05
Sideritis arguta	–	7.78±0.78	12.04±1.24	0.49±0.06	0.66±0.12	1.19±0.09
Sideritis congesta	–	2.50±0.65	5.56±0.88	0.50±0.01	0.67±0.06	1.02±0.08
Sideritis libanotica subsp. *linearis*	4.82±0.83	8.15±0.66	12.87±0.65	0.26±0.01	0.44±0.04	0.58±0.13
Sideritis perfoliata	–	13.52±0.52	20.84±3.27	0.42±0.02	0.86±0.03	1.03±0.09
Sideritis pisidica var. *termessi*	–	–	6.30±1.01	0.33±0.01	0.70±0.06	0.78±0.13
Reference						
BHA	ND[c]	21.71±1.10	26.94±1.48	2.49±0.01	ND	ND

[a]Standard error mean; [b]no activity; [c]not determined

CONCLUSIONS

The current survey showed that 7 plant species (*Salvia fruticosa*, *Sideritis congesta*, *Salvia tomentosa*, *Sideritis pisidica* var. *termessi*, *Sideritis arguta*, *Sideritis perfoliata* and *Sideritis libanotica* subsp. *linearis)* are sold under the name "sage" in aktars (traditional herbal stores) in Turkey. In previous reports, some *Stachys* species were also recorded to be known as sage in some parts of Turkey by local people. Since sage has been used for simple disorders in the Anatolian folk medicine, correct identification of the plant species is quite important in terms of their biological activity and phytochemical content. The present data showed that the most common species known as sage in Turkey are *S. fruticosa* and *S. congesta* and their antioxidant activity displays a great variation depending on diverse factors. Thus, the obtained results underline the importance and necessity of a serious inspection on plant species sold in aktars by authorities such as the Ministry of Health from the viewpoint of human health.

Acknowledgements. This work constitutes the major part of the master thesis of E. Baki (Pharm.D.) supervised by Prof. Dr. I. Erdogan Orhan (one of the authors) at the Institute of Health Sciences, Gazi University, Ankara, Turkey. F. S. Şenol expresses her sincere thanks to the Turkish Scientific and Technical Research Council (TÜBITAK) for the scholarship provided for her Ph.D. program.

И З В О Д

ВРСТЕ ЖАЛФИЈЕ ПОРЕКЛОМ ИЗ ТУРСКЕ И ЊИХОВА АНТИОКСИДАТИВНА АКТИВНОСТ

ILKAY ERDOGAN-ORHAN[1], ELIF BAKI[1,2], SEZER ŞENOL[1] и GÜLDEREN YILMAZ[3]

[1]*Department of Pharmacognosy, Faculty of Pharmacy, Gazi University, Ankara,* [2]*Social Security Institution, Ministry of Labor and Social Security, Ankara и* [3]*Department of Pharmaceutical Botany, Faculty of Pharmacy, Ankara University, Ankara, Turkey*

Жалфија се уобичајено користи за чај у Анадолији и то не само врсте *Salvia*, већ и врсте *Sideritis*. Проучавали смо биљке које се сматрају жалфијом, а продају се у локалним продавницама. Осамдесет седам узорака насумично купљене жалфије у 21 провинцији Турске је идентификовано и систематизовано у 7 врста: *Salvia tomentosa*, *Salvia fruticosa*, *Sideritis congesta*, *Sideritis pisidica* var. *termessi*, *Sideritis arguta*, *Sideritis perfoliata* и *Sideritis libanotica* subsp. *linearis*. Екстракти свих узорака су прелиминарно тестирани ради утврђивања антиоксидативне активности, а 7 типичних узорака је даље анализирано тестовима: а) DPPH, за одређивање слободних радикала, б) FRAP, за одређивање способности хелатирања феро-јона и редукције фери-јона и в) тестом за одређивање анти-ацетилхолинестеразне активности. Екстракти су подвргнути DPPH биоаутографском тесту, чији су резултати довели до закључка да су флавоноидни деривати одговорни за антиоксидативну активност врста *S. congesta* и *S. pisidica* var. *termessi*.

(Примљено 22. марта, ревидирано 30. априла 2010)

REFERENCES

1. T. Baytop, *Therapy with Medicinal Plants in Turkey (past and present*), Istanbul University Publications No. 3255, Nobel Presshouse, Istanbul, 1999, p. 211

2. E. Sezik, N. Ezer, *Doğa Bilimleri Dergisi* **7** (1983) 163 (in Turkish)
3. G. Yilmaz, A. Güvenç, *J. Fac. Pharm. Ankara Univ.* **36** (2007) 87
4. I. C. Hedge, in *Flora of Turkey and the East Aegean Islands*, Vol. 10, P. H. Davis, Ed., Edinburgh University Press, Edinburgh, 1988, p. 400
5. A. Huber-Morath, in *Flora of Turkey and the East Aegean Islands*, Vol. 10, P. H. Davis, Ed., Edinburgh University Press, Edinburgh, 1988, p. 178
6. H. Duman, in *Flora of Turkey and the East Aegean Islands*, Vol. 11, A. Güner, N. Özhatay, T. Ekim, K. H. C. Başer, Eds., Edinburgh University Press, Edinburgh, 2000
7. N. Perry, G. Court, N. Bidet, J. Court, E. K. Perry, *Int. J. Ger. Psych.* **11** (1996) 1063
8. L. S. Schneider, *Clin. Geriatr. Med.* **17** (2001) 337
9. M. S. Blois, *Nature* **181** (1958) 1199
10. M. T. Chua, Y. T. Tung, S. T. Chang, *Biores. Technol.* **99** (2008) 1918
11. M. Oyaizu, *Jpn. J. Nutr.* **44** (1986) 307
12. G. L. Ellman, K. D. Courtney, V. Andres, R. M. Featherstone, *Biochem. Pharmacol.* **7** (1961) 88
13. F. S. Şenol, I. Orhan, F. Celep, A. Kahraman, M. Dogan, G. Yilmaz, B. Şener, *Food Chem.* **120** (2010) 34
14. V. L. Singleton, J. A. Rossi Jr., *Am. J. Enol. Viticult.* **16** (1965) 144
15. R. Woisky, A. Salatino, *J. Apicol. Res.* **37** (1998) 99
16. S. U. Savelev, E. J. Okello, E. K. Perry, *Phytother. Res.* **18** (2004) 315
17. A. Yildirim, A. Mavi, M. Oktay, A. A. Kara, Ö. F. Algur, V. Bilaloğlu, *J. Agric. Food Chem.* **48** (2000) 5030
18. K. Triantaphyllou, G. Blekas, D. Boskou, *Int. J. Food. Sci. Nutr.* **52** (2001) 313
19. V. Exarchou, N. Nenadis, M. Tsimidou, I. P. Gerothanassis, A. Troganis, D. Boskou, *J. Agric. Food Chem.* **50** (2002) 5294
20. L. Pizzale, R. Bortolomeazzi, S. Vichi, E. Überegger, L. S. Conte, *J. Sci. Food Agric.* **82** (2002) 1645.

Journal of the Serbian Chemical Society
JSCS-info@shd.org.rs • www.shd.org.rs/JSCS
J. Serb. Chem. Soc. 75 (11) 1503–1513 (2010)
JSCS–4072
UDC 635.71+66.048+66.061+543.544.3:665.52/.54
Original scientific paper

The chemical composition and antioxidant activities of basil from Thailand using retention indices and comprehensive two-dimensional gas chromatography

PATCHAREE PRIPDEEVECH[1]*, WATCHARAPONG CHUMPOLSRI[2], PANAWAN SUTTIARPORN[2] and SUGUNYA WONGPORNCHAI[2]

[1]*School of Science, Mae Fah Luang University, Chiang Rai, 57100 and* [2]*Department Center of Excellence for Innovation in Chemistry, Department of Chemistry, Faculty of Science, Chiang Mai University, Chiang Mai, 50200, Thailand*

(Received 3 February, revised 12 June 2010)

Abstract: The chemical compositions of essential oils obtained from *Ocimum basilicum* var. *thyrsiflora* (1.39 % dry weight) and *Ocimum basilicum* (0.61 %) were analyzed by GC–MS. Seventy-three constituents representing 99.64 % of the chromatographic peak area were obtained in the *O. basilicum* var. *thyrsiflora* oil, whereas 80 constituents representing 91.11 % observed in the essential oil of *O. basilicum* were obtained. Methyl chavicol (81.82 %), β-(*E*)-ocimene (2.93 %) and α-(*E*)-bergamotene (2.45 %) were found to be the dominant constituents in *O. basilicum* var. *thyrsiflora* oil while *O. basilicum* contained predominantly linalool (43.78 %), eugenol (13.66 %) and 1,8-cineole (10.18 %). The clear separation of the volatiles in all samples, demonstrated by the application of GC×GC, resulted in significantly different fingerprints for the two types of basil. The *O. basilicum* oil showed strong antioxidant activity while the oil of *O. basilicum* var. *thyrsiflora* exhibited very low activity, which was attributed to the significant differences in linalool and eugenol contents in these essential oils.

Keywords: *O. basilicum*; *O. basilicum* var. *thyrsiflora*; DPPH radical scavenging activity; simultaneous distillation and extraction (SDE); comprehensive two-dimensional gas chromatography; GC×GC.

INTRODUCTION

Basil (*Ocimum basilicum*), belonging to the Lamiaceae family, is one of the most popular plants grown extensively in many continents around the world, especially in Asia, Europe and North America. Basil is believed to have originated in Iran and/or India. At least 150 species of the genus *Ocimum* are widely

* Corresponding author. E-mail: patcharee_pri@mfu.ac.th
doi: 10.2298/JSC100203125P

cultivated in other countries of Asia.[1] Although several basil species are found in many regions, the species *O. basilicum* is the most cultivated variety in the world.[2–4] Basil has been planted as a popular culinary and medicinal herb from ancient time until now and the leaves and flowers have been used for the treatment of headaches, coughs, diarrhea, worms and kidney malfunctions, as well as for its carminative, galactagogue, stomachic and antispasmodic properties.[1,5–7] Basil contains a wide range of phenolic compounds displaying various antioxidant activities, depending on the basil species and cultivars.[8–11] The extracts of basil obtained by different methods are considered to be antimicrobial,[12–14] insecticidal[15] and useful in a number of medical treatments.[16–18] The essential oils of basil are used in the flavoring of food and in perfumery because of their aromatic properties.[19] There are significant differences in the chemical composition and amounts and kinds of aromatic components in the essential oils of basil depending on the species and environmental conditions of the cultivation location. For instance, basil having dark green leaves and white flowers, the popular cultivars for the fresh market and garden, possesses a rich spicy pungent aroma due to the presence of linalool, methyl chavicol and 1,8-cineole.[19] Lesser cultivars vary in growth habit, size, and color, and can display a wide range of aromas including, lemon, rose, camphor, licorice, wood and fruit.[19] The dark opal cultivar with purple color in all parts contains linalool and 1,8-cineole as the major components while camphor is dominant in the basil camphor cultivars.[19] The basil cultivars of India, Pakistan and Guatemala exhibit methyl cinnamate as the dominant component.[20,21] Basil essential oils include mainly the group of terpenoid components, which includes monoterpenes and sesquiterpenes as well as their oxygenated derivatives.[22,23]

The similarity of the structures of the constituents has obstructed component identification. To date, gas chromatography–mass spectrometry (GC–MS) has played the most important role in the identification of the chemical composition of basil essential oils. Nevertheless, incomplete identification was achieved by the use of GC–MS due to the complex nature of the constituents of the essential oil. Comprehensive two-dimensional gas chromatography (GC×GC) is a powerful technique that has been successfully used for the separation of the volatile constituents in highly complex samples, especially essential oils.[24–26] This technique is a combination of two columns with different separation mechanisms coupled *via* a cryogenic modulator interface. Many co-eluting components on the first column are separated in the second column. This rapid technique displays significant differences between samples, making it a valuable technique for application in qualitative analysis. The application of comprehensive two-dimensional gas chromatography coupled to time-of-flight mass spectrometry (GC×GC–––TOFMS) has been employed to analyze the aromatic compounds of basil samples.[27] Linalool, methyl chavicol, eugenol, and 1,8-cineole were the dominant com-

pounds identified in these samples. The relative abundances of the different constituents allowed differentiation between the examined cultivars.

In the present study, *O. basilicum* var. *thyrsiflora* and *O. basilicum* plants were grown in northern Thailand. The chemical compositions of the essential oils of the leaves of both cultivars were identified by using GC–MS and confirmed by the linear retention indices. The use of GC×GC with a longitudinally modulated cryogenic system (LMCS) was also employed to clearly differentiate between the fingerprints of these oil samples. Additionally, the analyses of the volatile constituents of all oils were completed by an evaluation and determination of the antioxidant activities of the essential oil samples.

EXPERIMENTAL

Plant materials and chemicals

Aerial parts of two varieties of basil, *O. basilicum* var. *thyrsiflora* and *O. basilicum*, were collected at flowering stage in the Chiang Rai province located in the northern part of Thailand (altitude 390 m) in June 2008. Voucher herbarium specimens (QBG No. 41462 and QBG No. 41463) of *O. basilicum* var. *thyrsiflora* and *O. basilicum* plant, respectively, were identified and deposited at the Queen Sirikit Botanic Garden, Mae Rim, Chiang Mai, Thailand. The morphology of *O. basilicum* var. *thyrsiflora* and *O. basilicum* plants differ significantly. *O. basilicum* var. *thyrsiflora* plant has narrow green leaves, purple–red stems and violet pink flowers, whereas *O. basilicum* plant has light-green stems, elliptic–ovate leaves and white flowers. The leaves were separated by hand and then dried in the shade for 10 days before being subjected to simultaneous distillation–extraction (SDE). All basil essential oil samples obtained were diluted 1:10 v/v with *n*-hexane prior to injection into the GC–MS and GC×GC instruments. All chemicals were of analytical grade and consisted of dichloromethane, anhydrous sodium sulfate, mixtures of C_8 to C_{22} *n*-alkanes and 2,2-diphenyl-1-picrylhydrazyl (DPPH) which were purchased from Merck (Darmstadt, Germany), and gallic acid, purchased from Sigma–Aldrich GmbH. (Steinheim, Germany).

Gas chromatography–Mass spectrometry (GC–MS)

The volatile constituents of basil leaf oils were analyzed using a Hewlett Packard model HP6890 gas chromatograph (Agilent Technologies, Palo Alto, CA, USA) equipped with an HP-5MS (5 % phenyl-polymethylsiloxane) capillary column (30 m×0.25 mm i.d., film thickness 0.25 μm; Agilent Technologies, USA) interfaced to an HP model 5973 mass-selective detector. The oven temperature was initially held at 100 °C and then increased at 2 °C min^{-1} to 220 °C. The injector and detector temperatures were 250 and 280 °C, respectively. Purified helium was used as the carrier gas at a flow rate of 1 mL min^{-1}. The EI mass spectra were collected at an ionization voltage of 70 eV over the *m*/*z* range 29–300. The electron multiplier voltage was 1150 V. The ion source and quadrupole temperatures were set at 230 and 150 °C, respectively. Identification of volatile components was performed by comparison of their Kováts retention indices, relative to C_8–C_{22} *n*-alkanes, and comparison of the mass spectra of individual components with the reference mass spectra in the Wiley 275 and NIST 98 databases and with the corresponding data for components in basil.[10,19,28,29]

Comprehensive two-dimensional gas chromatography (GC×GC)

A gas chromatograph, model HP 6890, equipped with an FID detector and an HP 6890 series auto sampler was used for the GC×GC–FID experiments and was operated at 100 Hz

data acquisition. The GC was retrofitted with a longitudinally modulated cryogenic system, LMCS (Chromatography Concepts, Doncaster, Australia). CO_2 was employed as the cryogen, which was thermostatically controlled at about –20 °C for the duration of each run. The injection temperature was 250 °C with an injection volume of 1.0 µL in the split mode with a split ratio of 100:1. The injection and detector temperature were operated at 250 °C. Hydrogen gas was used as the carrier gas at a flow rate of 1.5 mL min^{-1}. The GC was operated in the constant flow mode. The column set for GC×GC analysis consisted of two capillary columns which were serially coupled by a zero-dead-volume fitting. The column sets and operation conditions used in this experiment are listed in Table I. The columns are available from SGE International (Ringwood, Australia). The GC×GC column set BPX5/BP20 (Column set 1) was 5 % phenyl polysilphenylene-siloxane connected to a polyethylene glycol phase, which separates most components according to boiling point rather than polarity, while the separation polar/non-polar was obtained using the column set Solgel wax/BP1 (Column set 2) which is the combination of an inverse phase of poly(ethylene glycol) and 100 % dimethylpolysiloxane. Both column sets were selected to investigate the basil volatiles in all samples due to the different properties of these column sets.

TABLE I. GC×GC column sets and temperature programs

Condition	Set 1		Set 2	
	^{1}D	^{2}D	^{1}D	^{2}D
Stationary phase	BPX5	BP20	Solgel Wax	BP1
Length, m	30	2.0	30	2.0
Diameter, mm	0.25	0.10	0.25	0.1
Film thickness, µm	0.25	0.10	0.25	0.10
Modulation period, s	6		6	
Temperature program	from 120 to 180 °C at 1 °C min^{-1}		from 80 to 250 °C at 2 °C min^{-1}	

Antioxidant activity

DPPH radical scavenging assay. The radical scavenging abilities of *O. basilicum* var. *thyrsiflora* and *O. basilicum* essential oils based on reaction with the 2,2-diphenyl-2-picrylhydrazyl radical (DPPH˙) were evaluated by a spectrophotometric method based on the reduction of a methanol solution of DPPH according to a modified method of Blois.[30] One milliliter of various concentrations of the each oil in methanol was added to 1 mL of a 0.003 % methanol solution of DPPH and the reaction mixture was shaken vigorously. The tubes were allowed to stand at room temperature (27 °C) for 30 min. Each reaction mixture was then placed in the cuvette holder of a Perkin Elmer-Lambda 25 UV/Vis spectrophotometer and monitored at 517 nm against a methanol blank. The scavenging ability was calculated as follows: scavenging ability = 100×(absorbance of control – absorbance of sample/absorbance of control). The antioxidant activity of all essential oils is expressed as IC_{50}, which is defined as the concentration (in µg mL^{-1}) of oil required to inhibit the formation of DPPH radicals by 50 %. The experiment was performed in triplicate.

Determination of the total phenolic contents. Total phenolic content of the essential oils obtained from *O. basilicum* var. *thyrsiflora* and *O. basilicum* leaves was determined using Folin–Ciocalteu reagent according to a modified method of Singleton and Rossi[31] using gallic acid as the standard. The oil solution (0.2 mL) was mixed with 1.0 mL of Folin–Ciocalteu reagent, 1.0 mL of a 7 % aqueous solution of Na_2CO_3 and 5.0 mL of distilled water. Then, the mixture was vigorously vortexed. The reaction mixtures were allowed to stand for 30 min

before the absorbance at 765 nm was measured. The concentration of both essential oils was set to 5 mg mL^{-1}. The same procedure was also applied to standard solutions of gallic acid. The calibration equation for gallic acid was:

$$y = 0.00515x - 0.00400 \ (R^2 = 0.999)$$

where y is the absorbance and x is the concentration of gallic acid in mg mL^{-1}.

RESULTS AND DISCUSSION

The essential oil of the leaves of *O. basilicum* var. *thyrsiflora* and *O. basilicum* were extracted using a modified Likens–Nickerson apparatus and appeared as viscous yellow liquids with a percentage yield of 1.39 and 0.61 (w/w), respectively. These essential oils were subjected to detailed GC–MS analysis in order to determine the volatile constituents. Overall, 81 volatile constituents were identified among the two basil leaf oil samples. The GC–MS chromatograms of all samples are shown in Fig. 1. The structures of the volatile components identified by GC–MS, their relative area percentages and their retention indices are summarized in Table II. Although the oils of the two *O. basilicum* species contained high percentages of the same group of monoterpenes and sesquiterpenes, the different varieties presented significant variability in their chemical compositions. A total of 73 constituents representing 99.64 % of the *O. basilicum* var. *thyrsiflora* leaf oil were established. The dominant components were methyl chavicol (81.82 %), *β*-(*E*)-ocimene (2.93 %), *α*-(*E*)-bergamotene (2.45 %), *α*-epi-cadinol (2.08 %), 1,8-cineole (1.62 %), methyl eugenol (1.10 %) and camphor (1.09 %). As indicated, pentyl butanoate was distinguished only in *O. basilicum* var. *thyrsiflora* essential oil. The present studies are similar to the published research of Simon *et al.*,[19] who reported methyl chavicol (60 %) and linalool (12 %) as the major constituents in the essential oil of *O. basilicum* var. *thyrsiflora*; Thai (Richters).

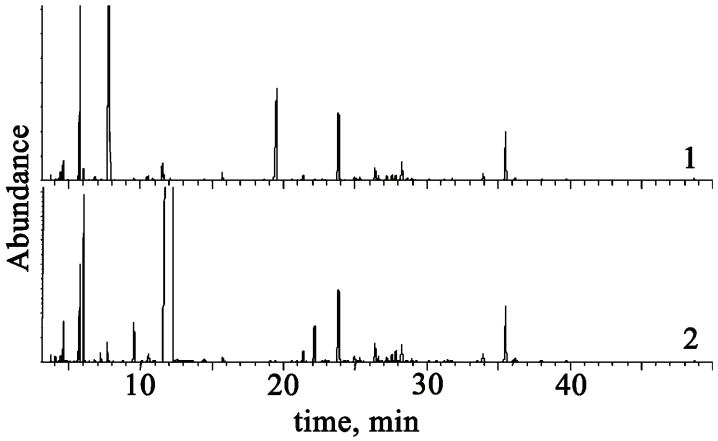

Fig. 1. GC-MS chromatogram of volatile component profiles of (1.1 above) *O. basilicum* essential oil, (1.2) *O. basilicum* var. *thyrsiflora* essential oil.

TABLE II. Structural assignment and relative peak area percent of the volatile components of the essential oil obtained from of *O. basilicum* (A) and *O. basilicum* var. *thyrsiflora* (B) leaves

Component	*LTPRI*[a]	Relative peak area, %		Component	*LTPRI*	Relative peak area, %	
		A	B			A	B
(*E*)-2-Hexenol	849	0.06	0.03	Methyl chavicol	1196	0.21	81.82
α-Thujene	924	0.01	t	Geraniol	1253	0.03	0.01
α-Pinene	932	0.19	0.07	Chavicol	1259	0.07	0.09
Camphene	949	0.03	0.06	*iso*-Bornyl acetate	1283	0.65	0.11
Sabinene	971	0.33	0.08	Carquejol acetate	1295	0.05	t
Amyl vinyl carbinol	974	0.04	0.02	*α*-Cubebene	1344	0.03	0.02
β-Pinene	978	0.57	0.16	Eugenol	1355	13.66	0.02
β-Myrcene	988	0.76	0.49	*exo*-2-Hydroxycineole acetate	1358	0.04	–
Dehydro-1,8-cineole	991	0.02	0.01	*α*-Ylangene	1373	0.08	0.02
para-Mentha-1(7),8-diene	1007	t	0.01	*β*-Bourbonene	1380	0.10	0.03
α-Terpinene	1017	0.02	0.01	*iso*-Longifolene	1385	0.06	0.03
ortho-Cymene	1024	0.01	0.01	*β*-Elemene	1387	0.47	0.31
Limonene	1028	0.23	0.15	Cyperene	1391	0.05	0.02
1,8-Cineole	1033	10.18	1.62	Methyl eugenol	1400	0.09	1.10
β- (*E*)-Ocimene	1044	0.57	2.93	*α*-Cedrene	1410	0.09	0.04
γ-Terpinene	1056	0.06	t[b]	(*E*)-Caryophyllene	1416	0.08	0.06
(*Z*)-Sabinene hydrate	1071	0.23	0.03	*β*-Cedrene	1420	0.04	0.02
Caprylyl acetate	1078	0.08	t	*β*-Copaene	1426	t	–
Terpinolene	1084	0.06	0.15	*α*-(*E*)-Bergamotene	1431	0.10	2.45
Linalool oxide	1087	0.07	–	*β*-(*Z*)-Farnesene	1438	0.05	0.05
Pentyl butanoate	1095	–	0.01	(*Z*)-Muurola-3,5-diene	1442	0.05	0.03
Linalool	1099	43.78	0.43	*α*-Humulene	1451	0.36	0.18
(*E*)-Sabinene hydrate	1099	0.17	–	*β*-(*E*)-Farnesene	1454	0.20	0.08
(*Z*)-Myroxide	1138	0.01	–	(*Z*)-Muurola-4(14),5-diene	1458	0.35	0.13
Camphor	1146	0.20	1.09	*β*-Acoradiene	1462	0.04	0.02
iso-Menthone	1162	0.03	0.03	*γ*-Gurjunene	1471	0.06	0.02
δ-Terpineol	1170	0.28	–	*γ*-Muurolene	1477	1.35	0.60
Borneol	1172	0.36	0.32	*γ*-Himachalene	1481	0.47	0.18
Terpinen-4-ol	1179	0.18	0.06	*β*-Selinene	1485	0.04	0.04
γ-Terpineol	1195	1.75	–	Bicyclogermacrene	1491	0.04	0.18
β-(*E*)-Guaiene	1498	0.59	0.27	1,10-Di-epi-cubenol	1611	0.76	0.29
γ-Patchoulene	1503	0.51	0.35	*β*-Acorenol	1629	0.05	0.01
β-Bisabolene	1505	0.09	0.04	*α*-Epi-cadinol	1640	5.76	2.08
γ-Cadinene	1509	1.99	0.57	*β*-Eudesmol	1650	0.11	0.09
(*E*)-Calamenene	1516	0.35	0.06	*α*-Cadinol	1652	0.32	0.14
(*Z*)-Nerolidol	1521	0.30	0.11	*α*-Epi-bisabolol	1683	0.06	0.03

TABLE II. Continued

Component	*LTPRI*[a]	Relative peak area, %		Component	*LTPRI*	Relative peak area, %	
		A	B			A	B
α-Cadinene	1533	0.03	0.01	α-Bisabolol	1685	0.10	0.04
Longicamphenylone	1560	0.08	0.02	Zierone	1698	0.03	t
Spathulenol	1573	0.25	0.03	β-(*Z*)-Santalol	1713	0.12	0.03
(*E*)-Sesquisabinene hydrate	1579	0.01	–	(*E*)-3-Tetradecen-5--yne	1889	0.24	0.05
β-(*Z*)-Elemenone	1580	0.06	0.03				

[a]Linear temperature program retention index; [b]trace amount, < 0.005 %

Individually, *O. basilicum* leaf oil yielded 80 identified constituents representing 91.11 % with dominant components consisting of linalool (43.78 %) followed by eugenol (13.66 %), 1,8-cineole (10.18 %), α-epi-cadinol (5.76 %), γ-cadinene (1.99 %), γ-terpineol (1.75 %) and γ-muurolene (1.35 %), respectively. As can be observed, eight components (linalool oxide, (*E*)-sabinene hydrate, (*Z*)-myroxide, δ-terpineol, γ-terpineol, *exo*-2-hydroxycineole acetate, β-copaene and (*E*)-sesquisabinene hydrate) were detected only in the essential oil of *O. basilicum*. These results are in a good agreement with those of most published studies on the chemical composition of *O. basilicum* essential oil in which linalool was found to be the predominant constituent: Kéita *et al.*[14] (69 %), Akgül[32] (45.7 %) and Gurbuz *et al.*[33] (41.2 %). In other studies, methyl chavicol (estragole) was represented as the major constituent in the *O. basilicum* leaf oils as can be seen in the study of Khatri *et al.*,[34] Telci *et al.*[10] and Chalchat *et al.*[28] Additionally, methyl eugenol was detected as the main component in *O. basilicum* leaf oil in Thailand by Suppakul *et al.*[29] These differences indicate that the chemical composition of the essential oils of *O. basilicum* varieties may be correlated with different environmental and ecological conditions, as well as by genetic factors.

The overall volatile constituents of the basil leaf oil samples were analyzed using the GC×GC technique. In this study, the conventional combination of columns BPX5/BP20 (Column set 1) and columns Solgel wax/BP1 (Column set 2) were also employed (Table I). The essential oil of *O. basilicum* leaves was used for the optimization of the conditions in both column sets due to the higher number of components identified by GC–MS than for the oil obtained from *O. basilicum* var. *thyrsiflora*. The resulting GC×GC–FID contour plots obtained by the two column sets for all samples are shown in Fig. 2. The component separation in the Column set 1 was based on boiling point and polarity in first and second columns, respectively, but the separation was the reverse in the Column set 2. As seen in the contour plots in Fig. 2, at least 101 and 87 individual components of *O. basilicum* leaf oils were resolved by the use of Column set 1 and 2 as shown in

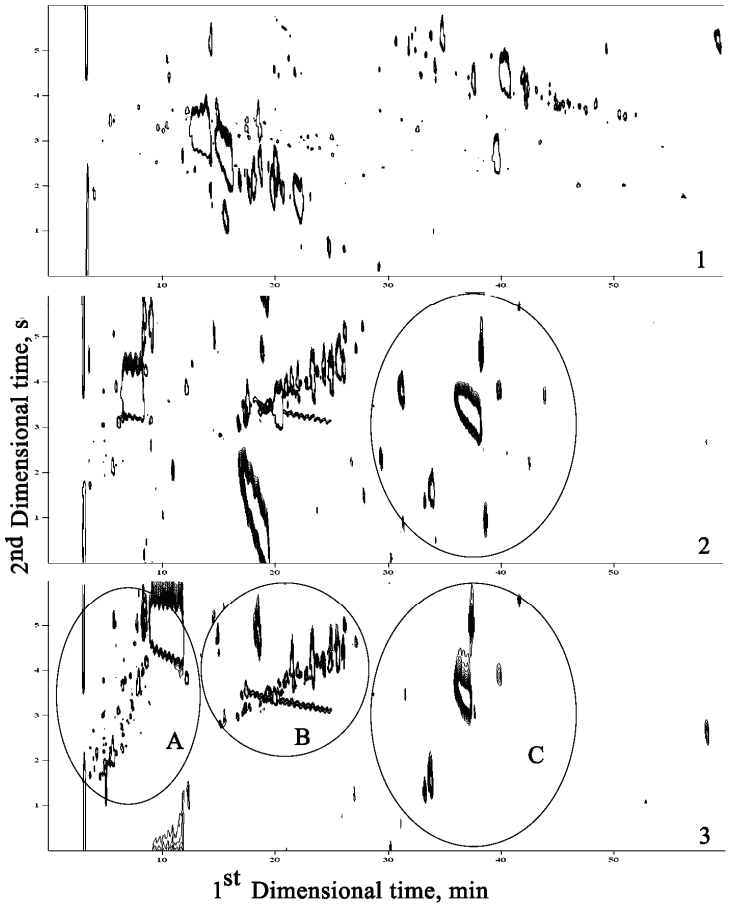

Fig. 2. The contour plots of the volatile component profiles of: 1) *O. basilicum* essential oil with the polar–non-polar column set, 2) *O. basilicum* essential oil with the non-polar-polar column set and 3) *O. basilicum* var. *thyrsiflora* essential oil with non-polar–polar column set. The components are grouped into 3 groups: monoterpenes (A), sesquiterpenes (B) and oxygenated sesquiterpenes (C).

Figs. 2(1) and 2(2), respectively. This indicates that a better resolution was achieved by the use of Column set 1, in which many overlapping peaks were resolved in the 2nd dimension, allowing additional volatile components to be detected. The differentiations of the chemical composition among two varieties by the Column set 1 are present as contour plots shown in Fig. 2(2) and 2(3), respectively. At least 92 and 101 volatile components were detected in *O. basilicum* var. *thyrsiflora* and *O. basilicum* leaf essential oil, respectively. Nevertheless, using GC×GC, more compounds were found and separated compared to those obtained by GC–MS. Grouping of the various components are highlighted in the circled areas: A includes the monoterpenes, B includes the sesquiterpenes, and C

includes the oxygenated sesquiterpenes. Although similar fingerprint patterns were exhibited in both essential oil profiles, the number of oxygenated monoterpenes (region A) of *O. basilicum* var. *thyrsiflora* essential oil was found to be significantly higher compared to that of the *O. basilicum* essential oil profile. The similar profiles of volatile sesquiterpenes (region B) in both essential oils are shown in Fig. 2(2) and 2(3), while numbers of oxygenated sesquiterpenes (region C) of *O. basilicum* essential oil were higher than that obtained from the essential oil of *O. basilicum var. thyrsiflora*.

The antioxidant activities of the essential oils of *O. basilicum* var. *thyrsiflora* and *O. basilicum* leaves were tested by DPPH radical scavenging. The violet color of the radical disappeared when mixed with the substances in the essential oil solution that can donate a hydrogen atom. The antioxidant activities of all the essential oils and eugenol are presented in Table III, in which lower IC_{50} values indicate higher antioxidant activity. The *O. basilicum* essential oil (IC_{50} = = 26.53±0.94 μg mL^{-1}) exhibited a higher scavenging ability for DPPH radicals than the essential oil of *O. basilicum* var. *thyrsiflora* (IC_{50} = 98.33±2.08 μg mL^{-1}). The other results show that a stronger antioxidant activity was found with standard linalool (IC_{50} = 0.61±0.05 μg mL^{-1}) and eugenol (IC_{50} = 2.83±0.08 μg mL^{-1}) than with either of the essential oils. Thus an essential oil containing a higher level of linalool and eugenol should provide a stronger antioxidant activity as was found by Jilisni and Simon[35] who reported that a stronger antioxidant activity was found in the essential oil containing a higher level of linalool. As a result, the *O. basilicum* essential oil was evaluated to be the stronger antioxidant than the essential oil of *O. basilicum* var. *thyrsiflora* according to the higher level of linalool and eugenol. The different levels of linalool and eugenol found between *O. basilicum* and *O. basilicum* var. *thyrsiflora* may be related to ecological conditions and genetic factors.

TABLE III. Antioxidant activities of basil essential oils, standard linalool and eugenol

Material	IC_{50} / μg mL^{-1} (DPPH)[a]	Total phenolic content[a] mg mL^{-1}
O. basilicum leaf oil	26.53±0.94	0.102±0.009
O. basilicum var. *thyrsiflora* leaf oil	98.33±2.08	0.070±0.004
Linalool	0.61±0.05	–[b]
Eugenol	2.83±0.08	–

[a]Values represent averages±standard deviations for triplicate experiments; [b]not studied

The amounts of total phenolic compounds in both the essential oils were investigated spectrometrically according to the Folin–Ciocalteu procedure, calculated as gallic acid equivalents. The essential oil of *O. basilicum* leaves contained higher amounts of total phenolic than that of *O. basilicum* var. *thyrsiflora* leaf oil, as can be seen in Table III. The total phenols of *O. basilicum* and *O. basilicum*

var. *thyrsiflora* essential oil are 0.102±0.009 and 0.070±0.004 mg mL^{-1}, respectively, at the same concentration of 5 mg mL^{-1}. In the present study, linalool (43.78 %) and eugenol (13.66 %), the major components in the essential oil of *O. basilicum*, would play an important role in the antioxidant activity. The low amounts of linalool (0.43 %) and eugenol (0.02 %) in *O. basilicum* var. *thyrsiflora* oil are reflected in its relatively low antioxidant activity.

CONCLUSIONS

Although the chemical compositions of the essential oils of *O. basilicum* var. *thyrsiflora* and *O. basilicum* leaves were similar, both oil samples had significant differences in their major constituents, as determined by GC–MS. In addition, GC×GC separation was utilized to monitor the profiles of both samples and good resolution was exhibited using a combination of non-polar and polar columns. Thus, this technique could be very useful for quality control during the industrial production of these essential oils. Finally, the high amount of linalool and eugenol in *O. basilicum* compared to *O. basilicum* var. *thyrsiflora* is likely responsible for the higher antioxidant activity of the former oil.

Acknowledgements. Great appreciation is given to the Thai Royal Project for providing sweet basil (*O. basilicum*) and Queen Sirikit Botanic Garden for helpful collecting and identification of *O. basilicum* and *O. basilicum* var. *thyrsiflora* plant. Mae Fah Luang University is acknowledged for instrument support of the GC–MS and funding. The Center of Excellence for Innovation in Chemistry (PERCH-CIC), Commission on Higher Education, Ministry of Education, is also acknowledged for its support of the GC×GC system.

ИЗВОД

ОДРЕЂИВАЊЕ ХЕМИЈСКОГ САСТАВА И АНТИОКСИДАТИВНЕ АКТИВНОСТИ БОСИЉКА ИЗ ТАЈЛАНДА ПРИМЕНОМ РЕТЕНЦИОНИХ ИНДЕКСА И ДВОДИМЕНЗИОНАЛНЕ ГАСНЕ ХРОМАТОГРАФИЈЕ

PATCHAREE PRIPDEEVECH[1], WATCHARAPONG CHUMPOLSRI[2], PANAWAN SUTTIARPORN[2] и SUGUNYA WONGPORNCHAI[2]

[1]*School of Science, Mae Fah Luang University, Chiang Rai, 57100 и* [2]*Department of Chemistry, Faculty of Science, Chiang Mai University, Chiang Mai, 50200, Thailand*

Хемијски састав етарског уља босиљка *Ocimum basilicum* var. *thyrsiflora* (1,39 % у односу на суву масу) и *Ocimum basilicum* (0,61 %) је анализиран методом GC–MS. Седамдесет три састојка, која чине 99,64% укупне површине испод хроматографских максимума, нађено је у уљу *O. basilicum* var. *thyrsiflora* и осамдесет (91,11 %) у уљу *O. basilicum*. Метил чавикол (81,82 %), *β*-(*E*)-оцимен (2,93 %) и *α*-(*E*)-бергамотен (2,45 %) су главни састојци уља *O. basilicum* var. *thyrsiflora*, док уље *O. basilicum* садржи највише линалола (43,78 %), еугенола (13,66 %) и 1,8-цинеола (10,18 %). Добро раздвајање испарљивих састојака у свим узорцима, постигнуто применом GC×GC, указује на значајну разлику у саставу две врсте босиљка. Антиоксидативна активност уља *O. basilicum* је велика, док је активност уља *O. basilicum* var. *thyrsiflora* мала. Разлика у активности потиче од значајне разлике у садржају линалола и еугенола у ова два етарска уља.

(Примљено 3. фебруара, ревидирано 12. јуна 2010)

REFERENCES

1. S. E. Sajjadi, *Daru* **14** (2006) 128
2. E. Bravo, S. Amrani, M. Aziz, H. Harnafi, M. Napolitano, *Fitoterapia* **79** (2008) 515
3. M. Ziaei, J. Tahsili, M. Sharifi, M. Behmanesh, K. Razavi, *J. Biotechnol.* **136** (2008) S55
4. P. Fandohan, B. Gnonlonfin, A. Laleye, J. D. Gbenou, R. Darboux, M. Moudachirou, *Food Chem. Toxicol.* **46** (2008) 2493
5. R. J. Grayer, R. F. Vieira, A. M. Price, G. C. Kite, J. E. Simon, A. J. Paton, *Biochem. Syst. Ecol.* **32** (2004) 901
6. M. Özcan, D. Arslan, A. Ünver, *J. Food Eng.* **69** (2005) 375
7. H. B. Heath, *Source book of flavor*, Avi Publications, Westport, CT, 1981
8. A. I. Hussain, F. Anwar, S. T. H. Sherazi, R. Przybylski, *Food Chem.* **108** (2008) 986
9. O. Politeo, M. Jukic, M. Milos, *Food Chem.* **101** (2007) 379
10. I. Telci, E. Bayram, G. Yılmaz, B. Avcı, *Biochem. Syst. Ecol.* **34** (2006) 489
11. S. Lee, K. Umano, T. Shibamoto, K. Lee, *Food Chem.* **91** (2005) 131
12. G. Opalchenova, D. Obreshkova, *J. Microbiol. Meth.* **54** (2003) 105
13. M. J. Pascual-Villalobos, M. C. Ballesta-Acosta, *Biochem. Syst. Ecol.* **31** (2003) 673
14. S. M. Kéita, C. Vincent, J. Schmit, J. T. Arnason, A. Bélanger, *J. Stored Prod. Res.* **37** (2001) 339
15. S. C. Umerie, H. U. Anaso, L. J. C. Anyasoro, *Bioresour. Technol.* **64** (1998) 237
16. E. Werker, E. Putievsky, U. Ravid, N. Dudai, I. Katzir, *Ann. Bot.* **71** (1993) 43
17. T. Dasgupta, A. R. Rao, P. K. Yadava, *Phytomedicine* **11** (2004) 139
18. T. Berić, B. Nikolić, J. Stanojević, B. Vuković-Gačić, J. Knežević-Vukčević, *Food Chem. Toxicol.* **46** (2008) 724
19. J. E. Simon, M. R. Morales, W. B. Phippen, R. F. Vieira, Z. Hao, *Perspectives on new crops and new uses*, J. Janick, Ed., ASHS Press, Alexandria, VA, 1999, p. 499
20. G. Vernin, J. Metzger, *Perfum. Flavor.* **9** (1984) 71
21. J. E. Simon, J. Quinn, R. G. Murray, in *Advances in New Crops*, J. Janick, J. E. Simon, Eds., Timber Press, Portland, OR, 1999, p. 484
22. M. C. Diaz-Maroto, M. S. Peréz-Coello, M. D. Cabezudo, *Chromatographia* **55** (2002) 723
23. M. E. Lucchesi, F. Chemat, J. Smadja, *J. Chromatogr. A* **1043** (2004) 323
24. P. Marriott, R. Shellie, J. Fergeus, R. Ong, P. Morrison, *Flavour Fragr. J.* **15** (2000) 225
25. J. Wu, X. Lu, W. Tang, H. Kong, S. Zhou, G. Xu, *J. Chromatogr. A.* **1034** (2004) 199
26. S. Zhu, X. Lu, L. Dong, J. Xing, X. Su, H. Kong, G. Xu, C. Wu, *J. Chromatogr. A.* **1086** (2005) 107
27. E. Klimánková, K. Holadová, J. Hajšlová, T. Čajka, J. Poustka, M. Koudela, *Food Chem.* **107** (2008) 464
28. J. Chalchat, M. M. Özcan, *Food Chem.* **110** (2008) 501
29. P. Suppakul, J. Miltz, K. Sonneveld, S. W. Bigger, *J. Agric. Food Chem.* **51** (2003) 3197
30. M.S. Blois, *Nature* **181** (1958) 1199
31. V. L. Singleton, J. A. Rossi, *Am. J. Enol. Vitic.* **16** (1965) 144
32. A. Akgül, *Spice science and technology*, Turkish Association Food Technologists Publ. No. 15, Ankara, 1993 (in Turkish)
33. B. Gurbuz, A. Ipek, D. Basalma, E. O. Sarihan, C. Sancak, S. Özcan, *Asian J. Chem.* **18** (2006) 285
34. L. M. Khatri, M. K. A. Nasir, R. Saleem, F. Noor, *Pak. J. Sci. Ind. Res.* **38** (1995) 281
35. H. R. Julisni, J. E. Simon, *Trends in new crops and new uses*, J. Janick, Ed., ASHS Press, Alexandria, VA**,** 2002, p. 575.

Journal of the Serbian Chemical Society
JSCS-info@shd.org.rs • www.shd.org.rs/JSCS
J. Serb. Chem. Soc. 75 (11) 1515–1531 (2010)
JSCS–4073
UDC 546.562'732'742+542.9+547.571+547.551:54–74:543.57
Original scientific paper

Transition metal M(II) complexes with isonicotinic acid 2-(9-anthrylmethylene)-hydrazide

MARIANA LOREDANA DIANU[1]*, ANGELA KRIZA[1], NICOLAE STANICA[2] and ADINA MAGDALENA MUSUC[2]

[1]*University of Bucharest, Faculty of Chemistry, Department of Inorganic Chemistry, 23 Dumbrava Rosie St., 020464 Bucharest and* [2]*Romanian Academy, "Ilie Murgulescu" Institute of Physical Chemistry, 202 Spl.Independentei, P.O. Box 12–194, 060021 Bucharest, Romania*

(Received 23 November 2009, revised 6 April 2010)

Abstract: New complexes of isonicotinic acid 2-(9-anthrylmethylene)-hydrazide with Cu(II), Co(II) and Ni(II) have been prepared and characterized by analytical and physico–chemical techniques, such as elemental and thermal analyses, magnetic susceptibility and conductivity measurements, and electronic, EPR and IR spectral studies. The infrared spectral studies revealed the bidentate or monodentate nature of the Schiff base in the complexes; the pyridine nitrogen does not participate in the coordination. A tetrahedral geometry is suggested for the nitrate complexes and an octahedral geometry for the others. Thermal studies support the chemical formulation of these complexes.

Keywords: IR spectra; isonicotinoylhydrazone; Schiff base; transition metal complexes; thermal analysis.

INTRODUCTION

It is generally known that hydrazones have significant antimicrobial, anticonvulsant, analgesic, anti-inflammatory and antitumoral activities.[1–6] The remarkable biological activity of acid hydrazides R–CO–NH–NH_2, their corresponding aroylhydrazones R–CO–NH–N=CH–R', and the dependence of their activity on the mode of chelating with transition metal ions have been of significant importance in the past.[7–10] Thermal analysis techniques (DTA, TG, DSC) play an important role in the study of the structure of metal complexes.[11–16]

As a continuation of our interest in the coordination behavior of Schiff bases with isonicotinoylhydrazones,[17] the synthesis and characterization of a series of copper(II), cobalt(II) and nickel(II) complexes with the isonicotinic acid 2-(9-anthrylmethylene)-hydrazide ligand are reported herein.

* Corresponding author. E-mail: maridianu@yahoo.com
doi: 10.2298/JSC091113121D

EXPERIMENTAL

Materials

All chemicals were of pure analytical grade and were purchased from Sigma-Aldrich and Fluka.

Methods and apparatus

The Schiff base ligand was prepared by a known method.[18] The metal(II) contents were determined by literature methods.[19] The carbon, hydrogen and nitrogen contents were determined using CHNS-O elemental combustion analysis with a Costech elemental analyzer, model ECS 4010. The melting temperatures of the complexes were directly measured with SMPI Melting Point apparatus. The molar conductance of the complexes was measured at a concentration of 1.0×10^{-3} M in DMF at room temperature using a Consort type C-533 conductivity instrument. The IR spectra were recorded between 4000–400 cm^{-1} in KBr pellets with a Bio-Rad FTS-135 instrument. The reflectance spectra of the complexes were recorded on a Jasco V-670 spectrophotometer. The EPR spectra for the copper(II) complexes were recorded using a Jeol JES–FA 100 X-band frequency spectrometer. Measurements of the magnetic susceptibility were realized at room temperature using the Faraday method and were corrected for diamagnetism.

The thermal experiments were performed on a Mettler Toledo TGA/SDTA 851^e thermal analyzer, within the temperature range 25–1000 °C, and a Mettler Toledo DSC 853^e differential scanning calorimeter, within the temperature range 25–600 °C. The TG curves were recorded under a dynamic nitrogen atmosphere at a flow rate of 50 mL min^{-1} and at a heating rate of 10 K min^{-1}. The DSC curves were obtained under a dynamic nitrogen atmosphere at 80 mL min^{-1} flow rate and the same heating rate. The samples were held in aluminum crucibles for the DSC experiments and Al_2O_3 crucibles for the TG/SDTA experiments, with a pinhole in the lid, for both methods, to prevent pressure build up due to gaseous products. The sample mass was between 0.8 and 3 mg for both methods. At the end of the heating process for the DSC experiments, the mass of the remaining sample represented approximately 30–40 % of the initial value for all the studied complexes. The TG and DSC curves were used to characterize the variation of mass and also thermal changes during the linear heating.

Synthesis of complexes

A methanolic solution (10 mL) of isonicotinoylhydrazide (1.0×10^{-3} M) and a methanolic solution (20 mL) of 9-anthraldehyde (1.0×10^{-3} M) were mixed with constant stirring at 50 °C for 30 min. The preparation of the complexes was performed by mixing methanolic solutions (1.0×10^{-3} M, 20 mL) of metal (Cu(II), Co(II) and Ni(II)) salts (nitrate, acetate and perchlorate) to a cold methanolic solution of the ligand. The reaction mixture was stirred under reflux for 3 h. The obtained precipitates were filtered, washed with methanol and dried under vacuum on anhydrous $CaCl_2$.

RESULTS AND DISCUSSION

The synthesized complexes have the general formulae $ML_2X_2{\cdot}xH_2O$, where M = Cu(II), Co(II) or Ni(II), L = Schiff base (Fig. 1) and X = NO_3^-, ClO_4^- or CH_3COO^-.

The complexes were characterized based on elemental analyses, magnetic susceptibility and electronic conductibility measurements, IR, UV–Vis–NIR and EPR spectroscopy and thermal studies. The M(II) complexes were colored pow-

ders with high melting points. They were soluble in acetone, DMF and DMSO and insoluble in methanol, ethanol, $CHCl_3$, CH_2Cl_2 and CCl_4.

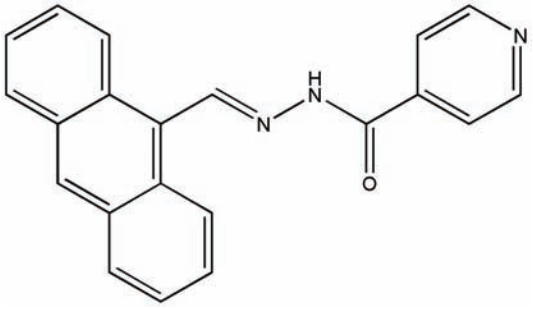

Fig. 1. Structural formula of isonicotinic acid 2-(9-anthrylmethylene)-hydrazide (L).

The analytical and physical data (color, melting point and molar conductivity in DMF (1.0×10^{-3} M, at room temperature)) of the complexes are given in Table I. The molar conductivity values show that the nitrate and perchlorate complexes were 1:2 electrolytes and the acetate complexes were non-electrolytes.[20]

TABLE I. Analytical and physical data of the complexes

Compound	Color	Found (Calcd.), %				M.p. °C	Λ_M[a] Ω^{-1} cm^2 mol^{-1}
		C	H	N	M		
$[CuL_2(H_2O)_2](NO_3)_2\cdot2H_2O$	Green	56.03	4.11	12.96	6.55	>320	154
(**I**)		(55.41)	(4.21)	(12.31)	(6.98)		
$[NiL_2(H_2O)_2](NO_3)_2\cdot4H_2O$	Yellowish	54.21	4.26	12.54	5.97	>320	148
(**II**)	green	(53.57)	(4.49)	(11.90)	(6.23)		
$[CuL_2(H_2O)_2](ClO_4)_2$	Reddish	53.88	3.34	9.16	6.23	285[a]	137
(**III**)		(53.14)	(3.61)	(8.85)	(6.69)		
$[CoL_2(H_2O)_2](ClO_4)_2$	Brick-red-	54.12	3.28	9.21	5.98	260[a]	175
(**IV**)	-colored	(53.40)	(3.63)	(8.89)	(6.24)		
$[NiL_2(H_2O)_2](ClO_4)_2$	Orange	53.69	3.76	9.26	6.32	250[a]	143
(**V**)		(53.41)	(3.63)	(8.90)	(6.21)		
$[CuL_2(CH_3COO)_2]$	Khaki	66.82	4.12	10.32	7.24	>320	3.4
(**VI**)		(66.37)	(4.36)	(10.09)	(7.63)		
$[CoL_2(CH_3COO)_2]\cdot2H_2O$	Brown-	64.42	4.33	10.16	6.63	>320	5.2
(**VII**)	reddish	(63.96)	(4.67)	(9.73)	(6.82)		
$[NiL_2(CH_3COO)_2]$	Green-	68.09	4.55	10.48	7.24	>320	4.5
(**VIII**)	khaki	(66.76)	(4.38)	(10.16)	(7.09)		

[a]With decomposition

Infrared spectra

The IR spectra of the Schiff base (L) and its metal complexes were recorded between 4000–400 cm^{-1} and the obtained data are summarized in Table II with some assignments of the important characteristic bands.

TABLE II. The characteristic IR bands (cm^{-1}) of the ligand and the complexes ($X^- = NO_3^-$, ClO_4^-, CH_3COO^-)

Compound	ν(O–H)	ν(C=O) Amide I	ν(C=N) Azomethine	δ(N–H) Amide II	ν_{X^-}	$\rho_r(H_2O)$
Ligand (L)	–	1654	1597	1520	–	–
$[CuL_2(H_2O)_2](NO_3)_2\cdot 2H_2O$ (**I**)	3421	1652	1558	1507	1384	849
$[NiL_2(H_2O)_2](NO_3)_2\cdot 4H_2O$ (**II**)	3430	1653	1550	1510	1384	849
$[CuL_2(H_2O)_2](ClO_4)_2$ (**III**)	3430	1637	1569	1510	1106, ν_3 623, ν_4	850
$[CoL_2(H_2O)_2](ClO_4)_2$ (**IV**)	3367	1635	1551	1521	1088, ν_3 625, ν_4	841
$[NiL_2(H_2O)_2](ClO_4)_2$ (**V**)	3420	1661	1564	1519	1108, ν_3 625, ν_4	845
$[CuL_2(CH_3COO)_2]$ (**VI**)	–	1653	1557	1520	1570, ν_{asym} 1493, ν_{sym}	–
$[CoL_2(CH_3COO)_2]\cdot 2H_2O$ (**VII**)	3390	1652	1547	1521	1571, ν_{asym} 1498, ν_{sym}	–
$[NiL_2(CH_3COO)_2]$ (**VIII**)	–	1653	1550	1522	1572, ν_{asym} 1450, ν_{sym}	–

The IR spectra of the complexes **I**–**V** and **VII** showed a broad band at 3400 cm^{-1} that can be assigned to the ν_a(OH) and ν_s(OH) vibration modes from water molecules.[21] The presence of coordinated water was confirmed by the medium strength bands at 840–850 cm^{-1}, characteristic of $\rho_r(H_2O)$ frequencies. These bands were not observed in the spectra of the complexes **VI** and **VIII**, indicating the absence of coordinated water molecules.

The IR spectrum of the ligand exhibits two medium bands at 3196 and 3047 cm^{-1}, which can be ascribed to the asymmetric and symmetric vibrational frequencies of the NH amide group, respectively. The band at 1520 cm^{-1} was assigned to δ(N–H) of amide II. This band appeared in the spectra of the ligand and complexes at the same position, confirming that the nitrogen atom of the NH moiety does not participate in the coordination. The observed minor shift to lower frequencies of δ(N–H) (amide II) for some complexes (**I**–**III**) may be due to the presence of the amide group in a chelate system rather than in the open system of the ligand.[14]

The band at 1654 cm^{-1}, attributable to the ν(C=O) stretching vibration of the Schiff base ligand[22] is shifted to another region in the complexes **III**–**V**, indicating coordination of the carbonyl oxygen to the metal ions. The presence of bands at 520–550 cm^{-1} in the IR spectra of complexes **III**–**V** is due to M–O stretching vibrations.[23]

The azomethine band at 1597 cm^{-1} was shifted to lower frequencies in the spectra of all the complexes, confirming the participation of the azomethine nitrogen atom in the coordination of the metal ions. In the IR spectra of these complexes, the new bands which appear in the 460–420 cm^{-1} region are assigned to the ν(M–N) vibration.[17]

The band at 1623 cm^{-1}, assigned to the vibration of the pyridine ring, remains at the same position in the spectra of the ligand and complexes, confirming that the nitrogen of pyridine group does not participate in the coordination.

The strong sharp band observed at 1384 cm^{-1} in the complexes **I** and **II** can be assigned to uncoordinated nitrate ion.[24] In the IR spectra of complexes **III**–**V**, the presence of strong ν_3 at about 1100 cm^{-1} and medium ν_4 at 625 cm^{-1} bands indicates that the T_d symmetry of the perchlorate anion is maintained.[25] The IR spectra of the acetate complexes **VI**–**VIII** display two bands assigned to the bidentate coordination of the acetate group ($\Delta\nu = \nu_{asym} - \nu_{sym}$, which were in the 73–122 cm^{-1} range).[26]

All of these IR data confirm a bidentate ligand coordination for complexes **III**–**V** and a monodentate one for the others.

Electronic and EPR spectra

In order to obtain information concerning the stereochemistry of the metal ions, the UV–Vis spectra of the ligand and complexes were recorded in the solid phase. The electronic spectral data and the magnetic moments for the ligand and its complexes are given in Table III.

TABLE III. Electronic spectral data and magnetic moments for the ligand and its complexes

Compound	Observed bands cm^{-1} / nm	Assignments	μ_{eff} μ_B	Symmetry
Ligand (L)	37313 / 268	$\pi \rightarrow \pi^*$	–	–
	24752 / 404	$n \rightarrow \pi^*$		
$[CuL_2(H_2O)_2](NO_3)_2 \cdot 2H_2O$ (**I**)	26316 / 380	$n \rightarrow \pi^*$	2.14	Td
	14925 / 670	$^2E \rightarrow {}^2T$		
$[NiL_2(H_2O)_2](NO_3)_2 \cdot 4H_2O$ (**II**)	39062 / 256	$\pi \rightarrow \pi^*$	4.45	Td
	25252 / 396	$n \rightarrow \pi^*$		
	17241 / 580 (ν_3)	$^3T_1 \rightarrow {}^3T_1(P)$		
	9950 / 1005 (ν_1)	$^3T_1 \rightarrow {}^3T_2$		
$[CuL_2(H_2O)_2](ClO_4)_2$ (**III**)	19608 / 510	TS	1.77	Distorted Oh (D_{4h})
	14204 / 704 ($\nu_1 + \nu_2$)	$d_{xz}, d_{yz} \rightarrow d_x2_{-y}2$		
	11223 / 891 (ν_3)	$d_{xy} \rightarrow d_x2_{-y}2$		
		$d_z^2 \rightarrow d_x^2{}_{-y}^2$		
$[CoL_2(H_2O)_2](ClO_4)_2$ (**IV**)	41841 / 239	$\pi \rightarrow \pi^*$	5.57	Oh
	25445 / 393	$n \rightarrow \pi^*$		
	20576 / 486 (ν_3)	$^4T_{1g} \rightarrow {}^4T_{1g}(P)$		
	8802 / 1136 (ν_1)	$^4T_{1g} \rightarrow {}^4T_{2g}$		

TABLE III. Continued

Compound	Observed bands cm^{-1} / nm	Assignments	μ_{eff} μ_B	Symmetry
$[NiL_2(H_2O)_2](ClO_4)_2$ (**V**)	39682 / 252	$\pi \rightarrow \pi^*$	3.05	Oh
	25445 / 393	$n \rightarrow \pi^*$		
	16129 / 620 (ν_2)	$^3A_{2g} \rightarrow {}^3T_{1g}(F)$		
	10438 / 958 (ν_1)	$^3A_{2g} \rightarrow {}^3T_{2g}$		
$[CuL_2(CH_3COO)_2]$ (**VI**)	24096 / 415	TS	2.27	Oh
	12820 / 780	$^2E_g \rightarrow {}^2T_{2g}$		
$[CoL_2(CH_3COO)_2]\cdot 2H_2O$ (**VII**)	25125 / 398	$n \rightarrow \pi^*$	5.26	Oh
	18182 / 550 (ν_3)	$^4T_{1g} \rightarrow {}^4T_{1g}(P)$		
	9901 / 1010 (ν_1)	$^4T_{1g} \rightarrow {}^4T_{2g}$		
$[NiL_2(CH_3COO)_2]$ (**VIII**)	39682 / 252	$\pi \rightarrow \pi^*$	3.34	Oh
	25252 / 396	$n \rightarrow \pi^*$		
	15949 / 627 (ν_2)	$^3A_{2g} \rightarrow {}^3T_{1g}(F)$		
	10309 / 970 (ν_1)	$^3A_{2g} \rightarrow {}^3T_{2g}$		

The UV–Vis spectrum of the Schiff base ligand is characterized mainly by two absorption bands at 37313 (268 nm) and 24752 cm^{-1} (404 nm), which may be assigned to $\pi \rightarrow \pi^*$ and $n \rightarrow \pi^*$ transitions. These transitions were also found in the spectra of the complexes, but they were shifted towards lower frequencies, confirming the coordination of the ligand to the metal ions.

The electronic spectrum of complex **I** showed a broad band at 14925 cm^{-1}, due to the $^2E \rightarrow {}^2T$ transition, in a tetrahedral geometry around the cooper(II) ion. The electronic spectra of complex **III** showed absorption bands at 14204 and 11223 cm^{-1}, assignable to d_{xz}, $d_{yz} \rightarrow d_{x^2-y^2} + d_{xy} \rightarrow d_{x^2-y^2}$ ($\nu_1 + \nu_2$) and $d_{z^2} \rightarrow$ $\rightarrow d_{x^2-y^2}$ (ν_3), respectively.[27] This is consistent for a D_{4h} geometry with a distorted octahedral environment around the cooper(II) ion. The absorption band at 19608 cm^{-1} may be reasonably assigned to a charge transfer transition.

The electronic spectrum of complex **VI** showed a broad band at 12820 cm^{-1}, corresponding to a $^2E_g \rightarrow {}^2T_{2g}$ transition in an octahedral stereochemistry around the cooper(II) ion. The observed magnetic moments 1.77 and 2.27 μ_B, for the complexes **III** and **VI**, respectively, usually correspond to an octahedral geometry.[28]

The electronic spectra of the Co(II) complexes **IV** and **VII** of high-spin systems exhibited bands at 8802 and 20576 cm^{-1} for complex **IV** and at 9901 and 18182 cm^{-1} for complex **VII**, which may be assigned to ν_1, $^4T_{1g} \rightarrow {}^4T_{2g}$ and ν_3, $^4T_{1g} \rightarrow {}^4T_{1g}(P)$ transitions, respectively. The observed magnetic moment values of 5.57 and 5.26 μ_B for the Co(II) complexes suggest an octahedral geometry.[29]

The electronic spectra of the Ni(II) complexes **V** and **VIII** also showed two bands at ≈ 16000 and ≈ 10400 cm^{-1}, assignable to $^3A_{2g} \rightarrow {}^3T_{1g}(F)$ (ν_2) and $^3A_{2g} \rightarrow {}^3T_{2g}$ (ν_1) transitions, respectively, in an octahedral geometry. The obser-

ved magnetic moment values 3.05 and 3.34 μ_B for the complexes **V** and **VIII** may be taken as additional evidence for their octahedral structure.[29]

The complex **II** displayed two bands at 9950 and 17241 cm^{-1}, due to ν_1: $^3T_1 \rightarrow {}^3T_2$ and ν_3: $^3T_1 \rightarrow {}^3T_1(P)$ transitions, respectively, and also, the magnetic moment value 4.45 μ_B indicates to a possible tetrahedral geometry.[30]

The ligand field splitting energy (10*Dq*), interelectronic repulsion parameter (*B*) and nephelauxetic ratio (β) for the Co(II) and Ni(II) complexes were calculated using the secular equations given by König.[31–33]

For the Ni(II) complexes **V** and **VIII**:

$$10Dq = \nu_1 \tag{1}$$

$$B = \frac{2\nu_1^2 + \nu_2^2 + 3\nu_1\nu_2}{15\nu_2 - 27\nu_1} \tag{2}$$

For the Ni(II) complex **II** and the Co(II) complexes **IV** and **VII**:

$$10Dq = 2\nu_1 - \nu_3 + 15B \tag{3}$$

$$B = \frac{1}{30}\sqrt{-\left(2\nu_1 - \nu_3\right) + \left(-\nu_1^2 + \nu_3^2 + \nu_1\nu_3\right)} \tag{4}$$

The values of the Racach parameter determined for the Ni(II) and Co(II) complexes are lower than usually observed for the free ions, 1041 and 971 cm^{-1}, respectively. The nephelauxetic ratio β depends on the ligand position on the nephelauxetic scale, indicating at the same time the degree of metal–ligand bond covalence.[34] For these complexes, the lower values suggest a larger degree of covalence.

The values of the electronic parameters, the ligand field splitting energy, the Racach interelectronic repulsion parameter and the nephelauxetic ratio are summarized in Table IV.

TABLE IV. Electronic parameters of the Co(II) and Ni(II) complexes

Compound	$10Dq$ / cm^{-1}	B / cm^{-1}	β
$[NiL_2(H_2O)_2](NO_3)_2{\cdot}4H_2O$ (**I**)	10944	552	0.53
$[NiL_2(H_2O)_2](ClO_4)_2$ (**V**)	10438	677	0.65
$[NiL_2(CH_3COO)_2]$ (**VIII**)	10309	673	0.65
$[CoL_2(H_2O)_2](ClO_4)_2$ (**IV**)	9992	864	0.89
$[CoL_2(CH_3COO)_2]{\cdot}2H_2O$ (**VII**)	10966	623	0.64

The room temperature EPR spectra of the Cu(II) complexes **I**, **III** and **VI** were recorded in solid state. From the EPR spectrum of complex **I** the exact geometry of the metal ion cannot be proposed. The "*g*" parameters have only one value ($g_{isotropic}$ = 2.14). The electronic spectra, the moment magnetic value and the relative isotropy of the "*g*" parameters indicate to the tetrahedral geometry of complex **I**.

An analysis of the EPR spectrum of complex **III** gave $g_{||}$ = 2.15 and $g_{\perp}$ = = 2.07. The trend $g_{||} > g_{\perp}$,[35] which was observed for this complex, indicates a distorted octahedral geometry.

The EPR spectrum of complex **VI** displayed an isotropic signal with g_i = = 2.12. The spectral data, magnetic susceptibility and isotropic value of the "*g*" factor suggest an octahedral geometry for this complex.

Thermal analysis

Thermal analysis by the TG and DSC techniques has proved to be very useful in determining the crystal water content in complexes and their thermal stability and decomposition mode under a controlled heating rate. Due to the explosive nature of perchlorate complexes, the thermal properties of only the nitrate and acetate complexes were investigated.[36,37]

The determined temperature ranges and the corresponding percent mass losses are given in Table V.

The DSC curves of the Schiff base ligand (Fig. 2) showed a melting process located at 545.16 K (peak temperature) with ΔH = 118.5 J g^{-1} (evaluated as the area of the endothermal DSC peak). The melting process is followed by exothermal decomposition with maximum at T_{max} = 600.16 K. The evaluation of the exothermal peak area gives a value of ΔH = – 465.4 J g^{-1}.

The thermal behavior of the complexes depended on the nature and the environment around the metal ion. The TG/DTG and DSC curves of $[CuL_2(H_2O)_2](NO_3)_2 \cdot 2H_2O$ complex are represented in Fig. 3. The decomposition of Cu(II) complex occurred in three stages.

The TG/DTG curves of $[CuL_2(H_2O)_2](NO_3)_2 \cdot 2H_2O$ complex (**I**) showed a mass loss between 303.16 and 391.16 K due to dehydration with a loss of two lattice water molecules (exp. 3.65, calcd. 3.96 %). The second stage, from 391.16 to 429.16 K, corresponded to the elimination of two molecules of HNO_3,[38,39] accompanied by the removal of two coordinated water molecules. The processes of elimination of molecules are indicated by the exothermal peak at 422.7 K on the DSC curve with ΔH = – 951.22 J g^{-1}. The final stage, which occurred in the 429.16–1259.16 K temperature range, appeared as a complex process with more than one exothermal peak. The overall mass loss was observed to be 54.38 %. On DSC curve, the violent decomposition showed a strong exothermal effect with two overlapping peaks with a heat of decomposition (calculated as the peak area neglecting the partial superposition) of ΔH = – 4670.22 J g^{-1}. This exothermal process is followed by another one with a maximum at 600.74 K and ΔH = = –948.57 J g^{-1}.The final residue, estimated as CuO and carbon[39,40], was 23.7 %.

The TG/DTG and DSC curves of the $[NiL_2(H_2O)_2](NO_3)_2 \cdot 4H_2O$ complex are represented in Fig. 4.

TABLE V. Thermoanalytical results for the M(II) complexes

Compound	TG range, K	Mass loss (found (calcd.), %)	Assignments
$[CuL_2(H_2O)_2](NO_3)_2{\cdot}2H_2O$	303.16–391.16	3.65 (3.96)	Loss of 2 lattice water molecules
	391.16–429.16	18.29 (17.80)	Loss of 2 coordinated water molecules + $2HNO_3$
	429.16–1259.16	54.38	Removal of the ligand
	>1259.16	23.68	CuO + C
$[NiL_2(H_2O)_2](NO_3)_2{\cdot}4H_2O$	303.16–393.16	7.47 (7.64)	Loss of 4 lattice water molecules
	393.16–537.16	26.40 (25.60)	Loss of 2 coordinated water molecules + 2 HNO_3+ removal of one Py molecule
	537.16–1123.16	39.51	Removal of the ligand
	>1123.16	26.62	NiO + C
$Cu(L)_2(CH_3COO)_2$	478.16–523.16	19.45 (19.00)	Removal of two Py molecules
	523.16–634.16	66.01 (66.15)	Removal of the ligand
	634.16–713.16	5.11 (5.29)	Loss of CO_2 molecule
	>713.16	9.42 (9.56)	CuO
$[CoL_2(CH_3COO)_2]{\cdot}2H_2O$	388.16–458.16	3.88 (4.17)	Loss of 2 lattice water molecules
	505.16–563.16	18.72 (18.31)	Removal of two Py molecules
	563.16–663.16	64.24 (63.13)	Removal of the ligand
	663.16–718.16	4.88 (5.10)	Loss of CO_2 molecule
	>445	9.04 (9.29)	Co_3O_4
$Ni(L)_2(CH_3COO)_2$	538.16–603.16	19.18 (19.12)	Removal of two Py molecules
	603.16–733.16	66.42 (66.54)	Removal of the ligand
	733.16–773.16	5.46 (5.32)	Loss of CO_2 molecule
	>773.16	8.94 (9.02)	NiO

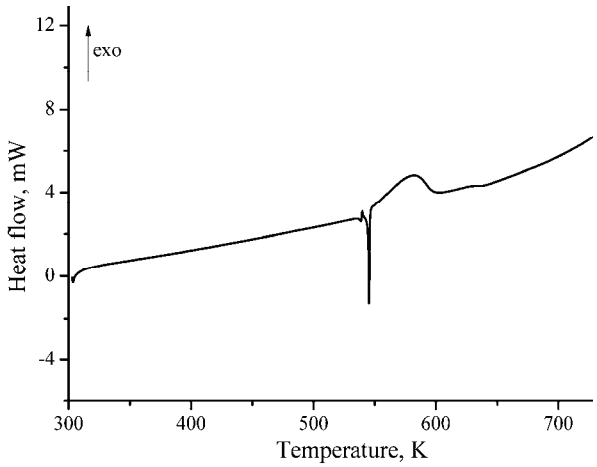

Fig. 2. DSC curve of the ligand.

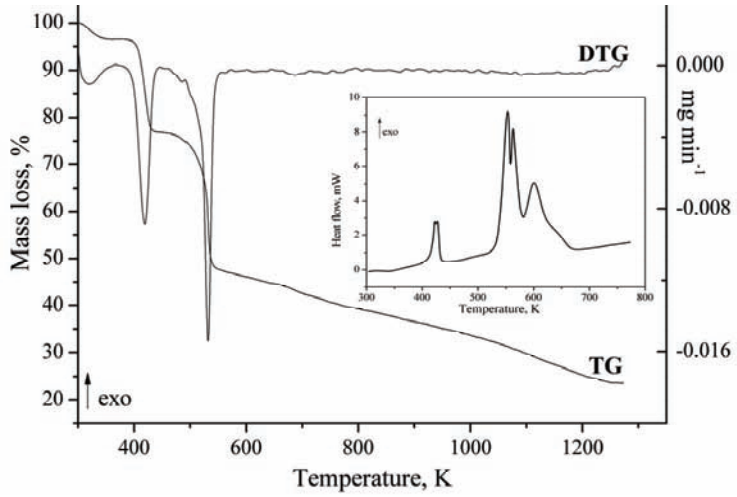

Fig. 3. TG, DTG and DSC (inset) curves of $[CuL_2(H_2O)_2](NO_3)_2 \cdot 2H_2O$ (**I**).

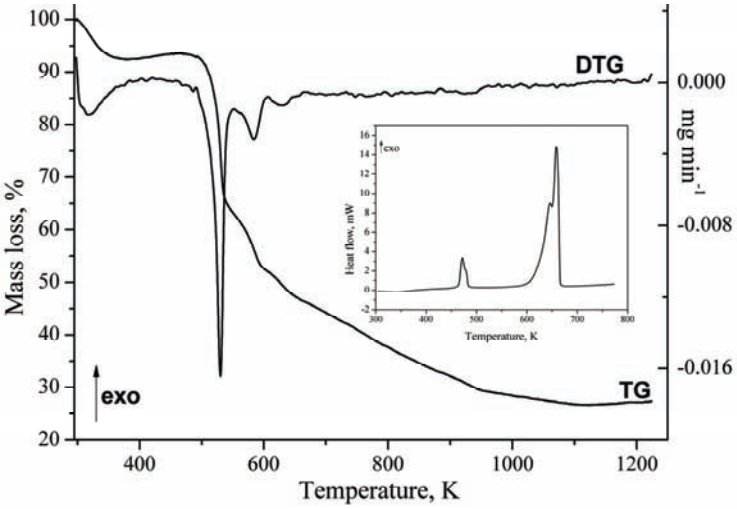

Fig. 4. TG, DTG and DSC (inset) curves of $[NiL_2(H_2O)_2](NO_3)_2 \cdot 4H_2O$ (**II**).

The $[NiL_2(H_2O)_2](NO_3)_2 \cdot 4H_2O$ complex showed almost the same three--stage decomposition process. The first stage occurred in the temperature range 303.16–393.16 K, with a mass loss of 7.47 % due to the removal of four lattice water molecules (calcd. 7.64 %). The second step, between 393.16 and 537.16 K, was complex and was also due to the loss of two coordinated water molecules together with the loss of two molecules of HNO_3 and one molecule of pyridine. The decomposition process is indicated by the DSC peak at 471.18 K, with ΔH = = –641.11 J g^{-1}. The third stage (from 537.16–1123.16 K) was due to the total

decomposition of the ligand. The observed mass loss was 39.51 %. This step was accompanied by an exothermal process at 658.69 K on the DSC curve, with ΔH = –7028.00 J g^{-1}. The residue at 1123.16 K amounted to 26.62 % and corresponded to nickel oxide and carbon.[39,40]

The absence of any mass loss under 473.16 K indicates that the Cu(II) and Ni(II) acetate complexes contained neither coordinated water molecules nor water of crystallization. Their thermal decompositions revealed them to be anhydrous, which is consistent with the elemental and spectral data.

The thermal decomposition of $Cu(L)_2(CH_3COO)_2$ proceeded in three stages. The TG, DTG and DSC curves are given in Fig. 5. The complex was stable up to 478.16 K. The first step of thermal decomposition occurred in the range 478.16––523.16 K and corresponds to the removal of two pyridine molecules (exp. 19.45, calcd. 19.00 %). The second (from 523.16–643.16 K) and third (from 643.16––713.16 K) stages may be due to the removal of the remaining part of the ligand and the acetate group.[41] The observed mass losses in these temperature ranges were 66.01 (calcd. 66.15 %) and 5.11 % (calcd. 5.92 %), respectively. On the DSC curve, the decomposition process is complex with at least three exothermal peaks with ΔH = –8234.40 J g^{-1} (obtained as the peak area in the 523.16–643.16 K temperature range, neglecting the partial superposition). The residue, estimated as copper oxide, had a mass of 9.42 %, compared with the calculated value of 9.56 %.

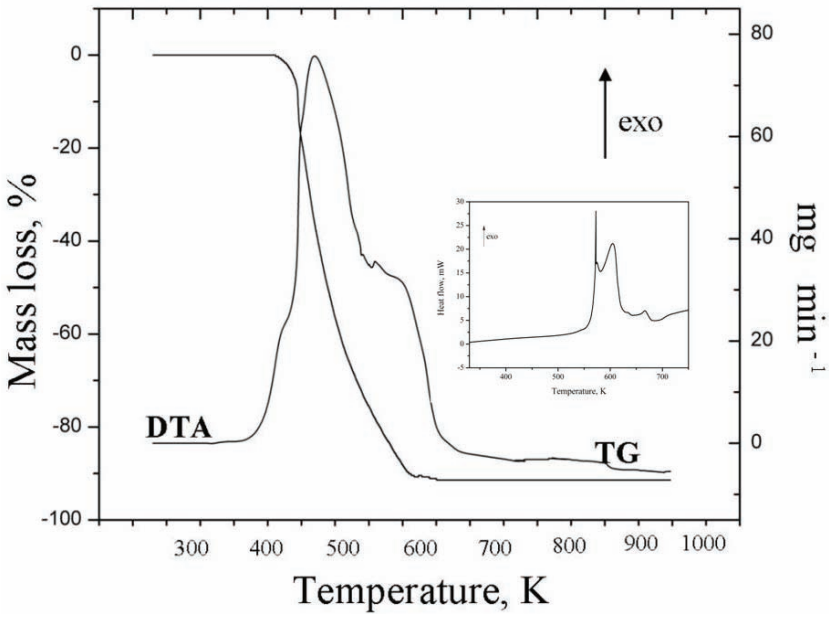

Fig. 5. TG, DTG and DSC (inset) curves of $Cu(L)_2(CH_3COO)_2$ (**VI**).

The TG, DTG and DSC curves of $[CoL_2(CH_3COO)_2]\cdot 2H_2O$ are shown in Fig. 6. The thermal decomposition of the Co(II) acetate complex proceeded in four stages. The thermal dehydration of this complex occurred between 388.16 and 458.16 K, with a mass loss of 3.88 % (calcd. 4.17 %). Two moles of lattice water molecules were removed in this dehydration stage. The process was accompanied by an endothermal effect at 425.78 K on the DSC curve, with ΔH = = 163.59 J g^{-1}. The elimination of crystal water molecules at ≈ 426 K suggests that these are strongly bound in the crystal lattice of the complex.[39] The second (from 505.16–563.16 K) and third (from 563.16–663.16 K) stages may be due to the decomposition of ligand with an observed mass losses of 18.72 (calcd. 18.31 %) and 64.24 % (calcd. 63.13 %), respectively. These steps were accompanied by a complex decomposition process with three consecutive and overlapping exothermal peaks on the DSC curve, with ΔH = –1303.68 J g^{-1} (obtained as the peak area in the 453.16–603.16 K temperature range, neglecting the partial superposition). The fourth stage occurred in the 663.16–718.16 K temperature range, corresponding to the loss of the acetate group, with a mass loss of 4.88 % (calcd. 5.10 %). The process is indicated by the DSC peak with maximum at 718.16 K. The heat of decomposition had a value of ΔH = –314.35 J g^{-1}. The final residue, estimated as Co_3O_4,[42,43] had a mass of 9.04 %, compared to the calculated value of 9.29 %.

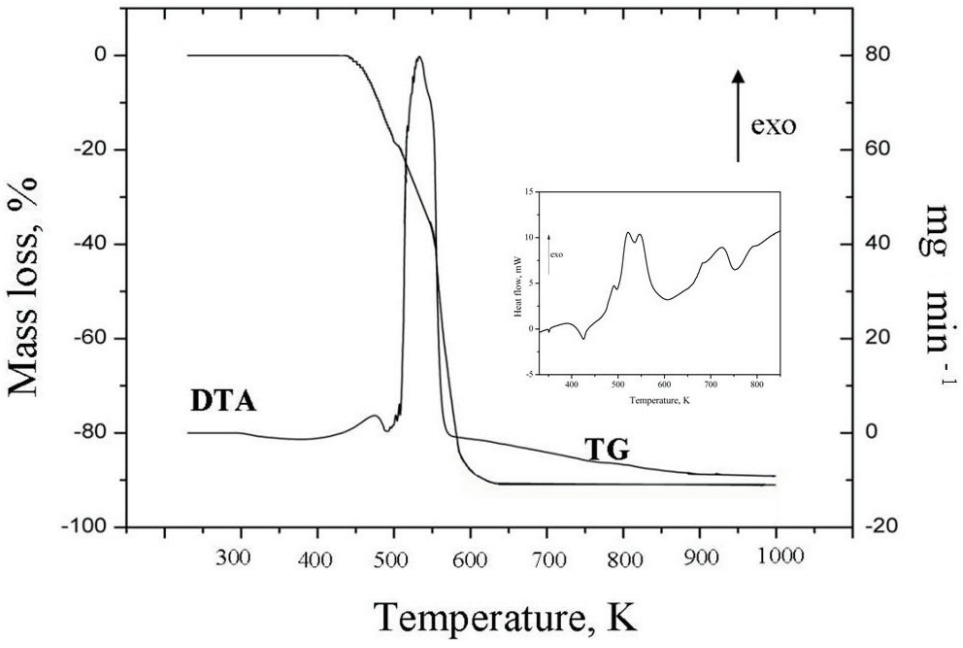

Fig. 6. TG, DTG and DSC (inset) curves of $[CoL_2(CH3COO)_2]\cdot 2H_2O$ (**VII**).

As predicted, the Ni(II) acetate complex was stable up to 538.16 K. The TG, DTG and DSC curves are shown in Fig. 7. According to the TG analysis, the thermal decomposition of this complex was a three-stage process. The first mass loss occurred between 538.16 and 603.16 K, with two exothermal peaks on the DSC curve at 545.16 K, with ΔH = –241.13 J g^{-1} and 582.46 K, with ΔH = = –92.15 J g^{-1}, and is attributed to the removal of two molecules of pyridine (exp. 19.18, calcd. 19.12 %). The removal of the remaining part of the ligand followed in the second stage, between 603.16 and 733.16 K, with a mass loss of 66.42 % (calcd. 66.54 %). The process was indicated by the DSC peak at 698.03 K, with ΔH = –3174.03 J g^{-1}. The third stage between 733.16–773.16 K with a DSC peak at 790.76 K and ΔH = –2689.41 J g^{-1} corresponds to the loss of the acetate group. The observed mass loss was 5.46 %, which is consistent with the theoretical value of 5.32 %. The residue, estimated as NiO, had a mass of 8.94 %, compared with the calculated value of 9.02 %.

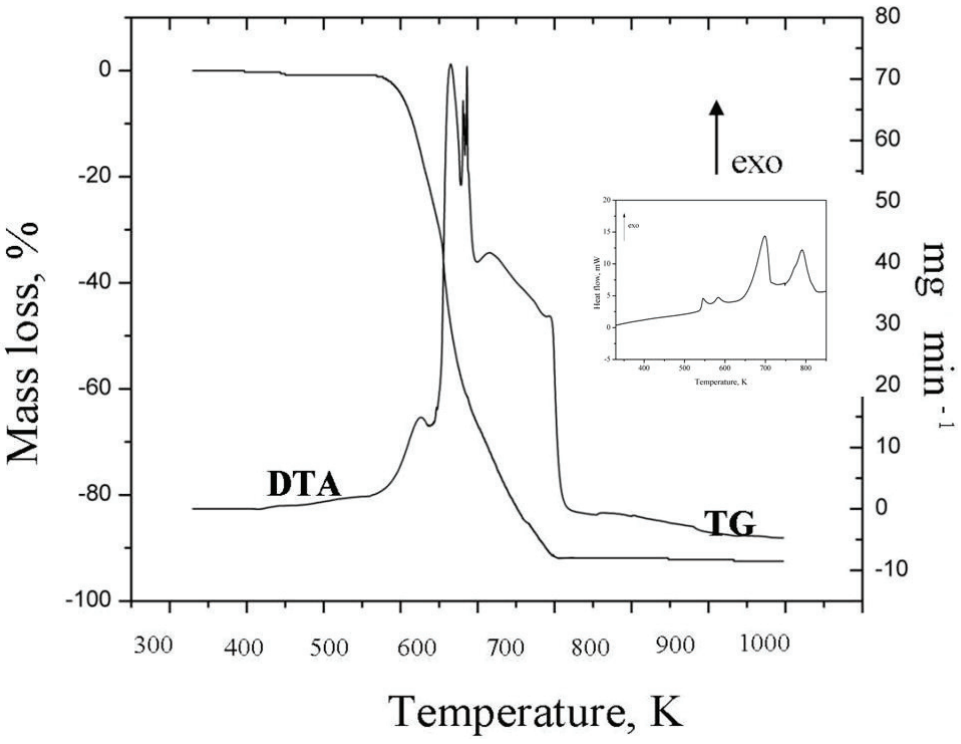

Fig. 7. TG, DTA and DSC (inset) curves of Ni(L)$_2$(CH$_3$COO)$_2$ (**VIII**).

From the thermal investigation of the Cu(II) and Ni(II) acetate complexes, it can be concluded that the decomposition proceeds in the following three stages:

$$M(C_{21}H_{15}N_3O)_2(CH_3COO)_2(s) \rightarrow M(C_{16}H_{10}N_2O)_2(CH_3COO)_2(s)+2C_5H_5N(g)$$
$$M(C_{16}H_{10}N_2O)_2(CH_3COO)_2(s)+93/2O_2(g) \rightarrow MCO_3(s)+36CO_2(g)+$$
$$+13H_2O(g)+4NO_2(g)$$
$$MCO_3(s) \rightarrow MO(s)+CO_2(g)$$

where M is Cu(II) or Ni(II).

Based on the above analytical, spectral and magnetic data together with the thermal decomposition studies, the structural formula and the stoichiometry, given in Fig. 8, are proposed.

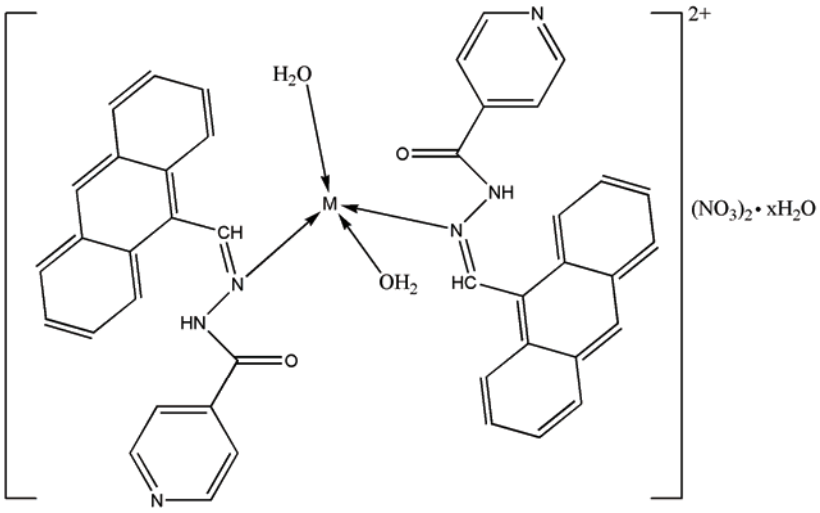

M=Cu(II) x=2, N i(II) x=4

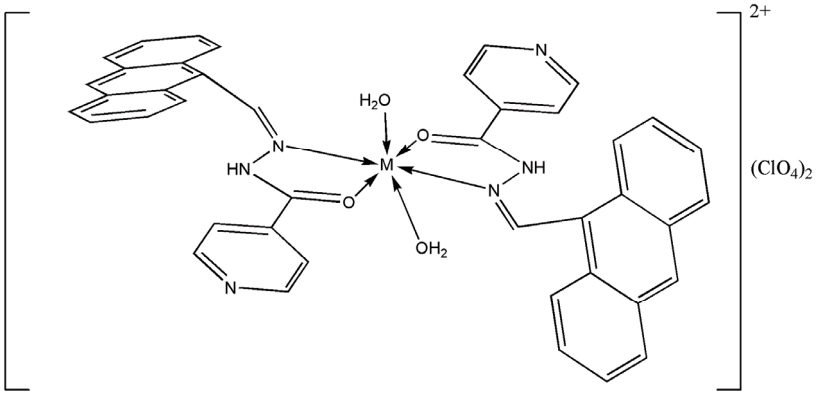

M=Cu(II), Co(II), Ni(II)

Fig. 8. Structural formula of the $ML_2X_2 \cdot xH_2O$ complexes.

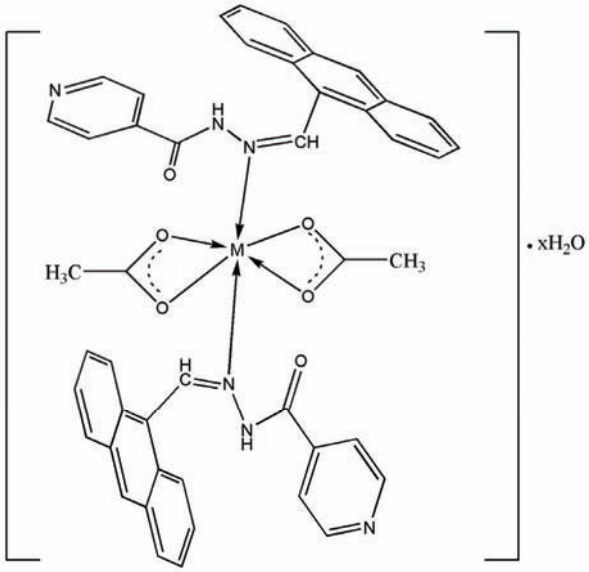

M=Cu(II), Ni(II) x=0, Co(II) x=2

Fig. 8 (continued). Structural formula of the $ML_2X_2 \cdot xH_2O$ complexes.

CONCLUSIONS

Eight new complexes of Cu(II), Co(II) and Ni(II) with isonicotinic acid 2-(9-anthrylmethylene)-hydrazide were synthesized and characterized by analytical, spectral and thermal studies. The spectral studies indicated that hydrazone act as a neutral monodentate ligand coordinating through the nitrogen of the azomethine group or as a bidentate ligand using both the azomethine nitrogen and the amide oxygen. The nitrate complexes have a tetrahedral geometry and the others an octahedral one around the metal ion. The thermal decomposition of the hydrated **I**, **II** and **VII** complexes began with the release of crystallization water in the first stage. During heating, the nitrate complexes lost two coordinated water molecules in the second stage. The anhydrous acetate complexes of Cu(II) and Ni(II) were the most stable. Their decomposition commenced above 473.16 K. The thermal data are in agreement with the spectral and elemental data.

ИЗВОД

КОМПЛЕКСИ ПРЕЛАЗНИХ МЕТАЛА(II) СА 2-(9-АНТРИЛМЕТИЛЕН)ХИДРАЗИДОМ ИЗОНИКОТИНСКЕ КИСЕЛИНЕ

MARIANA LOREDANA DIANU[1], ANGELA KRIZA[1], NICOLAE STANICA[2] и ADINA MAGDALENA MUSUC[2]

[1]*University of Bucharest, Faculty of Chemistry, Department of Inorganic Chemistry, 23 Dumbrava Rosie St., 020464 Bucharest и* [2]*Romanian Academy, „Ilie Murgulescu“ Institute of Physical Chemistry, 202 Spl. Independentei, P.O. Box 12–194, 060021 Bucharest, Romania*

Синтетизовани су и окарактерисани нови комплекси Cu(II), Co(II) и Ni(II) са 2-(9-антрилметилен)хидразидом изоникотинске киселине. За карактеризацију комплекса употребљене су различите аналитичке и физичкохемијске методе, као што су елементална и термална анализа, магнетна и кондуктометријска мерења, електронски, ESR и IR спектри. Инфрацрвена спектроскопска испитивања су показала да су у испитиваним комплексима одговарајући лиганди типа Шифових база монодентатно, или бидентатно координовани, као и да пиридински атом азота код ових лиганада не учествује у координацији. Одговарајућим нитратним комплексима приписана је тетраедарска, док је за остале испитиване комплексе претпостављена октаедарска геометрија. Добивени резултати термалних испитивања су у складу са претпостављеним формулама испитиваних комплекса.

(Примљено 23. новембра 2009, ревидирано 6. априла 2010)

REFERENCES

1. S. Rollas, S. G. Küçükgüzel, *Molecules* **12** (2007) 1910
2. E. W. Ainscough, A. M. Brodie, W. A. Denny, G. J. Finlay, S. A. Gothe, J. D. Ranford, *J. Inorg. Biochem.* **77** (1999) 125
3. B. Bottari, R. Maccari, F. Monforte, F. Ottana, E. Rotondo, M. G. Vigorita, *Bioorg. Med. Chem. Lett.* **10** (2000) 657
4. S. K. Sridhar, M. Saravanan, A. Ramesh, *Eur. J. Med. Chem.* **36** (2001) 615
5. K. B. Koçyiğit, S. Rollas, *Farmaco* **57** (2002) 595
6. R. K. Agarwal, D. Sharma, L. Singh, H. Agarwal, *Bioinorg. Chem. Appl.* **2006** (2006) 1
7. N. K. Singh, N. Singh, A. Sodhi, A. Shrivastava, *Transition Met. Chem.* **21** (1996) 556
8. N. K. Singh, N. Singh, G. C. Prasad, A. Sodhi, A. Shrivastava, *Bioorg. Med. Chem.* **5** (1997) 245
9. B. V. Agarwala, S. Hingorani, G. A. Nagna Gowda, *Inorg. Chim. Acta* **176** (1990) 149
10. R. C. Maurya, R. Verma, T. Singh, *Synth. React. Inorg. Met.-Org. Chem.* **33** (2003) 309
11. M. Donia, H. A. El-Boraey, M. F. El-Samalehy, *J. Therm. Anal. Calorim.* **73** (2003) 987
12. M. Amirnasr, R. Houriet, S. Meghdadi, *J. Therm. Anal. Calorim.* **67** (2002) 523
13. M. Sekerci, F. Yakuphanoglu, *J. Therm. Anal. Calorim.* **75** (2004) 189
14. H. A. El-Boraey, *J. Therm. Anal. Calorim.* **81** (2005) 339
15. S. A. AbouEl-Enein, *J. Therm. Anal. Calorim.* **91** (2008) 929
16. C. K. Modi, B. T. Thaker, *J. Therm. Anal. Calorim.* **94** (2008) 567
17. L. Mitu, N. Raman, A. Kriza, N. Stanica, M. Dianu, *Asian J. Chem.* **21** (2009) 5749
18. L. Mitu, N. Raman, A. Kriza, N. Stanica, M. Dianu, *J. Serb. Chem. Soc.* **74** (2009) 1075
19. G. Macarovici, *Inorganic Quantitative Chemical Analysis*, Ed. Academiei, Bucharest, 1979
20. W. J. Geary, *Coord. Chem. Rev.* **7** (1971) 81
21. K. Nakamoto, *Infrared and Raman Spectra of Inorganic and Coordination Compounds*, Wiley, New York, 1986

22. R. S. Baligar, V. K. Revankar, *J. Serb. Chem. Soc.* **71** (2006) 1301
23. A. Z. El-Sonbati, *Transition Met. Chem.* **16** (1991) 45
24. K. B. Yatsimirskii, *Pure Appl. Chem.* **49** (1977) 115
25. S. D. Ross, *Spectrochim. Acta* **18** (1962) 225
26. U. Casellato, P. A. Vigato, N. Vidali, *Coord. Chem. Rev.* **26** (1978) 85
27. B. P. Lever, *Inorganic Electronic Spectroscopy*, 2nd ed., Elsevier Science, New York, 1984
28. R. L. Carlin, *Magnetochemistry*, Springer, Berlin Heidelberg, 1986
29. F. A. Cotton, G. Wilkinson, *Advanced Inorganic Chemistry*, Wiley Interscience, New York, 1976
30. C. I. Lepadatu, M. Andruh, *Forma moleculelor anorganice. O introducere in stereochimia anorganica*, Ed. Academiei Romane, Bucharest, 1998 (in Romanian)
31. E. König, S. Kremer, *Ber. Bunsenges Phys. Chem.* **78** (1974) 786
32. E. König, R. Schnakig, *Phys. Status Solidi* **B77** (1976) 657
33. E. König, *Struct. Bond.* **9** (1971) 175
34. D. Marinescu, *Chimie Coordinativa – Principii generale*, Ed. Universitatii, Bucharest, 1995 (in Romanian)
35. S. Chandra, X. Sangeetika, *Spectrochim. Acta A* **60** (2004) 147
36. C. Wei, W. J. Rogers, M. S. Mannan, *J. Therm. Anal. Calorim.* **83** (2006) 125
37. G. Sing, D. K. Pande, *J. Therm. Anal. Calorim.* **82** (2005) 353
38. Z. H. A. El-Wanab, M. M. Mashaly, A. A. Salma, B. A. El-Shetary, A. A. Faheim, *Spectrochim. Acta A* **60** (2004) 2861
39. M. Lalia-Kantouri, L. Tzavellas, D. Paschalidis, *J. Therm. Anal. Calorim.* **91** (2008) 937
40. S. U. Din, M. Umar, *J. Therm. Anal. Calorim.* **58** (1999) 61
41. G. G. Mohamed, Z. H. A. El-Wahab, *J. Therm. Anal. Calorim.* **73** (2003) 347
42. D. Czakis-Sulikowska, J. Radwańnska-Doczekalska, M. Markiewicz, M. Pietrzak, *J. Therm. Anal. Calorim.* **93** (2008) 789
43. G. Bannach, A. B. Siqueira, E. Y. Ionashiro, E. C. Rodrigues, M. Ionashiro, *J. Therm. Anal. Calorim.* **90** (2007) 873.

Journal of the Serbian Chemical Society
JSCS-info@shd.org.rs • www.shd.org.rs/JSCS
J. Serb. Chem. Soc. *75* (11) 1533–1548 (2010)
JSCS–4074
UDC 635.71:616.936:530.145:543:51–3
Original scientific paper

A study of new antimalarial artemisinins through molecular modeling and multivariate analysis

JOÃO E. V. FERREIRA[1]*, ANTONIO F. FIGUEIREDO[1], JARDEL P. BARBOSA[1], MARIA G. G. CRISTINO[1], WILLIAMS J. C. MACEDO[1], OSMARINA P. P. SILVA[1], BRUNO V. MALHEIROS[1], RAYMONY T. A. SERRA[2] and JOSE CIRIACO-PINHEIRO[1]

[1]*Laboratório de Química Teórica e Computacional, Faculdade de Química, Instituto de Ciências Exatas e Naturais, Universidade Federal do Pará, Avenida Augusto Correa, 01, CP 101101, CEP 66075-110, Belém, PA, Amazônia and* [2]*Centro de Ciências Biológicas e da Saúde, Universidade Federal do Maranhão, CEP 65085-580, São Luis, MA, Brasil*

(Received 26 January, revised 12 June 2010)

Abstract: Artemisinin and 18 derivatives with antimalarial activity against W-2 strains of *Plasmodium falciparum* were studied through quantum chemistry and multivariate analysis. The geometry optimization of the structures was realized with the Hartree-Fock (HF) theory and 3-21G** basis set. Maps of molecular electrostatic potential (*MEP*) and molecular docking were used to investigate the interaction between the ligands and the receptor (heme). Principal component analysis (PCA) and hierarchical cluster analysis (HCA) were employed to select the most important descriptors related to activity. A predictive model was generated by the partial least square (PLS) method through 15 molecules and 4 used as an external validation set, which were selected in the training set, the validation parameters of which are Q^2 = 0.85 and R^2 = 0.86. The model included as molecular parameters the radial distribution function, *RDF060e*, the hydration energy, *HE*, and the distance between the O1 atom from the ligand and the iron atom from heme, d(Fe–O_1). Thus, the synthesis of new derivatives may follow the results of the *MEP* maps and the PLS analysis.

Keywords: Malaria; artemisinin; molecular docking; *MEP* maps; QSAR.

INTRODUCTION

Malaria is a very serious infectious disease caused by protozoans of the genus *Plasmodium* and is transmitted by the bite of infected female *Anopheles* mosquitoes. Every year, over one million people die owing to malaria, especially in tropical and subtropical areas. Most of the deaths are attributed to the parasite species *Plasmodium falciparum*. Many drugs have been investigated for their efficacy in the treatment of the disease, but resistant strains of *P. falciparum* to some

* Corresponding author. E-mail: joao.elias@yahoo.com.br
doi: 10.2298/JSC100126124F

of these drugs have appeared.[1–6] Hence, further discovery of new classes of more potent compounds against the disease is necessary.

However, drug design is a process involving high cost and time. Computational and quantitative structure–activity relationship (QSAR) studies have been of great value in medicinal chemistry.[7–15] Statistical tools can be used for the prediction of the biological activities of new compounds based only on the knowledge of their chemical structures, *i.e.*, not depending on experimental data, which are unknown. Such a strategy gives very useful information for the understanding of the mechanisms of the action of drugs and proposals for syntheses, in this way rationalizing drug discovery. As Doweyko[16] states "QSAR is alive and well", thus it is still of relevance today.

Some of the effective drugs used in the clinical treatment of *P. falciparum* malaria are artemisinin or *qinghaosu* and its derivatives. Artemisinin (compound **1**, Fig. 1) is a sesquiterpene containing the 1,2,4-trioxane ring system. Currently,

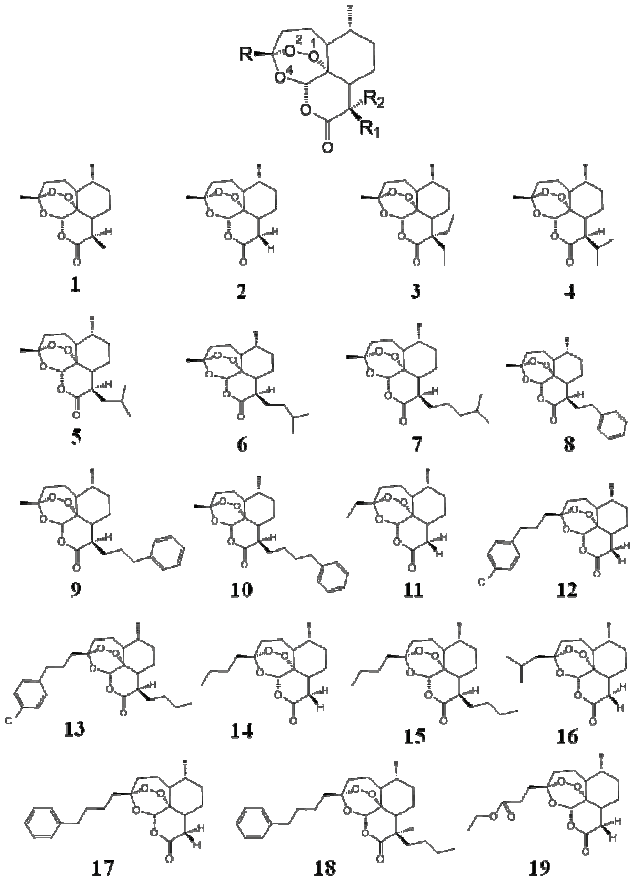

Fig. 1. Artemisinin and derivates with antimalarial activity against W-2 strains of *P. falciparum*.

semi-synthetic artemisinin derivatives play an important role in the treatment of *P. falciparum* malaria.[1,17–19] Even though the true mechanism of their biological activity against malaria has not been elucidated completely yet, various studies suggest that the trioxane ring is essential for antimalarial activity owing to the properties displayed by the endoperoxide linkage. Literature also suggests that free heme (Fig. 2) could be the molecule targeted by artemisinin in biological systems and that Fe^{2+} interacts with the peroxide when artemisinin reacts with heme.[20–23]

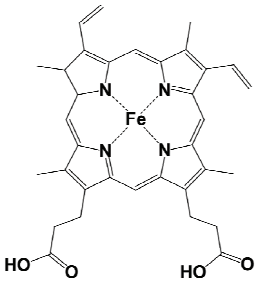

Fig. 2. Two-dimensional structure of the heme.

In this article, a quantum chemical and multivariate study of artemisinin and 18 derivatives, the training set (Fig. 1), with different antimalarial activities, tested *in vitro* against *P. falciparum*, was performed. Initially, the structures were modeled and many different molecular descriptors were computed. Maps of the molecular electrostatic potential (*MEP*) and molecular docking were employed to better understand the correlation between structure and activity, and the interaction between the ligands (artemisinin and derivatives) and the receptor (heme). Methods of multivariate analysis[24] were used to deal with such a large number of descriptors and find a predictive model. First principal component analysis (PCA) and hierarchical cluster analysis (HCA) were employed in order to choose those molecular descriptors that are most related to the biological property investigated. Then, a QSAR model was elaborated through the partial least square (PLS) method to aid future studies searching for others new drugs against malaria.

COMPUTATIONAL METHODS

The compounds studied

Initially, 19 molecules were selected from the literature[6] to build a training set (Fig. 1). They were associated to their *in vitro* bioactivity against the drug-resistant malarial strain *P. falciparum* (W-2 clone), which is cloroquine resistant but mefloquine sensitive. The samples include artemisinin (**1**) and analogs substituted in the R, R1 and R2 positions around the tetracyclic framework of the parent structure **1**. The atomic numbering adopted in this work is the same as that used in a previous work.[10] Considering that the biological data was available from different sources, the logarithm of the IC_{50} value of artemisinin over the IC_{50} value of the compounds (logarithm of relative activity, log *RA*) was used to reduce inconsistencies caused by individual experimental environments:

$$\log RA = \log (IC_{50} \text{ of artemisinin} / IC_{50} \text{ of an analog}) \quad (1)$$

where IC_{50} means the 50 % inhibitory concentration. In this work, the following classification based on the antimalarial responses was adopted: compounds with log $RA \geq 0.00$ were assumed as more potent analogs (**1**, **2**, **8**–**11**, **17** and **19**) and those with log $RA < 0.00$ were considered as less potent analogs (**3**–**7**, **12**–**16** and **18**).

Molecular modeling

The starting point in the molecular modeling step was the construction of the structures of the molecules with the aid of GaussView software.[25] To model all the compounds, it was necessary to use a quantum chemistry method and a basis set able to describe well the region around the 1,2,4-trioxane ring, which was indicated as being crucial for the antimalarial efficacy of artemisinin, as previously stated. Hence, the complete geometry optimization for all structures was performed with the Hartree-Fock (HF) method[26] and the 3-21G** basis set,[27] incorporated in the Gaussian 98 program.[28] This procedure gives good results for the geometrical parameters when compared to the experimental (crystallographic) results, as verified by Cardoso *et al.*[11]

Descriptors

After molecular modeling, various descriptors were computed for each molecule in the training set. They represent different source of chemical information (features) regarding the molecules and include geometric, electronic, quantum-chemical, physical–chemical and topological descriptors and others. They are important for the quantitative description of molecular structure and to find appropriate predictive models.[29] The descriptors computed were dipole moment, molecular weight, molecular volume, surface area, molecular refractivity, molecular polarizability, molecular hardness, molecular softness, O1–O2 bond length, atomic charge on the atoms O1, O2 and O4, logarithm of octanol–water partition coefficient (log *P*), hydration energy (HE), radial distribution functions (RDF030e and RDF060e), total energy, frontier orbital energies (HOMO, HOMO-1, LUMO, LUMO+1), maximal electrotopological negative variation (MAXDN), maximal electrotopological positive variation (MAXDP), information index on molecular size (ISIZ), energy of the interaction of the heme–ligand complex, distance between the O1 atom from the ligand and the iron atom from heme, *d*(Fe–O1), and the distance between the O2 atom from the ligand and the iron atom from heme, *d*(Fe–O2). The computation of the descriptors was performed employing the following software: Gaussian 98, e-Dragon,[30,31] Autodock 4.0,[32] Molekel,[33] and HyperChem 6.02.[34]

Molecular electrostatic potential maps

An important aspect explored in this research was the correlation of the structure–activity of the species studied here through the characteristics of the electrostatic potential in the region of the 1,2,4-trioxane-ring, since in the literature[8,11,12] it is stated that artemisinin and its derivatives with antimalarial activities present similar patterns in their *MEP* maps. Such a method enables a qualitative analysis to be used to localize reactive sites in a molecule and the role played by both the electronic and steric (size/shape) effects on its potency. It is worthwhile to point out that visualization of *MEP* maps gives qualitative information on molecules such as the behavior in the interaction between ligand and receptor. *MEP* maps for artemisinin, derivatives and heme were computed from the atomic charge at the HF/3-21G** level using the Gaussian 98 program and the results are displayed with Molekel software.

Molecular docking

The interaction between the ligands and the receptor was studied with aid of molecular docking in order to find the best geometry for the complex formed between these two molecules. The geometry of artemisinin and the derivatives (ligands) was designed with the HF/3--21G** level of theory, whereas the geometry of heme (receptor) was obtained from the protein data bank (PDB) RCSB, identified by the code 1A6M, according to the work of Vojtechovsky *et al*.[35] The arrangement in the docking calculation took into account the presence of the proximal histidine residue under the plane of the porphyring ring. This histidine unity is, as usual, coordinated perpendicularly to Fe^{2+} through its sp^2 nitrogen atom of its imidazole ring. Such an arrangement will allow the Fe^{2+} to attain a nearly octahedral hexacoordinated arrangement after binding to the artemisinin molecule.[22] The orientation of the ligand was set just above the plane of heme. Then, for each ligand/receptor interaction, 20 (twenty) conformations were calculated and the most probable one, based on the lowest energies of interaction, was selected to evaluate the distance between the O1 atom from the ligand and the iron atom from heme, *d*(Fe–O1), and the distance between the O2 atom from ligand and the iron atom from heme, *d*(Fe–O2). Automated docking calculations were performed to develop possible conformations for the complex employing the Lamarckian Genetic Algorithm implemented in the package Autodock 4.0. This program starts the docking displaying the ligand in an arbitrary conformation and position and look for the favorable dockings with the receptor using both simulating annealing and genetic algorithms. AutoDock uses a random number generator to create new poses for the ligand during its search and estimates the free energy of binding of a ligand to its target. The resulting conformations were ranked in order of increasing binding energy of the lowest binding energy conformation in each cluster.

Multivariate analysis

A multivariate analysis was performed in order to extract meaningful information efficiently from the data computed. However, prior to performing the exploratory data analysis, all variables were auto-scaled as a preprocessing so that they could be standardized and this way could have the same importance regarding the scale. Furthermore, given the large quantity of multivariate data available, it was necessary to reduce the number of variables. Thus, if two any descriptors had a high Pearson correlation coefficient ($r > 0.8$), one of the two was randomly excluded from the matrix, since theoretically they describe the same property,[36] that is, they also have a high correlation with antimalarial activity and it is sufficient to use only one of them as an independent variable in a predictive model. Moreover those properties that showed either the same values for most of the samples or a small correlation with activity ($r < < 0.2$) were also eliminated.

After this data compression, two complementary methods for exploratory data analysis, HCA and PCA, were employed to study intersample and intervariable relationships and to select the properties that better contribute to the classification of the compounds into two groups: one for more potent analogs and other for less potent analogs. The PCA was employed to reduce the dimensionality of the data, find descriptors that could be useful in characterizing the behavior of the compounds acting against malaria and look for natural clustering in the data and outlier samples. While processing PCA, several attempts to obtain a good classification of the compounds were made. At each attempt, the score and loading plots were analyzed based on the variables employed in the analysis. The score plot gives information about the compounds (similarity and differences). The loading plot gives information about the variables (how they are connected to each other and which are the best to describe the variance in the original data). Then the descriptors selected by PCA were used to perform

HCA and PLS. The objective of HCA was also to present the compounds distributed in natural groups and the results confirm the PCA results. Thus, several approaches to establish links between samples/cluster were attempted. All of them were of an agglomerative type, since each sample was first defined as its own cluster, then others were grouped together to form new clusters until all samples were part of a single cluster.

The final purpose of the multivariate analysis was the construction of a mathematical model to predict antimalarial activity. The samples selected to compose the external validation set were **5**, **8**, **15** and **19**. In order to evaluate the statistical significance of the model, some validation parameters were calculated as recommended,[24,36,37] which included the total variance explained, R^2 (correlation between the estimated values predicted by the model built with the full data set and actual values of y), Q^2 (the cross-validated correlation coefficient), *PRESS* (prediction residual error sum of squares), *SEP* (standard error of the prediction), s (standard deviation) and F (Fisher test). The statistical analysis, including both calculations and plots was realized with Pirouette software.[38]

RESULTS AND DISCUSSION

Molecular electrostatic potential maps

The molecules in the training set have similar *MEP* maps (Fig. 3). They display contour surfaces close to that of the 1,2,4-trioxane ring, which is characterrized by negative electrostatic potentials (red color), on which the lowest values for charge were about –0.30 au (atomic unit). Such a characteristic indicates a concentration of the electron density due to the lone electron pairs on the oxygen atoms (O_1, O_2 and O_4). These molecules also have contour surfaces characterrized by positive electrostatic potentials (blue color), the highest values of which are about 0.30 au. The distribution of electron density on the molecules around the trioxane ring induces their activity against malaria, a belief supported by the fact that the complexation of artemisinin with heme involves particularly the interaction between the peroxide bond, the most negatively charged zone on the ligand, and Fe^{2+}, the most positively charged zone on heme (the receptor molecule).[14,23] The *MEP* map for heme (Fig. 4) displayed a contour surface around the porphyrin ring associated to negative electrostatic potentials (red color) and the zone above Fe^{2+} is presented as having a positive electrostatic potential (blue color). Hence, the presence of a surface in red close to the trioxane ring suggests these compounds have a reactive site for electrophilic attack and must possess antimalarial potency; consequently they are interesting to be investigated. Thus, in the case of an electrophilic attack of the iron of heme against an electronegative zone, this attack has a great preference to occur through the involvement of the endoperoxide linkage. Such a pattern of *MEP* maps is an indication that the compounds in the test set are all active against the malarial strain *P. falciparum* (W-2 clone). Thus by analyzing *MEP* maps, the selection of inactive compounds is avoided.

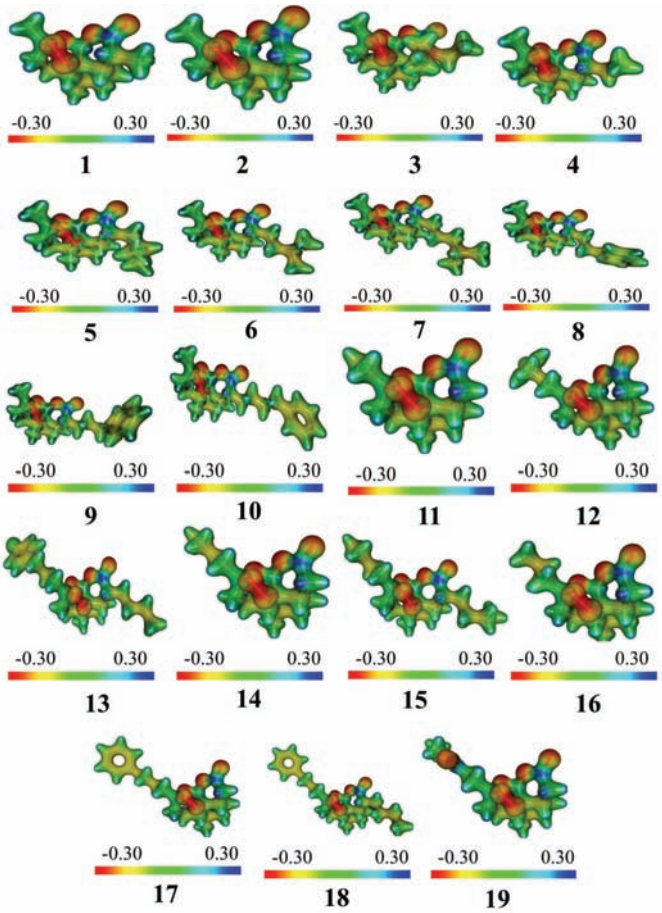

Fig. 3. *MEP* maps (values in atomic unit) for artemisinin and derivatives with antimalarial activity against W-2 strains of *P. falciparum*.

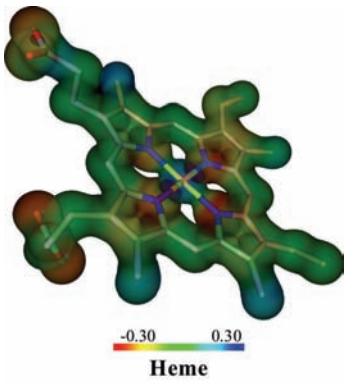

Fig. 4. *MEP* map (values in atomic unit) for heme.

Molecular docking

Docking calculations showed that the entire molecules of the ligands are placed parallel to the plane of the porphyrin ring of heme and the polar part of the ligands containing peroxide bond is directed towards the polar part of the heme system containing Fe^{2+}. This interaction for compounds **2** and **14**, the most active and the least active in the training set, respectively, is visualized in Fig. 5. Such orientations were assumed as the most favorable and so represent the real system under investigation, considering they were chosen based on the lowest free-energy of binding (interaction energy). For compounds in the training set, the values of d(Fe–O_1) ranged from 2.48 to 2.89 Å; however this interval for the d(Fe–O_2) distances ranged from 2.79 to 3.93 Å. For artemisinin (**1**), the d(Fe–O_1) calculated distance was found to be 2.68 Å, which is very close to the value reported (2.7 Å) in other theoretical studies.[40,41] A clear trend occurs involving the interatomic separation between Fe^{2+} and the oxygen atom in the trioxane ring because the distances are shorter for the O_1 atom than for the O_2 atom. This result reinforces the conception that the O_1 atom from artemisinin binds to Fe^{2+} from heme more preferably than the O_2 atom. Compounds **9**, **10**, **17** and **19** have higher activity than artemisinin and also higher values of d(Fe–O_1). They have a large substituent which certainly causes repulsion due to the steric effect which prevents them from approaching closer to the heme. Now considering the interaction energy for the ligand/receptor complex, it showed a poor linear correlation with activity (r = –0.04) and ranged from –6.80 to –5.53 kcal mol^{-1}. In fact, it was verified that even though some orientations were associated with the lowest interaction energy, they seemed strongly favorable with respect to being active against malaria for they presented the endoperoxide bond apart from Fe^{2+}.

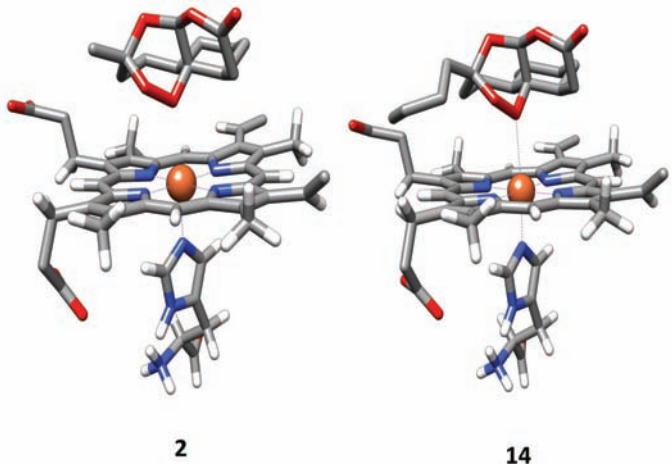

Fig. 5. Molecular docking between heme and artemisinin derivatives. Molecules **2** and **14** are the most and the least potent in the training set, respectively.

Nowadays, the most accepted mechanism of antimalarial action involves the formation of a complex between heme and artemisinin derivatives in which the iron of heme interacts with O_1 of the endoperoxide.[40] Moreover substituent and conformation effects may affect the charge distribution at the oxygen and even the Fe–O_1 bond.[9] An increase in the polar area of artemisinin increases the space with polar interactions between heme, ligand and globin.

PCA method

The first three principal components, PC1, PC2 and PC3 explained 57.89, 24.23 and 17.88 % of the total variance, respectively. Fig. 6 shows the PC1–PC2 scores for the samples **1**–**19**, which are distributed into two distinct separated zones in PC1. The left side has samples with the lowest PC1 values, corresponding to the more potent analogs (associated with a plus sign), whereas the right side has samples with the highest PC1 values, corresponding to less potent analogs (associated with a minus sign). The molecular parameters of the training set responsible for such a distinct classification were the radial distribution function 6.0 weighted by the atomic Sanderson electronegativities, *RDF060e*,[39] hydration energy, *HE*, and *d*(Fe–O_1). They were selected among the descriptors initially computed and are believed to be closely related to the investigated biological response. According to Table I, the Pearson correlation coefficient between log *RA* and these variables are moderate: *RDF060e* (–0.55), *HE* (–0.71) and *d*(Fe–O_1) (0.68); however, between the variables it is, in absolute values, less than 0.45. The other variables were not selected because they either had a poor linear correlation with activity or they did not give a distinct separation of the two classes. The PC1–PC2 loadings (Fig. 7) revealed that the compounds with a higher activity have the main contribution from the *d*(Fe–O_1) descriptor, while the compounds with lower activities have the major influence from the *RDF060e* and *HE* descriptors.

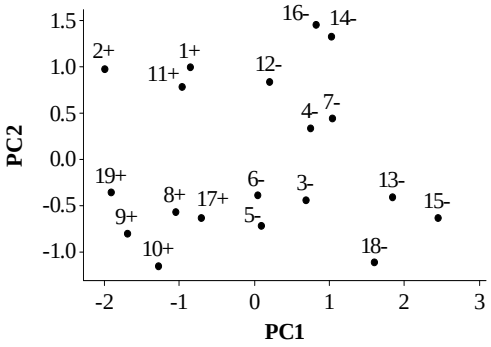

Fig. 6. Plot of PC1–PC2 scores for artemisinin and derivates with antimalarial activity against W-2 strains of *P. falciparum*. Plus sign for more potent analogs and minus sign for less potent analogs.

The radial distribution function descriptors are based on the distance distribution of the molecules and are related to the three-dimensional arrangement of

the atoms. Thus, the *RDF* of an ensemble of *n* atoms can be interpreted as the probability distribution of finding an atom in a spherical volume of radius *R*,[39] The spherical volume comprises the inner part of the molecule. For *RDF060e* this radius was fixed at 6.0 Å from the geometrical center of each molecule under investigation. High values for *RDF060e* are attributed to the presence of electronegative atoms in the inner part of the molecule limited by this spherical volume.

TABLE I. Values of the three properties (descriptors) that classify artemisinin and its 18 derivatives (training set) and their respective experimental log *RA* (W-2) values. The table also shows the correlation matrix (+: more active analogs, –: less active analogs)

Compound	*RDF060e*	*HE*[a] / kcal mol^{-1}	*d*(Fe–O_1) / Å	log *RA* (ref. 6)
1+	21.89	–3.00	2.68	0.00
2+	17.35	–3.52	2.79	0.81
3–	32.87	–1.38	2.73	–0.42
4–	31.00	–2.06	2.59	–0.080
5–	32.28	–1.89	2.82	–0.61
6–	29.53	–1.44	2.81	–0.010
7–	29.98	–1.09	2.62	–0.14
8+	31.28	–4.48	2.74	0.00
9+	28.22	–4.02	2.89	0.64
10+	31.27	–3.72	2.89	0.48
11+	22.00	–2.83	2.73	0.050
12–	29.78	–3.92	2.48	–0.060
13–	40.06	–2.14	2.51	–0.49
14–	27.30	–1.82	2.48	–0.78
15–	40.03	–0.17	2.60	–0.59
16–	25.58	–1.77	2.50	–0.39
17+	31.95	–3.86	2.75	0.31
18–	42.27	–2.19	2.60	–0.51
19+	25.76	–4.37	2.85	0.27
Descriptor			Correlation coefficient	
RDF060e	–	0.38	–0.28	–0.55
HE	–	–	–0.44	–0.71
d(Fe–O_1)	–	–	–	0.68

[a]1 kcal = 4.184 kJ

In a similar study, Pinheiro *et al.*[9] performed an investigation on artemisinin derivatives with antimalarial activities against *P. falciparum* with the aid of computation and multivariate analysis and selected an *RDF* descriptor. Their work indicated the *RDF030m* (the radial distribution function centered at 3.0 Å interatomic distance and weighted by atomic mass) as a property closely related to antimalarial potency of molecules. They associated the compounds with high activity to low values of *RDF030m*. The more potent analogs exhibited, in general, lower values of *RDF060e* and the most potent **2** presented the lowest *RDF060e*. In addition, compounds **1**, **2** and **11** with small substituents (hydrogen atom, methyl or

ethyl) presented lower values for *RDF060e*. The presence of large substituents at the R and R1 position (**13**, **15** and **18**) caused an increase in *RDF060e* due to the presence of more electronegative atoms.

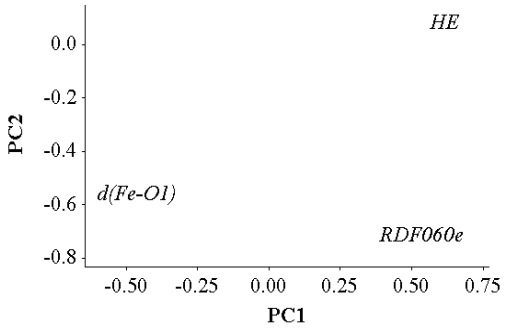

Fig. 7. Plot of the PC1–PC2 loadings with the three descriptors selected to build the PLS model of artemisinin and derivatives with biological activity against W-2 strains of *P. falciparum*.

Regarding the *HE*, more potent analogs showed trends in having more negative energies involved in the hydration process. The *HE* descriptor is a physicochemical property that is a measure of the energy released when water molecules surrounds certain molecules. Its presence means that the mechanism of molecules against malaria is dependent on a hydration process which is related to solubility. Actually, the study of Costa *et al.*[40] led to the conclusion that the presence of water changed the dihedral angle involved in the complex heme–artemisinin (C–Fe––O_1–O_2). Thus, this effect is believed to influence the process of molecular recognition between artemisinin and derivatives and heme in aqueous biological systems. Finally, the selection of the *d*(Fe–O_1) descriptor suggests that the action of drugs against malaria depends on electrophilic attack on the endoperoxide bond, particularly on the O_1 atom. This result was confirmed by both an analysis of the *MEP* maps and by molecular docking as discussed before.

HCA method

The best approach chosen in HCA to group samples into two main classes (one for more potent analogs and the other for less potent analogs) was based on the Euclidean distance and the average group method.[38] This method established links between samples/cluster. The distance between two clusters was computed as the distance between the average values (the mean vector or centroids) of the two clusters. The descriptors employed in HCA were the same in PCA, that is, *RDF060e*, *HE* and *d*(Fe–O_1). The representation of clustering results is shown by the dendrogram in Fig. 8, which depicts the similarity of samples. The branches on the bottom of the dendrogram represent single samples. The length of the branches linking two clusters is related to their similarity. Long branches are related to low similarity while short branches mean high similarity. On the scale of similarity, a value of 100 is assigned to identical samples and a value of 0 to the most dissimilar samples.

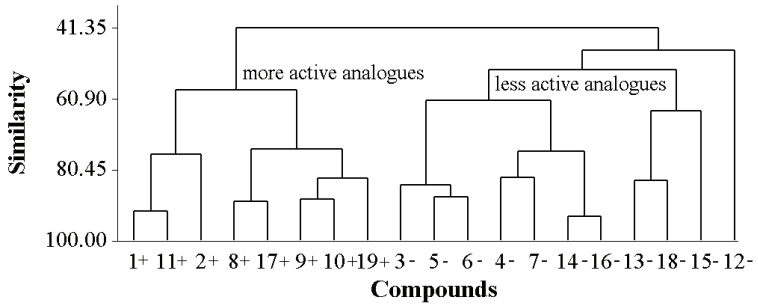

Fig. 8. HCA dendrogram for artemisinin and derivatives with biological activity against W-2 strains of *P. falciparum.* Plus sign for more potent analogs and minus sign for less active compounds.

The dendrogram shows, like the PCA plot, the compounds separated into two different classes according to their activities with no sample incorrectly classified. More active compounds are on the left side and are divided into two groups. In one group consisting of **1**, **2** and **11**, the most active compound 2 is present. The substituents are small (hydrogen atom, methyl or ethyl) and the values for *RDF060e* are the lowest. They present the largest range for activity since it varies from the highest value for log *RA*, 0.81 to 0.00, the activity of artemisinin. The other group consisting of **8**–**10**, **17** and **19** has structures presenting a hydrogen atom or methyl as one of the substituents whereas the other substituent has either a phenyl attached at the end of its alkyl chain with two to four carbons or an ester functional group. They present the most negative values of *HE*. Now considering the less active compounds, there are three main groups. One of them consisting of **13**, **15** and **18** has a phenyl attached at the end of an alkyl chain of three or four carbons in length at R and *n*-butyl at R1; the exception is **15** which has an *n*-butyl at both positions. These analogs present the highest *RDF060e*. A second group consisting of **3**, **5** and **6** has a methyl at R and an alkyl chain of two to five carbons at R1. It is worthwhile mentioning that analog **3** is the only one that has a substitution at R2. A third group consisting of **4**, **7**, **12**, **14** and **16** has compounds with hydrogen atom or methyl as one of the substituents while the other substituent has an alkyl chain length of three to six carbons. Compound **12** is classified as outlier. It presents the most negative hydration energy among the compounds classified as less active. This compound has only a substitution at R, which is a phenyl group with a chlorine atom in the *p* position attached at the end of its alkyl chain. Others compounds classified as less active, the substitution of which occurs only at R, have completely different substituents, they are **14** (*n*-butyl) and **16** (*i*-butyl). Another conclusion from cluster analysis is that the presence of either an *n*-butyl or *i*-butyl at R or R1 causes a great decrease in antimalarial activity, as is verified by analogs **5**, **13**–**16** and **18**.

PLS method

The model built with the aid of the PLS method was based on three latent variables and 15 compounds selected from the training set. The equation which relates the descriptors and biological activity is:

$$\log RA = -0.30RDF060e - 0.45HE + 0.49d(\mathrm{Fe–O_1}) \quad (2)$$

The traditional validation parameters expressed in QSAR terms are: total variance explained = 100 %, R^2 = 0.86, Q^2 = 0.85, *PRESS* = 0.42, *SEP* = 0.17, *s* = = 0.17 and $F_{3,11}$ = 22.52. They support the fact that the model is efficient and hence satisfactory if the complexity of the antimalarial mechanisms and the small number of descriptors (three) selected to build the QSAR model are considered.

According to the PLS equation, the three variables present almost the same magnitude of the coefficients of regression (in absolute value). The model reveals that to achieve high biological potency against *P. falciparum*, a combination of higher values of $d(\mathrm{Fe–O_1})$, lower values of *RDF060e* and more negative values for *HE* are necessary. The predicted and experimental activities reveal a good numerical comparison (Table II). The plot of the correlation between the measured and the predicted log *RA* is shown in Fig. 9. The PLS plot identifies compounds with higher activity (located up) and compounds with lower activity (located down) separately, including compounds from the external validation set. Such classifi-

TABLE II. Experimental and estimated antimalarial activity (log *RA*) by PLS and residuals for the compounds from the training set

Compound	Experimental (ref. 6)	Predicted[a]	Experimental – Predicted
1	0.00	0.22	–0.22
2	0.81	0.60	0.21
3	–0.42	–0.26	–0.16
4	–0.080	–0.29	0.21
5[b]	–0.61	–0.040	–0.57
6	–0.010	–0.050	0.040
7	–0.14	–0.43	0.29
8[b]	0.00	0.41	–0.41
9	0.64	0.61	0.030
10	0.48	0.48	0.00
11	0.050	0.26	–0.21
12	–0.060	–0.080	0.020
13	–0.49	–0.60	0.11
14	–0.78	–0.44	–0.34
15[b]	–0.59	–0.85	0.26
16	–0.39	–0.38	–0.010
17	0.31	0.28	0.030
18	–0.51	–0.49	–0.020
19[b]	0.27	0.67	–0.40

[a]PLS model using three latent principal components and leave-one-out cross-validation; [b]compounds from the external validation set

cation is the same as that achieved by the PCA and HCA methods: no sample appearing in a different class.

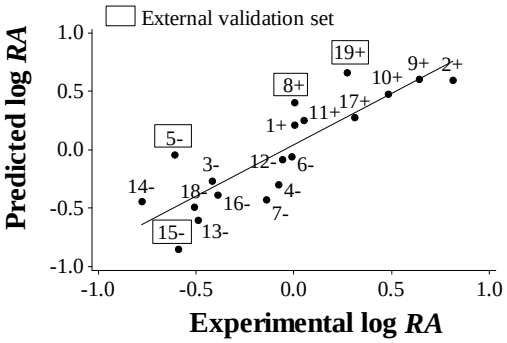

Fig. 9. Experimental *vs.* predicted log *RA* (W-2) for artemisinin and derivatives plotted by PLS model using three latent variables. External validation compounds included.

CONCLUSIONS

The HF method and the 3-21G** basis set revealed themselves to be adequate to optimize the structures of artemisinin and derivatives and consequently their study. *MEP* maps characterized the region of the 1,2,4-trioxane ring for artemisinin and derivatives as a region of negative electrostatic potential. Molecular docking calculations revealed that the Fe^{2+} ion from heme attacks the O_1 from artemisinin more preferably than O_2. The PCA and HCA methods enabled the compounds in the training set to be classified into two groups according to their degree of antimalarial activity against *P. falciparum*. The descriptors *RDF060e*, *HE* and d(Fe–O_1) were the properties responsible for distinguishing compounds with higher or lower antimalarial activity. The combination of these structural attributes is believed to govern the antimalarial response of the compounds studied in this work. The PLS model revealed that the more active compounds have higher values of d(Fe–O_1), lower values of *RDF060e* and more negative values of *HE*. By this strategy, useful information was obtained that could be of use in experimental processes of syntheses and biological evaluation in order to find new efficient drugs against malaria.

Acknowledgements. We acknowledge the financial support of the Brazilian agency Conselho Nacional de Desenvolvimento Científico e Tecnológico. We also thank the Instituto de Química-Araraquara for the use of the GaussView software and the Swiss Center for Scientific Computing for the use of the Molekel software. We employed the computing facilities at the Centro Nacional de Processamento de Alto Desempenho, Universidade Estadual de Campinas, and at the Laboratório de Química Teórica e Computacional, Universidade Federal do Pará.

ИЗВОД

СТУДИЈА НОВИХ АНТИМАЛАРИЈСКИХ АРТЕМИЗИНИНА ПОМОЋУ МОЛЕКУЛСКОГ МОДЕЛИРАЊА И МУЛТИВАРИЈАНТНЕ АНАЛИЗЕ

JOÃO E. V. FERREIRA[1], ANTONIO F. FIGUEIREDO[1], JARDEL P. BARBOSA[1], MARIA G. G. CRISTINO[1], WILLIAMS J. C. MACEDO[1], OSMARINA P. P. SILVA[1], BRUNO V. MALHEIROS[1], RAYMONY T. A. SERRA[2] и JOSE CIRIACO-PINHEIRO[1]

[1]*Laboratório de Química Teórica e Computacional, Faculdade de Química, Instituto de Ciências Exatas e Naturais, Universidade Federal do Pará, Avenida Augusto Correa, 01, CP 101101, CEP 66075-110, Belém, PA, Amazônia и* [2]*Centro de Ciências Biológicas e da Saúde, Universidade Federal do Maranhão, CEP 65085-580, São Luis, MA, Brasil*

Артемизинин и његових 18 деривата који имају антималарично дејство на W-2 сој *Plasmodium falciparum*-а проучаване су методама квантне хемије и мултиваријантне анализе. Оптимизација геометрије је изведена помоћу Хартри-Фокове (ХФ) теорије са базним сетом 3-21G** . Мапе молекулског електростатичног потенцијала (*MEP*) и молекулско доковање су употребљени за истраживање интеракција између лиганда и рецептора (хема). Анализа главне компоненте (*Principal Component Analysis*, PCA) и хијерархијска кластерска анализа (*Hierarchical Cluster Analysis*, HCA) су примењени да би се изабрали најважнији дескриптори у односу на активност. Помоћу методе парцијалних најмањих квадрата (*Partial Least Square*, PLS) генерисан је одговарајући предиктивни модел. Конструкција тог модела базирана је на 15 молекула и још 4 коришћена као сет за спољашњу валидацију; параметри валидације су Q^2 = 0,85 и R^2 = 0,86. Модел укључује следеће молекулске параметре: радијалну функцију расподеле, *RDF060e*, енергију хидратације, *HE*, и растојање између атома O_1 у лиганду и атома гвожђа у хему, d(Fe–O_1). На тај начин могу се синтетисати нови деривати на основу мапа *MEP* и PLS анализе.

(Примљено 26. јануара, ревидирано 12. јуна 2010)

REFERENCES

1. D. M. Opsenica, B. A. Šolaja, *J. Serb. Chem. Soc.* **74** (2009) 1155
2. R. Arav-Boger, T. A. Shapiro, *Annu. Rev. Pharmacol. Toxicol.* **45** (2005) 565
3. N. J. White, *J. Clin. Invest.* **113** (2004) 1084
4. R. G. Ridley, *Nature* **424** (2003) 887
5. P. M. O'Neill, N. L. Searle, K. W. Kan, R. C. Storr, J. L. Maggs, S. A. Ward, K. Raynes, B. K. Park, *J. Med. Chem.* **42** (1999) 5487
6. J. R. Woolfrey, M. A. Avery, A. M. Doweyko, *J. Comput.-Aided Mol. Des.* **12** (1998) 165
7. M. A. Rafiee, N. L. Hadipour, H. Naderi-Manesh, *J. Chem. Inf. Model.* **45** (2005) 366
8. G. Bernardinelli, C. W. Jefford, D. Marić, C. Thomson, J. Weber, *Int. J. Quantum Chem.: Quantum Biol. Symp.* **21** (1994) 117
9. J. C. Pinheiro, R. Kiralj, M. M. C. Ferreira, O. A. S. Romero, *QSAR Comb. Sci.* **22** (2003) 830
10. J. C. Pinheiro, M. M. C. Ferreira, O. A. S. Romero, *J. Mol. Struct. Theochem* **572** (2001) 35
11. F. J. B. Cardoso, A. F. Figueiredo, M. S. Lobato, R. M. Miranda, R. C. O. Almeida, J. C. Pinheiro, *J. Mol. Modell.* **14** (2008) 39
12. F. J. B. Cardoso, R. B. Costa, A. F. Figueiredo, J. P. Barbosa, I. Nava-Junior, J. C. Pinheiro, O. A. S. Romero, *Internet Electon. J. Mol. Des.* **6** (2007) 122

13. R. Guha, P. C. Jurs, *J. Chem. Inf. Comput. Sci.* **44** (2004) 1440
14. F. Cheng, J. Shen, X. Luo, W. Zhu, J. Gu, R. Ji, H. Jiang, K. Chen, *Bioorg. Med. Chem.* **10** (2002) 2883
15. A. K. Bhattacharjee, K. A. Carvalho, D. Opsenica, B. A. Šolaja, *J. Serb. Chem. Soc.* **70** (2005) 329
16. A. Doweyko, *J. Comp.-Aided Mol. Des.* **22** (2008) 81
17. D. J. Creek, D. K. Chalmers, W. N. Charman, B. J. Duke, *J. Mol. Graphics Modell.* **27** (2008) 394
18. P. M. O'Neill, *Expert Opin. Invest. Drugs* **14** (2005) 1117
19. G. A. Biagini, P. M. O'Neill, P. G. Bray, S. A. Ward, *Curr. Opin. Pharmacol.* **5** (2005) 473
20. R. K. Haynes, S. C. Vonwiller, *Tetrahedron Lett.* **37** (1996) 253
21. G. H. Posner, D. Wang, J. N. Cumming, C. H. Oh, A. N. French, A. L. Bodley, T. A. Shapiro, *J. Med. Chem.* **38** (1995) 2273
22. J. Q. Araújo, J. W. M. Carneiro, M. T. Araújo, F. H. A. Leite, A. G. Taranto, *Bioorg. Med. Chem.* **16** (2008) 5021
23. C. W. Jefford, *Curr. Med. Chem.* **8** (2001) 1803
24. P. Gramatica, *QSAR Comb. Sci.* **26** (2007) 694
25. *GaussView 1.0*, Gaussian, Inc., Pittsburgh, PA, 1997
26. C. C. J. Roothaan, *Rev. Mod. Phys.* **23** (1951) 23, 69
27. J. S Binkley, J. A. Pople, W. J. Hehre, *J. Am. Chem. Soc.* **102** (1980) 939
28. *Gaussian 98, revision A.7*, Gaussian, Inc., Pittsburgh, PA, 1998
29. E. Estrada, E. Molina, *J. Mol. Graphics Modell.* **20** (2001) 54
30. *Virtual Computational Laboratory*, VCCLAB 2005, http://www.vcclab.org (accessed January 2010)
31. I. V. Tetko, J. Gasteiber, R. Todeschini, A. Mauri, D. Livingstone, P. Ertl, V. A. Palyulin, E. V. Radchenko, N. S. Zefirov, A. S. Makarenko, V. Y. Tanchuk, V. V. Prokopenko, *J. Comput.-Aided Mol. Des.* **19** (2005) 453
32. *Auto-Dock 4.0*, The Scripps Research Institute, Department of Molecular Biology, MB-5, La Jolla, CA, 2007
33. *Molekel 4.3*, Swiss Center for Scientific Computing, Manno, Switzerland, 2000
34. *ChemPlus, Modular Extensions to HyperChem, Release 6.02*, Molecular Modeling for Windows, Hyper, Inc., Gainesville, 2000
35. J. Vojtechovsky, K. Chu, J. Berendzen, R. M. Sweet, I. Schlichting, *Biophys. J.* **27** (1999) 2153
36. M. M. C. Ferreira, C. A. Montanari, A. C. Gaudio, *Quim. Nova* **3** (2002) 439
37. A. Golbraikh, A. Tropsha, *J. Mol. Graphics Modell.* **20** (2002) 269
38. *Pirouette 3.01*, Infometrix, Inc., Woodinville, WA, 2001
39. M. C. Hemmer, V. Steinhauer, J. Geisteiger, *Vib. Spectrosc*. **19** (1999) 151
40. M. S. Costa, R. Kiralj, M. M. C. Ferreira, *Quim. Nova* **30** (2007) 25
41. S. Tonmunphean, V. Parasuk, S. Kokpol, *J. Mol. Modell.* **7** (2001) 7 26.

Journal of the Serbian Chemical Society
JSCS-info@shd.org.rs • www.shd.org.rs/JSCS
J. Serb. Chem. Soc. 75 (11) 1549–1557 (2010)
JSCS–4075
UDC 546.791.6+546.795.4+546.141+546.181–31:66.061:620.168.3
Original scientific paper

Extraction and separation of U(VI) and Th(IV) from hydrobromic acid media using Cyanex-923 extractant

SNEHAL M. GHAG and SURESH D. PAWAR*

Department of Chemistry, Siddharth College of Arts, Science and Commerce, Dr. D. N. Road, Fort, Mumbai – 400 001, India

(Received 17 June 2009, revised 12 July 2010)

Abstract: A systematic study of the solvent extraction of uranium(VI) and thorium(IV) from hydrobromic acid media was performed using the neutral phosphine oxide extractant Cyanex-923 in toluene. These metal ions were found to be quantitatively extracted with Cyanex-923 in toluene in the acidity range 5×10^{-5}–1×10^{-4} M and 5×10^{-5}–5×10^{-3} M, respectively, and they are stripped from the organic phase with 7.0 M $HClO_4$ and 2.0–4.0 M HCl, respectively. The effect of the equilibrium period, diluents, diverse ions and stripping agent on the extraction of U(VI) and Th(IV) was studied. The stoichiometry of the extracted species of these metal ions was determined based on the slope analysis method. The extraction reactions proceed by solvation and their probable extracted species found in the organic phase were $UO_2Br_2\cdot2$Cyanex-923 and $ThBr_4\cdot2$Cyanex-923. Based on these results, a sequential procedure for their separation from each other was developed.

Keywords: solvent extraction; uranium(VI); thorium(IV); Cyanex-923; stripping; separation.

INTRODUCTION

In last few years, organophosphorous compounds have found wide application in nuclear establishments for the extraction, enrichment and reprocessing of uranium, thorium and plutonium. The new extractant di-(2-ethylhexyl) sulphoxide (DEHSO) is used for the reprocessing of spent Th–U fuel and extraction of U(VI) and Th(IV) from dilute HNO_3 media.[1] Preston *et al.*[2] performed the extraction of U(VI) and Th(IV) from $NaNO_3$ media using *N*-alkylcarboxylic acid amide. Quantitative extraction of Th(IV) and U(VI) from HNO_3 media was investigated by Dhadke *et al.*[3] using bis-(2-ethylhexyl) phosphinic acid (PIA-8) and bis(2-ethylhexyl) phosphoric acid (HDEHP).

* Corresponding author. E-mail: sureshpawar_2004@rediffmail.com
doi: 10.2298/JSC090617118G

The extraction of U(VI) with Th(IV) was performed from nitrate media using extractants such as *N,N'*-tetrahexylbipocolinamide(THBPA) and *N,N'*-tetra(2-ethylhexyl)bipicolinamide, *O*-methyleneoxyphenyldiphosphine dioxide and butyl bis(dibutoxyphosphinylmethyl) phosphinate.[4–6] The separation of Th, La, Eu ions was realised using the acidic extractant bis(2-ethylhexyl) phosphoric acid (DEHPA) in cyclohexane using 2-nitrobenzo-18-crown-6 [NB18(6)].[7] LIX-360 (HX) in kerosene and Versalic-10 was also used for extraction studies of U(VI).[8] In addition, 2-hydroxy-1-naphthaldehyde thiosemicarbazone was used to study the extraction behaviour of Th(IV) from HNO_3 in the presence of donors, trioctylphosphine oxide (TOPO), Calix[3]OH[3]OMe[6]arene, trioctyl amine (TOA) and DMSO in ethyl acetate solvent.[9]

A new chelating polymeric sorbent was developed using Merrifield chloromethylated resin anchored with di-bis(2-ethylhexyl)malonamide (DB2EHM) for the selective extraction of U(VI) and Th(IV) from an acidic stream.[10] The branched chain di(2-ethylhexyl) isobutyramide (D2EHIBA) was chosen as a promising alternative to tri-*n*-butyl phosphate (TBP) for the recovery of U from irradiated Th.[11]

EXPERIMENTAL

Apparatus and reagents

The extractant Cyanex-923, supplied by Cytec Industries Inc. Canada, was used without further purification. Known amounts of uranyl nitrate $UO_2(NO_3)_2{\cdot}6H_2O$ and thorium nitrate $Th(NO_3)_4{\cdot}5H_2O$ were dissolved in water and diluted to 1.0 dm^3 with double distilled water. All other employed chemical were of analytical grade. An Equip-Tronic model EQ-614 pH meter with a combined electrode was used for H^+ concentration studies and an Elico UV–Vis SL-27 spectrophotometer with 10 mm cortex quartz cuvettes was employer for the absorbance measurements.

Procedure

An aliquot of solution containing U(VI) (20 μg) or Th(IV) (20 μg) was taken, diluted to 10 ml and equilibrated with an equal volume of Cyanex-923 diluted in toluene for the required shaking time of 10 min, after adjusting the acidity of the aqueous solution to 1.0×10^{-4} and 1.0×10^{-3} M HBr, respectively. The organic phase containing the extracted metal species was then stripped with different stripping agent, such as HCl, HNO_3, $H2SO_4$ and $HClO_4$. It was found that U(VI) and Th(IV) can be quantitatively stripped from the metal loaded organic phases of Cyanex-923 with 7.0 M $HClO_4$ and 2.0 HCl solutions, respectively, as was determined spectrophotometrically using Arsenazo-I and Thoron-I indicators, respectively.[12] All the experiments were performed at room temperature, except when the effect of temperature on the distribution equilibria was studied.

RESULTS AND DISCUSSION

Effect of acidity and reagent concentration on the percentage extraction of U(VI) and Th(IV)

The effect of acidity on the percentage extraction of U(VI) and Th(IV) with Cyanex-923 in toluene was studied for the acidic range from 5×10^{-5}–1.0 M HBr.

The percentage extraction is the amount of U(VI) or Th(IV) extracted into the organic phase containing Cyanex-923 in toluene. It was found that the extraction of U(VI) and Th(IV) into the organic phase of 0.0025 and 0.001 M Cyanex-923 was quantitative in the acidic range of 5×10^{-5}–1.0×10^{-4} M and 5×10^{-5}–5×10^{-3} M, respectively. Hence, all the extractions of U(VI) and Th(IV) with Cyanex-923 in toluene were performed at a fixed acidic concentration of 1×10^{-4} and 1.0×10^{-3} M HBr solution, respectively (Fig. 1).

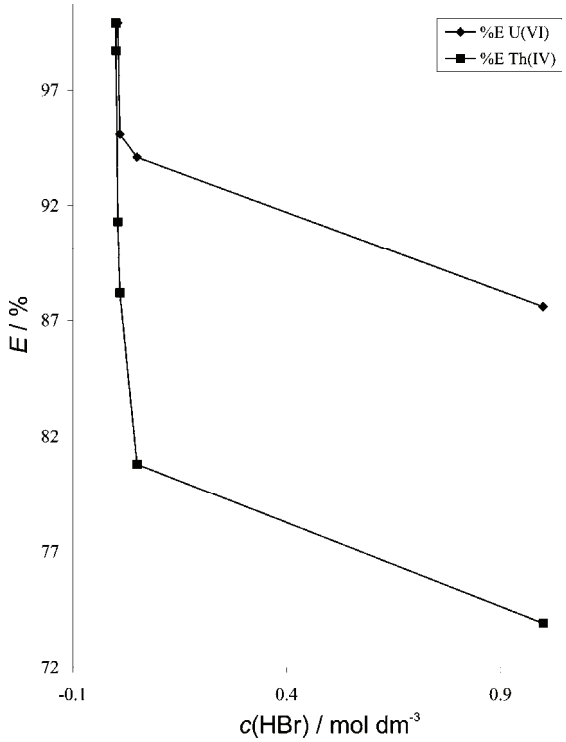

Fig. 1. Effect of acidity on the percentage extraction of U(VI) and Th(IV) with Cyanex-923.

These metal ions were extracted with varying concentrations of Cyanex-923 in toluene from 5×10^{-5}–5×10^{-3} M, while keeping the other parameters, such as pH, period of equilibration, diluent and temperature, constant. The extraction was found to increase with increasing reagent concentration. The extraction of U(VI) and Th(IV) was quantitative with 2.5×10^{-3} and 1×10^{-3} M Cyanex-923, respectively.

Effect of stripping agent

The metal ions were stripped from the metal-loaded organic phases of Cyanex-923 with different strengths of acids such as HCl, HNO_3, H_2SO_4 and $HClO_4$. This process is termed percentage recovery. The complete stripping of U(VI) was observed with 7.0 M $HClO_4$ solution from the organic phase of Cyanex-923.

Th(IV) was stripped quantitatively with 2.0–4.0 M HCl and 1.0–4.0 M HNO_3 solutions (Table I).

TABLE I. Effect of the stripping agent on the percentage extraction of U(VI) and Th(IV) from metal-loaded organic phases of Cyanex-923 in toluene; U(VI): 20 μg; Cyanex-923: 2.5×10^{-3} M; acidity: 1.0×10^{-4} M; Th(IV): 20 μg; Cyanex-923: 1.0×10^{-3} M Acidity;: 1×10^{-3} M

Acid	Acid concentration, mol dm^{-3}							
	1.0	2.0	3.0	4.0	5.0	6.0	7.0	8.0
				U(VI)				
HCl	43.5	42.3	35.5	23.9	14.1	6.7	3.6	1.2
HNO_3	0.0	4.3	6.1	10.4	20.8	36.2	19.6	16.6
H_2SO_4	1.8	3.7	15.9	18.4	–	–	–	–
$HClO_4$	31.9	39.3	41.1	46.6	58.8	66.3	99.9	80.5
				Th(IV)				
HCl	76.2	99.9	99.9	99.9	–	–	–	–
HNO_3	99.9	99.9	99.9	99.9	–	–	–	–
H_2SO_4	3.9	17.8	27.7	46.5	–	–	–	–
$HClO_4$	48.5	62.4	63.4	74.3	77.3	53.5	41.6	38.6

Effect of various diluents

The extraction of U(VI) and Th(IV) was performed with Cyanex-923 using various aromatic and aliphatic organic diluents, such as xylene, benzene, chloroform, *n*-hexane, carbon tetrachloride and cyclohexane. Quantitative extraction of U(VI) was observed with all the diluents. In the case of Th(IV), the extraction was quantitative with all solvents except for *n*-hexane and carbon tetrachloride. Toluene was considered the best diluent for the extraction of U(VI) and Th(IV) since it provided better phase separation (Table II).

TABLE II. Effect of various diluents on the percentage extraction of U(VI) and Th(IV) with Cyanex-923; U(VI): 20 μg; Cyanex-923: 2.5×10^{-3} M; acidity: 1.0×10^{-4} M; Th(IV): 20 μg; Cyanex-923: 1×10^{-3} M; Acidity: 1×10^{-3} M

Diluent	Percentage extraction (*E* / %)	
	U(VI)	Th(IV)
Toluene	99.9	99.9
Cyclohexane	99.9	99.9
n-Hexane	99.9	95.0
Xylene	99.9	99.9
Chloroform	99.9	99.9
Carbon tetrachloride	99.9	97.0

Effect of period equilibration

The extraction equilibrium was studied for different periods of shaking ranging from 1–30 min. It was observed that a 1-min shaking period was sufficient for the quantitative extraction of U(VI) and Th(IV) with Cyanex-923 in toluene,

but there was no adverse effect when the extraction period was extended up to 30 min.

Nature of the extracted species

It was necessary to evaluate the distribution ratio (*D*) while varying the extractant concentration to ascertain the nature of the extracted species. The distribution ratio is the ratio of the concentration of solute in the organic phase to the concentration of the solute in the aqueous phase. Therefore, the composition of the extracted species was first ascertained from graphs of log *D* *vs*. log *R* at a fixed HBr concentration of 1.0×10^{-4} and 1.0×10^{-3} M (Fig. 2). The slopes obtained were 1.92 and 1.83 respectively for U(VI) and Th(IV), indicating that two molecules of ligand react with one molecule of U(VI) and Th(IV). Hence, the probable ratio of the extracted species of U(VI) and Th(IV) with Cyanex-923 was found to be 1:2. Therefore, the probable extracted species of U(VI) and Th(IV) in the organic phase are $UO_2Br2\cdot2$Cyanex-923 and $ThBr_4\cdot2$Cyanex-923.

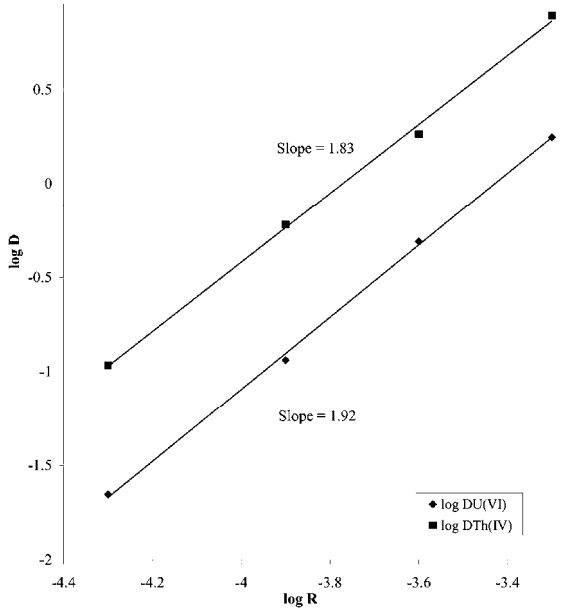

Fig. 2. Effect of reagent concentration on the distribution ratio of U(VI) and Th(IV).
(log *R* = log [Cyanex-923]).

Influence of temperature

Extractions of uranium(VI) and thorium(IV) with 2.5×10^{-3} and 1.0×10^{-3} M Cyanex-923 in toluene at a fixed HBr concentration of 1.0×10^{-4} and 1.0×10^{-3} M were performed at different temperatures (up to 343 K). The distribution ratio decreased with increasing temperature. The Van't Hoff Equation is given by:

$$\log D = -\frac{\Delta H}{2.303RT} + C$$

where D represents the distribution ratio, ΔH is the enthalpy change for the reaction and C is a constant. The slope obtained from the plots of log D *vs.* $1/T$ were 2.45×10^{-3} and 2.77×10^{-3} K for the extraction of U(VI) and Th(IV), respectively (Fig. 3). The obtained ΔH values were – 46.9 and –53.0 kJ mol^{-1}, respectively, indicating that the reaction are exothermic in nature.

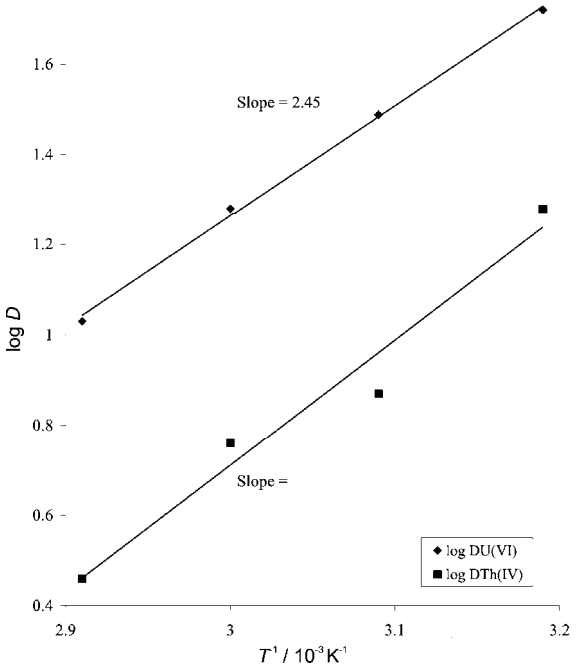

Fig. 3. Effect of temperature on distribution ratio of U(VI) and Th(IV) with Cyanex-923.

Effect of diverse ions

The effects of diverse ions on the extraction of U(VI) and Th(IV) by Cyanex-923 in toluene were studied at a fixed HBr concentration of 1.0×10^{-4} and 1.0×10^{-3} M, respectively. The tolerance limit was set so that the error in the percentage recovery was not more than ±2.0 %.

In case of U(VI), ions such as thiocyanate, thiourea and Zr^{4+} interfere the most with the percentage extraction of U(VI), while ions such as Na^+, K^+, Cs^+, Pb^{2+}, Rb^+, Mg^{2+}, Ca^{2+}, Ba^{2+} and Sr^{2+} are tolerated to a greater extent. In case of Th(IV), ions such as thiocynate, thiourea, Al^{3+}, Be^{2+} and Zr^{4+} interfere to the maximum in the percentage extraction of Th(IV), while Na^+, K^+, Cs^+, Rb^+, Mg^{2+}, Ca^{2+}, Ba^{2+}, Sr^{2+}, Cl^-, Br^-, I^- and SO_3^{2-} are tolerated to a larger extent. The other ions which show intermediate effects are indicated in Table III.

TABLE III. Effect of various diverse ions on the percentage extraction of U(VI) and Th(IV) Cyanex-923 in toluene; U(VI): 20 µg; Cyanex-923: 2.5×10^{-3} M; Acidity: 1.0×10^{-4} M; Th(IV): 20 µg; Cyanex-923: 1.0×10^{-3} M; acidity: 1.0×10^{-3} M

Uranium(VI)						
1:32	1:27	1:22	1:17	1:10	1:6	Strongly interfere
Na^+, K^+, Cs^+, Pb^{2+}, Rb^+, Mg^{2+}, Ca^{2+}, Ba^{2+}, Sr^{2+}	Bi^{3+}, Zn^{2+}, Fe^{3+}, Cr^{3+}	Mn^{2+}, Co^{2+}, Cu^{2+}, Cd^{2+}, Pd^{2+}, Os^{8+}	Rh^{3+}, Au^{3+}, Ru^{3+}	V^{5+}, Mo^{6+}, Pt^{2+}, Ce^{3+}, La^{3+}	Citrate, Oxalate	Thiocynate, thiourea, Zr^{4+}
Thorium(IV)						
Na^+, K^+, Cs^+, Rb^+, Mg^{2+}, Ca^{2+}, Ba^{2+}, Sr^{2+}	Mn^{2+}, Co^{2+}, Cu^{2+}, Cd^{2+}	Cr^{3+}, Fe^{3+}, Zn^{2+}, Bi^{3+}	Pt^{2+}, Pd^{2+}, Os^{8+}, Ru^{3+}	Ce^{3+}, La^{3+}	SO_3^{2-}, Cl^-, I^-, Br^-, citrate, oxalate	Thiocynate, thiourea, Al^{3+}, Be^{3+}, Zr^{4+}, V^{6+}

Mutual separation of uranium(VI) and thorium(IV) with Cyanex-923

The proposed method provides mutual separation of U(VI) and Th(IV). U(VI) was separated mainly from Th(IV) and various other metal ions. This was enabled by exploiting the differences in their respective extracting and stripping conditions. In order to separate U(VI) and Th(IV), the difference in their stripping agents was exploited.

A mixture of U(VI) (20 µg) and Th(IV) (20 µg) was taken and the acidity of the solution was adjusted to 1.0×10^{-4} M. The final volume was made up to 10 ml by the addition of double distilled water. It was then equilibrated with an equal volume of 1.0×10^{-3} M Cyanex-923 in toluene by shaking it in a separating funnel for 10 min at room temperature, whereby both the metal ions were extracted simultaneously. Taking advantage of the difference in the stripping agents, both the metal ions were separated. Th(IV) was stripped first with 1.0 M HNO_3 followed by U(IV) with 7.0 M $HClO_4$.

Separation of U(VI) from Th(IV) was possible. In addition, U(VI) was separated from a mixture containing Be(II), Ce(IV), La(III) and Zr(IV), while Th(IV) was separated from a mixture containing La(III), Zr(IV) and Ce(IV) (Table IV).

TABLE IV. Separation of U(VI) and Th(IV) from multicomponent mixtures with Cyanex-923 in toluene; Acidity: 1.0×10^{-4} HBr; Extractant, Cyanex-923: 1.0×10^{-3} M

No.	Metal ion	Amount taken, µg	Stripping agent	Recovery, %
1.	U(VI)	20	8.0 M $HClO_4$	99.5
	Th(IV)	20	1.0 M HNO_3	99.3
2.	U(VI)	20	8.0 M $HClO_4$	99.5
	Be (II)	50	1.0 M NaOH	99.2
3.	La(III)	50	2.0 M HCl	99.2
	U(VI)	20	8.0 M $HClO_4$	99.5

TABLE IV. Continued

No.	Metal ion	Amount taken, μg	Stripping agent	Recovery, %
4.	U(VI)	20	8.0 M $HClO_4$	99.5
	Th(IV)	20	1.0 M HNO_3	99.3
	Zr(IV)	20	0.5 M NaF	98.8
5.	U(VI)	20	8.0 M $HClO_4$	99.5
	Th(IV)	20	1.0 M HNO_3	99.3
	Ce(IV)	50	Unextracted	99.1
6.	La(II)	50	2.0 M HCl	99.2
	Th (IV)	20	1.0 M HNO_3	99.3
	Ce(IV)	50	Unextracted	99.1

CONCLUSIONS

The U(VI) and Th(IV) were extracted quantitatively in the acid concentration range 5.0×10^{-5}–1.0×10^{-4} M and 5.0×10^{-5}–5.0×10^{-3} M, respectively. The minimum reagent concentration required for the complete extraction of U(VI) and Th(IV) was 2.5×10^{-3} and 1.0×10^{-3} M in toluene, respectively.

A thermodynamic study of the extraction reaction of U(VI) and Th(IV) with Cyanex-923 in toluene was also performed. It revealed that the extraction reaction is exothermic in nature with a value of the enthalpy change of –46.9 and –53.0 kJ mol^{-1}, respectively.

Quantitative extraction of U(VI) and Th(IV) was not possible from HNO_3 media using 4-benzoyl-2,4-dihydro-5-methyl-2-phenyl-3*H*-pyrazol-3-thione (HBMPPT). The addition of petroleum sulphoxides (PSO) was required for significant improvement in the extraction of U(VI) and Th(IV).[13] Cyanex-923 does not require the addition of any other extractant for the quantitative extraction.

The extraction of Th(IV) was possible with 1-phenyl-3-methyl-4-benzyl-5-pyrazolone in 1–1.5 M HCl only when ascorbic acid and ammonium oxalate were used for the extraction,[14] while complete extraction of Th(IV) was possible with Cyanex-923 without a salting out agent.

Tri-*n*-octylphenoxide was used for the separation of Th(IV) and U(VI), but for complete separation, the use of ascorbic acid solution together with an NH_4I/HCl mixture was required.[15] With the proposed method, complete separation of U(VI) and Th(IV) was realized without the addition of such mixtures.

Extraction of U(VI) with Primene JMT required a minimum reagent concentration of 0.3 M in benzene,[16] while Cyanex-923 required a lower concentration, *i.e.*, 2.5×10^{-3} M.

Acknowledgement. The authors are thankful to Cytec Industries Inc. Canada for supplying the gift sample of Cyanex-923.

И З В О Д

ЕКСТРАКЦИЈА И РАЗДВАЈАЊЕ U(VI) И TH(IV) ИЗ БРОМОВОДОНИЧНЕ КИСЕЛИНЕ ПОМОЋУ CYANEX-923 ЕКСТРАКТАНТА

SNEHAL M GHAG и SURESH D PAWAR

Department of Chemistry, Siddharth College of Arts, Science and Commerce, Dr. D. N. Road, Fort, Mumbai – 400 001, India

У раду је систематски испитивана екстракција уранијума(VI) и торијума(IV) из бромоводоничне киселине коришћењем неутралног фосфин-оксида Cyanex-923 у толуену као средству за екстракцију. Нађено је да се ови метални јони квантитативно екстрахују са Cyanex-923 у толуену у осегу концентрације киселине $5{,}0\times10^{-5}$–$1{,}0\times10^{-4}$ и $5{,}0\times10^{-5}$–$5{,}0\times10^{-3}$ M, респективно, и да се из органске фазе одвајају са 7,0 M $HClO_4$ и 2,0–4,0 M HCl, респективно. Испитиван је ефекат дужине успостављања равнотеже, разблаживања, других јона и средства за одвајање на екстракцију U(VI) и Th(IV) и одређен стехиометријски састав екстрахованих врста. Екстракција се одиграва солватацијом, а вероватне екстраховане врсте нађене у органској фази су UO_2Br_2·2Cyanex-923 и $ThBr_4$·2Cyanex-923. На основу ових резултата развијен је и секвенционални поступак за њихово раздвајање.

(Примљено 17. јуна 2009, ревидирано 12. јула 2010)

REFERENCES

1. B. Borong, B. Yazhi, S. Chaohong, W. Gaodong, J. Qian, C. Zhengbai, *J. Radioanal. Nucl. Chem.* **162** (1992) 391
2. J. S. Preston, A. C. du Preez, *Solvent Extr. Ion. Exch.* **13** (1995) 391
3. D. V. Koladkar, P. M. Dhadke, *J. Radioanal. Nucl. Chem.* **253** (2002) 297
4. E. A. Mowafy, A. M. Shalash, I. M. El-Naggar, *Indian J. Chem. A* **42** (2003) 3012
5. A. N. Turanov, V. K. Karandashev, A. M. Fedoseev, N. I. Rodygina, V. E. Baulin, *Radiochemistry* **47** (2005) 177
6. A. N. Turanov, V. K. Karandashev, A. N. Yarkevich, *Radiochemistry* **47** (2005) 570
7. A. A. Zamani, M. R. Yaftian, *Sep. Purif. Technol.* **40** (2004) 115
8. S. P. Mohanty, I. Mohanty, S. Mishra, V. Chakravortty, *J. Radioanal. Nucl. Chem.* **227** (1998) 99
9. S. Banerjee, S. Basu, *Radiochim. Acta* **91** (2003) 97
10. D. Prabhakaran, M. S. Subramanian, *Talanta* **65** (2005) 179
11. P. N. Pathak, D. R. Prabhu, A. S. Kanekar, P. B. Raikar, A. Bhattacharyya, P. K. Mohapatra, V. K. Manchanda, *Ind. Eng. Chem. Res.* **43** (2004) 4369
12. W. W. Philip, C. Maria, *Anal. Chem.* **21** (1949) 628
13. S. Yu, L. Ma, B. Bao, *J. Radioanal. Nucl. Chem.* **241** (1999) 347
14. H. C. Arora, *J. Indian Chem. Soc.* **69** (1992) 346
15. A. M. Afinogenov, Y. A. Spazhnikov, I. P. Yefimov, V. M. Ivanov, *Vestn. Mosk. Univ., Ser. 2: Khim.* **41** (2000) 62 (in Russian)
16. P. Nekovar, D. Schroetterova, M. Mrnka, *J. Radioanal. Nucl. Chem.* **223** (1997) 17.

Journal of the Serbian Chemical Society
JSCS-info@shd.org.rs • www.shd.org.rs/JSCS
J. Serb. Chem. Soc. 75 (11) 1559–1574 (2010)
JSCS–4076
UDC 547.262+66.094.3:546.92+544.478:539.12
Original scientific paper

Comparative study of ethanol oxidation at Pt-based nanoalloys and UPD-modified Pt nanoparticles

AMALIJA V. TRIPKOVIĆ*#, JELENA D. LOVIĆ# and KSENIJA DJ. POPOVIĆ#

ICTM – Institute of Electrochemistry, University of Belgrade, Njegoševa 12, P.O. Box 473, 11000 Belgrade, Serbia

(Received 19 May, revised 30 June 2010)

Abstract: The activity of two alloys, Pt_3Sn/C and Pt_3Ru_2/C, was compared with the activity of Pt/C modified with corresponding amounts of Sn_{UPD} (≈25 %) and Ru_{UPD} (≈40 %) in the oxidation of ethanol. Pt_3Sn/C, Pt_3Ru_2/C and Pt/C catalysts were characterized by XRD analysis. To establish the activity and stability of the catalysts, potentiodynamic, quasi steady-state and chronoamperometric measurements were performed. Both alloys are more active than Sn_{UPD}- or Ru_{UPD}-modified Pt/C catalysts. The electronic effect determining dominantly the activity of Pt_3Sn/C is the main reason for its higher activity compared to Pt_3Ru_2/C. Since Sn_{UPD} and Ru_{UPD} do not provoke any significant modification of electronic environment, both modified Pt/C catalysts were less active than the corresponding alloys. More pronounced difference in activity between Pt_3Sn/C and Sn_{UPD}-modified Pt/C than between Pt_3Ru_2/C and Ru_{UPD}-modified Pt/C is caused by the electronic effect in Pt_3Sn/C. The high activity of Pt_3Sn/C modified with a small amount of Sn_{UPD} (≈10 %) can be explained by combining the electronic effect, causing less strongly bonded adsorbate on Pt sites and easier mobility of the Sn_{UPD}, with an enhanced amount of oxygen-containing species on the Sn sites, resulting finally in a reinforcement of the bi-functional mechanism.

Keywords: ethanol oxidation; platinum–tin nanocatalyst; platinum–ruthenium nanocatalyst, platinum nanocatalyst; underpotential deposition.

INTRODUCTION

Ethanol is promising fuel for direct alcohol low temperature fuel cells due to is low toxicity, high energy density, mass production from renewable sources and easy storage and transportation. However, the lack of an efficient and selective anode catalyst able to break the C–C bond providing complete oxidation to CO_2 with an exchange of 12 e^- per molecule and to oxidize the adsorbed fragments

* Corresponding author. E-mail: amalija@tmf.bg.ac.rs
# Serbian Chemical Society member.
doi: 10.2298/JSC100519093T

produced by ethanol dissociation is, at present, the main problem for a practical use of ethanol in a direct ethanol fuel cell (DEFC).

Despite of fact that platinum is generally known as one of the best electrocatalysts for alcohol oxidation at low temperatures, it has limited capability for C–C bond scission and is easily poisoned by CO and other carboneous intermediates.[1–5] To improve its electrocatalytic activity, especially at potentials of technical interest (E < 0.6 V *vs*. RHE), Pt is modified by the addition of transition metals, providing oxygen-containing species at low potentials which facilitate the oxidative removal of poisoning species through a bifunctional mechanism.[6] The addition of the second metal to platinum (by underpotential deposition or alloying) creates bimetallic catalysts and changes the electronic and structural properties of the base material thereby influencing its catalytic properties. It also alters the number of large Pt ensembles on platinum surfaces, which are important for site demanding processes such as C–C bond cleavage. All these effects influence ethanol oxidation on bimetallic catalysts.

Of all other studied bimetallic catalysts, PtSn/C and PtRu/C catalysts demonstrated the best performance in ethanol oxidation.[7–15]

The electronic effect induced by charge transfer from Sn to Pt was reflected as a negative shift in the Pt 4f binding energies in the XPS spectra of various PtSn/C catalysts.[16] This finding was supported by 1.1 eV shift in the X-ray near edge spectrum (XANES)[17] as well as by X-ray absorption spectroscopic studies (XAS), which demonstrated a partial filing of the Pt 5d-bands.[18]

The relevant results obtained for PtRu/C catalysts by means of different spectroscopic techniques are rather controversial. The XAS spectra revealed electron transfer from Pt to Ru in Pt–Ru/C catalysts,[18] while, on the contrary, the XPS data showed no significant electronic effect in Pt–Ru alloys.[16] The latter results were explained by the similar electronegativity values for Pt and Ru, in contrast to the values for Pt and Sn which differ appreciably.

Incorporation of Sn atoms in the *fcc* Pt lattice enhances the Pt–Pt bond distance, thereby altering the structural characteristic of the base metal. The extended Pt–Pt distance could facilitate the dissociative adsorption of ethanol molecules and promote the reaction.[15,19–21] However, the reduced Pt–Pt distance caused by the addition of Ru to Pt should not be favorable for dissociative adsorption of ethanol.[10,15,19]

From the viewpoint of the role of an ensemble effect in the oxidation of ethanol on PtRu/C[7] and PtSn/C[22] catalysts with different ratios between Pt and the alloying atoms, it was suggested that an increase of the Ru or Sn content may cause a negative effect on the selectivity of the catalysts towards CO_2 formation by decreasing the Pt ensembles required for the dissociative adsorption of ethanol.

Recently, the activity of Pt–Sn/C and Pt–Ru/C in ethanol oxidation was correlated with the degree of alloying. Although the results reported so far are ge-

nerally not unambiguous, most of them indicate that highly alloyed catalysts promote ethanol oxidation.[8,23–27]

Underpotential deposition (UPD) of Sn or Ru at Pt/C does not significantly perturb Pt structurally or electronically, as was shown in spectroscopic studies.[16,18,28] The catalytic action of both atoms was associated mostly with their ability to adsorb oxygenated species at lower potentials than Pt, permitting the bifunctional mechanism to proceed.

In this work, ethanol oxidation was studied at two alloys, Pt_3Sn/C and Pt_3Ru_2/C, as well as at a Pt/C catalyst modified with the corresponding amounts of Sn_{UPD} (25 %) and Ru_{UPD} (40 %). This comparative investigation based on the effects influencing the catalytic properties of these electrodes enabled a better understanding of the differences in the activities of the alloys, as well as those of the alloys and Pt/C modified by underpotentially deposited Sn and Ru. This approach, which to the best of our knowledge, has not been used so far, resulted finally in the comprehension of the superior activity of the catalyst created by modification of Pt_3Sn/C with a small amount of Sn_{UPD} (≈ 10 %).

EXPERIMENTAL

Electrode preparation

Commercially available Pt-based catalysts supported on high surface area carbon were used: Pt_3Sn/C (20 wt. %) provided by E-Tek, and Pt_3Ru_2/C (33.5 wt. %) and Pt/C (47.5 wt. %) provided by Tanaka Precious Metals Group (Kikinzoku International K.K). The catalysts were applied to a glassy carbon substrate in the form of a thin-film.[10] A suspension of 5 mg of the catalyst in a mixture of 1 ml water, 1 ml ethanol and 50 μl of a 5 % aqueous Nafion solution was prepared in an ultrasonic bath and 10 μl of the suspension was placed onto the substrate (5 mm diameter) and dried at room temperature to form a homogenous catalyst layer. The resulting metal loading was 25 μg cm^{-2}.

To avoid the contribution of any other anions, Sn or Ru adlayers were prepared by holding freshly prepared electrodes at –0.2 V in 0.1 M $HClO_4$ solution containing Sn or Ru ions, generated by dissolution of Sn or Ru from the alloy matrix during cycling (20 cycles) of the Pt_3Sn/C and Pt_3Ru_2/C electrodes up to 0.70 V or 1.10 V, respectively. The Sn or Ru modified electrode was then rinsed with water and transferred to the electrochemical cell.

Characterization of the catalysts

The Pt/C, Pt_3Ru_2/C and Pt_3Sn/C catalysts were characterized by X-ray diffraction (XRD) analysis. The XRD measurements were realized using a Siemens D5005 (Bruker-AXS) diffractometer with a Cu Kα source operating at 40 mA and 40 kV and a graphite monochromator.

The quantitative analysis of the phase content and crystallite size calculations were performed by multiphase Rietveld refinement using Topas software and the Fundamental Parameters approach for the modeling of the peak shape. The Pt(220) diffraction peak was used to calculate the average crystallite size according to the Scherrer Equation.

Electrochemical measurements

Electrochemical measurements were performed at room temperature in a nitrogen-purged 0.1 M $HClO_4$ solution in a standard three compartment electrochemical cell with a Pt wire

as the counter electrode and a saturated calomel electrode (SCE) as the reference. The employed reagents were of p.a. purity (Merck) and the solutions were prepared with high purity water ("Millipore", 18 MΩ cm resistivity). Ethanol (0.5 M) was added to the solution while holding the electrode potential at –0.2 V. The catalytic activity was measured using the potentiodynamic (sweep rate 20 mV s^{-1}), quasi-steady-state (sweep rate 1 mV s^{-1}) and chronoamperometric methods. The current–time transient curves were recorded during 30 min upon the immersion of the electrode in the solution at –0.2 V and holding for 2 s prior to stepping at 0.2 V. For the CO stripping measurements, pure CO was bubbled through the electrolyte for 20 min while keeping the electrode potential at –0.2 V *vs.* SCE. After purging the electrolyte with N_2 for 30 min to eliminate the dissolved CO, the adsorbed CO was oxidized in an anodic scan (20 mV s^{-1}). Two subsequent voltammograms were also recorded to verify the completeness of the CO oxidation.

A VoltaLab PGZ402 (Radiometer Analytical, Lyon, France) was used in the electrochemical experiments.

The potentials are given *versus* SCE. The current densities are normalized to the active surface area.

The active surface area for Pt_3Sn/C, Pt_3Ru_2/C and Pt/C was calculated from the the charge of CO stripping, assuming 420 μC cm^{-2} for a CO monolayer (Fig. 1). The CO stripping voltammograms were corrected for the background currents to eliminate the contribution of the double layer charge, as well as Sn and Ru oxidation charges.[29]

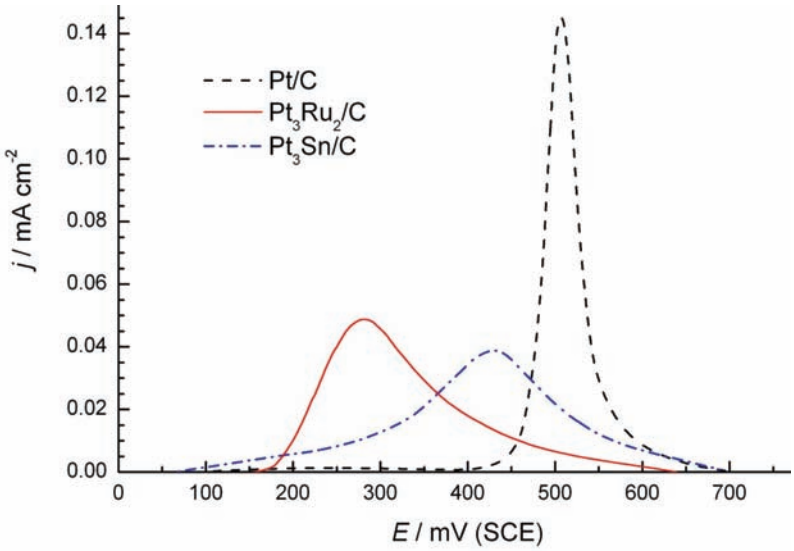

Fig. 1. CO stripping voltammograms at Pt/C, Pt_3Ru_2/C and Pt_3Sn/C catalysts in 0.1 M $HClO_4$ corrected for the background current; ν = 20 mV s^{-1}.

RESULTS AND DISCUSSION

Catalysts characterization

The X-ray diffraction patterns of Pt_3Sn/C, Pt_3Ru_2/C and Pt/C catalysts are presented in Fig. 2. All samples display four characteristic peaks of the face cen-

tered cubic (*fcc*) crystalline structure of Pt, *i.e.*, (111), (200), (220) and (311). No peaks for either Sn or Pt oxides were found. However, this does not mean that they were not present; they could be present but in undetectably small amounts or in an amorphous form. The poorly resolved peak at ≈ 43.8° on the diffractogram for the Pt_3Ru_2/C catalyst is assigned to the hexagonal Ru phase (*hcp*). Two broad peaks that appeared at 14.0 and 30.9° are related to the carbon support material.

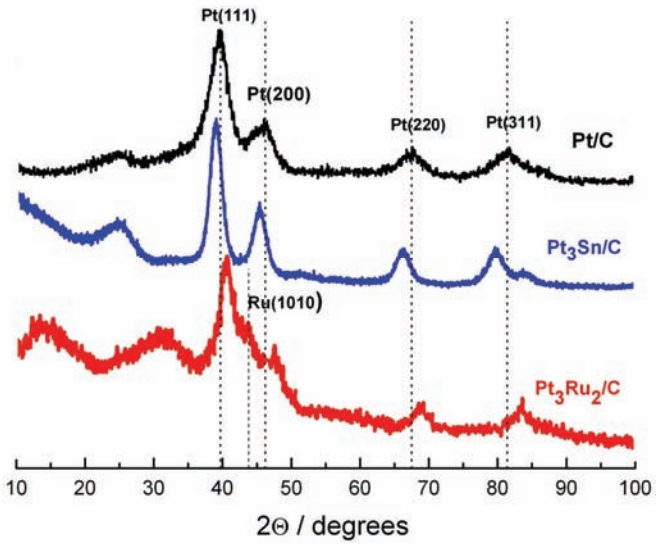

Fig. 2. XRD Patterns of Pt_3Sn/C, Pt_3Ru_2/C and Pt/C catalysts. Vertical lines represent the position of the peaks of pure Pt and pure Ru.

Addition of Sn or Ru to Pt leads to an expansion or contraction of the Pt lattice, respectively, caused by their different atomic sizes in respect to that of Pt (R_{Sn} = 1.61 Å, R_{Ru} = 1.34 Å, R_{Pt} = 1.39 Å), which correspondingly shifts the peaks in opposite directions compared to Pt/C.

The lattice parameters calculated from the (220) peak as well as the mean crystallite diameters are listed in Table I. The atomic fractions of Sn and Ru (x_{Me}) and alloying degree (M_{alloy} / %) calculated *via* the Vegard law[8] are also given in Table I. The atomic fraction of Sn, x_{Sn} = 0.243 is close to the nominal content of 0.25 in the Pt_3Sn/C catalyst, indicating that almost all the Sn atoms

TABLE I. XRD Analysis of Pt/C, Pt_3Ru_2/C and Pt_3Sn/C catalysts

Catalysts	Nominal content (Pt:Me)	Mean crystallite diameter, nm	Lattice parameter nm	x_{Me}	M_{alloy} %
47.5 wt. % Pt/C	–	3.9	0.39166	–	–
33.5 wt. % Pt_3Ru_2/C	60:40	4.5	0.3871	0.368	87.4
20 wt. % Pt_3Sn/C	75:25	5.2	0.398385	0.243	96.4

were alloyed to Pt. The atomic fraction of Ru, x_{Ru} = 0.368, is slightly below the nominal content of 0.4 in Pt_3Ru_2/C, implying that most of the Ru atoms were incorporated in the *fcc* Pt structure. This was confirmed by the corresponding alloying degrees of 96.4 % for Pt_3Sn/C and 87.4 % for Pt_3Ru_2/C.

Ethanol oxidation

The polarization curves for ethanol oxidation on Pt_3Sn/C, Pt_3Ru_2/C and Pt/C catalysts in acid solution are given in Fig. 3. The positive potentials were limited to 0.3 V to avoid any Sn or Ru dissolution.

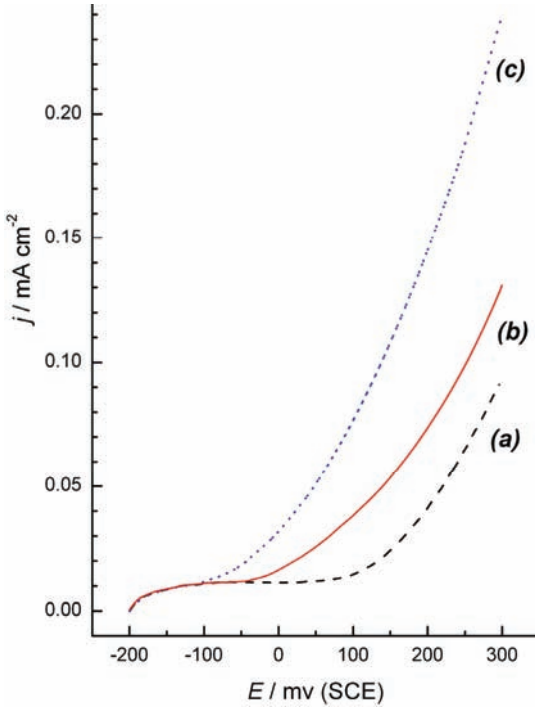

Fig. 3. Potentiodynamic curves for the oxidation of 0.5 M C_2H_5OH at Pt/C (curve a), Pt_3Ru_2/C (curve b) and Pt_3Sn/C (curve c) catalysts in 0.1 M $HClO_4$; ν = 20 mV s^{-1}.

The Pt/C catalyst exhibited a low activity (curve a). The reaction commenced at ≈ 0.1 V when the dissociative adsorption of water occurred, providing OH_{ad} species[30] needed for the oxidation of adsorbate containing C_1 fragments (mostly CO_{ad}[11,14] and CH_x[5]) and C_2 fragments generated by the dissociative adsorption of ethanol.[3,8]

Both alloys were more active than Pt/C. The onset potentials on the Pt_3Ru_2/C (curve b) and Pt_3Sn/C (curve c) catalysts are shifted to less positive potentials with respect to Pt/C by ≈ 0.15 and ≈ 0.25 V, respectively. The catalytic action of Sn or Ru in the corresponding Pt-based alloys was correlated generally by their ability to dissociate water at lower potentials than Pt, enabling the bifunctional

mechanism between the adsorbate on the Pt and the OH species adsorbed on the added metals to proceed.[6] However, the superior activity of Pt_3Sn/C with respect to Pt_3Ru_2/C catalyst requires further analysis.

Alloying Sn to Pt causes an electronic modification due to the Pt–Sn interaction. An electronic modification in the unfilled d-band states of Pt atoms in various PtSn catalysts has been evidenced by spectroscopic techniques.[16–18,22] Characteristic for Sn is the decrease of the local density of states at the Fermi level, which is in direct correspondence with the lowering of the energy of the d-band center. Therefore, CO binds more weakly on a Pt_3Sn surface than on a pure Pt surface, which is in accordance with the downshift of the d-band centers of the platinum atoms.[31,32] The Sn atom is not a strong acceptor of electrons from water molecules and forms a weak bond with OH.[22,33] Both phenomena should be beneficial for ethanol oxidation.

Incorporation of Sn atoms in the *fcc* Pt lattice leads to an expansion of the lattice parameter, as revealed by XRD analysis (Table I), changing the structure of the Pt-based material. The elongation of lattice parameter may facilitate C–C bond cleavage thus improving the catalytic activity.[15,20,21] A DFT calculation supports this assumption, indicating that surface transition species originating from ethanol are sensitive to the bond length and angle.[34]

As the Pt_3Sn/C catalyst had the high alloying degree of 96.4 %, it is reasonable to assume that both effects, electronic and structural, could be the origin of its high activity. On the other hand, C–C bond cleavage is a site demanding process requiring at least two adjacent (ensemble) binding Pt sites as the C–C bond length is 1.5 Å and the atomic diameter of Pt is 1.39 Å. This means that larger Pt ensembles are required for C–C bond breakage, while on smaller Pt ensembles, incomplete ethanol oxidation to acetaldehyde and acetic acid should be promoted. The number of the large Pt ensembles is generally diminished by incorporation of Sn into the Pt lattice, but it may be simultaneously compensated with the structural effect originating from the expansion of the Pt–Pt distance (Table I). However, it should be pointed out that the selectivity of Pt_3Sn/C or other PtSn/C catalysts towards CO_2 formation was not improved significantly with respect to a Pt/C catalyst.[4,7,8,10,23]

Electron transfer from Pt to Ru in the Pt_3Ru_2/C catalyst[18] decreases the bond strength between Pt and adsorbate produced from ethanol.[32] Moreover, the decreased Pt–Pt bond distance seems to be unfavorable for C–C bond cleavage.[10]

If electronic and structural effects are not beneficial for ethanol oxidation, than the promotion of catalytic activity of Pt_3Ru_2/C with respect to Pt/C arises mainly from the ability of Ru atoms to dissociate water at lower potentials compared to Pt, providing oxygen-containing species to oxidize the adsorbed fragments generated from ethanol. However, although the capability of Ru atoms to dissociate water is larger than Sn atoms,[16] Pt_3Ru_2/C is significantly less active

than Pt_3Sn/C in ethanol oxidation most likely due to the slightly stronger bonded adsorbate, *i.e.*, higher poisoning of the surface.

Electronic effect dominantly determined the activity of the Pt_3Sn/C catalyst in ethanol oxidation and it is the main reason for its higher activity with respect to Pt_3Ru_2/C.[35] The structural or ensemble effects seems to be less important, since the selectivity for oxidation to CO_2 is not significantly increased on both catalysts compared to Pt/C.[19]

The stability of the catalysts was studied in chronoamperometric experiments (Fig. 4). The highest initial current density at 0.2 V on Pt_3Sn/C related to the other two catalysts is in accordance with the potentiodynamic measurements (Fig. 3). The currents decay rapidly at Pt/C and Pt_3Ru_2/C catalysts, reaching their steady state values within a few minutes. On the other hand, the initial current decreases slightly at Pt_3Sn/C and stabilizes in the experimental period of time at a value which is about two times higher than at the Pt_3Ru_2/C catalyst. The Pt_3Sn/C catalyst is evidently less poisoned than Pt_3Ru_2/C or Pt/C.

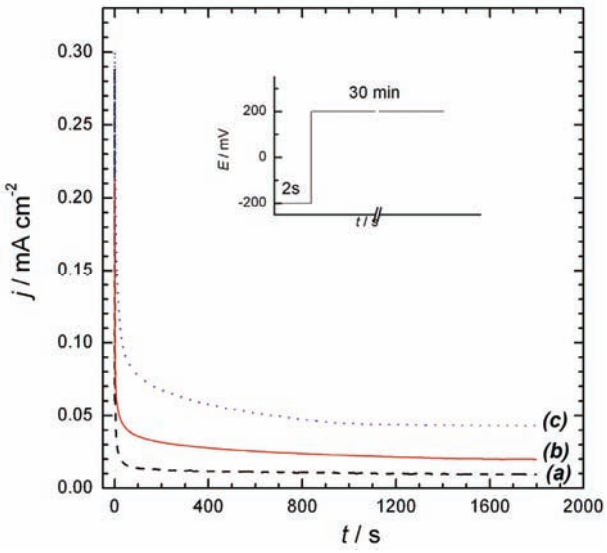

Fig. 4. Chronoamperometric curves for the oxidation of 0.5 M C_2H_5OH at 0.2 V at Pt/C (curve a), Pt_3Ru_2/C (curve b) and Pt_3Sn/C (curve c) catalysts in 0.1 M $HClO_4$.

Ethanol oxidation at Pt_3Sn/C, Pt/C and the Sn_{UPD}-modified Pt/C and Pt_3Sn/C catalysts and the corresponding basic voltammograms are displayed in Fig. 5.

The decrease of charge in the hydrogen region of ≈ 25 % between Pt/C and the Sn_{UPD}-modified Pt/C catalyst (Fig. 5A) can be related to the coverage with Sn_{UPD}, assuming that hydrogen does not adsorb on Sn.[36]

The activity of Pt/C catalyst was improved by the Sn_{UPD} layer (Fig. 5C). The reaction commences at ≈ 0.0 V (curve a'), *i.e.*, at ≈ 0.1 V less positive potentials relative to Pt/C (curve a).

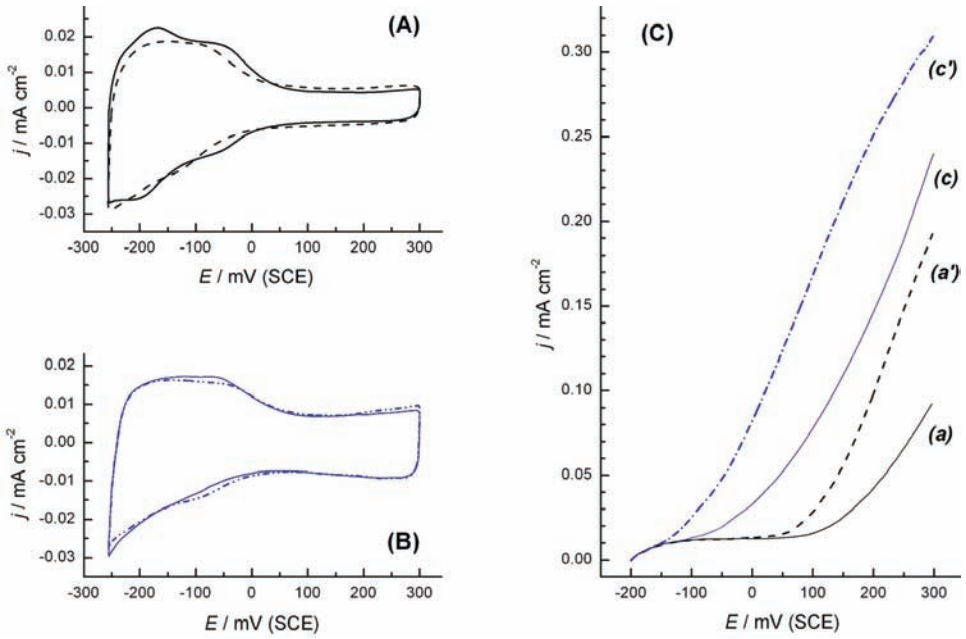

Fig. 5. (A) Basic voltammograms of Pt/C (solid line) and Pt/C modified with 25 % Sn_{UPD} (dash line); (B) basic voltammograms of the Pt_3Sn/C electrode (solid line) and Pt_3Sn/C modified with 10 % Sn_{UPD} (dash-dot line); (C) potentiodynamic curves for the oxidation of 0.5 M C_2H_5OH in 0.1 M $HClO_4$ at Pt/C (curve a), at Pt/C modified with 25 % Sn_{UPD} (curve a'), at Pt_3Sn/C (curve c) and at Pt_3Sn/C modified with 10 % Sn_{UPD} (curve c'); $\nu = 20$ mV s^{-1}.

Comparison of Pt_3Sn/C containing ≈ 25 at. % of Sn (curve c) with Pt/C modified by the same amount of Sn_{UPD} (curve a') reveals clearly that the alloy is considerably more active. The onset of the reaction at Pt_3Sn/C is shifted by more than 0.1 V to less positive potentials and the current densities are enhanced. Spectroscopic analysis of Sn_{UPD} on Pt/C shows that the Sn_{UPD} interacts with oxygen species similarly as in Pt_3Sn/C alloy, but the underpotential deposition of Sn on Pt/C induces much smaller electronic changes in Pt/C than in Pt_3Sn/C.[28] This means that Sn_{UPD} does not interfere remarkably with the ability of Pt to adsorb strongly ethanol or the adsorbate generated by ethanol dissociation, which should be the main reason for the lower activity of the Sn_{UPD} modified Pt/C with respect to Pt_3Sn/C.

The small amount of Sn (≈ 10 %) electrodeposited on Pt_3Sn/C (Fig. 5B) promotes the activity of the alloy (Fig. 5C, curve c'), creating a powerful catalyst for ethanol oxidation as was shown in the literature.[37] The high activity of this catalyst can be explained by combining the electronic effect, causing less strongly bonded adsorbate on the Pt sites, and the easier mobility of Sn_{ad},[38] with enhanced amount of oxygen-containing species on the Sn sites, resulting, as a final consequence, in a reinforcement of the bifunctional mechanism.

Using the same approach, ethanol oxidation was examined at Pt_3Ru_2/C containing 40 % of Ru (Fig. 6B) and compared with the Pt/C catalyst modified with approximately the same amount (≈ 40 %) of Ru_{UPD}, (Fig. 6C, curves b and a", respectively). The decrease of charge in the hydrogen region of ≈ 40 % between Ru_{UPD} modified and unmodified Pt/C catalyst (Fig. 6A) can be attributed to the coverage with Ru_{UPD} on the Pt sites, assuming that the maximal coverage of Ru by H adatoms is ≈ 15 %.[39,40]

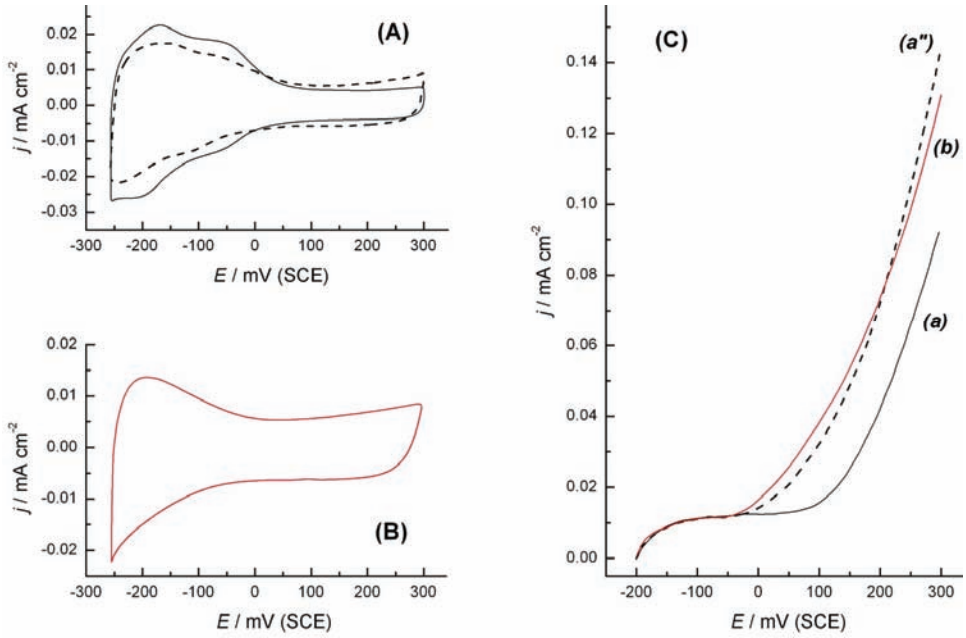

Fig. 6. (A) Basic voltammograms of Pt/C (solid line) and Pt/C modified with 40 % Ru_{UPD} (dash line); (B) basic voltammogram of Pt_3Ru_2/C electrode; (C) potentiodynamic curves for the oxidation of 0.5 M C_2H_5OH in 0.1 M $HClO_4$ at Pt/C (curve a), at Pt/C modified with 40 % Ru_{UPD} (curve a'') and at Pt_3Ru_2/C (curve b); ν = 20 mV s^{-1}.

Inspection of the results given in Fig. 6C shows a significant difference in respect to the corresponding results obtained at Pt_3Sn/C and Sn_{UPD} modified Pt/C catalysts (Fig. 5C). The substantial easily recognized contrast is the small difference between the activity of Pt_3Ru_2/C (curve b) and that of the Pt/C modified by the same amount of underpotentially deposited Ru (curve a"). This is reliable proof that electronic or structural effects do not provoke a significant influence on the activity of Ru alloyed Pt catalysts. In this context, the high alloying degree of 87.4 % (Table I) is not as relevant for an estimation of the catalytic properties of Pt_3Ru_2/C as it is in a case of the Pt_3Sn/C catalyst. Since underpotential deposition of Ru on Pt/C does not provoke significant electronic changes in Pt/C,[16,18] ethanol oxidation on the respective catalysts obeys the con-

ditions relevant for the bifunctional mechanism. In this sense, the ratio between Pt sites, which adsorb ethanol, and Ru sites, which nucleate oxygen species to oxidize that adsorbate, becomes crucial. The ratio Pt/Ru = 60:40 fulfilled in Pt_3Ru_2/C as well as in Pt/C modified by 40 % of Ru_{UPD} provide the best catalytic performance.[41] The addition of ≈ 10 % Ru_{UPD} on Pt_3Ru_2/C or enhancement of the amount of Ru_{UPD} on Pt/C at 50 % decreases the activity of both catalysts, respectively (not shown).

The activities of the catalysts studied in ethanol oxidation obtained under quasi-steady state conditions are given in Figs. 7 and 8. In these plots, the cur-

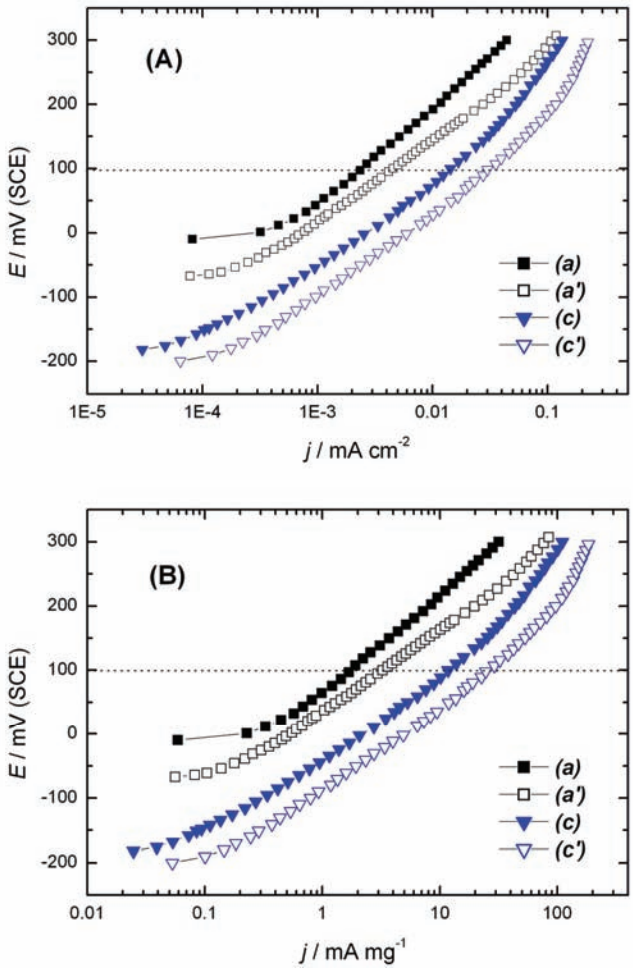

Fig. 7. Tafel plots for the oxidation of 0.5 M C_2H_5OH in 0.1 M $HClO_4$ solution at: Pt/C (curve a), Pt/C modified with 25 % Sn_{UPD} (curve a'), Pt_3Sn/C (curve c) and Pt_3Sn/C modified with 10 % Sn_{UPD} (curve c'). (A) Current density normalized to the active surface area of the respective catalysts; (B) mass specific current density; ν = 1 mV s^{-1}.

rents are given either as active surface area normalized current densities (Figs. 7A and 8A) or as mass normalized currents (Figs. 7B and 8B). The Pt_3Sn/C is more active than the Pt/C modified by Sn_{UPD} (≈ 25 %) catalysts (Fig. 7) and considerably more active than Pt/C. The activity of Pt_3Ru_2/C and Pt/C modified by Ru_{UPD} (≈ 40 %) are similar, but both catalysts are more active than Pt/C (Fig. 8). The activity of the respective catalysts at E = 0.1 V (SCE) summarized in Table II show that the ratio of the activity between the alloys and corresponding Sn_{UPD}- or Ru_{UPD}-modified Pt/C is generally maintained regardless of whether the currents are given as active surface area or as mass specific currents.

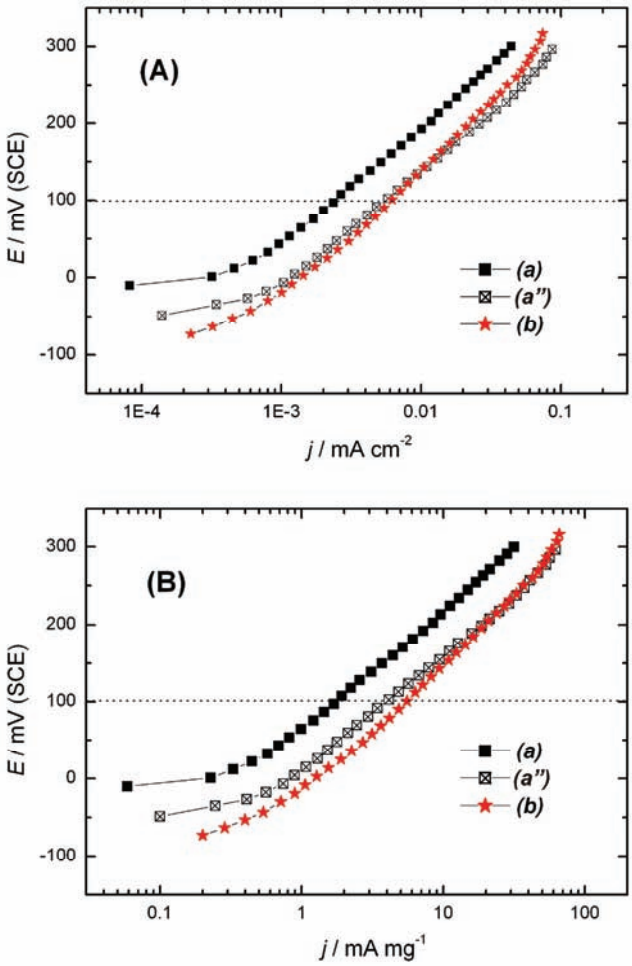

Fig. 8. Tafel plots for the oxidation of 0.5 M C_2H_5OH in 0.1 M $HClO_4$ solution at: Pt/C (curve a), Pt/C modified with 40 % Ru_{UPD} (curve a'') and Pt_3Ru_2/C (curve b). (A) Current density normalized to the active surface area of the respective catalysts; (B) mass specific current density; ν = 1 mV s^{-1}.

Pt_3Sn/C modified by ≈ 10 % Sn_{UPD} is the best catalyst studied. Its activity enhanced more than two times in respect to Pt_3Sn/C catalyst is close to the activity attained at ternary Pt/Rh/SnO_2 catalyst.[42–44]

TABLE II. Activity of the respective catalysts at E = 0.1 V (SCE)

Catalysts	Pt/C	Pt/C + 25 % Sn_{UPD}	Pt_3Sn/C	Pt_3Sn/C + 10 % Sn_{UPD}	Pt_3Ru_2/C	Pt/C + 40 % Ru_{UPD}
j / mA mg^{-1}	1.69	3.25	11.75	25.6	5.45	4.02
j / mA cm^{-2}	2.4×10^{-3}	4.6×10^{-3}	14.2×10^{-3}	31.3×10^{-3}	6.2×10^{-3}	5.5×10^{-3}

Tafel slopes of ≈ 120 mV dec^{-1} obtained at Pt_3Sn/C and Sn_{UPD} modified Pt/C catalysts indicate that the first electron transfer could be the rate determining step.[23] Higher Tafel slopes of 140–150 mV dec^{-1} at Pt/C, Pt_3Ru_2/C and Ru_{ad} modified Pt/C catalysts are caused by a large poisoning of Pt.[45]

CONCLUSIONS

According to the results obtained in this work dealing with the effects influencing the overall ethanol oxidation on the studied catalysts, the following conclusions can be reached.

Both alloys are more active than Pt/C. Pt_3Sn/C is more active than Pt_3Ru_2/C or the corresponding Sn_{UPD}- or Ru_{UPD}-modified Pt/C catalysts as revealed from potentiodynamic and quasi steady state measurements. Its high activity originates mainly from the electronic effect causing the weakly bonded adsorbate generated by ethanol adsorption on the Pt sites and the appropriate amount of oxygen-containing species labile bound to Sn to oxidize the adsorbate through the bifunctional mechanism. It was concluded that the promoted OH generation is the primary reason for the enhanced activity towards ethanol oxidation on the Pt_3Ru_2/C catalyst.

Since underpotential deposition of Sn or Ru does not provoke any significant electronic effect, both the modified Pt/C catalysts were less active than the corresponding alloys. Accordingly, the more pronounced difference between the Pt_3Sn/C and the Sn_{UPD}-modified Pt/C (25 % Sn) as compared to the difference between Pt_3Ru_2/C and the Ru_{UPD}-modified Pt/C (40 % Ru) is caused by the electronic effect in Pt_3Sn/C.

Modification of Pt_3Sn/C with a small amount of Sn_{UPD} (≈ 10 %) creates a powerful catalyst for overall ethanol oxidation.

Acknowledgements. This work was financially supported by the Ministry of Science and Technological Development of the Republic of Serbia, Contract No. H-142056.

ИЗВОД

УПОРЕДНО ИСПИТИВАЊЕ ОКСИДАЦИЈЕ ЕТАНОЛА НА ПЛАТИНСКИМ НАНОЛЕГУРАМА И Pt НАНОЧЕСТИЦАМА МОДИФИКОВАНИМ ПОДПОТЕНЦИЈАЛНОМ ДЕПОЗИЦИЈОМ

АМАЛИЈА В. ТРИПКОВИЋ, ЈЕЛЕНА Д. ЛОВИЋ и КСЕНИЈА Ђ. ПОПОВИЋ

ИХТМ – Центар за електрохемију, Универзитет у Београду, Његошева 12, п. пр. 473, 11000 Београд

Активност две легуре, Pt_3Sn/C и Pt_3Ru_2/C, упоређене су са активностима Pt/C модификованим одговарајућим количинама Sn_{UPD} (≈ 25 %) или Ru_{UPD} (≈ 40 %) у реакцији оксидације етанола. Катализатори су окарактерисани дифракцијом X-зрака (XRD) и одређен је степен легирања. Њихова активност и стабилност испитивана је потенциодинамичким, квази-стационарним и хроноамперометријским мерењима. Добијени резултати су показали да су обе легуре активније од Sn_{UPD} и Ru_{UPD} модификованог Pt/C катализатора. Активност Pt_3Sn/C катализатора одређена је значајним електронским ефектом, што је и главни разлог његове веће активности у односу на Pt_3Ru_2/C. Одсуство електронског ефекта код Sn_{UPD} и Ru_{UPD} модификованог Pt/C катализатора чини ове електроде мање активним од одговарајућих легура, тј. од Pt_3Sn/C и Pt_3Ru_2/C. Већа разлика у активности између Pt_3Sn/C и Sn_{UPD} модификованог Pt/C катализатора него између Pt_3Ru_2/C и Ru_{UPD} модификованог Pt/C катализатора изазвана је елктронским ефектом у Pt_3Sn/C катализатору. Велика активност Pt_3Sn/C катализатора модификованог малом количином Sn_{UPD} (≈ 10 %) може се објаснити комбинацијом електронског ефекта, тј. слабијом везом адсорбата на Pt местима и већом мобилношћу Sn_{UPD}, и повећаном количином OH_{ad} честица на Sn местима, што као крајњи резултат има побољшање бифункционалног механизма реакције.

(Примљено 19. маја, ревидирано 30. јуна 2010)

REFERENCES

1. G. A. Camara, T. Iwasita, *J. Electroanal. Chem.* **578** (2005) 315
2. H. Wang, Z. Jusys, R. J. Behm, *J. Phys. Chem. B* **108** (2004) 19413
3. M. H. Shao, R. R. Adžić, *Electrochim. Acta* **50** (2005) 2415
4. C. Coutanceau, S. Brimaud, C. Lamy, J.-M. Leger, L. Dubau, S. Rousseau, F. Vigier, *Electrochim. Acta* **53** (2008) 6865
5. S. C. S. Lai, E. F. Kleyn, V. Rosca, M. T. Koper, *J. Phys. Chem. C* **112** (2008) 19080
6. M. Watanabe, S. Motoo, *J. Electroanal. Chem.* **60** (1975) 267
7. H. Wang, Z. Jusys, R. J. Behm, *J. Power Sources* **154** (2006) 351
8. L. Colmenares, H. Wang, Z. Jusys, L. Jiang, S. Yan, G. Q. Sun, R. J. Behm, *Electrochim. Acta* **52** (2006) 221
9. E. Antolini, *J. Power Sources* **170** (2007) 1
10. Q. Wang, G. Q. Sun, L. H. Jiang, Q. Xin, S. G. Sun, Y. X. Jiang, S. P. Chen, Z. Jusys, R. J. Behm, *Phys. Chem. Chem. Phys.* **9** (2007) 2686
11. F. C. Simoes, D. M. dosAnjos, F. Vigier, J.-M. Leger, F. Hahn, C. Coutanceau, E. R. Gonzalez, G. Tremiliosi-Filho, A. R. deAndrade, P. Olivi, K. B. Kokoh, *J .Power Sources* **167** (2007) 1
12. S. Delime, J.-M. Leger, C. Lamy, *J. Appl. Electrochem.* **29** (1999) 1249
13. A. O. Neto, M. J. Giz, J. Perez, E. A Ticianelli, E. R. Gonzalez, *J. Electrochem. Soc.* **149** (2002) A272

14. J.-M. Leger, S. Rousseau, C. Coutanceau, F. Hahn, C. Lamy, *Electrochim. Acta* **50** (2005) 5118
15. W. J. Zhou, Z. H. Zhou, S. Q. Song, W. Z. Li, G. Q. Sun, P. Tsiakaras, Q. Xin, *Appl. Catal. B* **46** (2003) 273
16. A. K. Shukla, A. S. Arico, K. M. El-Khatib, H. Kim, P. L. Antonucci, V. Antonucci, *App. Suf. Sci.* **137** (1999) 20
17. A. S. Arico, V. Antonucci, N. Giordano, A. K. Shukla, M. K. Ravikumar, A. Roy, S. R. Barman, D. D. Sarma, *J. Power Sources* **50** (1994) 295
18. S. Mukerjee, J. McBreen, in *Proceedings of 2nd International Symposium on New Materials for Fuel Cells and Modern Battery Systems*, O. Savadoga, P. R. Roberge, Eds., Ecole Polytechnique, Montreal, 1997, p. 548
19. H. Li, G. Sun. L. Cao, L. Jiang, Q. Xin, *Electrochim. Acta* **52** (2007) 6622
20. W. J. Zhou, S. Q. Song, W. Z. Li, Z. H. Zhou, G. Q. Sun, Q. Xin, S. Douvartzides, P. Tsiakaras, *J. Power Sources* **140** (2005) 50
21. W. J. Zhou, S. Q. Song, W. Z. Li, G. Q. Sun, Q. Xin, S. Kontou, K. Poulianitis, P. Tsiakaras, *Solid State Ionics* **175** (2004) 797
22. J. H. Kim, S. M. Choi, S. H. Nam, M. H. Seo, S. H. Choi, W. B. Kim, *Appl. Catal. B* **82** (2008) 89
23. M. Zhu, G. Sun, Q. Xin, *Electrochim. Acta* **54** (2009) 1511
24. F. Colmati, E. Antolini, E. R. Gonzalez, *J. Power Sources* **154** (2006) 98
25. P. W. Albers, W. Weber, K. Kunzmann, M. Lopez, S. F. Parker, *Surf. Sci.* **602** (2008) 3611
26. S. Sen Gupta, S. Singh, J. Datta, *Mater. Chem. Phys.* **116** (2009) 223
27. R. F. B. De Souza, L. S. Parreira, D. C. Rascio, J. C. M. Silva, E. Teixeira-Neto, M. L. Calegaro, E. V. Spinace, A. O. Neto, M. C. Santos, *J. Power Sources* **195** (2010) 1589
28. S. Mukerjee, J. McBreen, *J. Electrochem. Soc.* **146** (1999) 600
29. M. Arenz, V. Stamenković, B. B. Blizanac, K. J. Mayrhofer, N. M. Marković, P. N. Ross, *J. Catal.* **232** (2005) 402
30. T. Iwasita, *Electrochim. Acta* **47** (2002) 3663
31. I. Pašti, S. Mentus, *Mater. Chem. Phys.* **116** (2009) 94
32. P. Liu, A. Logadottir, J. K. Norskov, *Electrochim. Acta* **48** (2003) 3731
33. A. B. Anderson, E. Grantscharova, P. Schiller, *J. Electrochem. Soc.* **142** (1995) 1880
34. R. Alcala, M. Mavrikakis, J. A. Dumesic, *J. Catal.* **218** (2003) 178
35. F. Vigier, C. Coutanceau, F. Hahn, E. M. Belgsir, C. Lamy, *J. Electroanal.Chem.* **563** (2004) 81
36. H. A. Gastaeiger, N. M. Marković, P. N. Ross, *Catal. Lett.* **36** (1996) 1
37. A. V. Tripković, K. Dj. Popović, J. D. Lović, V. M. Jovanović, S. I. Stevanović, D. V. Tripković, *Electrochem. Commun.* **11** (2009) 1030
38. Y. Yao, Q. Fu, Z. Zhang, H. Zhang, T. Ma, D. Tan, X. Bao, *Appl. Surf. Sci.* **254** (2008) 3808
39. S. Szabo, I. Bakos, F. Nagy, *J. Electroanal. Chem.* **271** (1989) 269
40. A. V. Tripković, G. Lj. Gojković, K. Dj. Popović, J. D. Lović, A. Kowal, *Electrochim. Acta* **53** (2007) 887
41. G. A Camara, R. B. de Lima, T. Iwasita, *Electrochem. Commun.* **6** (2004) 812
42. A. Kowal, M. Li, M. Shao, K. Sasaki, M. B. Vukmirović, J. Zhang, N. S. Marinković, P. Liu, A. I. Frenkel, R. R. Adžić, *Nat. Mat.* **8** (2009) 325

43. A. Kowal, S. Lj. Gojković, K.-S. Lee, P. Olszewski, Y.-E. Sung, *Electrochem. Commun.* **11** (2009) 724
44. M. Li, A. Kowal, K. Sasaki, N. Marinković, D. Su, E. Korach, P. Liu, R. R. Adžić, *Electrochim. Acta* **55** (2010) 4331
45. J. D. Lović, A. V. Tripković, S. Lj. Gojković, K. Dj. Popović, D. V. Tripković, P. Olszewski, A. Kowal, *J. Electroanal. Chem.* **581** (2005) 294.

Journal of the Serbian Chemical Society
JSCS-info@shd.org.rs • www.shd.org.rs/JSCS
J. Serb. Chem. Soc. 75 (11) 1575–1582 (2010)
JSCS–4722
UDC 628.1.033:543.551+543.554:
544.362.2:544.6.076.32–43
Original scientific paper

Coulometric–potentiometric determination of the autoprotolysis constant and the relative acidity scale of water

RADMILA M. DŽUDOVIĆ[1]* and LJILJANA N. JAKŠIĆ[2]

[1]*Faculty of Sciences, University of Kragujevac, Radoja Domanovića 12, 34000 Kragujevac and* [2]*University of Belgrade, Faculty of Mining and Geology, Đušina 7, 11000 Belgrade, Serbia*

(Received 16 March, revised 6 July 2010)

Abstract: The autoprotolysis constant and the relative acidity scale of water were determined by applying the coulometric–potentiometric method and a hydrogen/palladium (H_2/Pd) generator anode. In the described procedure for the evaluation of the autoprotolysis constant, a strong base, coulometrically generated *in situ* at the platinum cathode in the electrolytic cell, in the presence of sodium perchlorate as the supporting electrolyte, was titrated with hydrogen ions obtained by the anodic oxidation of hydrogen dissolved in the palladium electrode. The titration was performed with a glass–SCE electrode pair at 25.0±0.1 °C. The obtained value, pK_w = 13.91±0.06, is in agreement with literature data. The range of the acidity scale of water was determined from the difference between the half-neutralization potentials of the electrogenerated perchloric acid and that of sodium hydroxide in a sodium perchlorate medium. The half-neutralization potentials were measured using both a glass–SCE and a $(H_2/Pd)_{ind}$–SCE electrode pair. A wider range of the relative acidity scale of water was obtained with the glass–SCE electrode pair.

Keywords: coulometry; potentiometry; autoprotolysis constant; relative acidity scale; hydrogen–palladium electrode.

INTRODUCTION

A variety of procedures have been used for the evaluation of autoprotolysis constants, mainly based on potentiometric titrations.[1] The classical potentiometric procedure for the determination of an autoprotolysis constant requires the preparation of standard solutions of strong acids and strong bases in the investigated solvent; the parameters, such as concentrations of the solutions and the presence of either acidic or basic impurities, must be accurately evaluated. The potentio-

* Corresponding author. E-mail: radadz@kg.ac.rs
doi: 10.2298/JSC100316094D

metric determination of autoprotolysis constants was simplified by generating the acid or base coulometrically.

Glab and Hulanicki[2] were the first to apply coulometric titrations for the determination of autoprotolytic constants. The values of pK_s of solvents were calculated from the potentials measured during the course of a titration of a strong acid (perchloric acid) with a cathodically generated base. In the described procedure, only one solution containing the acid and the conducting electrolyte had to be prepared, and its concentration was determined from the coulometric alkalimetric titration curve, assuming 100 % current efficiency for the generation of the base. The same authors[3,4] applied the coulometric titration technique for the determination of the protonation constants of acids and bases in water and non-aqueous solvents.

In previously published papers,[5,6] it was shown that the use of a standard perchloric acid solution for titration of bases in aqueous and non-aqueous media can be avoided by generating perchloric acid coulometrically at a H_2/Pd generator anode. Furthermore, a H_2/Pd anode was applied as the source of hydrogen ions in the coulometric determination of the dissociation constant of bases in some aprotic solvents, as well as in the determination of autoprotolysis constants and relative acidity scales of some non-aqueous solvents.[6,7] In the present study, a H_2/Pd generator electrode was used for the coulometric-potentiometric determination of the autoprotolysis constant of water as well as for the evaluation of relative acidity scale of water.

EXPERIMENTAL

Apparatus

The apparatus and the electrodes used in this work were described previously.[7]

Reagents

Water, twice distilled. Sodium perchlorate, analytical grade. A 0.10 M aqueous sodium perchlorate solution was used as the supporting electrolyte solution. Tris(hydroxymethyl)aminomethane (THAM), analytical grade. THAM was used to prepare a primary standard solution (0.0676 M).

Procedures

Determination of the autoprotolysis constant. The supporting electrolyte was poured into both the generating (35.0 mL) and the auxiliary (10.0 mL) compartment of the coulometric cell. For the generation of the base, both electrodes in the generating circuit were made of platinum; the surface of the generating cathode was about 2 cm^2. Base was generated by passing a constant current of 15 mA to give a concentration of 0.006 M. The generator H_2/Pd anode and the electrode pair glass–SCE were then placed in the generating compartment. Titration of the base was performed with hydrogen ions generated at the H_2/Pd anode, at a current of 15 mA. The total concentration of the generated acid was equal to double the initial concentration of the titrated base. Possible interferences due to the diffusion of the solution through the porous diaphragms, separating the anode from the cathode compartment, were avoided by occasional replacement of the catholyte with fresh supporting electrolyte solution. The titration

end-point (EP) was determined by the Gran method, which was modified for the coulometric titration. The slope of the glass electrode was 59 mV.

Determination of the relative acidity scale. The range of the relative acidity scale of water (mV) was determined from the difference in the half-neutralization potentials during the reaction of perchloric acid with sodium hydroxide, generated coulometrically in an aqueous solution of sodium perchlorate.

a) Determination of the half-neutralization potential of an acid. The supporting electrolyte solution was poured into the anode (35.0 mL) and cathode (10.0 mL) compartment of the coulometric cell. The $(H_2/Pd)_{gen}$ anode and the Pt-cathode were immersed into the anolyte and the catholyte, respectively. The perchloric acid was generated using a current strength of 15 mA, until a concentration of 0.007 M was achieved. The Pt-electrode and the glass–SCE (or a $(H_2/Pd)_{ind}$–SCE) pair was then immersed in the anolyte, and the acid was titrated with cathodically generated base. The half-neutralization potentials of acid were determined graphically (Fig. 1).

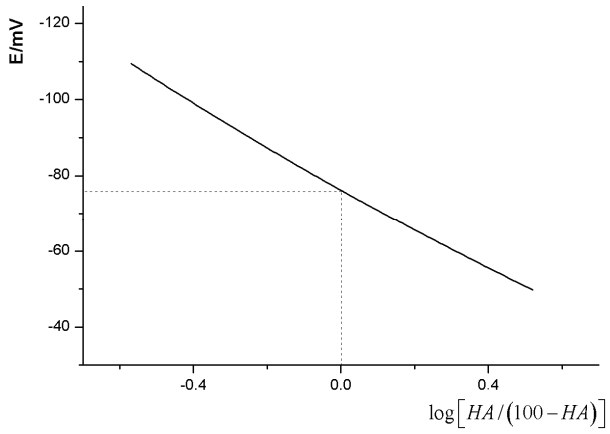

Fig. 1. The dependence of the potential of the cell on log [*HA*/(100 – *HA*)], where *HA* represent the percent of neutralized acid. The graphical determination of the half-neutralization potential of perchloric acid is illustrated.

b) Determination of the half-neutralization potential of a base. The supporting electrolyte solution was poured into the generating (35.0 mL) and the auxiliary (10.0 mL) compartment of the coulometric cell. The base was generated at the Pt-cathode with the current strength of 15 mA, until a concentration of 0.007 M was achieved, and then titrated with the acid generated at the H_2/Pd anode. The potentials were measured by means a glass–SCE or a $(H_2/Pd)_{ind}$–SCE electrode pair. The half-neutralization potential of the base was also determined graphically.

All measurements were carried out at 25.0±0.1 °C in solutions stirred with a magnetic stirrer.

Coulometric–potentiometric titration of THAM in water. A THAM solution (2.00 mL) and the sodium perchlorate solution (18.0 mL) were put into the anode compartment of the coulometric cell, and the sodium perchlorate solution (5.0 mL) was poured into the cathode compartment. The auxiliary electrode (a Pt-wire) was immersed in the catholyte. The $(H_2/Pd)_{gen}$ anode and the electrode pair glass–SCE or $(H_2/Pd)_{ind}$–SCE were placed in the anolyte. The titration of the base was performed with hydrogen ions generated discontinually at the H_2/Pd anode, under continuous registration of the potential.

RESULTS AND DISCUSSION

The autoprotolysis constant of water was determined by the coulometric procedure in which a strong base was first generated cathodically in the electrolytic cell and then titrated with hydrogen ions generated by the anodic oxidation of hydrogen dissolved in palladium, in an aqueous sodium perchlorate solution. The concentration of the base was determined from the coulometric acidimetric titration curve, assuming 100 % current efficiency for the generation of hydrogen ions at the $(H_2/Pd)_{gen}$ anode. The changes in hydrogen ion concentration were followed with a glass electrode. For calibration of glass electrode the so-called "E^0-titration"[8] was used; at a constant ionic strength, the e.m.f. of the cell is a linear function of the logarithm of hydrogen ion concentration.

The experimental data obtained in the course of the coulometric–potentiometric titration of the electrogenerated base with perchloric acid generated at a $(H_2/Pd)_{gen}$ anode at a given ionic strength (0.10 M) were used to calculate the autoprotolysis constant of water. The concentration constant of water autoprotolysis ($pK_w^c = -\log K_w^c$) was calculated by means of the expression:

$$pK_w^c = \frac{E_b^0 - E_a^0}{59.16}$$

were the potentials E_b^0 and E_a^0 represent the specific cell constants for the basic and acid regions, respectively, involving the standard potential of the glass electrode, the potential of the reference electrode, the diffusion potential and the activity factors. The values E_b^0 (mV) and E_a^0 (mV) were calculated from a definite number of points along the titration curve before and after the equivalence point, respectively, using the equations:

$$E_b^0 = E - 59.16 \log \frac{Q_{EP} - Q}{FV}$$

$$E_a^0 = E + 59.16 \log \frac{Q - Q_{EP}}{FV}$$

where Q_{EP} (C) denotes the amount of charge generated up to the end point of titration of the base, Q (C) is the quantity of the charge generated up to the measured potential E (mV), V is the solution volume (mL) and F is the Faraday constant (96500 C mol^{-1}). The constancy of E_b^0 and E_a^0 over the whole range indicates the proper functioning of the indicator electrode and the absence of systematic errors. The detailed record for this procedure is given in Table I.

The concentration constant was recalculated to obtain the thermodynamic value:

$$pK_w = pK_w^c - \log f_+ f_-$$

by using the known ionic strength (in 0.10 M ionic strength, f_+ = 0.83 and f_- = = 0.76).[9]

TABLE I. Coulometric determination of the autoprotolysis constant of water; the base in 35 mL cell was generated at a Pt-cathode and then titrated with electrogenerated acid by the use of an $(H_2/Pd)_{gen}$ anode; current 15 mA; equivalence point for acid generation corresponds to Q_{EP} = 19310 mC; the supporting electrolyte was 0.10 M sodium perchlorate;

$$pK_w^c = \frac{459.6-(-351.0)}{59.16} = 13.70\ ;\ pK_w = 13.89$$

Q / C	E / mV	E_b^0 / mV	E_a^0 / mV
1.80	322	457.4	–
2.70	321	457.8	–
3.60	319	457.2	–
4.50	318	457.7	–
5.40	317	458.4	–
6.30	317	460.1	–
7.20	316	460.9	–
8.10	314	461.0	–
9.00	312	461.1	–
9.90	311	462.5	–
10.80	307	461.2	–
11.70	305	462.0	–
12.60	300	458.4	–
13.50	295	459.2	–
24.30	–183	–	–352.5
25.20	–188	–	–350.6
26.10	–192	–	–351.0
27.00	–195	–	–350.9
27.90	–198	–	–351.1
28.80	–200	–	–350.6
29.70	–202	–	–350.3
30.60	–204	–	–350.2
31.50	–206	–	–350.2
32.40	–208	–	–351.4
33.30	–210	–	–350.7
34.20	–212	–	–351.1
35.10	–214	–	–351.6
36.00	–215	–	–351.2
Average	–	459.6	–351.0

The pK_w values determined coulometrically using a H_2/Pd anode, as well as the literature date, are listed in Table II. The pK_w value obtained experimentally in this study agrees well with the literature data.[10] This indicates that the procedure proposed here delivers fair results, but that special attention must be paid to avoid the diffusion of the solution through the porous separator.

TABLE II. Autoprotolysis constant of water obtained by coulometry at 25.0±0.1 °C

$pK_w^c \pm SD$[a]	$pK_w \pm SD$[a]	pK_w Literature data[10]
13.71±0.06	13.91±0.06	14.0

[a]Standard deviation, number of determinations: 6

The relative acidity scale

The relative acidity scale (E_S) of a solvent defines the approximate potential range which can be used for potentiometric acid–base titrations in the given solvent under the determined experimental conditions. The value of the practical E_S scale can be determined from the difference between the half-neutralization potentials of a strong acid and a strong base in the applied solvent.[11]

The relative acidity scale of water was determined in this study coulometrically from the difference between the half-neutralization potentials of solutions of perchloric acid and sodium hydroxide.

$$E_S = E_{1/2(HClO_4)} - E_{1/2(NaOH)}$$

The half-neutralization potentials of the acid were determined graphically from the experimental data obtained in the course of the titration of electrogenerated perchloric acid with the coulometrically generated base in sodium perchlorate media (Fig. 1). The potentials were measured using both a glass–SCE and a $(H_2/Pd)_{ind}$–SCE electrode pairs at 25.0±0.1 °C. The half-neutralization potentials of the base were also determined graphically, from the experimental data obtained in the course of the titration of coulometrically generated sodium hydroxide with perchloric acid generated at an $(H_2/Pd)_{gen}$ anode in an aqueous solution of sodium perchlorate.

The ranges of the relative acidity scale of water obtained by the coulometric––potentiometric procedure using a $(H_2/Pd)_{gen}$ electrode, as well as literature data, are summarized in Table III.

TABLE III. The relative acidity scale of water obtained by coulometry at 25.0±0.1 °C; supporting electrolyte, 0.10 M sodium perchlorate

Electrode pair	$E_{1/2}$(acid)±*SD*[a] mV	$E_{1/2}$(base)±*SD* mV	E_S±*SD* mV	E_S / mV (literature data[11])
Glass–SCE	–79±3	411±7	490±6	540
$(H_2/Pd)_{ind}$–SCE	66±4	276±14	210±9	–

[a]Standard deviation, number of determinations: 4

The experimentally determined E_S values of the acidity scale of water obtained in this study by coulometry differ from the ones obtained by the classic potentiometric method.[11] This difference can be explained by differences in the experimental conditions (titrant, electrode pair, ionic strength, *etc.*) in the present work in comparison to those applied by other authors.

As can be seen (Table III), a wider E_S scale of water was obtained when a glass–SCE electrode pair was used to measure the half-neutralization potentials. This significant difference between the values of E_S scales obtained with a glass––SCE and a $(H_2/Pd)_{ind}$–SCE electrode pairs is probably caused by the lower sen-

sitivity of the $(H_2/Pd)_{ind}$ electrode compared with the glass electrode. Previously, it was shown that the slopes of the potential response of the $(H_2/Pd)_{ind}$ electrode in aqueous media were sub-Nernstian.[12] Based on this fact, it could expected that the highest potential jumps at the end-point would be obtained if a glass electrode were used as an indicator electrode.

Thus, for example, in the coulometric titration of THAM in aqueous media (Fig. 2), the potential jumps at the end-point were, respectively, about 140 and 70 mV when a glass and a $(H_2/Pd)_{ind}$ electrode were used, (for a base concentration 0.0070 M). Hence, a relative acidity scale of water determined by coulometry may be a practical and useful criterion for the choice of the optimal conditions (for example, the choice of a favorable electrode pair) in coulometric-potentiometric acid–base titration in this solvent.

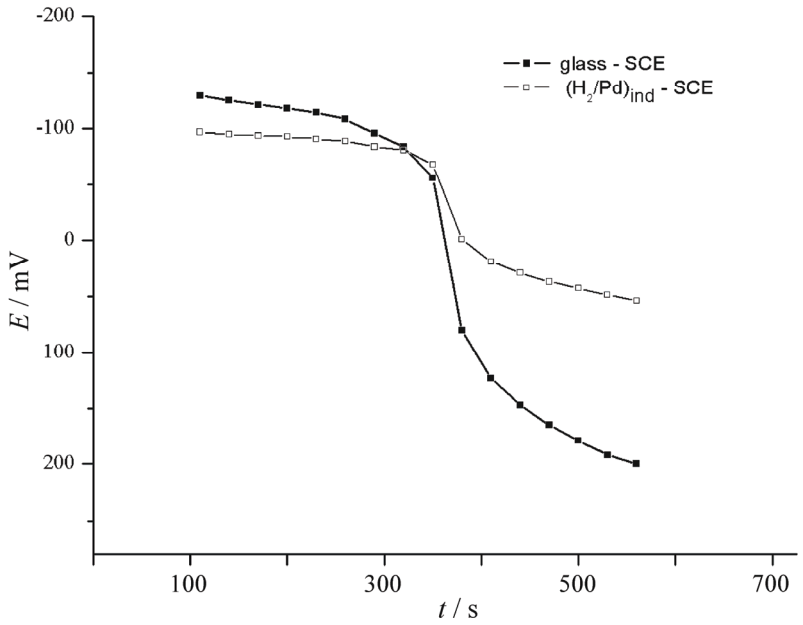

Fig. 2. Coulometric–potentiometric titration curves of tris(hydroxymethyl)aminomethane in aqueous media.

CONCLUSIONS

The autoprotolysis constant and relative acidity scale of water were determined by applying the coulometric–potentiometric method and a hydrogen/palladium generator electrode. By employing a hydrogen/palladium anode as the source of hydrogen ions, the preparation of a standard solution of acid was avoided and the titrated volume and the ionic strength remained unchanged. This procedure is more rapid and simpler than the classical potentiometric procedure.

Acknowledgement. The authors are grateful to the Ministry of Science and Technological Development of the Republic of Serbia for financial support (Project No. 142060).

И З В О Д

КУЛОМЕТРИЈСКО–ПОТЕНЦИОМЕТРИЈСКО ОДРЕЂИВАЊЕ КОНСТАНТЕ АУТОПРОТОЛИЗЕ И РЕЛАТИВНЕ СКАЛЕ КИСЕЛОСТИ ВОДЕ

РАДМИЛА М. ЏУДОВИЋ[1] и ЉИЉАНА Н. ЈАКШИЋ[2]

[1]*Природно–математички факултет, Универзитет у Крагујевцу, Радоја Домановића 12, 34000 Крагујевац и* [2]*Рударско–геолошки факултет, Универзитет у Београду, Ђушина 7, 11000 Београд*

Константа аутопротолизе и релативна скала киселости воде одређене су применом кулометријско–потенциометријске методе и водоник/паладијумове (H_2/Pd) генераторске аноде. У приказаном поступку за одређивање константе аутопротолизе воде, јака база генерисана *in situ* кулометријски на Pt-катоди, у раствору натријум-перхлората као електролита, титрисана је водониковим јонима добијеним анодном оксидацијом водоника раствореног у паладијуму. Титрација је извођена применом електродног пара стаклена електрода–ЗКЕ на 25,0±0,1 °C. Добијена вредност pK_w = 13,91±0,06 је у сагласности са литературним подацима. Релативна киселинска скала воде одређена је из разлике полу-неутрализационих потенцијала раствора електрогенерисане перхлорне киселине и натријум-хидроксида у натријум-перхлоратној средини. За мерење полу-неутрализационих потенцијала коришћени су електродни парови стаклена електрода–ЗКЕ и $(H_2/Pd)_{инд}$–ЗКЕ. Применом електродног пара стаклена електрода–ЗКЕ добијене су веће вредности за релативну скалу киселости воде.

(Примљено 16. марта, ревидирано 6. јула 2010)

REFERENCES

1. A. Albert, E. P. Serjeant, *The Determination of Ionization Constants*, Chapman Hall, London, 1971
2. S. Glab, A. Hulanicki, *Talanta* **28** (1981) 183
3. S. Glab, E. Skrzydlewska, A. Hulanicki, *Talanta* **37** (1987) 411
4. S. Glab, U. Nowicka, *Mikrochim. Acta* **2** (1987) 229
5. R. P. Mihajlović, V. J. Vajgand, Lj. N. Jakšić, *Talanta* **38** (1991) 333
6. R. P. Mihajlović, Lj. N. Jakšić, R. M. Džudović, *Anal. Chim. Acta* **557** (2006) 37 (and references therein)
7. R. M. Džudović, Lj. N. Jakšić, *J. Serb. Chem. Soc.* **73** (2008) 871
8. A. Johansson, S. Johansson, *Analyst*, **103** (1978) 305
9. J. Kielland, *J. Am. Chem. Soc.* **59** (1937) 1675
10. R. A. Robinson, R. H. Stokes, *Electrolyte Solutions*, 2nd ed., Butterworths, London, 1968, p. 230
11. A. P. Kreshkov, Analytical Chemistry of Non-Aqueous Solutions, Khimiya, Moscow, 1982, p. 183 (in Russian)
12. Lj. N. Jakšić, R. M. Džudović, R. P. Mihajlović, *J. Serb. Chem. Soc.***70** (2005) 243.

Journal of the Serbian Chemical Society
JSCS-info@shd.org.rs • www.shd.org.rs/JSCS
J. Serb. Chem. Soc. *75* (11) 1583–1594 (2010)
JSCS–4078
UDC *Digoxin+544.35+543.544.5.068.7
Original scientific paper

An HPLC method for the determination of digoxin in dissolution samples

MIROSLAV Ž. MILENKOVIĆ[1]*, VALENTINA D. MARINKOVIĆ[1], PREDRAG S. SIBINOVIĆ[1], RADOSAV M. PALIĆ[2#] and DRAGAN M. MILENOVIĆ[1#]

[1]*Pharmaceutical and Chemical Industry Zdravlje-Actavis, Vlajkova 199, Leskovac and* [2]*Department of Chemistry, Faculty of Science and Mathematics, University of Niš, Višegradska 33, Niš, Serbia*

(Received 6 January, revised 13 September 2010)

Abstract: An HPLC method for digoxin quantification in dissolution samples obtained as per the official British Pharmacopeia (BP) method is presented in this paper. The chromatography was performed at 20 °C on a Symmetry C18; 3.5 μm, 75 mm×4.6 mm column with water–acetonitrile (72:28, v/v), as the mobile phase and UV detection at 220 nm. The method was found to be selective, linear, accurate and precise in the specified ranges. The *LOD* and *LOQ* were 0.015 and 0.050 μg mL^{-1}, respectively. Robustness testing was conducted to evaluate the impact of minor changes in the chromatographic parameters (*i.e.*, acetonitrile fraction, flow rate of the mobile phase, column temperature and column length) on the characteristics of the digoxin peak. A full factorial design (2^4) was used to investigate the influence of the four variables The presented HPLC method was applied in quality and stability testing of digoxin tablets 0.25 mg.

Keywords: digoxin; tablets; dissolution testing; HPLC; validation; experimental design.

INTRODUCTION

Digoxin is a cardiac glycoside that is widely used in the treatment of congestive heart failure and certain cardiac arrhythmias. This drug is characterized by a narrow therapeutic range (typically 0.5–2.0 ng mL^{-1} in serum), wide individual variability in dosage requirements and complex metabolic pathways.[1]

As is known, dissolution testing is a routine quality control procedure in good manufacturing practice (GMP), and the dissolution data are a substantial parameter for the estimation of the bioavailability of solid oral dosage forms.

* Corresponding author. E-mail: mirmilenkovic@actavis.rs
# Serbian Chemical Society member.
doi: 10.2298/JSC100106123M

Numerous high performance liquid chromatographic (HPLC) methods have been reported for the determination of digoxin.[2–13] There are some methods reported for digoxin determination after a dissolution test.[14–16]

In the United States Pharmacopoeia (USP), 0.1 M hydochloric acid (HCl) and in the Japanese Pharmacopoeia (JP), diluted HCl is used as the dissolution medium,[17,18] while distilled water is employed as the dissolution medium in the British Pharmacopeia (BP).[19] As some degradation could occur by acid-catalyzed hydrolysis of digoxin[16], dissolution testing with water as the dissolution medium was used in this study. Quantification of digoxin in the dissolution samples is, as per all three compendia (*i.e.*, the BP, USP and JP), based on measurement of fluorescence induced by exposing digoxin to drastic conditions (*i.e.*, ascorbic acid–methanol solution and hydrochloric acid, followed by hydrogen peroxide–methanol solution over a period of 2 h). Here, a fast and simple HPLC method is applied for digoxin determination after dissolution and filtration without any derivatization.

The Pharmacopoeias state that digoxin (Fig. 1) is practically insoluble in water. It can also be found on the web that the solubility of digoxin is 0.07 and 0.0648 mg mL^{-1}.[20,21] When the described BP dissolution test conditions are applied to 0.25 mg digoxin tablets, the resulting concentration should be about 0.42 μg mL^{-1} when the whole dose is dissolved (*i.e.*, 0.25 mg in 600 mL). This concentration can be determined by the HPLC method without any additional sample treatment, except filtration, when an aliquot of 100 μl is injected.

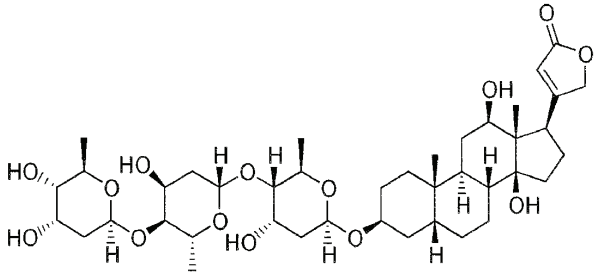

Fig. 1. Structural formula of digoxin.

A robustness test was performed to indicate factors that could affect the results. Evaluating robustness according to the International Conference on Harmonization (ICH) definition is possible by two approaches: one variable at a time or experimental design. For several reasons (too many experiments, no interactions terms, *etc.*), the univariate approach, although often performed and described in the literature, is not recommended for robustness testing.[22]. Full factorial design, as a powerful statistical tool, was employed in this study.

EXPERIMENTAL

Equipment

Development and validation of the method were realised on a Agilent HPLC system HP 1200 series equipped with a binary pump G1312A, a vacuum degasser G1379B, an autosampler G1329A, a thermostated column compartment G1316A and a UV detector G1315D, from Agilent Technologies (Waldbronn, Germany). Data acquisition, data collection and system control was provided by Chemstation software, revision B.03.01-SR1, from the same company.

A Symmetry C18, 3.5 µm, 75 mm×4.6 mm column purchased from Waters (Wexford, Ireland) was used.

The dissolution tests were performed using an Erweka DT700LH Dissolution apparatus (USP I) (Heusenstamm, Germany). The dissolution medium was filtered through Whatman 25 mm, blue ribbon glass microfibre filters (Maidstone, UK).

Other equipment used was a Sartorius MC 1 analytical balance with a precision of 0.1 mg (Göttingen, Germany) and a Bandelin Sonorex ultrasonic bath (Berlin, Germany).

Design-Expert software, version 7.1.6, Stat-Ease Inc. (Minneapolis, USA), was used for the experimental design of the robustness test.

Reagents and solutions

HPLC-grade acetonitrile and HPLC-grade methanol were purchased from Merck KgaA (Darmstadt, Germany), while the HPLC-grade water was obtained from a Sartorius Stedim Biotech water system (Göttingen, Germany).

As the standard, an in-house working standard provided by Roche Diagnostics GmbH, Mannheim, Germany, (assay calculated on “as is” substance, 96.46 %) was used and standardised against digoxin EPCRS (assay calculated on “as is” substance, 98.50 %) as reference. Digoxin tablets (dilacor 0.25 mg tablets) manufactured by Zdravlje Actavis, Leskovac, Serbia, were used for validation purposes. One tablet weighed 120 mg and contained 0.250 mg of digoxin.

A digoxin stock solution was prepared by dissolving 21.0 mg of reference substance digoxin in 90 m of a mixture of methanol–acetonitrile–water (20:20:60, v/v) and diluted to 100.0 mL with the same solvent mixture, c = 0.21 mg mL^{-1}. A standard solution of digoxin was prepared by diluting 1 volume of stock solution to 500 volume with water, c = 0.42 µg mL^{-1}.

Sample solutions were prepared by performing the dissolution test.

For the selectivity test the following samples were prepared in 600 mL of the dissolution medium:

– Excipients (mixture of lactose monohydrate, maize starch, soluble starch, colloidal anhydrous silica and magnesium stearate), in the same amount as present in one tablet.

– Digoxin, in the same amount as present in one tablet.

– Digoxin and excipients in the same amount as present in one tablet.

The linearity stock solution was prepared by diluting 1.0 mL of digoxin stock solution to 50 mL with water, c = 4.2 µg mL^{-1}. Six linearity solutions were prepared by diluting of linearity stock solution.

A set of dilute solutions were prepared for the determination of the limit of detection (*LOD*) and limit of quantification (*LOQ*). After determination of the *LOD* and *LOQ*, one solution with the *LOD* concentration and six solutions with *LOQ* concentration were prepared by diluting the standard solution.

Experimental conditions

The experimental conditions described in the BP were used for the dissolution tests. For dissolution experiments, digoxin tablets were weighed and placed in the dissolution apparatus in batches of six. Sample aliquots (*ca*. 10 mL) were withdrawn at 5, 10, 15, 20, 30, 45 and 60 min and filtered through Whatman 25 mm, blue ribbon filters, whereby the first portion of the filtrate was discarded. No additional pretreatment was required prior to HPLC analysis.

HPLC Chromatography was performed with a column temperature of 20 °C and the mobile phase (mixture of water and acetonitrile, 72:28 % v/v) was pumped at a flow rate of 0.8 mL min^{-1}.[2] The run time cycle was completed in 10 min, while for the robustness test, it was set on 20 min. Peak areas registered at 220 nm were used for digoxin quantification.

RESULTS AND DISCUSSION

Method validation

The parameters to be validated for the HPLC assay were according to the ICH guidelines.[24]

System suitability. The USP states the tailing should be in the interval 0.8––1.5; the *RSD* derived from six injections of standard solution should be less than 2.0 % and number of theoretical plates per column for the digoxin peak should be not less than 2000. This parameter was demonstrated throughout the validation work. The results obtained in the beginning, as well as the results obtained when performing the intermediate precision by a second analyst are given in Table I.

TABLE I. Results for system suitability test

Run	Analyst 1			Analyst 2		
	Area of digoxin peak	USP Tailing	Theoretical plates	Area of digoxin peak	USP Tailing	Theoretical plates
1	52.6	1.028	6952	46.1	1.073	6877
2	52.4	1.054	6861	45.9	1.084	6838
3	52.2	1.064	7069	45.1	1.092	6836
4	54.1	1.101	6867	44.9	1.100	6748
5	54.5	1.032	6730	44.6	1.104	6659
6	52.7	1.021	6883	43.8	1.112	6671
Mean	53.08	1.05	6894	45.1	1.094	6772
SD	0.97	0.03	112.09	0.85	0.014	92.76
RSD / %	1.82	2.84	1.63	1.89	1.296	1.37

Selectivity. In order to determine the selectivity of the dissolution medium, placebo solutions, sample and standard solutions were filtrated and injected into HPLC system. Representative chromatograms are shown in Fig. 2.

In the placebo solutions, no interfering peaks were observed at the expected retention time of the active ingredient.

Linearity. The linearity of digoxin (area of peak against concentration) was verified within the range 20–120 % of the reference solution, which corresponds to concentrations 0.084–0.504 μg mL^{-1} of digoxin. The best-fit line through un-

weighted least squares linear regression was generated. Digoxin gave a linear response over the tested range and the linear regression equation was obtained:

$$y = 129.69x / 0.0867 \quad (1)$$

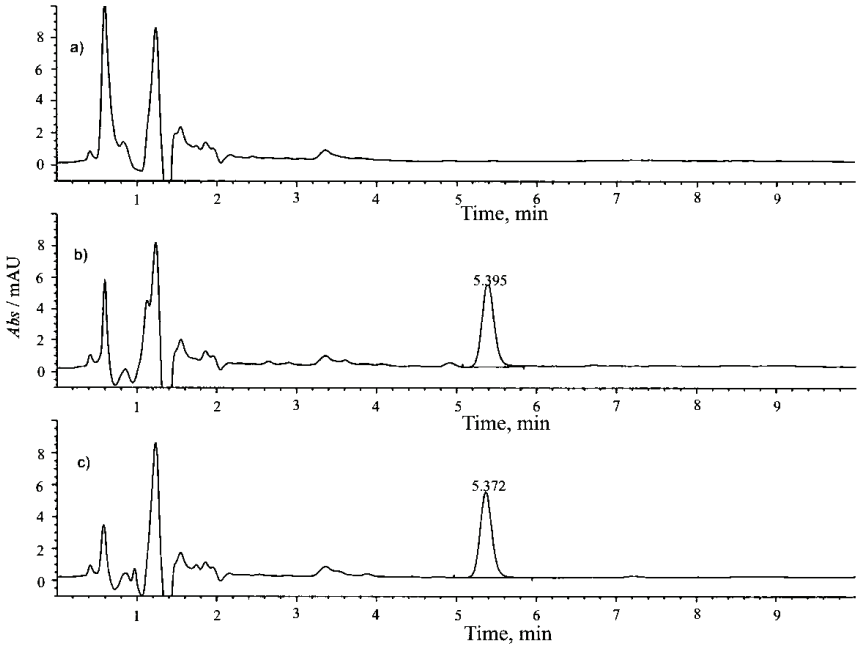

Fig. 2. Chromatograms of placebo solution (a), standard solution (b) and sample solution (c) under the described conditions.

The raw data for the best line calculation is given in Table II as well as the calculated peak areas of the best line, the peak area residual values and the relative peak area residual values.

TABLE II. Linearity of the response for digoxin (peak area residuals)

c / μg mL^{-1}	Area, mAU s	Best line peak area	Peak area residuals	Relative peak area residuals
0.084	12.1	10.98	1.12	10.19
0.168	21.2	21.88	–0.68	–3.09
0.252	32.3	32.77	–0.47	–1.43
0.336	43.3	43.66	–0.36	–0.83
0.420	53.8	54.56	–0.76	–1.39
0.504	66.6	65.45	1.15	1.75

The correlation coefficient (r) was 0.999. No apparent non-linearity was observed. This indicates functional linearity between the concentration of analyte and the digoxin peak area.

Limit of detection and limit of quantification. The *LOD* and *LOQ* values were determined based on the *S*/*N* criteria and were found to be 0.015 μg mL^{-1} (*S*/*N* = 3) and 0.050 μg mL^{-1} (*S*/*N* = 10), respectively. The *LOQ* solutions were tested against the standard solution (c = 0.42 μg mL^{-1}). The *RSD* value of 8.9 % and a mean recovery of 103.4% show that acceptable accuracy and precision were obtained.

Precision. In order to determine the repeatability, the dissolution test was performed as previously described. To determine the intermediate precision of the method, a second analyst performed the repeatability determination on the same batches of 0.25 mg digoxin tablets on a different day, using a different dissolution apparatus and a different HPLC system. The results of the precision testing are given in Table III.

TABLE III. Repeatability and intermediate precision results for digoxin

Sample	Digoxin dissolved, %	
	Analyst 1, day 1	Analyst 2, day 2
1	100.07	101.63
2	101.96	99.66
3	98.75	98.76
4	104.42	98.40
5	101.20	98.04
6	106.69	104.50
Mean	102.18	100.17
SD	2.92	2.48
RSD / %	2.86	2.48
RSD / % of 12 samples	2.76	
95 % confidence intervals	99.85–104.52	98.18–102.15

Accuracy. The accuracy was tested as the recovery of digoxin at levels 80, 100 and 120 % of the declared content of digoxin, with 100 % content of placebo. Placebo (120 mg) and the appropriate amount of digoxin, *i.e.*, 0.200, 0.250 or 0.300 mg of digoxin, were added in the form of a solution of concentration 0.10 mg mL^{-1} (*i.e.*, 2.0, 2.5 or 3.0 mL, respectively) into dissolution vessels filled with 600 mL of dissolution medium (three replicates for each concentration level) and the dissolution testing was performed as per the method.

The accuracy results for digoxin in all samples showed good recovery and are summarized in Table IV.

Stability of solution. The stability of digoxin in the test solution and the stability of digoxin in the standard solution during a period of 48 h were determined. Three test solutions representing 100 % of the 0.25 mg digoxin tablets were used to determine the stability of the test solutions. The initial concentration of digoxin was compared to the concentration of digoxin in same solutions after 24 and 48 h. The test solutions and standard solution were stored in autosampler

vials at ambient temperature. The results show that the solutions were stable when stored in autosampler for a period of 48 h, since the measured content of digoxin in the stored solutions differed by not more than 2.0 % from the initially measured content.

TABLE IV. Accuracy results for digoxin (accurate concentrations of digoxin were 0.336, 0.420 and 0.504 μg mL^{-1}, respectively)

Sample	Determined concentration μg mL^{-1}	Recovery	Determined concentration μg mL^{-1}	Recovery	Determined concentration μg mL^{-1}	Recovery
	80 % level		100 % level		120 % level	
1	0.327	97.32	0.415	98.81	0.509	100.99
2	0.321	95.54	0.419	99.76	0.499	99.01
3	0.321	95.54	0.422	100.48	0.491	97.42
Mean	0.323	96.13	0.419	99.68	0.500	99.14
SD	0.003	1.031	0.004	0.836	0.009	1.789
RSD / %	1.072	1.072	0.839	0.839	1.805	1.805
95 % Confidence interval	0.319–0.327	94.96–97.30	0.415–0.423	98.74––100.6	0.489–0.510	97.12––101.2

Robustness. Critical chromatographic parameters, such as the percentage of acetonitrile in the mobile phase, flowrate of the mobile phase, column temperature and column length, were deliberately varied to test their impact on the digoxin determination. The characteristics of the digoxin peak, such as peak area, retention time, USP tailing, symmetry, number of theoretical plates per column (half-width method) and capacity factor, were used to observe the influence of these changes in the method. The experimental results of the robustness study are summarized in Table V.

The number of experiments required for a study depends on the number of independent variables. The responses are measured for each trial and then the interactive model ($Y = b_0 + b_1X_1 + b_2X_2 + b_3X_3 + b_{12}X_1X_2 + b_{13}X_1X_3 + \cdots$) is fitted by performing multiple regression analysis and *F*-statistics to identify the statistically significant terms.[25]

The estimated effects were graphically and statistically interpreted to determine their significance. The half-normal probability plot was used as a graphical tool to assess significance of the effects. In this plot, the non-significant effects are found on a straight line through zero, while the significant deviate from this line. An example of the graphical method is given in Fig. 3, which shows that changing the flow rate has statistically the most significant effect on the area of the digoxin peak.

The interactive statistical first-order model was generated completely to evaluate the digoxin peak area. The final equation was given in terms of the actual factors:

TABLE V. Robustness – 2^4 full factorial design layout

No	Variable level in actual form				Responses					
	Acetonitrile fraction, %	*t* °C	Flow rate mL min^{-1}	Column length mm	Area mAU s	Retention time min	USP Tailing	Symmetry	Theoretic plates per column	*k*'
1	25.0	18.0	0.6	75.0	69.6	12.0	1.11	0.87	8317	8.64
2	25.0	22.0	0.6	75.0	67.8	12.9	1.10	0.87	8672	9.37
3	25.0	18.0	1.0	75.0	44.1	7.5	1.07	0.91	6439	9.06
4	25.0	22.0	1.0	75.0	41.6	8.1	1.09	0.90	7009	9.83
5	31.0	18.0	0.6	75.0	69.2	6.2	1.19	0.86	15612	4.00
6	31.0	22.0	0.6	75.0	78.5	4.4	1.21	0.82	5946	2.55
7	31.0	18.0	1.0	75.0	48.2	2.6	1.21	0.81	4660	2.49
8	31.0	22.0	1.0	75.0	46.7	2.7	1.06	0.83	4831	2.72
9	25.0	18.0	0.6	100.0	72.5	17.5	0.98	1.02	11297	9.51
10	25.0	22.0	0.6	100.0	69.7	18.7	0.95	1.01	11920	10.26
11	25.0	18.0	1.0	100.0	44.3	9.4	1.00	1.00	9086	8.48
12	25.0	22.0	1.0	100.0	43.7	10.2	1.00	0.97	9424	9.20
13	31.0	18.0	0.6	100.0	70.6	4.8	1.05	0.94	10082	1.88
14	31.0	22.0	0.6	100.0	71.9	4.9	1.06	0.94	9907	1.99
15	31.0	18.0	1.0	100.0	44.4	2.9	1.07	0.92	6742	1.95
16	31.0	22.0	1.0	100.0	41.1	3.1	1.05	0.94	7108	2.07

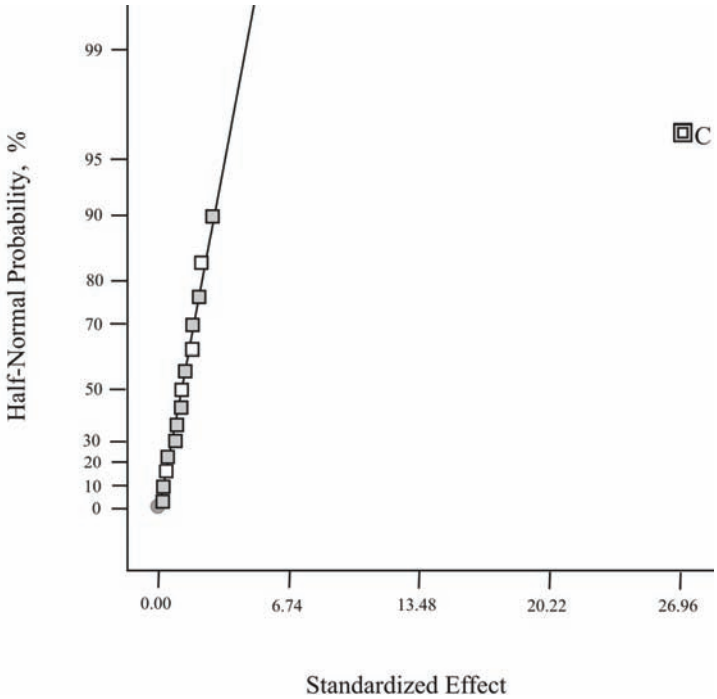

Fig. 3. Half-normal probability plot – effect of flow rate on the digoxin peak area.

$$\text{Dioxin peak area} = 111.67 - 67.41c \quad (2)$$

Equations for other responses were also generated:

$$\text{Retention time} = -161.24 + 5.72A + 1.49B + 133.98C + 2.57D - \\ -0.05AB - 4.73AC - 0.09AD - 2.22CD + 0.07ACD \quad (3)$$

$$\text{USP Tailing} = 1.11 + 0.01A - 4.4\times10^{-3}D \quad (4)$$

$$\text{Symmetry} = 0.086 - 0.01A + 4.15\times10^{-3}D \quad (5)$$

$$\text{Theoretic plates} = -2.05\times10^{6} + 82476.83A + 94770.67B + \\ +2.01\times10^{6} + 20173.27D - 3821.04AB - 81230.83AC - \\ -808.69AD - 92704.17BC - 923.86BD - 19611.22CD + \\ +3751.04ABC + 37.36ABD + 792.12ACD + 903.75BCD - \\ -36.65ABCD \quad (6)$$

$$\text{Capacity factor} = 37.58 - 1.13A \quad (7)$$

where A is the % acetonitrile, B is the temperature (°C), C is the flow rate (mL min^{-1}) and D is the column length (mm).

From the generated equations, it can be observed:

– statistically, the most significant factors that have an influence on the USP tailing and symmetry, are the % acetonitrile and the column length;

– statistically, the most significant factor which has an influence on the capacity factor is the % acetonitrile;

– statistically, all factors have a significant influence on the number of theoretical plates (N) and the retention time.

After construction, model was interpreted graphically by drawing 2D contour plots. A 2D contour plot shows the iso-response lines as a function of two levels of two factors. As an example, the graphical representation of the dependence of the number of theoretical plates on the % acetonitrile and temperature is shown in Fig. 4.

Finally, the robustness of the method can be seen in Fig. 5.

For the construction of the overlay plot, it was taken that the response factors were peak area above 50; retention time less than 10 min; symmetry, min 0.85; USP tailing, 0.8–1.2; number of theoretical plates (N) more than 2000 and capacity factor, 2–10.

In addition, the temperature and column length were chosen to be constant.

From the figure, it can be seen that the chosen experimental conditions are in the middle of the graph.

Dissolution profile. Method described above was used to analyse commercial batches of digoxin tablets. As per the applied BP dissolution test method, the requirement for released digoxin is a minimum of 75 % in 60 minutes. The dissolution profile of one of the batches with error bars is shown in Fig. 6.

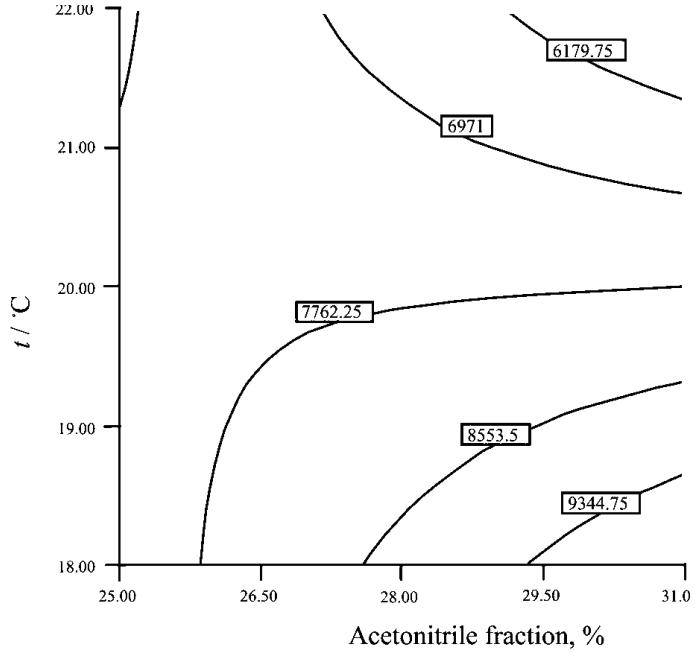

Fig. 4. 2D Contour plot – number of theoretical plates.

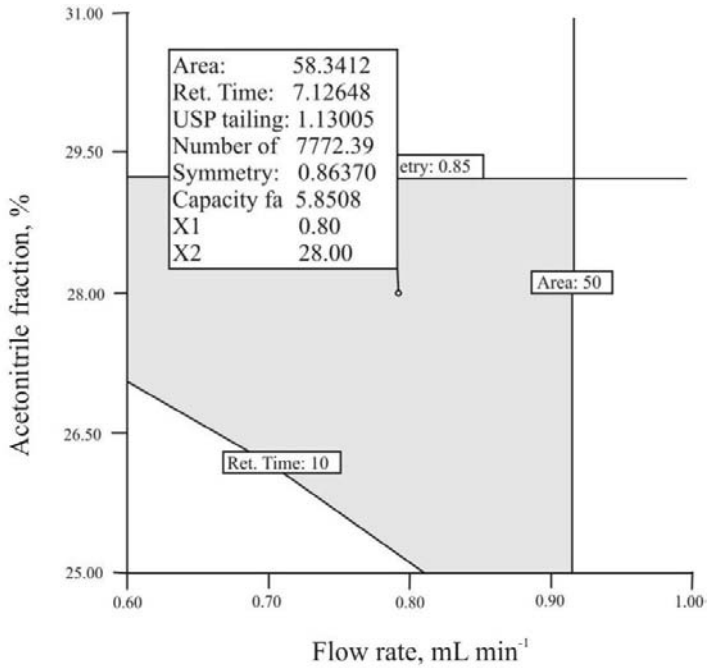

Fig. 5. Overlay plot – robustness of the method.

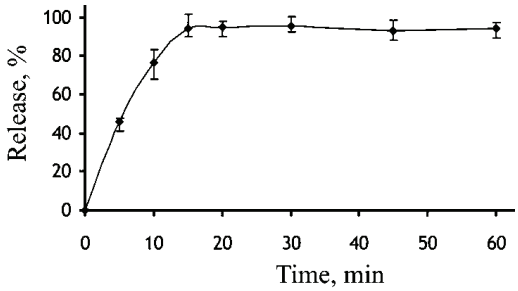

Fig. 6. Dissolution profile of digoxin.

CONCLUSIONS

In this work, an HPLC method for the evaluation of the dissolution of digoxin tablets in water is presented and validated by the modification of an existing in-house HPLC method. By this method, using the BP dissolution conditions, it is possible, simply and exactly, to determine digoxin in the dissolution medium without fluorescence detection or any additional sample pre-treatment. The acquired validation parameters indicate that this method is selective, accurate, precise and linear. In addition, by 2^4 full factorial design, it was shown that the method is robust and hence suitable for routine analyse of the dissolution of digoxin tablet.

ИЗВОД

HPLC МЕТОДА ЗА ОДРЕЂИВАЊЕ ДИГОКСИНА У РАСТВОРЕНИМ УЗОРЦИМА

МИРОСЛАВ Ж.МИЛЕНКОВИЋ[1],ВАЛЕНТИНА Д. МАРИНКОВИЋ[1],ПРЕДРАГ С. СИБИНОВИЋ[1], РАДОСАВ М. ПАЛИЋ[2] и ДРАГАН М.МИЛЕНОВИЋ[1]

[1]Фармацеутско хемијска индустрија Здравље–Актавис, Влајкова 199, Лесковац и [2]Универзитет у Нишу, Природно–математички факултет, Одсек за хемију, Вишеградска 33, Ниш

У овом раду представљена је HPLC метода за одређивање дигоксина у узорцима након теста растворљивости, по Британској фармакопеји (БФ). Хроматографија је изведена на 20 °C, на Symmetry C18 колони, 3,5 µm, 75 mm ×4,6 mm, са мобилном фазом вода–ацетонитрил (72:28, v/v) и УВ детекцијом на 220 nm. Установљено је да је метода селективна, линеарна, тачна и прецизна у специфицираном опсегу. *LOD* и *LOQ* вредности износиле су 0,015 µg mL^{-1} и 0,050 µg mL^{-1}. Тест робусности је такође изведен да би показао ефекат минорних промена у хроматографским параметрима (тј. у уделу ацетонитрила, протоку мобилне фазе, температури колоне и дужини колоне) на карактеристике пика дигоксин система. Потпуни факторијелни дизајн (2^4) је употребљен да би се показао утицај четири променљиве. Представљена метода је примењена у контроли квалитета и у тестовима стабилности дигоксин таблета.

(Примљено 6. јануара, ревидирано 13. септембра 2010)

REFERENCES

1. M. C. Tzou, R. A. Sams, R. H. Reuning, *J. Pharm. Biomed. Anal.* **13** (1995) 1531
2. Z. B. Todorović, M. L. Lazić, V. B. Veljković, D. M. Milenović, *J. Serb. Chem. Soc.* **74** (2009) 1143

3. X. Ouyang, Y. He, *Yaowu Fenxi Zazhi* **24** (2004) 213 (in Chinese) (*CA* 142/2004 397882)
4. S. H. Chen, H. L. Wu, J. C. Chang, S. M. Wu, S. J. Lin, *J. Liq. Chromatogr. Related Technol.* **22** (1999) 2321
5. F. C. Braga, W. Kreis, R. A. Recio, A. B. Oliveira, *Quim. Nova* **20** (1997) 481
6. D. Ivanovic, M. Medenica, D. Radulovic, Z. Djugumovic, *Drug Dev. Ind. Pharm.* **21** (1995) 1789
7. M. C. Tzou, *Diss. Abstr. Int. B* **55** (1994) 2175
8. B. Pekic, B. Slavica, *Memoir of Matica Srpska for Natural Sciences* **84** (1993) 73
9. H. Wiegrebe, M. Wichtl, *J. Chromatogr.* **630** (1992) 402
10. Y. Ikeda, Y. Fujii, M. Yamazaki, *J. Nat. Prod.* **55** (1992) 748
11. R. Bottler, *Pharm. Anal. Qualitaetskontrolle* **2** (1978) 36
12. G. W. Ponder, J. T. Stewart, *J. Chromatogr. A* **659** (1994) 177
13. D. M. Popova, T. N. Konyakhina, V. A. Semenova, A. P. Arzamastsev, *Farm. Zh. (Kiev)* **3** (1983) 44 (in Ukrainian)
14. T. Hagiwara, K. Akiyama, *Bunseki Kagaku* **36** (1987) 73 (*CA* 106/1987 144053)
15. T. Hagiwara, K. Nakayama, K. Akiyama, M. Doguchi, Iyakuhin *Kenkyu* **20** (1989) 679 (*CA* 111/1989 140376)
16. A. Jedlicka, T. Grafnetterova, V. Miller, *J. Pharm. Biomed. Anal.* **33** (2003) 109
17. USP31–NF26, United States Pharmacopeia Convention, Inc., Rockville, MD, 2008, p. 1965
18. The Japanese Pharmacopoeia XIII, Official Monographs for part I, 1996, p. 337
19. British Pharmacopoeia, Specific Monographs, 2007
20. Sigma-Aldrich, http://www.sigmaaldrich.com/life-science/cell-culture/learning-center/ cyclodextrin.html (accessed 21 November, 2009)
21. *Wikipedia*, http://en.wikipedia.org/wiki/Digoxin (accessed 21 November, 2009)
22. B. Dejaegher, Y. V. Heyden, *J. Chromatogr. A* **1158** (2007) 138
23. Y. Fujii, Y. Ikeda, M. Yamazaki, *J. Chromatogr.* **448** (1988) 157
24. International Conference on Harmonisation of Technical Requirements for Registration of Pharmaceuticals for Human Use (I.C.H.), Q2/R1 Validation of analytical procedures. Text and methodology, 1995
25. M. C. Gohel, A. F. Amin, *J. Controlled Release* **51** (1998) 115.

Journal of the Serbian Chemical Society
JSCS-info@shd.org.rs • www.shd.org.rs/JSCS
J. Serb. Chem. Soc. 75 (11) 1595–1604 (2010)
JSCS–4079
UDC 548.2+531.3+541.124+546.32'82'289'21:666.11
Original scientific paper

Crystal growth of $K_2TiGe_3O_9$ in the glass

SNEŽANA R. GRUJIĆ[1*#], NIKOLA S. BLAGOJEVIĆ[1#], MIHAJLO B. TOŠIĆ[2#], VLADIMIR D. ŽIVANOVIĆ[2] and ZAGORKA S. AĆIMOVIĆ-PAVLOVIĆ[1]

[1]*Faculty of Technology and Metallurgy, 4 Karnegijeva St., 11000 Belgrade and* [2]*Institute for Technology of Nuclear and other Mineral Raw Materials, Franchet d' Esperey 86, 11000 Belgrade, Serbia*

(Received 18 November 2009, revised 29 July 2010)

Abstract: The kinetics and mechanism of isothermal crystal growth of $K_2TiGe_3O_9$ from a glass of the same stoichiometric composition were studied. The crystal growth rate, U, in the range 1×10^{-11}–1.27×10^{-10} m s^{-1} was experimentally determined in the temperature interval 540–600 °C. In the range of high undercooling, Δt, 435–375 °C, spherical crystals growing at (374±19) kJ mol^{-1} was observed.

Keywords: crystal growth; $K_2TiGe_3O_9$; kinetics; mechanism; glass.

INTRODUCTION

Binary alkali germanates exhibit a characteristic behavior known as the "germanate anomaly effect".[1–3] This behavior means the presence of extremes on the curves showing the dependence of some properties (density, refractive index, glass transition temperature and viscosity) on the content of the alkali oxide. Studies of the behaviors of ternary germanate glasses are not very numerous. Recent investigations[4–6] showed that during crystallization of some K_2O–TiO_2–GeO_2 glasses with a high content of TiO_2, crystals of $K_2TiGe_3O_9$ were formed. The presence of these crystals enables non-linear optical materials showing second harmonic generation to be obtained.[6] Such materials have great potential for different applications. Due to this, the phase formation of $K_2TiGe_3O_9$ has been a subject of reinforced interest because knowledge of crystal nucleation and growth processes of $K_2TiGe_3O_9$ is important for the preparation of crystallized glasses possessing the desired microstructure and properties.

The results of a study of $K_2TiGe_3O_9$ crystal nucleation in a $K_2O{\cdot}TiO_2{\cdot}3GeO_2$ undercooled melt were previously published.[7] In the present study, attention was

* Corresponding author. E-mail: grujic@tmf.bg.ac.rs
# Serbian Chemical Society member.
doi: 10.2298/JSC091118120G

focused on the kinetics and mechanism of crystal growth of $K_2TiGe_3O_9$ from its undercooled melt.

EXPERIMENTAL

The $K_2O{\cdot}TiO_2{\cdot}3GeO_2$ glass was prepared by melting a homogeneous mixture of reagent grade K_2CO_3, TiO_2 (both Fluka Chemica,) and GeO_2 (electronic grade) in a platinum crucible. The melting was performed in an electric furnace, Carbolite BLF 17/3, at t = 1300 °C during τ = 2 h. The glass was obtained by quenching the melt on a steel plate. Powder X-ray diffraction analysis (XRD) confirmed the quenched melts to be vitreous. The glass samples were transparent, without visible residual gas bubbles.

The experiments were performed under isothermal conditions with bulk samples in a one-stage regime in an electric furnace, Carbolite CWF 13/13, with automatic regulation and a temperature accuracy of ±1°C. The glass samples were heated at a heating rate β = 10 °C min^{-1} up to the desired temperature of heat treatment and maintained at the chosen temperature for different times. The heat treatment temperatures, t_c, were in the range 540–600 °C. The samples were maintained at the selected temperature for times, τ_c, in the range 10–1000 min. Finally, the samples were removed from the furnace and crushed in an agate mortar for X-ray and SEM analyses.

A Jeol JSM 6460 microscope was used for the scanning electronic microscopy (SEM) investigations. The samples for SEM investigation were gold sputtered. The diameters of circular intersections of the particles were determined from the SEM micrographs. The crystal growth rate, U, at the treatment temperature, t, was determined from the time dependence of the largest circular cross-section diameter, d.

The XRD method was used to determine the phase composition. The XRD patterns were obtained on a Philips PW-1710 automated diffractometer using a Cu tube operated at 40 kV and 32 mA. The instrument was equipped with a diffracted beam curved graphite monochromator and a Xe-filled proportional counter. The diffraction data were collected in the 2θ Bragg angle range from 4 to 70°, counting for 0.25 s at every 0.02° step. The divergence and receiving slits were fixed 1 and 0.1, respectively. The XRD measurements were performed at room temperature in a stationary sample holder.

RESULTS AND DISCUSSION

The results of the chemical analysis show that a glass composition: $19.27K_2O{\cdot}16.8TiO_2{\cdot}63.93GeO_2$ (wt. %) was obtained. This composition is close to the stoichiometric one $K_2O{\cdot}TiO_2{\cdot}3GeO_2$.

The XRD patterns of samples thermally treated under different conditions are shown in Fig. 1, from which it can be seen that $K_2TiGe_3O_9$ was the only phase formed during the crystallization of this glass, *i.e.*, polymorphic crystallization occurred.[8]

The SEM micrographs of these samples are presented in Fig. 2. It is obvious that the nucleation process commenced within the bulk of the melt and that the morphology of the growing crystals was spherical.

A previous investigation of the nucleation of this glass showed that the temperature ranges of nucleation and crystal growth partly overlapped.[7] Accordingly, isothermal, single-stage heat treatment experiments were performed. The

largest circular cross-section diameters, *d*, measured as a function of time at 540, 560, 580, 590 and 600 °C are shown in Figs. 3a–3d. The crystal growth rates were obtained from the slope of the lines.

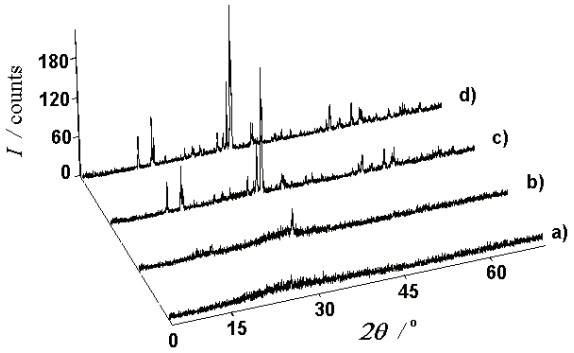

Fig. 1. XRD Patterns of: a) glass, b) sample crystallized at t = 580 °C for τ = 38 min, c) sample crystallized at t = 590 °C for τ = 30 min and d) sample crystallized at t = = 640 °C for τ = 1000 min.

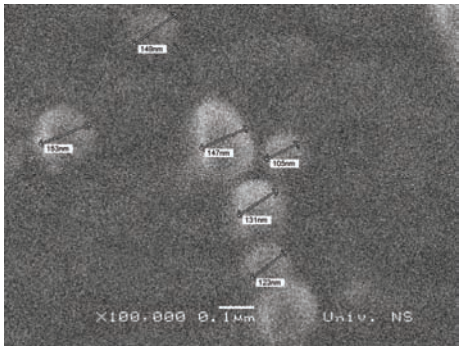

(a)

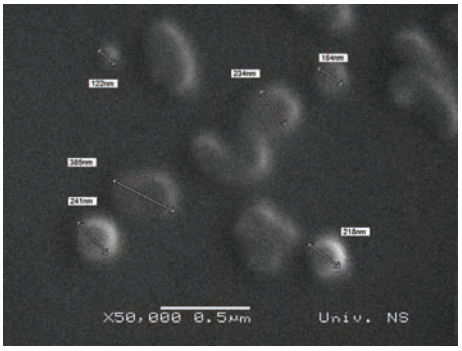

(b)

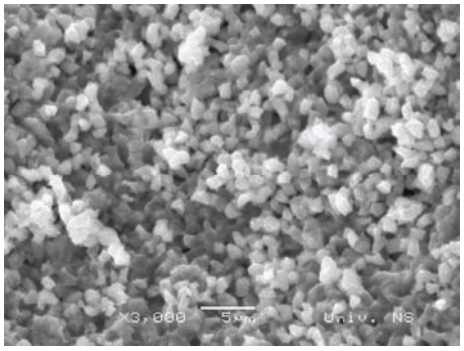

(c)

Fig. 2. SEM Micrographs of crystallized samples after heat treatment at: a) t = 580 °C for τ = 38 min, b) t = 590 °C for τ = 30 min and c) t = 640 °C for τ = 1000 min.

The experimentally determined crystal growth rate and nucleation rate as a function of temperature are presented in Fig. 4.

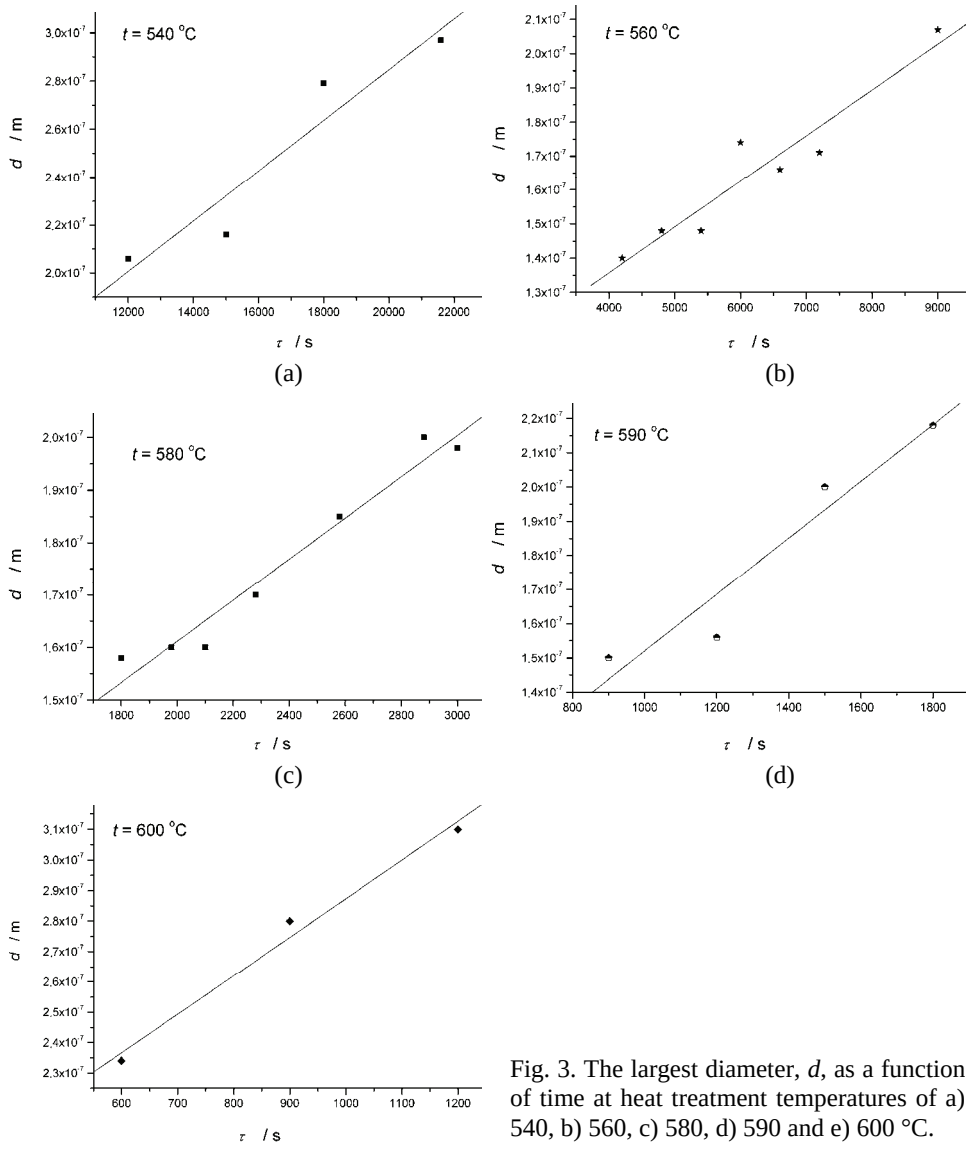

Fig. 3. The largest diameter, *d*, as a function of time at heat treatment temperatures of a) 540, b) 560, c) 580, d) 590 and e) 600 °C.

The kinetics and morphology of crystals growing from the melt are determined by the following factors: a) interface kinetics – the movement of material across the interface and its attachment to the crystal surface; b) material transfer – the diffusion of material in melt; c) heat transfer – the removal of latent heat of crystallization from the growing crystal surface and c) reconstructive transformation – the arrangement of atoms or ions species at the solid–liquid interface.[9] Crystal growth from the melt is realized by different mechanisms. The condition

of the surface of a growing crystal and the degree of undercooling of the melt play decisive roles on the action of certain growth mechanisms. Three standard models are employed to describe crystal growth and to predict the kinetic behavior and morphology: normal growth, screw dislocation growth and surface nucleation growth.[10–13] An appropriate method for the estimation of the surface condition of a growing crystal (crystal–liquid interface) and for the prediction of the growth mechanism is the Jackson criterion.[13] Accordingly, for materials with small entropies of fusion $\Delta S_m < 2R$, the solid–liquid interface should be rough on an atomic scale. If the interface is atomically rough, continuous growth with non-faceted interface morphology occurs and the anisotropy of the growth rate is small, hence normal growth is expected. In contrast, for materials with large entropies of fusion $\Delta S_m > 4R$, the solid–liquid interface should be smooth. If the interface is atomically smooth, layer growth with faceted interface morphology occurs, either by a screw dislocation or a surface nucleation growth mechanism. Previous experimental studies showed that for numerous organic and inorganic glasses, screw dislocation growth is operative. For glasses, crystallization with normal growth is less characteristic while surface nucleation growth is not usual.[10]

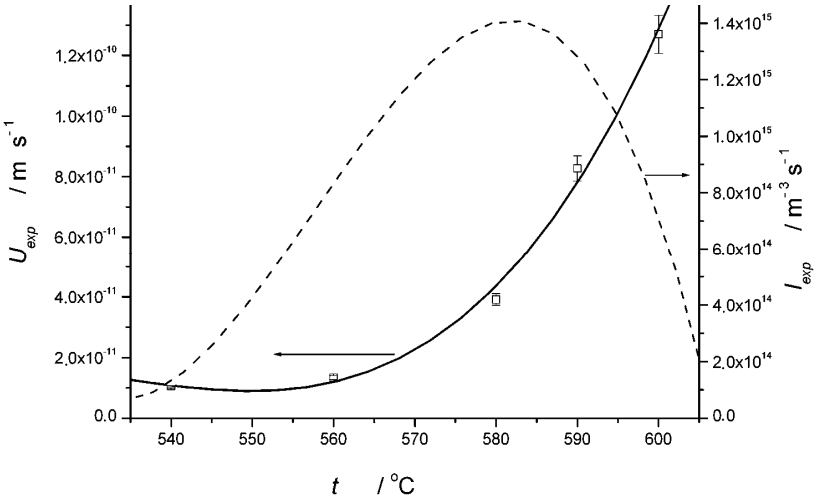

Fig. 4. U_{exp} and I_{exp}[7] in the temperature range 540–600 °C.

When the melt and crystal have the same chemical composition, for the case of growth at step sites provided by a screw dislocation intersecting the interface, the growth rate may be expressed by the relation:[13]

$$U = f\lambda v\left[1-\exp\left(-\frac{\Delta G}{RT}\right)\right] \quad (1)$$

where U is the growth rate per unit area of the interface, f is the fraction of preferred growth sites on the interface and υ is a frequency factor for transport at the interface, λ is the jump distance (of the order of atomic/molecular dimensions), ΔG is the free energy of crystallization (free energy difference in the transformation liquid-crystal, *i.e.*, the thermodynamic driving force for crystallization), T, is the temperature in Kelvin and R is the gas constant. The factor f is proportional to the undercooling $\Delta T = T_m - T$ according to the expression:

$$f = \frac{\lambda \Delta H_m \Delta T}{4\pi\sigma V_m T_m} \tag{2}$$

where T_m is the melting temperature, V_m is the molar volume of the crystalline phase, σ is the crystal/liquid interfacial and ΔH_m is the enthalpy of melting per mole. The frequency factor for transport at the interface, υ, may be expressed as:

$$\upsilon = \upsilon_0 \exp\left(-\frac{\Delta G_D}{RT}\right) \tag{3}$$

where υ_0 is the vibration frequency of the growth controlling atoms, ΔG_D is the activation free energy for diffusion across the interface (the activation energy of crystal growth).

Under the assumption that the molecular mobility necessary for crystal growth is similar to the transport of molecules in the bulk melt, then the activation energy for diffusion across the interface, ΔG_D, is equal to the activation energy for viscous flow, ΔG_η ($\Delta G_D \approx \Delta G$). Considering viscosity as an activated process, then it can be approximated by an equation of the form:[14]

$$\eta = \eta_0 \exp\left(\frac{\Delta G_\eta(T)}{RT}\right) \tag{4}$$

$$\eta_0 = \frac{kT}{l^3}\tau_0 \tag{5}$$

where l is the metal–oxygen bond length (Ge–O), τ_0 is a time of the order of the period of atomic vibration ($\tau_0 \approx 1/\upsilon_0$) and k is the Boltzmann constant.

By substitution of Eq. (5) into Eq. (4) and then into Eq. (3), the following expression is obtained:

$$\upsilon = \frac{kT}{l^3\eta} \tag{6}$$

Introducing Eqs. (2) and (6) into Eq. (1), Eq. (7) is obtained:

$$U = \frac{\lambda^2 \Delta H_m k}{4\pi\sigma V_m l^3} \frac{T\Delta T}{T_m} \frac{1}{\eta}\left[1 - \exp\left(-\frac{\Delta G}{RT}\right)\right] \tag{7}$$

Using Eq. (7) and the values of the parameters given in Table I, the theoretical rate of $K_2TiGe_3O_9$ crystal growth can be calculated.

TABLE I. The parameters of $K_2TiGe_3O_9$ used for the estimation of U_{calc}

k / J K^{-1} (Ref. 13)	1.3807×10^{-23}
λ / m (Ref. 15)	5.6×10^{-10}
l / m (Ref. 15)	1.77×10^{-10}
V_m / m^3 mol^{-1} (Ref. 8)	123.6×10^{-6}
σ / J m^{-2} (Ref. 8)	0.17
ΔG / J mol^{-1} (Ref. 7)	$\Delta G(T) = -102.97(1308.16 - T) + 108.27[(1308.16 - T) - T(\ln(1308.16/T)]$, T in K
η / Pa s (Ref. 5)	$\eta = -0.286 + 1739/(T - 684)$, T in K

To obtain a more exact insight into the relation between the theoretical and experimental values of the growth rate of $K_2TiGe_3O_9$ crystals, this relation in a narrow temperature range 540–600 °C is presented in Fig. 5, from which it may be seen that a good agreement between the theoretical and experimental values of the growth rate of $K_2TiGe_3O_9$ crystals exists in the temperature interval 540–600 °C. This enables the crystal growth mechanism and the activation energy of crystal growth to be determined based on experimental values.

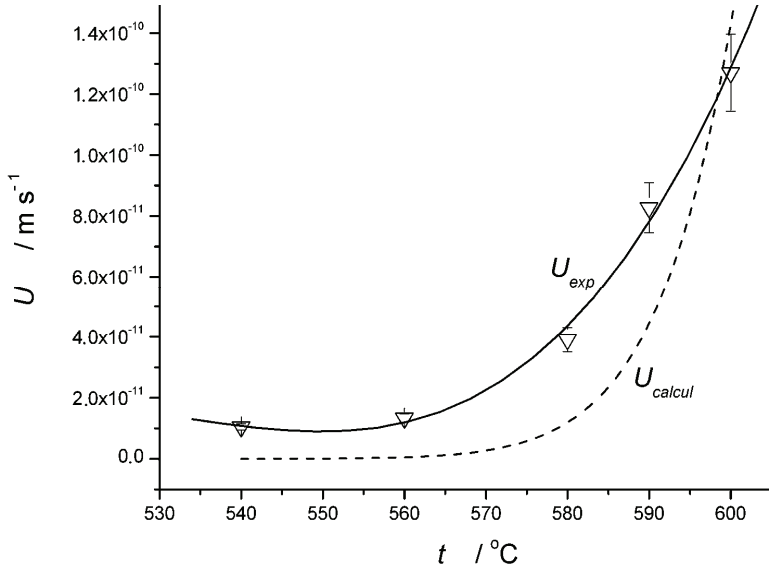

Fig. 5. Experimental (▽) and calculated (---) crystal growth rates according to Eq. (7) *vs.* t in the range 540–600 °C.

If in Eq. (1) the exponential factor expands in the series:

$$\exp^{-\frac{\Delta G}{RT}} = 1 - \frac{\Delta G}{RT} + \frac{1}{2!}\left(\frac{\Delta G}{RT}\right)^2 - \frac{1}{3!}\left(\frac{\Delta G}{RT}\right)^3 + \cdots \quad (8)$$

and as significant, the first two terms in the series are taken into consideration, the following replacement can be made

$$\left[1 - \exp\left(-\frac{\Delta G}{RT}\right)\right] = \frac{\Delta G}{RT} = \frac{\Delta H_\mathrm{m}}{RT}\frac{\left(T_\mathrm{m} - T\right)}{T_\mathrm{m}} = \frac{\Delta H_\mathrm{m}}{RT}\frac{\Delta T}{T_\mathrm{m}} \quad (9)$$

Replacement of Eq. (2), (3), (9) and $\upsilon_0 = kT/h$, $k = R/N_\mathrm{A}$ (where h is the Planck constant and N_A is the Avogadro constant) in Eq. (1) gives:

$$U = \frac{\lambda^2 \Delta H_\mathrm{m}{}^2}{4\pi\sigma V_\mathrm{m} h N_\mathrm{A} T_\mathrm{m}{}^2}(\Delta T)^2 \exp(-\frac{\Delta G_\mathrm{D}}{RT}) \quad (10)$$

The first term of the right side in Eq. (10) is independent of temperature, hence Eq. (10) may be written as:

$$U = K_1(\Delta T)^2 \exp\left(-\frac{\Delta G_\mathrm{D}}{RT}\right) \quad (11)$$

where $K_1 = \lambda^2 \Delta H_\mathrm{m}{}^2/(4\pi\sigma V_\mathrm{m} h N_\mathrm{A} T_\mathrm{m}{}^2)$.

Using the experimental data of the crystal growth rate at temperatures in the interval 540–600 °C according to Eq. (11), the relation $\ln[U_\mathrm{exp}/(\Delta T)^2]$ *vs.* $1/T$ shown in Fig. 6 was obtained. As can be seen in Fig. 6, the relationship can be described by a straight line of negative slope. This suggests that growth of

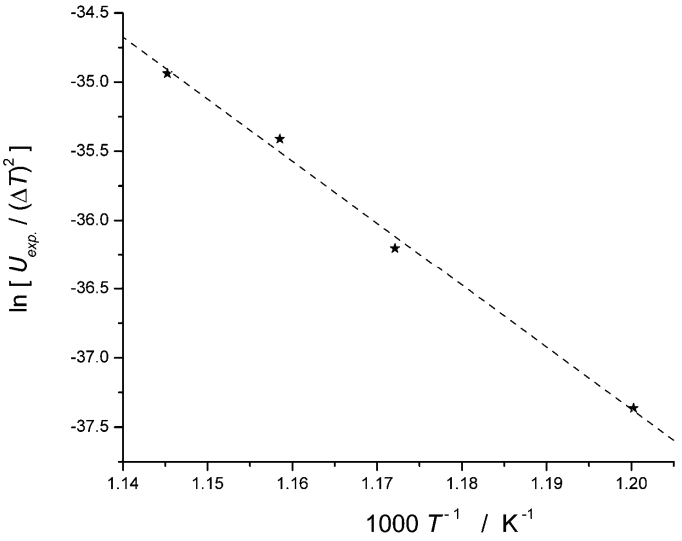

Fig. 6. Plot of $\ln[U_\mathrm{exp}/(\Delta T)^2]$ *vs.* $1/T$.

$K_2TiGe_3O_9$ crystals occurs by the screw dislocation mechanism in the region of undercooling, Δt, 435–475 °C. From the slope of this line, the activation energy of crystal growth ΔG_D = (374±19) kJ mol^{-1} was calculated.

In the range of large undercooling, the temperature dependence of the crystal growth rate substantially follows that of the viscosity of the liquid which crystallizes polymorphic and where crystal growth occurs by the screw dislocation growth mechanism. For comparison, the activation energy of viscous flow, $\Delta G_\eta(T)$, was calculated. Since $\Delta G_\eta(T)$ is temperature-dependent, the temperature range was selected in which the isothermal experiments were performed. The calculation was realized using data from Table I and Eq. (4). A value of $\Delta G_{\eta,560–600}$ = (372±12) kJ mol^{-1} was obtained, which is in good agreement with ΔG_D.

CONCLUSIONS

The crystal growth kinetics of $K_2TiGe_3O_9$ from its melt under isothermal conditions was studied. The experiments were performed in the temperature range 540–600 °C. The crystal growth rates determined by SEM were in the range from 1×10^{-11} to 1.27×10^{-10} m s^{-1}. In this temperature range, the agreement between the theoretical and experimental values of the crystal growth rate of $K_2TiGe_3O_9$ is good. The analysis showed that in the region of high undercooling, Δt, 435–475 °C, the crystals of $K_2TiGe_3O_9$ grew by the screw dislocation mechanism. The activation energy of crystal growth ΔG_D = (374±19) kJ mol^{-1} was calculated. This value corresponds to the activation energy of viscous flow in this temperature range.

Acknowledgment. The authors are grateful to the Ministry of Science and Technological Development of the Republic of the Serbia for financial support (Project No. 142041).

ИЗВОД

РАСТ КРИСТАЛА $K_2TiGe_3O_9$ У СТАКЛУ

СНЕЖАНА Р ГРУЈИЋ[1], НИКОЛА С БЛАГОЈЕВИЋ[1], МИХАЈЛО Б ТОШИЋ[2], ВЛАДИМИР Д ЖИВАНОВИЋ[2] и ЗАГОРКА С АЋИМОВИЋ-ПАВЛОВИЋ[1]

[1]Технолошко-металуршки факултет, Карнегијева 4, 11000 Београд и [2]Институт за технологију нуклеарних и других минералних сировина, Франше д'Епереа 86, 11000 Београд

Под изотермским условима проучавана је кинетика и механизам раста $K_2TiGe_3O_9$ кристала из стакла истог стехиометријског састава. У интервалу температуре 540–600 °C експериментално су одређене брзине раста кристала, U, 1×10^{-11}–1.27×10^{-10} m s^{-1}. Показано је да се у области високих потхлађења, Δt, 435–375 ° C, раст сферних кристала ове фазе одвија по механизму завојне дислокације. Добијена је енергија активације раста кристала ΔG_D = = (374±19) kJ mol^{-1}.

(Примљено 18. новембра 2009, ревидирано 29. јула 2010)

REFERENCES

1. M. K. Murthy, E. M. Kirby, *Phys. Chem. Glasses* **5** (1964)144

2. J. E. Shelby, *J. Am. Ceram. Soc.* **57** (1974) 436
3. E. F. Riebling, *J. Chem. Phys.* **39** (1963) 1889
4. S. R. Grujić, N. S. Blagojević, M. B. Tošić, V. D. Živanović, *Ceram. Silik.* **49** (2005) 278
5. S. Grujić, N. Blagojević, M. Tošić, V. Živanović, B. Božović, *J. Therm. Anal. Calor.* **83** (2006) 463
6. T. Fukushima, Y. Benino, T. Fujiwara, V. Dimitrov, T. Komatsu, *J. Solid State Chem.* **179** (2006) 3949
7. S. R. Grujić, N. S. Blagojević, M. B. Tošić, V. D. Živanović, J. D. Nikolić, *Ceram. Silik.* **53** (2009) 128.
8. Joint Committee on Powder Diffraction Standards (JCPDS), *Powder Diffraction File*, Card No. 27-0394, 1975
9. V. J. Fratello, J. F. Hays, F. Spaepen, D. Turnbull, *J. Appl. Phys.* **51** (1980) 6160
10. D. R. Uhlmann, in *Advances in Ceramics*, J. H. Simmons, D. R. Uhlmann, D. H. Beal, Eds., American Ceramic Society, Westerville, OH, 1982, p. 80
11. V. M. Fokin, M. L. F. Nascimento, E. D. Zanotto, *J. Non-Cryst. Solids* **351** (2005) 789
12. N. Diaz-Mora, E. D. Zanotto, V. M. Fokin, *Phys. Chem. Glasses* **39** (1998) 91
13. W. D. Kingery, H. K. Bowen, D. R. Uhlmann, *Introduction to Ceramics*, Wiley Interscience, New York, 1976, p. 340
14. I. Gutzow, J. Schmelzer, *The Vitreous State*, Springer, Berlin, 1995, p. 169
15. G. S. Henderson, H. M. Wang, *Eur. J. Mineral.* **14** (2002) 733.

Journal of the Serbian Chemical Society
JSCS-info@shd.org.rs • www.shd.org.rs/JSCS
J. Serb. Chem. Soc. 75 (11) 1605–1616 (2010)
JSCS–4080
UDC 665.73/.75+504.53.054:
620.95:628.516
Original scientific paper

Change of isoprenoids, steranes and terpanes during *ex situ* bioremediation of mazut on the industrial scale

VLADIMIR P. BEŠKOSKI[1*#], MILOŠ TAKIĆ[2], JELENA MILIĆ[1#], MILA ILIĆ[1#], GORDANA GOJGIĆ-CVIJOVIĆ[1#], BRANIMIR JOVANČIĆEVIĆ[1,2#] and MIROSLAV M. VRVIĆ[1,2#]

[1]*Department of Chemistry, Institute of Chemistry, Technology and Metallurgy, Njegoševa 12, P.O. Box 473, 11001 Belgrade and* [2]*Faculty of Chemistry, University of Belgrade, Studentski trg 16, P.O. Box 51, 11158 Belgrade, Serbia*

(Received 5 May, revised 22 June 2010)

Abstract: This paper presents the results of an *ex situ* bioremediation of soil contaminated by mazut (heavy residual fuel oil) in the field scale (600 m^3). The treatment-bed (thickness 0.4 m) consisted of mechanically mixed mazut-contaminated soil, softwood sawdust as an additional carbon source and crude river sand, as a bulking and porosity increasing material. The inoculation/reinoculation was conducted periodically using a biomass of a consortium of zymogenous microorganisms isolated from a bioremediation substrate. The biostimulation was performed through addition of nutritious substances (N, P and K). The aeration was improved by systematic mixing of the bioremediation system. After 50 days, the number of hydrocarbon degraders had increased a 100 fold. Based on the changes in the group composition, the average biodegradation rate during bioremediation was 24 mg kg^{-1} day^{-1} for the aliphatic fraction, 6 mg kg^{-1} day^{-1} for the aromatic fraction and 3 mg kg^{-1} day^{-1} for the nitrogen–sulphur–oxygen compounds (NSO)–asphaltene fraction. In the saturated hydrocarbon fraction, gas chromatography–mass spectrometry (GC–MS) in the single ion-monitoring mode (SIM) was applied to analyse isoprenoids pristane and phytane and polycyclic molecules of sterane and triterpane type. Biodegradation occurred during the bioremediation process, as well as a reduction of the relative quantities of isoprenoids, steranes, tri- and tetracyclic terpanes and pentacyclic terpanes of the hopane type.

Keywords: mazut; bioremediation; field experiment; zymogenous microbial consortia; isoprenoids, steranes and terpanes.

* Corresponding author. E-mail: vbeskoski@chem.bg.ac.rs
# Serbian Chemical Society member.
doi: 10.2298/JSC100505091B

INTRODUCTION

Mazut is a low quality, heavy residual fuel oil (chain length 12–70 C atoms).[1,2] In the United States and western Europe, heavy fuel oil is blended or broken down with the end product being diesel. Mazut is widely used in eastern Europe as a heating agent. Its long-term storage and use leads to the formation of a reservoir of hydrocarbon sediment with a high content of various mechanical impurities and water, which may potentially be hazardous for the environment.

The accumulated sediment is periodically taken off by mechanical means. Common practice dictates that the removed sediment should be placed into metal barrels or discarded reservoirs. In the case of incidents and mazut spills onto concrete surfaces, it is habitual to add sand to prevent further spreading, which is then covered and discarded along with the removed contaminated soil on a watertight material. Improper disposal of such material leads to contamination of the environment, in particular contamination of soil, and represents a grave hazard for the subterraneous waters.

Among numerous technologies for the cleansing of contaminated sites, bioremediation by means of zymogenous microorganisms[3] is the most commonly used method.[4,5]

Oil-degrading mixed cultures can be constructed either by combining a number of strains with known complementary degradative capabilities (defined consortia) or by direct enrichment procedures (non-defined consortia).[6]

Enrichment procedures with selected oil products or with some specific components can provide non-defined, metabolically specialized microbial consortia. The result is a microbial population naturally selected by its metabolic cooperation in the degradation of each mixture, with potentially higher efficiency in degrading identified and non-identified components.[7]

Studies conducted to date of bioremediation of soil polluted by mazut, performed in laboratories on the level of model systems, have proven the presence of bioremediation potential for stimulated self-purification.[8]

Although the most suitable criteria for optimising the bioremediation process are known (careful control of temperature, aeration, particle size, moisture, macro and micronutrients in the mass to be composted, C/N ratio of the materials, *etc*.),[9] so that the microbial activity necessary for treating this organic matter can be encouraged, very few studies have attempted to treat mazut and heavy fuel oil on the industrial scale.[10–14]

The fraction of saturated hydrocarbons is dominant in most oils compared to aromatic hydrocarbons and nitrogen-sulphur-oxygen compounds (NSO).[15–17] The fraction shows the highest presence of *n*-alkanes and isoprenoid aliphatic alkanes. The *n*-alkanes in oils may be present in different ranges, most frequently *n*-C_{10}–C_{35}, while the most represented isoprenoids are C_{19}, pristane and C_{20}, phytane.

Polycyclic hydrocarbons of the sterane (C_{27}–C_{29}) and terpane type (tri-, tetra-, and pentacyclic; C_{19}–C_{35}) are most commonly found in much smaller quantities. Due to their great biomarker potential, these compounds are highly important in both organo-geochemical and bioremediation testing.

Previous field scale application showed that the oil pollutant mixture in the soil treated by *ex situ* bioremediation behaved in a complex way: different degradation rate and time evolution were observed for the different fractions of the hydrocarbon mixture, which are characterised by different molecular weight and structure.[18,19] It was also concluded that a stable microbial community had been formed after initial fluctuations and that the microorganisms which decompose hydrocarbons were dominant in the microbial population at the end of the bioremediation process, with a share of more than 80 % (range 10^7 CFU/g).[20]

This paper presents transformations of saturated hydrocarbons of petroleum type pollutants (isoprenoids and polycyclic alkanes of the sterane and terpane type) during *ex situ* bioremediation of soil contaminated by mazut of approximately 600 m^3. Dominant hydrocarbon utilizing strains from mazut-contaminated soil were selected and used for reinoculation as the active zymogenous microbial consortium in this study. Experiments of biostimulation, bioventilation and reinoculation were performed during five months.

EXPERIMENTAL

Preparation of the biomass of the zymogenous consortium

The consortium of microorganisms was obtained from a mazut-contaminated soil by the method of enrichment using a mineral medium (10 mass %),[21] in which the mazut was used as the sole source of energy and carbon at a concentration of 2000 ppm in one-litre Erlenmeyer flasks with 200 mL medium.

Suspensions of the microorganisms were concentrated and used as inoculum to seed four 5-litre Erlenmeyer flasks containing 2000 mL of a medium containing 23 g of nutritious bouillon, 100 mL of soil extract and 20 g of mazut.[22] A commercial non-toxic and readily biodegradable surfactant, Biosolve® Clear® supplied by the Westford Chemical Corporation, (Westford, MA, USA) was used as a surface active agent to solubilise the mazut. The original solution supplied by the manufacturer was used at a concentration 1 mL L^{-1}. The growth conditions were as follows: temperature, 28 °C; 120 rpm; pH 7.0 (adjusted with 1.0 M HCl or NaOH); duration of growth: 96 h.

The microbial populations from all four flasks were used to inoculate (approx. 1 % v/v) a self-designed and produced mobile bioreactor (total volume 1000 L) with a working volume of 800 L, to produce the microbial consortium. The medium was 12 g L^{-1} of meat peptone (Torlak, Belgrade, Serbia); 0.2 g L^{-1} $(NH_4)_2HPO_4$; 25 g L^{-1} of an in autoclave sterilized soil sample from an undisturbed deciduous woodland; and 10 g L^{-1} of mazut. The growth conditions: non-sterile, 25 °C, aeration and agitation 0.70 volume of air/volume of medium/min, pH 7.0 (adjusted with 10 M HCl or NaOH), duration 48 h and sunflower oil (1 mL L^{-1}) as an antifoaming agent.

Experimental treatment bed, design and treatment

The treatment bed for bioremediation was set up on a watertight asphalt base with an approximate area of 1500 m^2 and a 1 % slope. A quantity of 270 m^3 of contaminated soil was mixed with 300 m^3 of crude river sand and 60 m^3 of softwood sawdust as the additional carbon source and bulking component. To ensure homogenization, the components were mixed 3 times with a front-end loader and finally fitted with a harrow. The final dimensions of the treatment bed at the bioremediation site were about 75 m×20 m with a height of 0.4 m, which means that the bioremediation substrate had a volume of approximately 600 m^3. A perimeter drain enclosed the entire treatment area and directed all leachate and runoff to a joint vessel, from where they were pumped back to the treatment bed. Based on the analysis, the optimal ratio C:N:P:K (approx.100:10:1:0.1) was secured by spraying a solution of ammonium nitrate, diammonium phosphate and potassium chloride using a tractor-powered agricultural sprinkler. This also provided for the required level of moisture (40–60 % of the water holding capacity--WHC). Moisture and aeration during bioremediation were maintained by 15-day watering, tumbling and mixing of the treatment-bed. Reinoculation with the prepared microbial biomass was performed in 30-day intervals, in the same manner as the moistening substrate was applied.

The treatment bed was also amended with BioSolve® Clear®, applied at a volume of 70 mL of original solution per cubic meter.

After mixing, the heaps were covered with polyethylene foil to prevent the direct influence of the weather conditions on the bioremediation substrate.

The bioremediation experiment was conducted from March to August 2009 and in this period, the average temperature was 18.2 °C (min. 0.3, and max. 35.4 °C).

Chemical and microbiological indicators of the bioremediation process were monitored immediately after application of the microbial biomass (time zero, sample S-0) and every 50 days over a period of 150 days (designations S-50, S-100, S-150).

Determination of the number of microoorganisms

The number of microorganisms was determined by the method of a serial dilution on agar plates incubated at 28 °C. For the total microorganisms, a nutrient agar was used and for hydrocarbon degraders, a mineral based medium with 2000 ppm diesel fuel.[21,23]

Determination of hydrocarbon fractions and GC–MS analysis

The organic substance of the bioremediation substrate was extracted by the Soxhlet method and the components of the group composition were quantified after chromatographic separation on an adsorbent column. The NSO-asphaltene fraction was calculated arithmetically.[24]

Isoprenoid aliphatic alkanes, pristane and phytane, and polycyclic alkanes of sterane and triterpane types in saturated hydrocarbon fractions were analysed by gas chromatography––mass spectrometry (GC–MS). An Agilent GC System 6890N gas chromatograph with an Agilent 7673 Series injector and Series 5973 mass detector fitted with J & W Scientific DB--5ms-ITD column (30 m, 0.25 mm id, 0.25 μm film) was used. Helium was employed as the carrier gas (flow rate 1 mL min^{-1}). The temperature program of the column was 50 to 285 °C at 10 °C min^{-1}. Isoprenoids were identified from the *m/z* 183, steranes from *m/z* 217 and triterpanes from *m/z* 191 fragmentograms obtained from analysis in the single ion-monitoring mode (SIM). The most relevant peaks were identified based on organic geochemical literature data,[17] or based on total mass spectra, using mass spectra databases.[25]

All the results were calculated to dry substance.

RESULTS AND DISCUSSION

Basic microbiological indicators

The initial concentration of the zymogenous population of hydrocarbon degrading bacteria in the sample S-0 was approximately 10^4 CFU g^{-1} (Fig. 1). Previously conducted studies had determined that the bioremediation would not be realised to a significant extent if the population of the microorganisms capable of degrading the target contaminant was smaller than 10^5 CFU g^{-1} of soil.[4] The concentration of these microorganisms was increased through reinoculation of the zymogenous microbial biomass and multiplication in the bioreactor. Following biostimulation and reinoculation, the number of hydrocarbon degrading microorganisms after 50 days had increased by as much as 100 times (from 10^4 to 10^6). Midway through the process, the proportion of oil hydrocarbon degraders in the total number of microorganisms had increased to 75 %. This proportion amounted to only < 1 % at the beginning of the process. A decreased hydrocarbon concentration brought this proportion down to 25 %. The population of the bacterial consortium able to consume diesel oil as a sole source of carbon was stable even after 150 days following the first application of the microbial consortium, indicating the very high survivability of the introduced strains.

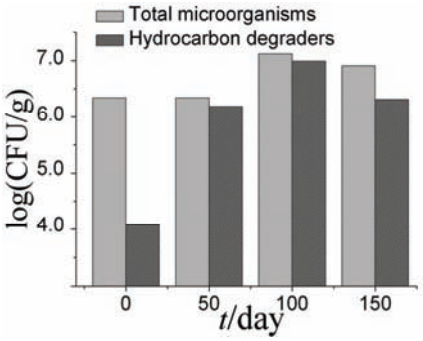

Fig. 1. Changes in the number of total microorganisms and hydrocarbon degraders during the bioremediation process.

Due to the toxic effect of the contaminant, the biodiversity of the contaminated soil decreased, whereas the concentration of the population of microorganisms degrading the contaminating substance rose.[26] Along with a decrease in the concentration of the contaminant towards the end of the remediation process, the share of hydrocarbon utilizing microorganisms in the total number decreased. Due to the reduced toxicity, the microbial population in the soil became more diverse.

Analysis of the hydrocarbon fractions

Biodegradation and the decreased concentration of the individual fractions within the hydrocarbons is shown in Fig. 2. The highest degree of degradation was noted in the most extensive aliphatic fraction. In sample S-0, the proportions

of aliphatic, aromatic and NSO-asphaltene fraction were 71.6, 17.0 and 11.4 %, respectively. Due to the intensive biodegradation processes, the share of individual fractions after 50 days compared to the initial concentration decreased to 27.0, 5.2 and 7.5 %. Since the *n*-alkane fraction was dominant and the most prone to bioremediation, the trend continued so that the percentages of the individual fractions amounted to 15.4, 3.3 and 6.4 after 100 days, *i.e.*, 3.1, 0.6 and 1.9 after 150 days.

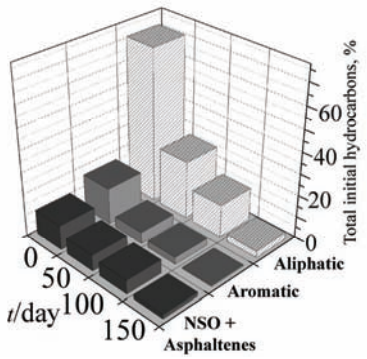

Fig. 2. Percent and decrease of the concentration of group composition components within the total initial hydrocarbons during *ex situ* bioremediation.

The average rate of decrease during the biodegradation of the heavy residual fuel oil was 23.7 mg kg^{-1} day^{-1} for the aliphatic fraction, 5.7 mg kg^{-1} day^{-1} for the aromatic fraction, and 3.3 mg^{-1} kg^{-1} day^{-1} for NSO and the asphaltene fraction. As expected, the asphaltene fraction was the most recalcitrant and the most persistent in the environment, which is the reason why it has the slowest rate of decomposition.[12] Considering the decomposition rate of the individual fractions, the relative ratios within the group composition change at the expense of decreased aliphatic and aromatic fractions and increased proportion of NSO and the asphaltene fraction. The increase in the proportion of NSO and the asphaltene fraction was followed by a decrease in the absolute value of all fractions in the group composition.

GC–MS Analysis of the aliphatic hydrocarbon fraction

Changes in the content of the alkane fraction were monitored by means of GC–MS analysis of samples S-0, S-50, S-100 and S-150. The total ion current (TIC) chromatograms of the alkane fraction of samples S-0 and S-150 are shown in Fig. 3. The SIM-chromatograms of isoprenoids (m/z = 183), terpanes (m/z = = 191) and steranes (m/z = 217) are presented in Figs. 4–6, respectively.

Based on the appearance of the TIC-chromatograms (for samples S-0 and S-150, Fig. 1), it may be concluded that alkane fractions of the tested samples are characterized by a high quantity of an unresolved complex mixture (UCM). This is an expected result, knowing that the soil tested in this study had been polluted

by mazut, a heavy oil fraction. The presence of peaks of individual *n*-alkanes is also visible, which is in accordance with the fact that the alkane fraction makes up over 75 % of the total hydrocarbons. As judged from the gas chromatograms, the hydrocarbons left in the soil had already been degraded to some extent during natural biodegradation processes since the abundances of C_{17} and C_{18} *n*-alkanes at time zero was somewhat smaller than the abundances of pristane (C_{19}) and phytane (C_{20}).

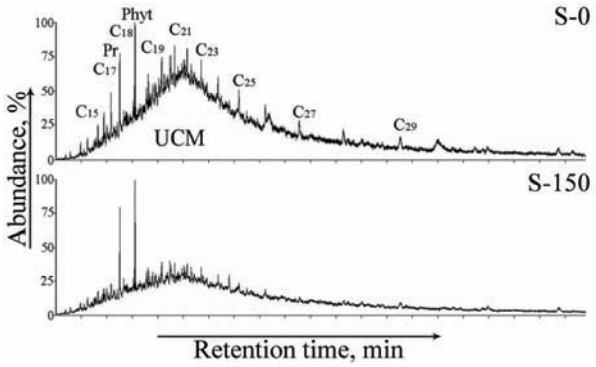

Fig. 3. TIC of the alkane fractions of extract samples S-0 and S-150; Pr: pristane; Phyt: phytane.

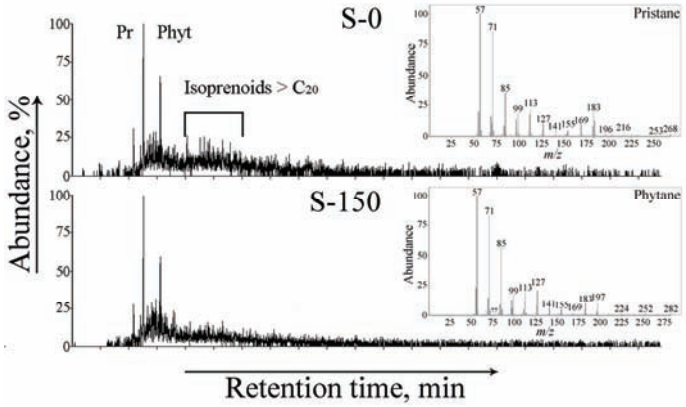

Fig. 4. Fragmentograms of the isoprenoids (SIM, *m/z* 183) of the alkane fractions in the samples S-0 and S-150 (full mass spectra corresponding to peaks of pristane C19 and phytane C20 for S-0 sample are also presented); Pr: pristane; Phyt: phytane.

The ratios Pr/*n*-C_{17} and Phyt/*n*-C_{18} may be used for differentiating between physical weathering and bioremediation.[27] Since the volatility of *n*-C_{17} and pristane are similar, as is the case with the volatility of *n*-C_{18} and phytane, a decrease in the concentrations of these substances over time should be attributed to weathering if their ratio remains the same. If with time, the ratios Pr/*n*-C_{17} and Phyt/

/*n*-C_{18} increase, the conclusion is that this occurs due to bioremediation, which is a consequence of the fact that bioremediation removes *n*-C_{17} and *n*-C_{18} at higher rates than pristane and phytane, respectively.[28]

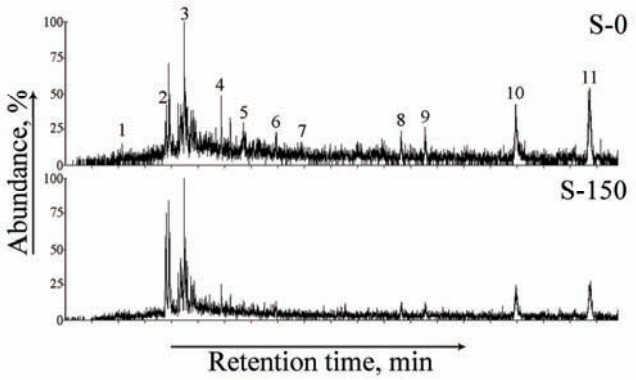

Fig. 5. Fragmentograms of the terpanes (SIM, *m/z* 191) of the alkane fractions in the samples S-0 and S-150. 1: C19 – tricyclic terpane; 2: C_{21} – tricyclic terpane; 3: C_{22} – tricyclic terpane; 4: C_{24} – tricyclic terpane; 5: C_{25} – tricyclic terpane; 6: C_{24} – tetracyclic terpane; 7: C_{28} – tricyclic terpane; 8: C_{27} – 18α(*H*)-22,29,30-trisnorhopane (Ts); 9: C_{27} – 17α(*H*),18α(*H*),21β(*H*)--25,28,30-trisnorhopane; 10: C_{29} – 17α(*H*),21β(*H*)-hopane; 11: C_{29} – 18α(*H*),21β(*H*)-30-norneohopane.

A decrease of the quantity of isoprenoid molecules over the course of the bioremediation process may also be noted based on the abundance of the peaks in chromatograms of the ion *m/z* 183, characteristic for these molecules (samples S-0 and S-150; SIM method; Fig. 4). In the chromatogram *m/z* 183 of all the samples, the pristane and phytane peaks are clearly differentiated, being the most intensive in the sample S-0. In this sample, individual peaks originating from the homologue strain > C_{20} isoprenoids are also observed, while in sample S-150 they are biodegraded.

The chromatogram of terpane in the initial sample S-0 (SIM, *m/z* 191, Fig. 5) is dominated by peaks originating from C_{19}–C_{28} tricyclic terpanes, C_{24} tetracyclic terpane and C_{27}–C_{29} pentacyclic terpanes, with a distribution not typical for raw heavy fuel oil (data not shown) rather for samples that had been exposed to weathering and biodegradation over extended periods of time.[17] This is in accordance with the ratio Pr/*n*-C_{17} and Phyt/*n*-C_{18} of the SIM isoprenoid fraction. Bearing in mind that terpanes are, generally speaking, more resistant to microbiological degradation compared to *n*-alkanes and isoprenoid aliphatic alkanes, their presence in the oil pollutant that had previously been exposed to natural biodegradation is not surprising. During the bioremediation process, the quantity of all tricyclic and tetracyclic terpanes decreased and in the sample S-150, the quantity of tricyclic (C_{19}, C_{24}, C_{25}, and C_{28}) and tetracyclic terpanes (C_{24}) is accord-

ing to their intensity virtually no different from the peaks overlapped by the background noise. In relation to them, the quantity of pentacyclic terpanes of the hopane type also decreased at an intensity that conforms to degradation of oil and oil derivatives under natural conditions.

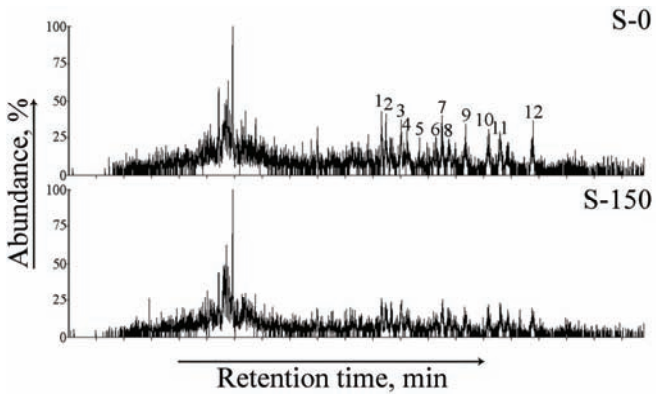

Fig. 6. Fragmentograms of the steranes (SIM, *m/z* 217) of the alkane fractions in the samples S-0 and S-150. 1: C_{27} – 13β(*H*),17α(*H*)-diasterane (20S); 2: C_{27} – 13β(*H*),17α(*H*)-diasterane (20R); 3: C_{27} – 13α(*H*),17β(*H*)-diasterane (20S); 4: C_{27} – 13α(*H*),17β(*H*) diasterane (20R); 5: C_{28} – 13β(*H*),17α(*H*)-diasterane (20R); 6: C_{28} – 13α(*H*),17β(*H*)-diasterane (20S) + C_{27} – – 14α(*H*),17α(*H*)-sterane (20S); 7: C_{29} – 13β(*H*),17α(*H*)-diasterane (20S) + C_{27} – – 14β(*H*),17β(*H*)-sterane (20R); 8: C_{27} – 14β(*H*),17β(*H*)-sterane (20S) + C_{28} – – 13α(*H*),17β(*H*)-diasterane (20R); 9: C_{29} – 13β(*H*),17α(*H*)-diasterane (20R); 10: C_{29} – 13α(*H*),17β(*H*)-diasterane (20R) + C_{28} –14β(*H*),17β(*H*)-sterane (20R); 11: C_{28} – 14α(*H*),17α(*H*)-sterane (20R); 12: C_{29} – 14α(*H*),17α(*H*)-sterane (20R).

Steranes and diasteranes are polycyclic alkanes that are degraded more quickly and easily than terpanes.[29] The decreased concentration due to intensive bioremediation processes makes their identification by the SIM method more difficult. Over the course of conducted bioremediation experiments, the fate of steranes and their more stable structural isomers, diasteranes, C_{27}–C_{29}, is similar to the fate of the terpanes (Fig. 6), and biodegradation, decrease and loss of resolution of the individual signals, was observed in the sample S-150.

CONCLUSIONS

This research monitored the effects of bioremediation of soil contaminated by mazut over a period of 150 days (March – July 2009). The bioremediation was stimulated through a two-week reinoculation with a zymogenous microbial consortium, along with mixing, watering and biostimulation. The analysis of change in the group composition evidenced that the average rate of decrease during the biodegradation of mazut was 23.7 mg kg^{-1} day^{-1} for the aliphatic fraction, 5.7 mg kg^{-1} day^{-1} for the aromatic fraction and 3.3 mg kg^{-1} day^{-1} for the NSO-asphaltene fraction. These findings indicate that the microorganisms

consumed all the components of the compounds of the hydrocarbon mixture, although at different biodegradation rates.

The participation of oil hydrocarbon degraders to the total number of microorganisms had increased to 75 % by the mid-cycle, compared to < 1 % during early bioremediation. The population of microorganisms capable of using diesel as their sole source of carbon remained stable even 150 days after the first reinoculation, which indicates that the natural ability of microorganisms to adapt to the environmental conditions significantly contributes to their extremely high survival rate.

The fate of the saturated hydrocarbons was monitored through changes in the composition of the alkane fraction. The abundance of *n*-C_{17}- and *n*-C_{18}-alkanes at time zero was somewhat smaller than the abundance of pristane (C_{19}) and phytane (C_{20}). This indicates that the process of hydrocarbon degradation had started before the design and application of the bioremediation procedure.

Polycyclic alkanes, steranes and diasteranes, as well as terpanes, were biodegraded in the sample S-150 and did not differ from peaks overlapped by the background noise. The zymogenous bacterial consortium used in this bioremediation study degraded isoprenoids with > C_{20}, and to a certain extent pristane and phytane as well, which are recalcitrant compounds resistant to biodegradation and hence commonly used as chemical markers against which the degree of biodegradation of the other compounds and oil maturation are measured.[27,30] Biodegradation of pristane and phytane means that these compounds are not suitable internal standards for monitoring bioremediation. Therefore, by comparing the content of other hydrocarbons relative to pristane and phytane, their degree of biodegradation may be underestimated, because branched pristane and phytane are also biodegradable, although in most cases with a lower biodegradation rate. However, the ratio Pr/*n*-C_{17} and Phyt/*n*-C_{18} may serve to differentiate between physical weathering and bioremediation.[27] The ratio Pr/*n*-C_{17} and Phyt/*n*-C_{18} increased over time of bioremediation because bioremediation removes *n*-C_{17} and *n*-C_{18} at a higher rate than pristane and phytane, respectively.

TIC confirmed a significant degradation of alkanes. This was followed by a decreased concentration of isoprenoids (> C_{20}), tricyclic (C_{19}–C_{26}) and tetracyclic terpanes (C_{24}), pentacyclic triterpanes (C_{27}–C_{30}) as well as by decreased sterane and diasterane contents (C_{27}–C_{29}).

Acknowledgements. This work was supported by the Ministry of Science and Technological Development of the Republic of Serbia under Grant Nos. ON 142018 and TR 20131B.

ИЗВОД

ПРОМЕНА ИЗОПРЕНОИДНЕ, СТЕРАНСКЕ И ТЕРПАНСКЕ ФРАКЦИЈЕ ТОКОМ *EX SITU* БИОРЕМЕДИЈАЦИЈЕ МАЗУТА НА ИНДУСТРИЈСКОМ НИВОУ

ВЛАДИМИР П. БЕШКОСКИ[1], МИЛОШ ТАКИЋ[2], ЈЕЛЕНА МИЛИЋ[1], МИЛА ИЛИЋ[1], ГОРДАНА ГОЈГИЋ-ЦВИЈОВИЋ[1], БРАНИМИР ЈОВАНЧИЋЕВИЋ[1,2] и МИРОСЛАВ М. ВРВИЋ[1,2]

[1]*Центар за хемију, Институт за хемију, технологију и металургију, Његошева 12, п. пр 473, 11001 Београд и* [2]*Хемијски факултет, Универзитет у Београду, Студентски трг 16, п. пр 51, 11158 Београд*

Приказани су резултати *ex situ* биоремедијације земљишта контаминираног мазутом на индустријском нивоу (600 m^3). Биоремедијациони материјал (дебљине 0,4 m) се састојао од механички помешаних мазутом загађеног земљишта, чамове пиљевине као додатног извора угљеника и непречишћеног речног песка, додатог у циљу мешања и повећања порозности. Инокулација/реинокулација (биоаугментација) је периодично рађена са биомасом конзорцијума зимогених микроорганизама изолованих из супстрата за биоремедијацију. Биостимулација је реализована додатком хранљивих супстанци (N, P и K). Аерација је побољшавана систематским мешањем биоремедијационог система. Након 50 дана број микроорганизама који деградирају угљоводонике повећан је 100 пута. На основу промена у групном саставу просечна стопа биодеградације током биоремедијације је била за алифатичну фракцију 24 mg kg^{-1} по дану, за ароматичну 6 mg kg^{-1} по дану и 3 mg kg^{-1} по дану за HCO-асфалтенску фракцију. У засићеној угљоводоничној фракцији методом GC–MS (SIM метод) анализирани су изопреноиди пристан и фитан и полициклични молекули стеранског и тритерпанског типа. Током биоремедијационог процеса дошло је до биодеградације и смањења релативних количина изопреноида, стерана, три- и тетрацикличних терпана и пентацикличних терпана хопанског типа.

(Примљено 5. маја, ревидирано 22. јуна 2010)

REFERENCES

1. *ASTM D396-09a, Standard Specification for Fuel Oils*, 2009
2. *ISO 8217:2005, Petroleum products – Fuels (class F) – Specifications of marine fuels*, 2005
3. U. Langer, L. Böhme, F. Böhme, *J. Plant Nutr. Soil Sci.* **167** (2004) 267
4. J. V. Forsyth, Y. M. Tsao, R. D. Bleam, in *Bioaugmentation for Site Remediation*, R. E. Hinchee, J. Fredrickson, B. C. Alleman, Eds., Battelle Press, Columbus, OH, 1995, p. 1
5. S. J. MacNaughton, J. R. Stephen, A. D. Venosa, G. A. Davis, Y. J. Chang, D. C. White, *Appl. Environ. Microbiol*. **65** (1999) 3566
6. M. Viñas, M. Grifoll, J. Sabaté, A. M. Solanas, *J. Ind. Microbiol. Biot.* **28** (2002) 252
7. F. M. Ghazali, R. N. Z. A. Rahman, A. B. Salleh, M. Basri, *Int. Biodeter. Biodegr*. **54** (2004) 61
8. A. M. Boronin, V. G. Grishchenkov, A. V. Karpov, S. G. Seleznev, V. G. Tokarev, M. U. Arinbasarov, R. R. Gajazov, N. P. Kuzmin, *Process Biochem*. **32** (1997) 13
9. A. Singh, O. P. Ward, *Biodegradation and bioremediation*, Springer-Verlag, Berlin, 2004, p. 1
10. J. A. Marín, J. L. Moreno, T. Hernández, C. García, *Biodegradation* **17** (2006) 251
11. S. J. McMillen, A. G. Requejo, G. N. Young, P. S. Davis, P. N. Cook, J. M. Kerr, N. R. Gray, in *Microbial Process for Bioremediation*, R. R. Hinchee, F. J. Brokman, C. M. Vogel, Eds., Battelle Press, Columbus, OH, 1995, p. 91

12. M. Nocentini, D. Pinelli, F. Fava, *Chemosphere* **41** (2000) 1115
13. K. Sugiura, M. Ishihara, T. Shimauchi, S. Harayama, *Environ. Sci. Technol*. **31** (1997) 45
14. S. Mishra, J. Jyot, R. C. Kuhad, B. Lal, *Curr. Microbiol*. **43** (2001) 328
15. B. P. Tissot, D. H. Welte, *Petroleum formation and occurrence*, Springer, Berlin, 1984, p. 1
16. D. Waples, *Geochemistry in petroleum exploration*, International Human Resources Development Corporation, Boston, USA, 1985, p. 1
17. K. E. Peters, C. C. Walters, J. M. Moldowan, *The biomarker guide*, Cambridge University Press, Cambridge, 2005, p. 1
18. B. Jovančićević, M. Antić, I. Pavlović, M. Vrvić, V. Beškoski, A. Kronimus, J. Schwarzbauer, *Water Air Soil Poll*. **190** (2008) 299
19. B. Jovančićević, M. Antić, M. Vrvić, M. Ilić, M. Novaković, R. M. Saheed, J. Schwarzbauer, *J. Serb. Chem. Soc*. **73** (2008) 577
20. J. S. Milić, V. P. Beškoski, M. V. Ilić, S. A. M. Ali, G. Dj. Gojgić-Cvijović, M. M. Vrvić, *J. Serb. Chem. Soc*. **74** (2009) 455
21. C. Loser, H. Seidel, A. Zehnsdorf, U. Stottmeister, *Appl. Microbiol. Biotechnol*. **49** (1998) 631
22. http://www.ccap.ac.uk/media/recipes/SE.htm (01.05.2010)
23. I. D. Bossert, L. M. Shor, D. S. Kosson, in *Manual of Environmental Microbiology*, 2nd Ed., C. J. Hurst, R. L. Crawford G. R. Knudsen, M. J. McInerney, L. D. Stetzenbach, Eds., ASM Press, Washington, DC, 2006, p. 934
24. B. S. Jovančićević, *Practical Organic Geochemistry with Fuel Chemistry*, Faculty of Chemistry, Belgrade, 1999, p. 13 (in Serbian)
25. *NIST/EPA/NIH Mass spectral library NIST2000*, Wiley
26. E. Katsivela, E. R. B. Moore, D. Maroukli, C. Strömpl, D. Pieper, N. Kalogerakis, *Biodegradation* **16** (2005) 169
27. Z. Wang, M. Fingas, S. Blenkinsopp, G. Sergy, M. Landriault, L. Sigouin, J. Foght, K. Semple, D. W. S. Westlake, *J. Chromatogr. A* **809** (1998) 89
28. M. P. Antic, B. S. Jovancicevic, M. Ilic, M. M. Vrvic, J. Schwarzbauer, *Environ. Sci. Pollut. Res*. **13** (2006) 320
29. W. K. Seifert, J. M. Moldowan, G. J. Demaison, *Org. Geochem*. **6** (1984) 633
30. N. L. Olivera, M. G. Commendatore, A. C. MorWan, J. L. Esteves, *J. Ind. Microbiol. Biot*. **25** (2000) 70.